CRANFIELD UNIVERSITY

JUDE EGBUE

CHARACTERIZATION OF TWO-PHASE FLOW IN A TYPICAL METROLOGICAL TEST FLOW LOOP

SCHOOL OF WATER, ENERGY AND ENVIRONMENT
Energy and Power

PhD
Academic Year: 2018- 2022

Supervisor: Dr Liyun Lao
Associate Supervisor: Dr Imma Bortone
September 2022

CRANFIELD UNIVERSITY

SCHOOL OF WATER, ENERGY AND ENVIRONMENT
Energy and Power

PhD

Academic Year 2018 – 2022

JUDE EGBUE

Characterization of Two-Phase Flow in a Typical Metrological Test Flow Loop

Supervisor: Dr Liyun Lao
Associate Supervisor: Dr Imma Bortone
September 2022

This thesis is submitted in partial fulfilment of the requirements for the degree of PhD

ABSTRACT

The understanding of the flow behaviour such as the flow regimes is important in multiphase flow metering for verification of the test meters especially during the reproducibility tests, as the meter could be transferred among different test flow loops or moved from one location to another within a flow loop. As the pipe geometry and configurations may vary for different testing laboratories and on the field, proper understanding of effect of geometrical variances on multiphase flow behaviour is deemed important for proper assessment of multiphase flow meter (MPFM) performance and as well developing testing protocols for commercial flow meters. To improve the performance assessment of MPFM, adequate understanding of the influence of pipe configurations on multiphase flow behaviour in a typical multiphase flow loop is important in order to design a flow loop for the purpose of calibration and validation of MPFM. To obtain this knowledge, a systematic study of flow characteristics transitioning from the horizontal to the vertical section in a typical MPFM testing installation with varying upstream and downstream configuration is needed to provide guidance on proper designing of MPFM calibration flow loop.

To this aim, an experimental study was carried out in a typical MPFM flow loop which consists of 19.2 m long horizontal section followed by a 2.6 m long vertical section. All the sections are at industrial scale, being made of inner diameter (ID) of 0.077 m clear PVC pipe that allows for gas-liquid two-phase flow behaviour to be observed and determined. The alteration of upstream and downstream geometries of the flow loop are also carried out to investigate the effect of geometrical variances on the flow. Air and water are the fluids used for this study.

The result of the study showed that the pipe configuration has significant effect on smooth stratified flow. The stratified flow regime observed in conventional straight pipe in horizontal section for low superficial velocities was observed to be absent in the present work. Instead, unstable wavy-slug (UWS) flow regime was observed. None of typical horizontal flow regime maps considered in this work were able to correctly predict UWS flow regime. The void fraction in the

horizontal section was observed to be influenced by the pipe configuration due to liquid accumulation in the horizontal section. This could contribute to measurement uncertainties of phase fractions in the horizontal section. Analyses of the experimental results showed that no significant change in flow regimes was observed in the horizontal section with different development lengths of 100D and 200D (D is the pipe diameter) from the gas injection points. This suggests that a length of 100D may be sufficient development length for air-water two-phase flow in the horizontal section for such flow loop. Furthermore, more liquid accumulation is observed in 200D as compared with 100D case, which leads to lower void fraction in 200D development length. Downstream effect of the pipe configuration due to backward flow of the liquid phase was noticed to have significant effect on the flow structure in the horizontal section as observed in the probability density function (PDF) signature of the flows. The experimental investigation of effect of blind tee length on pressure fluctuation has shown that the 90-degree bend (equivalent to a blind length of 0D) has the highest-pressure fluctuation while the blind tee with 0.154 m clearance (2D length) has the lowest pressure fluctuation. The magnitude of pressure fluctuation is observed to be higher for intermittent flows than that of separated flows. The influence of blind tee length on pressure fluctuation tends to decrease with distance away from the blind tee in straight pipes.

A set of guidelines for the MPFM test flow loop were proposed based on the outcome of the current studies.

ACKNOWLEDGEMENTS

My appreciation goes to Petroleum Technology Development Fund (PTDF) for granting me full scholarship to start this programme. With gratitude in my heart, I say thank you for catering for my tuition fee and my stipends. I also want to address my appreciation to the European Metrology Programme for Innovation and Research (EMPIR) for providing the funding for the construction of the 3in EMPIR flow loop.

My Sincere appreciation goes to my supervisors, Dr Liyun Lao and Dr Imma Bortone who helped and supported me during the difficult times. I cannot thank you enough for the technical advice and contributions all through this research. Thank you for all those numerous extra minutes we spend deliberating on some of the challenges and forging way forward during the supervisory meeting. I am also very grateful for your patience and understanding.

Special thanks to Stan Collins, the PSE Manager for his technical support during the process of commissioning of the 3in EMPIR rig. I appreciate all the help rendered in locating and installing some of the sensors. I also want to thank Dr Edem Eyo and all the technical team including Euan Hakon, and Marcello Spinelli for their support during the construction of the EMPIR 3in flow loop. My appreciation also goes to the administrative staff and the King Norton Library team for all the support they provided in my PhD journey.

Words are not enough to thank my siblings, my mother and late father who supported and encouraged me both in good and hard times. Your love and kindness kept me going all through this journey.

And finally, to my family, Laurette, Nasya-mira and Judenn, thank you all for your patience and understanding. Thank you for all the sacrifices you made for my sake so that I could focus on my research. You are my backbone and source of inspiration. From the depth of my heart, I say thank you.

Table of Contents

LIST OF FIGURES

LIST OF TABLES

LIST OF EQUATIONS

LIST OF ABBREVIATIONS

CR	Conductivity ring
ECT	Electrical capacitance tomography
EIT	Electrical impedance tomography
EMT	Electromagnetic tomography
ERT	Electrical resistance tomography
EVT	Electromagnetic velocity tomography
GVF	Gas volume fraction
HZDR	Helmholtz-Zentrum Dresden Rossendorf
ID	Inner diameter
LDV	Laser doppler velocity
MAPE	Mean absolute percentage error
MIT	Magnetic induction technology
MP	Multiphase
MPFM	Multiphase flow meter
MWT	Microwave tomography
NMR	Nuclear magnetic resonance
PDF	Probability density function
PNA	Pulsed neutron activation
UWS	Unstable wavy slug
VFM	Virtual flow meter
WMS	Wire mesh sensor

NOMENCLATURES

A	Constant in slip ratio generic formula for void fraction model
A_l	Liquid cross-sectional area, m^2
B	Build up factor (of gamma ray attenuation)
C	Conductivity between the twin ring electrodes of a conductivity ring sensor, S
C_m	Capacitance of the flow mixture, F (farads)
C_{max}	Maximum conductivity probe output voltage (water), V
C_{min}	Minimum conductivity probe output voltage (air), V
C_o	Distribution coefficient, dimensionless

C_p	Capacitance of the pipe wall, F (farads)
D	Diameter of the pipe, m
f	Frequency, Hz
Fgh	Raw gas flowrate from the test loop, m^3/hr
FL	Liquid flowrate, l/min
f_l	Liquid friction factor coefficient, dimensionless
Fr	Froude number, dimensionless
Fr_g	Gas Froude number, dimensionless
f_w	Excitation frequency of detection module, Hz
G	Gas injection point
g	Acceleration due to gravity, m/s^2
h	Parameter in Cioncollini and Thome void fraction model
h_{L1}	Liquid holdup calculated from conductivity ring 1
h_{L2}	Liquid holdup calculated from conductivity ring 2
I_0	Gamma ray source intensity, keV
K_L	Liquid phase coefficient, dimensionless
I	Measured gamma ray intensity, keV
L	Distance between two sensors, m
l_E	Entry length, m
N	Total number of measurements
n	Parameter in Cioncollini and Thome void fraction model
M	Total mass flowrate, kg/s
m	Mass of fluid and carrying probe, kg
P	Pressure, bar
$Pavg$	Average pressure, bar
Pbt	Pressure at blind tee, bar
$Pstdv$	Standard deviation of pressure measurement, bar
R	Measured resistance of the flow, Ohm
Re	Reynolds number, dimensionless
R_m	Resistance of the flow mixture, Ohm
R_{xy}	Cross correlation function value of x and y signals, dimensionless
S_L	Slippage number, dimensionless
r	Constant in slip ratio void fraction model generic formular
s	Constant in slip ratio void fraction model generic formular
SD	Standard deviation

t	Time, s
T	Period
U	Flow velocity, m/s
U_T	Tracer signal velocity, m/s
U_{gm}	Drift velocity, m/s
U_{sg}	Liquid superficial velocity, m/s
U_{sl}	Gas superficial velocity, m/s
U_m	Mixture superficial velocity, m/s
v	Fluid velocity, m/s
We	Weber number, dimensionless
w	Angular velocity, rad/s
X	Lockhart and Martinelli Parameter, dimensionless
$\overline{x}$	Mean value of sample from the data set.
x_h	Flow quality, dimensionless
$x(t)$	Downstream signal from sensor, V
$y(t)$	Upstream signal from sensor, V
Y	Normalized voltage from CR sensor, dimensionless
μ	Viscosity of fluid, Pa.s
μ_{ag}	Linear attenuation coefficient of gas component, m^{-1}
μ_{al}	Linear attenuation coefficient of liquid component, m^{-1}
ε	Fluid permittivity, farad/meter ($C^2.s^{2/}kg.m^3$)
ε_H	Permittivity of fluid with higher permittivity, farad/meter ($C^2.s^{2/}kg.m^3$)
ε_L	Permittivity of fluid with lower permittivity, farad/meter ($C^2.s^{2/}kg.m^3$)
σ	Surface tension, N/m
τ	Delayed time for signal y, s
τ^*	Time lag between two signals (x and y), s
ρ_H	Homogenous density of the flow, kg/m^3
ρ_g	Density of gas phase, kg/m^3
ρ_l	Density of the liquid phase, kg/m^3
ρ_m	Mixture density, kg/m^3
β	Beta ratio, dimensionless
α	Void fraction, dimensionless
α_l	Liquid holdup, dimensionless
$\Delta\rho$	Density difference of the liquid and gas phase, kg/m^3
ΔP	Pressure difference, Pa

1 INTRODUCTION

1.1 Background

Multiphase flow refers to the simultaneous flow of a stream consisting of more than one phase or component in a system (Brennen, 2005). The stream could be made up of different components from the same phase for instance oil and water, a single component with different phases such as steam and water, or different components with different phases such as gas, oil and water (Falcone, 2009). This phenomenon is encountered both in nature and in many industrial processes. Some examples of multiphase flow occurrences in nature include: the blood flow in the body, movement of reservoir fluids through the pores of rocks, steam condensation on windows, and the formation process of sand dunes. In industrial processes, gas-solid flow in pneumatic conveyors, gas-liquid flow in nuclear reactors, gas-liquid flows in evaporators, gas-liquid flow in production strings in oil and gas wells, etc., are some of the examples of multiphase flow. Due to these various occurrences, application of multiphase flow meter (MPFM) is needed for the measurement of these flows.

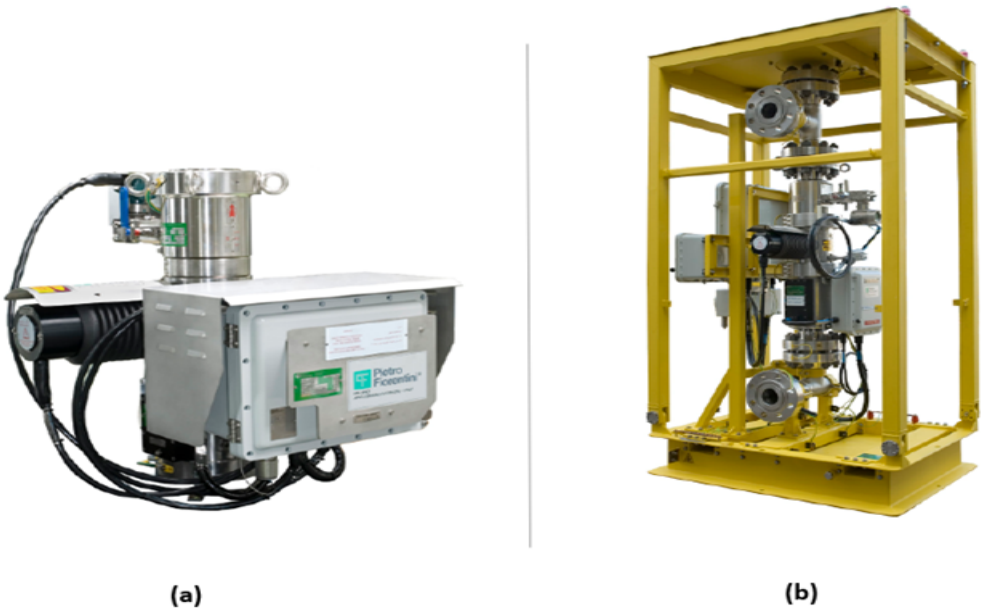

Figure 1-1 A typical (a) inline MPFM and (b) skid mounted MPFM (Pietro Fiorentini, 2021).

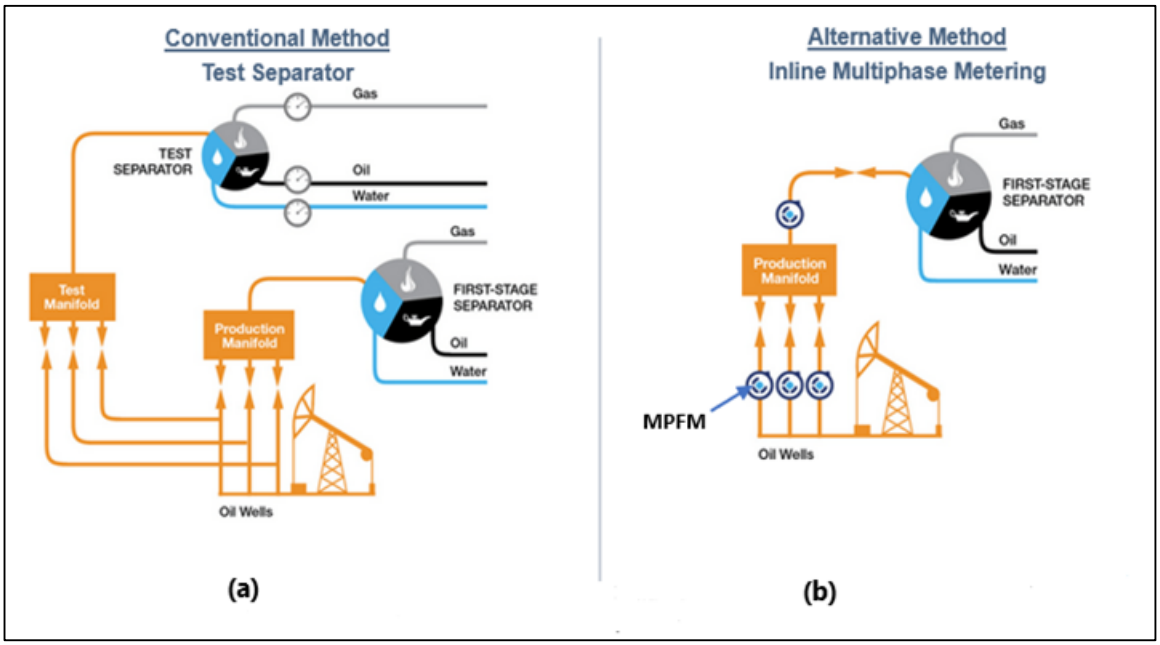

Figure 1-2 Well pad designs with (a) test separator (b) MPFM (Schafer, 2017).

Multiphase flow metering play an important role in many industrial processes such as nuclear industry, aerospace industry, petroleum industry, among others. The performance of multiphase metering, driven by industrial demands, has been gaining increasing attention over the last decades. In the petroleum industry for instance, as the need for cost effective production and metering of crude oil arises, MPFM are widely implemented. The MPFM can be installed inline, or skid mounted (Figure 1.1) depending on the operational requirements. The skid mounted type has the advantage of a smaller number of wirings which improves its installation, commissioning and start up time in the field. However, Inline MPFM is preferred in most facilities where there is space constraint due to its smaller footprint. The conventional method using test separators for measurements of flowrates of produced fluids are often replaced with MPFM (Figure 1-2) during field development nowadays. Aside the advantage of smaller footprint, and lesser pipping, MPFM eliminates space and cost of installing new separators, especially in marginal fields where construction of new infrastructures is not economically viable. Furthermore, the implementation of MPFM increases production optimization as it allows for continuous flow measurements and reduced well intervention time as compared to test separators. Subsequently, many oil and gas companies have heavily invested

on research and on the development of multiphase flow metering techniques mainly for production allocation, production monitoring, reservoir management, and well testing.

Without adequate understanding of multiphase flow behaviour in a flowline, it is almost impractical to choose the best metering technique, as MPFMs are application dependent (Tan et al., 2018). This implies that certain measurement strategy can be only efficient for one or a range of applications. And as a result, the systemic study of multiphase flow features, such as void fraction, flow regime and its development help to provide better measurement strategies and enhance meter accuracy. Further on this, in order to properly evaluate the performances of MPFMs, the systemic study of multiphase flow features in an experimental flow loop is also essential. However, due to the complex nature of multiphase flow, evaluating and improving the MPFM performances can be quite challenging, as different flow regimes may occur in pipeline and the uncertainties associated with the flow prediction. In literature, it is shown that flow regime has significant influence on MPFM performances, for which the MPFM measurement accuracy varies with different flow regimes. In general, adequate understanding of multiphase flow behaviour is crucial for the precise prediction of the flow patterns, which in turn is important for both accurate multiphase flow measurement and optimal design of pressure management and fluid handling system. The problem of understanding the flow behaviour and the associated impact on metering is compounded given the dependency of flow regimes on several factors, such as phase properties, operating conditions (e.g., temperature and pressure, pipe geometry & configurations, etc.).

Since the use of MPFM provides means for production optimization in oilfields, which has led to increase in demand and interest in research and development, it is necessary that extensive research is regularly carried to improve the performance assessment of MPFM and its accuracy. As the assessment of MPFM can be dependent on the flow behaviour, it is important that the state-of-the-art technology is implemented for the research on flow behaviour and its development in flow loop for accurate assessment of MPFM performance. The

last two decades has seen a shift from the use of pressure sensors to flow image acquisition for characterization of two-phase flow (Neogi et al., 2022). The use of sensors that provide cross-sectional imaging of the flow is usually implemented. This helps to provide the phase distribution and morphology of the flow in the pipeline. Most of the flow loops in national and industrial laboratories used for validation of MPFM employ tomography sensors and a viewing (clear) section for characterization of flow behaviour in the flow loop. Similar technology is implemented in this research. Majority of studies on flow behaviour available in literature is either dedicated to horizontal/near horizontal flows or vertical/near vertical flows, with very limited studies on flow transitions from horizontal to vertical section – which is a common configuration of most flow loops used in calibration and validation of MPFM. As a result, this research on flow behaviour in a typical metrological and laboratory-scaled flow loop, including effect of geometrical variances on flow behaviour is deemed relevant to provide insight on flow behaviour on such pipe configuration.

For the application purposes, it is also important that the MPFM performance results obtained by testing different flow loops in different laboratories can be harmonised, i.e., the results are comparable, transferable and traceable, provided that the flow loops' design and operation are following certain protocols. A key to achieve this is to have a good knowledge of the flow behaviours in a testing flow loop, which can further be used to provide guidance to design a rig satisfying for harmonisation requirements. The flow loop for calibration and validation of MPFM is usually made of different elements of joints of pipes, connection type, and instrumentation, which may vary for different flow laboratories used for validation purposes. Since pipe geometry and configuration affect flow regime and other flow behaviours, these geometrical variances in flow loop design for different laboratories may influence the MPFM performance. For this reason, it is therefore paramount to investigate the effect of flow loop design on multiphase flow behaviour in view of improving the assessment of MPFM performance. As stated in previous paragraph, most industrial flow loops for testing MPFM performance are mostly made of horizontal pipes with conjoined vertical configuration. Such flow loop

with horizontal to vertical configuration has shown to minimise the effect of flow regime on MPFM performance testing. It is therefore important to gain better understanding of flow behaviour as it transitions from the horizontal to the vertical section of the MPFM testing flow loop. The overall results of the experimental studies on effect of geometrical variances on flow behaviour in a typical metrological flow loop will help to provide guidance on flow loop design for adequate assessment of MPFM performance.

1.2 Thesis outline

The thesis consists of 7 chapters, and they are presented as follows:

Chapter 1: This chapter covers the introductory aspect of the research, by describing the research concept, highlighting the rationales of the research.

Chapter 2: A critical literature review is presented in this chapter, covering the published studies on flow regime and its development, and the effect of flow regime on multiphase flow metering. Based on the knowledge gaps identified, the aim and objectives of this study are outlined.

Chapter 3: This chapter describes the methodological approach adopted to achieve the aims and objectives of this research. This chapter includes the overview of the research methodology, description of the test facility and the experimental schematisation.

Chapter 4: This chapter covers the characteristics of flow transitioning from the horizontal to the vertical section of the flow. Comparison of some of the flow features such as flow regime and void fraction, for horizontal and vertical sections of the flow loop are presented in this chapter.

Chapter 5: Experimental study of flow regime development by using two injection positions for pipe lengths equal to 100 and 200 times the pipe diameter called respectively 100D and 200D, is presented in this chapter. Using combination of visual observation with probability density function (PDF) and time series plots, comparison and analyses of the two development lengths were carried out in this section. Furthermore, effect of backward flow was

investigated by using two different downstream configurations to understand their effect on flow regime development. Flow characteristics such as void fraction and flow regime were compared for the different configurations.

Chapter 6: In this chapter, effect of blind tee pipes on multiphase flow behaviour was studied by using blind tee of different lengths. Effect of blind tee length on pressure fluctuation was analysed using pressure transducer installed at dead-end of the blind tee.

Chapter 7: The conclusions on the research findings including recommendations for flow loop design are summarised and presented in this chapter.

2 LITERATURE REVIEW

2.1 Flow regime and its development

2.1.1 Flow regimes in horizontal and vertical pipes

Several flow regime may occur when fluids of different phases flow in a pipeline or conduit, depending on factors such as flow rates, fluid properties, pipe inclination with respect to the horizontal, and pipe geometry and size (Cheng et al., 2008; Falcone, 2009; Hassan et al., 2005). The understanding of flow regime is the first step to design and operate the two-phase gas-liquid flow system (Khan et al., 2023). Although this work is dedicated to gas-liquid two-phase flow, the gas-liquid-liquid three-phase flow is a common type of multiphase flow found predominantly in the oil and gas industry where MPFM is largely implemented. The gas and oil mixture produced from petroleum reservoir may consist of large amount of water depending on the maturity of the field. Significant increase in the ratio of water in the produced fluid is usually observed in the mature fields or during enhanced oil recovery process when water is pumped into the reservoir to increase the pressure and force the hydrocarbons out of the reservoir. Understanding the flow regimes is important for designing the pipelines and processing equipment. The gas-liquid-liquid three phase flow regimes are usually more complex than gas-liquid flow regimes. Three-phase flow regimes are usually distinguished based on gas-liquid and liquid-liquid interface (Yaqub & Pendyala, 2018). The characterisation of three-phase flow is complex as result of the uncertainty in predicting the form of both the gas-liquid and oil-water interfaces (Robert & Hall, 1992). The liquid phase (oil and water) could flow as separated layers or as a mixed liquid mixture or as one liquid acting like a continuous phase, and the other one as dispersed phase (Keskin et al., 2007). Some of the common gas-liquid-liquid three-phase flow regimes are presented in Appendix A. More detailed analyses of three phase flow can be found in the work of Khor (1998), Spedding et al. (2005) and Yaqub et al. (2020) for horizontal flows and Kjølaas et al. (2022), Rocha et al. (2017) and Wang et al. (2010) for vertical three phase flow.

Since the present work is focused on characterisation of gas-liquid two-phase flow in a laboratory-scaled flow loop, understanding of the flow regimes is considered necessary as it is one of the important characteristics of two-phase flow (Al-Hadhrami et al., 2014). Some flow regimes may be undesirable in certain industrial processes, for instance in oil and gas industry, slug flow regimes could pose a serious risk to the operations due to slugging effect that could lead to pipe vibration, and wears and tears of the pipeline.

Primary flow regimes in horizontal pipes can be classified as: stratified flow, wavy flow, plug flow, slug flow, dispersed bubble flow, and annular flow, which are shown in Figure 2-1. Stratified flow regime is usually associated with low superficial gas and liquid velocities (Li et al., 2018). Increasing the superficial velocity of gas causes the smooth interphase of the flow to become rippled, resulting to wavy flow regime. If only the liquid flow rate is increased significantly instead, plug flow regime may develop. Increasing both the liquid and gas flow rate will result to more bubbles coalescing, forming larger bubbles that are seen in between intermittently flowing liquid phase, leading to the so-called slug regime flow. Annular flow regime is mainly observed in flows with relatively high flowrate of gas and low liquid flow rate. Some authors have also reported mist flow regimes, mostly witnessed when the gas flow rate is further increased at a relatively low liquid flow rate (Cheng et al., 2008). Dispersed bubble flow regime is often witnessed in flows with high liquid flowrate and low flow rate of gas (Brauner, 2001).

For vertical flows, the most common flow regimes observed (Figure 2-2) can be classified as bubble, slug, churn, and annular flows (Wu et al., 2017). Other authors (Brauner & Barnea, 1986; Taitel et al., 1980) included a dispersed bubble flow regime detected at high liquid flow rates in vertical pipes. Bubble flow is witnessed when a small quantity of gas is injected or mixed with a moderate liquid flow rate (Shaban & Tavoularis, 2014; Wu et al., 2017).

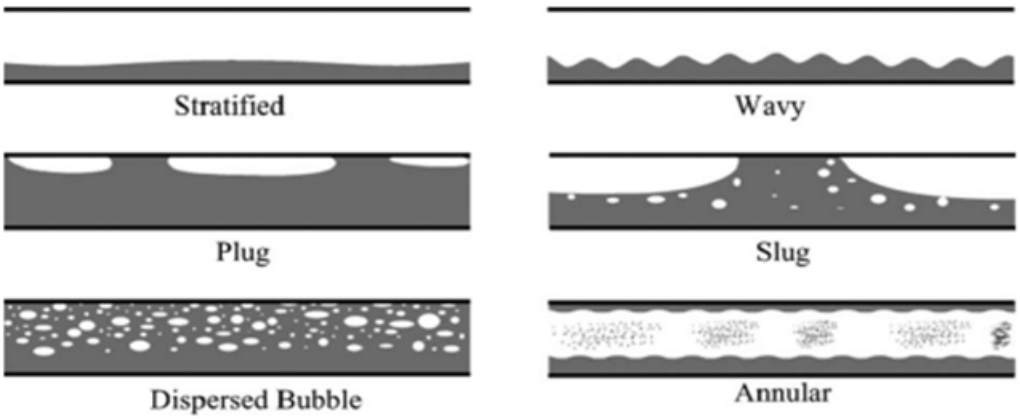

Figure 2-1 Horizontal gas-liquid flow regimes (Cheng et al., 2008).

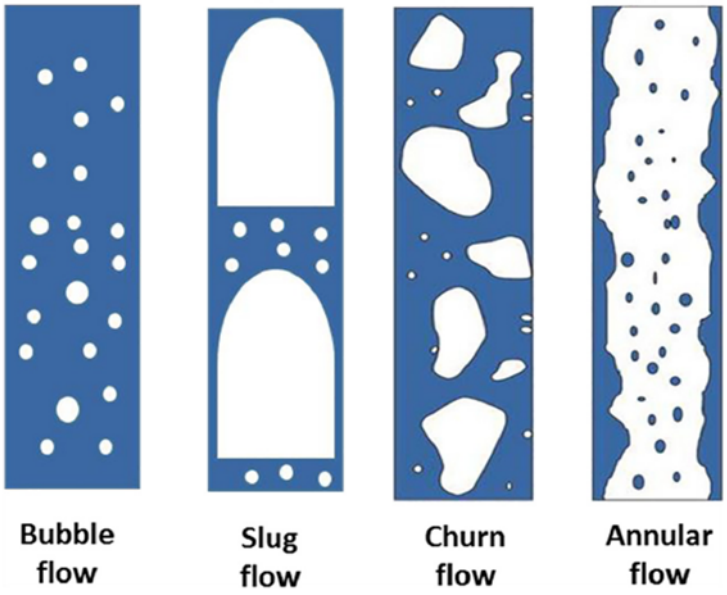

Figure 2-2 Most common vertical upwards two-phase gas-liquid flow regimes (Wu et al., 2017).

Increasing the gas flow rate may lead to slug flow regime, where bubbles coalesce to form a regular set of large bubbles separated by liquid slug (Rouhani & Sohal, 1983). Sometimes it is referred to as Taylor bubble flow (McQuillan & Whalley, 1985; Rouhani & Sohal, 1983). If the increase in gas flowrate is continued, the slugs will collapse, and unstable flow structures known as churn flow regime will occur (Hewitt & Roberts, 1969). Annular flow regime is usually associated with flows with high gas flowrate and relatively low liquid flowrate, where gas phase occupies the core of the pipe, pushing the liquid film to the conduit walls. Wispy annular flow regime is not documented in

many studies. This flow is the transition from churn to annular flow regime. Mist flow regime is observed at an even higher gas flow rate as the liquid film is pushed away from the walls of the pipe (Cheng et al., 2008).

2.1.2 Dimensionless parameters in characterisation of two-phase flow

The past decades have seen different authors implement non-dimensionless parameters for two-phase flow characterisation. These are usually used as mapping parameters for characterisation of two-phase flow. The use of flow regime maps is one of the common methods of flow regime characterisation. Various types of flow regime maps have been developed for prediction of flow regimes under various flow conditions (Spedding & Spence, 1993). Many researchers have used different varying nomenclature for the observed respective flow regimes, hence making it more challenging to have a generalized standard flow patterns and flow pattern map. The use of superficial gas and liquid velocities have been one of the most widely used coordinates for flow regime maps. The Mandhane et al. (1976) and Barnea (1987) are some of the widely used flow regime maps for characterization of horizontal and vertical flows respectively. However, the use of superficial phase velocities only as coordinate parameters have been found to be inadequate to flow regime prediction when extended outside the range of flow conditions for which the map was developed (Rouhani & Sohal, 1983).

Although different authors have suggested different coordinates for flow regime mapping such as mass momentum of the fluids (Hewitt & Robert, 1969) and mass flux of the fluids (Hapanowicz, 2010), there has not been a universally agreed method or mapping coordinates for characterisation of two-phase flow. More robust approach has been identified to include the use of dimensionless parameters to accounts for the flow's governing forces (inertia force, force of gravity, and surface tension). Troniewski & Ulbrich (1984) suggested that parameters, relating to physical properties of the fluid (i.e., Reynolds number) are the most likely universal solution to evaluating flow regime map. The

Reynolds number – a dimensionless parameter is the ratio of the inertial force to the viscous force and defined as

$$Re = \frac{\rho U D}{\mu} \quad \textbf{(2-1)}$$

where ρ is density of the fluid, U is velocity of the flow, D is the pipe diameter, and μ is viscosity of the fluids.

Da Hlaing et al. (2007) investigated the effect of viscosity on gas-liquid two-phase flow regimes using Reynolds number of the fluids as coordinates of the flow regime map to characterise the flow. The effect of viscosity was observed to be more pronounced for bubble, bubble-slug, and slug flow regimes - having low air critical Reynolds numbers. For churn, annular and mist flow, the critical Reynolds number of air were observed to be high, and flow regimes were turbulent in nature. The effect of viscosity was witnessed to be relatively less pronounced for such flow regimes.

Weber number, which characterizes the importance of fluid's inertia against its surface tension is expressed as,

$$We = \frac{\rho U^2 D}{\sigma} \quad \textbf{(2-2)}$$

where σ is the surface tension of the interface. A small Weber number indicates a surface tension force dominating an inertia force.

Weber number was suggested by Chen (2006) as the best options to be used in correlating flow regime transitions due to transition between continuous phase and dispersed phase. This deduction by Chen may only be valid for pipe diameters less than 5 mm. For pipes of larger diameters (greater than 9 mm), Reynolds and Froude numbers were suggested to be greatest importance for multiphase flow regime correlation (Fukano & Kariyasaki, 1993). The effect of Weber number on characteristics of bubble break up was studied by Shao et al. (2018), who observed that the initial large-scale spherical droplet tends to break down into dispersed small droplets with increase in Weber number. It has also been witnessed that with the increase of Weber number, larger droplets

penetrate well into smaller droplets, forcing the droplets to spread on its surface rather than along the symmetry axis (Nikolopoulos et al., 2012).

Froude number is another dimensionless parameter for characterisation of multiphase flow, which is described as the ratio of the inertia force to gravitational force as given in equation (2-3).

$$Fr = \frac{U^2}{gD} \tag{2-3}$$

where *U* is the velocity of the flow, *g* is acceleration due to gravity, and D is the diameter of the pipe.

The Froude number has been recommended by Paglianti et al. (1996) as means to distinguish the whole region of intermittent flow. Plug flow was observed to occur at low Froude numbers, elongated dispersed bubble at intermediate Froude numbers, while slug flow was witnessed at high Froude numbers. Furthermore, experimental studies by Gualtieri & Chanson (2007) showed that hydraulic jump, due to high inlet Froude number is associated with mixing of the two-phase flow and large-scale turbulence. High inlet Froude leads to increase in air entrainment in open channel flow, and consequently the increase in the void fraction.

Slippage number and mixture Froude number has been suggested as flow regime map coordinates (Abdelsalam et al., 2016). The slippage number considers the slippage between two-phases and is expressed as

$$S_L = \frac{(\rho_m - \rho_H)gD}{\rho_g U_{sg}^2} \tag{2-4}$$

where ρ_H is the homogenous or no-slip density, ρ_m is the mixture density, ρ_g is gas density, and U_{sg} is the superficial gas velocity. It was observed that the slippage number increases exponentially with the mixture Froude number. The slippage number was observed to be largest for annular flow regime and smallest for bubble flow regime. This proposed flow regime map coordinates however, do not include the effect of fluid viscosity, surface tension of the fluids

and as well as flow inclinations, which are influential parts of liquid holdup characterisation of flow regimes (Wu et al., 2017).Till date, there has not be any universally accepted flow regime map coordinates for characterisation of multiphase flow.

2.1.3 Flow regime development in pipes

Flow regime transitions may occur as the flow develops along the pipe, taking different patterns based on the phase distribution. Several factors may influence flow regime transition in the pipeline such as pipe geometry, fluid properties and flow parameters (temperature, pressure, and flow rates). Understanding the criteria for flow regime transition is important for accurate prediction of the flow patterns in a pipe and pressure drop in the system (Wu et al., 2017). Different transition criteria have been proposed by different authors for vertical flows (Barnea, 1987; Mishima & Ishii, 1984; McQuillan & Whalley, 1985; Taitel et al., 1980; Tengesdal et al., 1999; Wu et al., 2017) and horizontal flows (Barnea, 1987; Dukler & Taitel, 1986; Cai et al., 1999; Netto et al., 1999; Thaker & Banerjee, 2017). The flow regime may keep changing or transitioning as it travels through the pipe until a fully developed flow is achieved. This would normally require adequate flow regime development length to enable the flow to stabilize and fully develop, which is a desirable condition for accurate measurements of flow parameters for multiphase flow metering.

Flow regime development of multiphase flow plays a vital role in the characterisation of multiphase flow. However it has also created lots of controversy over time in the literature as different authors have suggested different flow regime development lengths in their respective works (Chidamoio et al., 2018; Reis & Goldstein, 2008; Wang et al., 2015).

Many researchers have used different flow parameters to characterise multiphase flow development. While some investigators (Mayor et al., 2008; Wang et al., 2015) have assigned a specific range of pipe length requirement for fully developed flow, others (Chen et al., 2006; Kaji et al., 2009; Lin & Hanratty, 1987) on the other hand, have studied the effect of pipe diameter on the flow regime transitions (Chidamoio et al., 2017).

A fully developed flow refers to flows whose behaviours do not change with the distance downstream (Abdulkadir et al., 2015). This generally involves that the velocity profile does not vary downstream of the fully developed flow region, and the wall shear stress remains fairly constant and perfectly symmetrical (Saffari et al., 2014).

It is well documented that a development length of 30D to 50D is sufficient for a fully developed flow in a turbulent regime for single-phase flow (Brennen, 2005). Earlier works on multiphase flow did not give significant details on multiphase flow regime development length, and in some cases, these earlier published works are believed to be for temporary or developing flow patterns (Brennen, 2005; Mayor et al., 2008; Morgado et al., 2016). For example, Hall & Reader-Harris (1999) were among the earliest pioneers of research on multiphase flow regime development, who observed that an entrance length is necessary to achieve satisfactory results for two-phase flow through horizontal pipes. However, they did not state the recommended flow regime development length.

Development lengths in horizontal two-phase bubbly flow was investigated by Warren & Klausner (1995) by measuring the local pressure drop for air-water two-phase flow and single-phase flow downstream of various orifices. The wall shear stress was determined from the pressure drop profile of the flow. The authors observed that the developing length of single-phase and two-phase bubbly flow downstream of orifice plate is dependent on the ratio of the orifice cross-sectional area to the duct cross-sectional area. Analyses of the photographs of the two-phase flow showed the flow structure varies along the pipe until a fully developed flow is achieved between 69-72 pipe diameters. This work however was only limited to single-phase and two-phase bubbly flow in horizontal pipe.

Vertical annular flow regime development was investigated by Wolf et al. (2001) by studying the local values of the flow properties such as film flow rate, disturbance wave, wall shear stress, film thickness and pressure gradient. The authors observed that the parameters associated to the interfacial wave structure, such as disturbance wave, frequency, and disturbance wave velocity

showed only a slight variation between 100D-300D. On the other hand, the mean film thickness and film flowrate showed a significant change between 100D-300D for high liquid flowrate. For the highest air mass flux (154 kg/m^{2}s), these flow parameters were observed to show little variation after 100D. However, the pressure gradient and the wall shear stress continued to change even after 100D. The authors therefore concluded that 100D is sufficient development for flows with high air flowrates. Any variation in the flow characteristics that continue to take place are mostly as a result of the change in gas density due to pressure drop in the pipeline.

Wang et al. (2006) studied the development of liquid slug length in air-water two-phase flow in horizontal PVC pipe. Conductivity probes were used to determine the liquid slug length distribution. The authors suggested that development length of slug flow is longer that 1157D due changes in slug lengths. In their work, slug and plug flow regimes were grouped together which could have contributed to inconsistency and changes in slug length.

The measurements of variation in liquid film thickness and passing wave frequency in the pipe were used by Hazuku et al. (2008) to describe a fully developed flow. The experimental work was performed in a vertical 3 m long, 0.011 m ID pipe with the measurements taken at 21 axial locations at interval of L/D= 50 – 250 along the pipe. The authors observed that the flows did not reach fully developed state at the end of the pipe as neither the liquid film thickness nor the wave frequency stopped to decrease as a function of distance.

Guo et al. (2009) in their study of slug flow in pipeline for different lengths of 256.6D, 336.6D and 376.6D observed that both the mean and the maximum slug length increases along the pipe as the number of slugs decreases. The authors noted that the more stabilized slug lengths were observed at 336.6D – 376.6D.

Kaji et al. (2009) performed experimental studies on the effect of the flow regime development on the structure of slug flow in two separate vertical pipes with internal diameters and lengths of 0.0512 m and 3.5 m, and 0.0523 m and 9 m, respectively. These authors observed that the slug frequency decreased with

distance and only stabilised at the end region of the pipe section. They also noted that the length of the liquid slug and Taylor bubble increased with distance, with stabilisation noticed at length-to-diameter ratio (L/D) = 100.

Julia et al. (2011) investigated the flow regime development in adiabatic upward air-water two-phase flow in a 4.3 m long vertical annulus of inner and outer diameter of 0.0191 m and 0.0381 m respectively. Measurements were taken at three axial positions of L/D equal to 52, 149 and 230 respectively. These authors also suggested that a flow regime development length of L/D ≥149 is necessary for a fully developed flow.

Successively, Waltrich et al. (2013) performed experimental studies on axial flow regime development of gas-liquid two-phase flow in a vertical 42 m long 0.048 m ID pipe. Conductivity probes were installed at locations L/D of 102, 521 and 815 to measure the liquid holdup and the frequency of the flow structure. The analyses of the behaviour of the liquid holdup showed reasonable axial variation at all measurement locations for higher liquid mass fluxes, while a more developed flow was reached at L/D=521 for lower liquid mass fluxes.

Imada et al. (2013) described a fully developed flow as that point at which the slug frequency becomes constant along the pipe length, and in their work, obtained a 60D development length. Rosa & Souza (2015) identified the fully developed slug flow regime as the flow where the gas and liquid velocity profiles no longer change within the liquid slug, the neighbouring Taylor bubbles do not join together, and the bubbles coalescence rate is null. Wang et al. (2015) recommended a development length between 100D and 200D while Reis & Goldstein (2010) suggested the flow regime development length to be greater than 140D for experimental tests in the annular region.

Abdulkadir et al. (2016) performed experimental work on hydrodynamic behaviour of slug flow in horizontal pipe. The authors used the average slug frequencies and the PDF of void fraction obtained from the electrical capacitance tomography (ECT) and wire mesh sensor (WMS) recording to determine changes in the flow characteristics along the pipe. Their work revealed that there was no significant change in the flow characteristics over the

three sensor locations (64D, 65D and 66.65D). They concluded that the slug flow is fully developed at 64D.

Dinaryanto et al. (2017) investigated initiation and development of slug flow for two-phase flow with observation sections at 25D, 50D, 75D, 180D and 210D respectively. The liquid and gas superficial velocities were observed to play important role in slug formation. The result revealed that at low superficial velocities (0.10 m/s and 1.88 – 6.20 m/s for liquid and gas respectively), role waves were formed by the wave coalescence. On the other hand, the slug flow was initiated by wave growth mechanism or Kelvin-Helmholtz instability at low superficial gas velocities and medium superficial liquid velocity (0.31 m/s). At superficial liquid velocity greater than 0.35 m/s, the slug formations were enhanced by the both the wave growth mechanism and wave coalescence, in addition to the disturbance wave. Generally, a developed flow regime was observed in the 180-210D test sections in their experimental work.

Chidamoio et al. (2017) examined the effect of length-to-diameter ratio (L/D) on vertical two-phase flow for L/D of 16.7, 83.3 and 166.7, respectively. The authors established in their work that by increasing the pipe length, the radial profile of the axial velocity of Taylor bubble tends to be parabolic. Although this trend was observed to be more noticeable on L/D of 166.7 as compared to L/D of 83.3 and 16.7 respectively, a fully parabolic profile was not achieved in the results.

Chidamoio et al. (2018) further investigated longer development length of vertical two-phase flow by assessing axial velocity of flow structures in two L/D geometries (833.3 and 1666.7) required to establish a fully developed parabolic profile. The radial component of the axial velocity is represented by a power law function, with the exponent of the function n=6.1 for L/D =833.3 and n=5.7 for L/D= 1666.7. It was observed that despite decrease in n exponent of the power law function as the L/D increases, the fully parabolic profile could not be attained. This observation leads to suggestion for further investigation on L/D ratio incorporating other factors that could affect flow regime development length.

Further experimental studies were performed by Abdulkadir et al. (2018) by investigating two-phase flow development and phase distribution in horizontal and vertical pipes. The measurements from two ECT and one WMS located at 64D, 65D and 66.65D respectively were used to analyse the flow characteristics. The results showed that the flow is fully developed for vertical two-phase flow, while a rapid developing flow was observed for the horizontal two-phase flow. The results were contrast to previous work where 64D was suggested as sufficient development length for slug flow regime.

The summary of the prominent works on flow regime development is shown in Table 2-1. Although there have been previous works on multiphase flow transition from vertical to horizontal pipe (Oliveira et al., 2009; Spedding et al., 2008), very limited data are available on flow transition from horizontal straight pipe to vertical straight pipe - which is a common configuration in most metrological flow loop. A recent study on three-phase flow transition from horizontal pipe to vertical pipe was conducted by Ma et al. (2021). Blind tee was used to transform the horizontal flow to upward vertical flow. Air, water, and refined transformer oil were used as the working fluid. This research, however, was only limited to stratified flow regime. Furthermore, the research was conducted in pipes of varying internal diameters (0.1 m ID and 0.66 m ID for horizontal and vertical pipe section) that could have significant impact on the results of the research on three-phase flow. A similar work was conducted by Razali et al. (2021) for two-phase flow transition into a vertical venturi, which was mounted on the blind tee. The research, however, was aimed at studying the effectiveness of the mixing effect of the blind tee to characterise the two-phase flow along the venturi. The comparison of gas-oil two-phase flow properties such as void fraction and flow regime development in the horizontal and vertical section (venturi) for different development lengths were not performed in their work.

Table 2-1 Summary of some of the prominent works on flow regime development for two-phase flow.

Pipe orientation	Author(s)	Pipe ID (m)	Working fluids	Results
Horizontal	Warren & Klausner (1995)	0.019	Air-water	Fully developed flow observed between L/D of 69 – 72. The wall shear stress, and analyses of the flow regime were used as criteria to determine the flow regime development.
	Wang, Guo, & Zhang (2006)	0.05	Air-water	Flow not fully developed at L/D = 1157. The mean liquid slug lengths were used as criteria to judge flow regime development
	Guo et al. (2009)	0.05	Air-water	A more stabilized slug lengths were observed between 336.6 – 376.6 pipe diameters. The mean and the maximum slug lengths were used as criteria to assess the flow regime development.
	Reis & Goldstein (2010)	0.034	Air-water	Fully developed flow was observed at L/D greater than 140.
	Wang et al. (2015)	0.076	Air-water	Fully developed flow between 100D-200D. No change in flow pattern.
	Abdulkadir et al. (2016)	0.067	Air-silicone oil	A fully developed flow observed between 66 – 73 pipe diameters. The average slug frequencies and the PDF of void fraction were implemented in assessing the flow regime development.
	Abdulkadir et al. (2018)	0.067	Air-silicone oil	Flow not fully developed at 66 pipe diameters. Partial flow regime development flow was observed, due to changes in flow pattern observed in PDF plots.

Pipe orientation	Author(s)	Pipe ID (m)	Working fluids	Results
Vertical	Wolf et al. (2001)	0.032	Air-water	100D was deemed sufficient for flows with high gas flowrate. No variation in flow properties.
	Hazuku, Takamasa, & Matsumoto (2008)	0.011	Air-water	Flow not fully developed with L/D = 250. Neither liquid thickness nor wave frequency stopped to decrease with distance.
	Kaji, Azzopardi, & Lucas (2009)	0.0523	Air-water	Flow developed at 100D. Slug frequency decreased with distance and only got stabilized at 100D.
	Julia et al. (2011)	0.0191	Air-water	Flow fully developed at L ≥149D. No change in flow pattern was observed.
	Waltrich, Falcone, & Barbosa (2013)	0.048	Air-water	Fully developed flow at L/D = 521 for lower liquid mass fluxes. Variation in liquid holdup was used at criteria.
	Imada, Saltara, & Balino (2013)	0.025	Air-water	Fully developed flow at 100D. Slug frequency was used as criteria. Slug frequency became constant at 100D.
	Rosa and Souza (2015)	0.026	Air-water	Fully developed flow at 360D. Gas and liquid velocity profiles did not change with distance. Bubble coalescence rate is null.
	Dinaryanto et al. (2017)	0.026	Air-water	Fully developed flow at 180-210D. No change in flow pattern.
	Chidamoio et al. (2018)	0.067	Air-water	A fully parabolic profile of the axial velocity not achieved at 1666.7D.
	Abdulkadir et al. (2018)	0.067	Air-silicone oil	Fully developed at 89.5D. Flow pattern did not change.

However, as shown in literature survey, adequate understanding of flow characteristics such as flow regime development in such pipe orientation is necessary for metrological characterisation of two-phase gas-liquid flow. Based on the literature survey, majority of the work done were mostly either devoted to horizontal or vertical flows. The sparsity of data on flow regimes and flow regime development for pipe configuration with conjoined horizontal and vertical orientation (horizontal to vertical flow configuration) has necessitated the need for this research. And as a result, part of this work will be focusing on flow regimes and flow regime development in the horizontal section with its transition to the vertical section of the pipe, to provide a better understanding of two-phase flow behaviour for such horizontal pipe with conjoined vertical pipe configuration.

2.2 Effect of flow regime on multiphase flow metering

Multiphase flow metering has wide application in many industrial processes such as nuclear, aerospace, pharmaceutical, petroleum and many others. Accurate measurement of multiphase flow in such industrial processes is very important to realise flow quantification, process optimization, product quality control, operation monitoring and good decision making (Yan et al., 2018).

Multiphase flow metering usually involves both measurement of the flow composition (phase fractions) and the individual phase velocities using combinations of sensors and/or flow meters to obtain the flow rate of the mixture. The common technologies for calculating the phase fractions and phase velocities are discussed briefly below.

2.2.1 Multiphase flow measurements

I. Phase fraction measurement

Measurement of phase fractions of multiphase flow can be challenging due the complex nature of the flow in conduit and the uncertainties associated with flow regime prediction and its transition (Zargar et al., 2021).

Gamma ray attenuation and electrical impedance techniques are the two common methods for measuring phase fractions (Falcone et al., 2014). Other methods include – microwave attenuation, nuclear magnetic resonance (NMR) and pulsed neutron activation (PNA).

Gamma ray attenuation

This method uses gamma ray source with one or two different energies to determine the component phase fractions of a multiphase flow. This method is sometimes referred to as gamma densitometry because the gamma ray attenuation coefficient is relatively equivalent to the average density of the volume covered by the beam (Thorn et al., 2013).

In this method, single or dual gamma ray source is placed on one side of the pipe through which the gas-liquid mixture flows, and the attenuation of the beam is then measured to infer the component fractions. Gamma ray attenuation working principle obeys the Lambert-Beer's exponential decay law, where the intensity *I* of the beam from the gamma source radiation I_0, after passing through gas-liquid two-phase flow is given as

$$\boldsymbol{I = I_0 B \exp\left[-d\left(\alpha_l \mu_{al} - \alpha \mu_{ag}\right)\right]} \quad \textbf{(2-5)}$$

where μ_{al} and μ_{ag} are the linear attenuation coefficients of the water and gas components, d is the effective diameter of the pipe, and *B* is the build-up factor due to scattered radiation. The linear attenuation coefficients (μ_{al} and μ_{ag}) and the build up factor (*B*) are obtained from calibration measurements. The gas void fraction (α) and the liquid fraction (α_l) can then be obtained using one or two independent measurements based on the mixture component phases. For two-phase flow, single energy gamma source can be implemented for the phase fraction measurements, while dual energy gamma ray source is required for three-phase flow.

In the case of three phase flow, two independent measurements are required for phase fraction measurements. Common method for this is the use of different technology such as capacitance measurement method to obtain the

second measurements. Alternatively, if the use of only one technology is adopted, then two separate measurements can be achieved by using the dual-energy method. With the dual energy attenuation method, two independent equations similar to the type shown in equation 2-1 can be obtained and combined to determine the component phase fractions. This approach has been investigated by different authors including Abouelwafa & Kendall (1980), Roach et al. (1994) and Van Santen et al. (1995).

Electrical impedance method (measures dielectric constant of the mixture)

This method involves measuring the resistance/capacitance of a system/circuit when current is passed through it. The electrical impedance is measured in multiphase flow test loop using conductivity or inductance probe that is fixed and smoothen into the flow channel so as not to disrupt the flow structure.

If two electrodes are fixed to a flow channel or pipe through which the multiphase fluid flows, the measured resistance (R) and capacitance (C_e) will be given as (Thorn et al., 2013):

$$\mathbf{R} = \frac{\mathbf{1} + \boldsymbol{f}_{\boldsymbol{w}}^{\mathbf{2}}\mathbf{R}_{\mathbf{m}}^{\mathbf{2}}(\mathbf{C}_{\mathbf{m}} + \mathbf{C}_{\mathbf{p}})^{\mathbf{2}}}{\boldsymbol{f}_{\boldsymbol{w}}^{\mathbf{2}}\mathbf{R}_{\mathbf{m}}\mathbf{C}_{\mathbf{p}}^{\mathbf{2}}} \tag{2-6}$$

$$\mathbf{C}_{\mathbf{e}} = \frac{\left[\mathbf{1} + \boldsymbol{f}_{\boldsymbol{w}}^{\mathbf{2}}\mathbf{R}_{\mathbf{m}}^{\mathbf{2}}\mathbf{C}_{\mathbf{m}}\left(\mathbf{C}_{\mathbf{m}} + \mathbf{C}_{\mathbf{p}}\right)\right]\mathbf{C}_{\mathbf{p}}}{\mathbf{1} + \boldsymbol{f}_{\boldsymbol{w}}^{\mathbf{2}}\mathbf{R}_{\mathbf{m}}^{\mathbf{2}}(\mathbf{C}_{\mathbf{m}} + \mathbf{C}_{\mathbf{p}})^{\mathbf{2}}} \tag{2-7}$$

where R_m is the resistance of the mixture, C_m is the capacitance of the mixture, f_w is the excitation frequency of the detection electronics, and C_p is pipe wall capacitance.

The resistance and Capacitance of the mixture are dependent on the permittivity and conductivity of the component phases of the mixture, the flow regime, the void fraction and liquid fraction of the flow.

As in gamma ray attenuation method, two independent measurements are required for obtaining phase fractions of the multiphase flow, while only one independent measurement is required for two-phase flow. A common strategy is

the use of combination of measurement of electrical parameter with another technology, usually the gamma ray attenuation method to obtain the phase fractions. More details on this strategy can be found in the work of Fischer (1994). The electrical impedance method is more efficient in gas continuous mixture, as calculating the Resistance (*R*) becomes more challenging for example in oil-continuous mixture with large *R*. Fischer (1994) have all implemented this technology in their various works.

Microwave phase fraction measurement

The microwave method is usually implemented for partially separated flows to measure water cut for oil-water stream. This method is based on measurement of the dielectric properties of the multiphase flow at microwave frequency, by measuring the change in amplitude and phase shift of the microwave signal as it passes through the flow (Ashton et al., 1994). The microwave could be extended to determining the gas volume fraction (GVF) by measuring the phase and loss of the received electromagnetic wave (Xie et al., 2011).

The microwave sensors have different operating principles which include measurement on a single frequency, transmission sensor, measurements on varying frequencies and resonator sensor. More details on the various available principle are presented in the work of Nyfors (2000). For the transmission sensor and measurement on a single frequency, a transmitter probe is used to send microwave radiation through the multiphase flow medium, with a receiver used to output the attenuation or phase change of the microwave signal. Varying frequency method is preferable when there is large attenuation of high frequency microwaves for water continuous flow.

Nuclear magnetic resonance

The nuclear magnetic resonance (NMR) is well known method used for analysing multiphase mixtures in many operations of the process industry (Thorn et al., 1997). In this approach, the meter is equipped with permanent magnets that produces a magnetic field that magnetizes the multiphase flow, which polarized the spins of hydrogen nuclei found in the flow (Bachman et al.,

2008). The realignment in spin state that occur once the flow has departed the magnetic field is related to the chemical composition of the mixture which can be used to deduct the phase fractions of the flow (Thorn et al., 2013).

II. Phase velocity measurements

Cross correlation method

Notably the most widely used technique for phase velocity measurements. This method involves using two sensors placed at L distance apart, and calculating the cross correlation of these signals x(t) and y(t) given as

$$\boldsymbol{R_{xy}(t) = \frac{1}{T}\int_0^T x(t)y(t-\tau)dt} \quad \textbf{(2-8)}$$

where R_{xy} is the cross-correlation function value, *x(t)* and *y(t)* are the downstream and upstream signals, τ is the delayed time for signal *y(t)*, and *T* is the duration of sensor data. The tracer signal velocity (U_T) at time lag τ^* (between the two sensors) at maximum cross-correlation function can be found as

$$\boldsymbol{U_T = L/\tau^*} \quad \textbf{(2-9)}$$

The measurement methods to which cross-correlation technique can be implemented include Gamma ray attenuation, electrical impedance, differential pressure, and acoustic transmission.

The effectiveness of the correlation used to link the velocity inferred from the correlation function's peak position to the average velocity of the flow is the major influencing factor to the accuracy of this measurement techniques. Beck & Plaskowski (1987) mentioned guidelines for good cross-correlation accuracy, including using large sensor bandwidth to enhance flow noise turbulence, and minimizing distance between the sensors (*L*) to decrease the probability of flow evolution between the sensors. One of the major limitations of cross-correlation techniques is that the mixture must be traveling with same velocity, as error will occur in the measurements if slip is present between the component phases.

Also, since a distinct feature (slug mostly) is required to measure velocity, and with the relationship between slug velocity and fluid velocity being very complex, fluctuation of slug velocity therefore poses another problem for cross-correlation techniques. Homogenization of the flow upstream of the sensors is one of the methods used to reduce the error due to slip. The traditional inline mixers are considered not suitable in this case as they are not capable of homogenizing the flow over the wide fraction range (Thorn et al., 1997). The use of a mixer based on twin-cell rotational principle has been proposed by Hewitt et al. (1995) with a claim of good homogenisation observed over a velocity range from 2 to 5.45 m/s. Another method to reduce error due to phase slip is the use of two sensors to measure the flow structures. Olsvik & Widerse (1995) used two sets of capacitance sensors to cross-correlate the gas phase velocity. One sensor to measure the velocity of the large gas bubble, assumed to be the dispersed phase, while the second sensor measures the small gas bubble which is assumed to be traveling at the same speed as the non-dispersed phase.

Another challenge associated with using cross correlation is selecting the optimal distance between the two sensors to efficiently measure the phase velocity over the widest possible range of flow rates. When the distance between the two sensors is high, the captured signal from the two sensors may not be similar enough, while for a short distance, a very high resolution of the timer is required, which is costly (Meribout et al., 2020).

Differential pressure measurement

This method is used for both single and multiphase flow measurements. The method implies using the measured pressure drop across the device to compute the flow rate. The venturi, orifice and V-cone utilize this principle for flow rate measurements, with venturi being the most widely used device of the three. The response of the devices are strongly influenced by the upstream condition of the flow (Falcone et al., 2014). The separated flow and homogenous flow models can be used for fully separated flows and homogenized flows, respectively. Separated flows have been observed to have

lower pressure drop than homogenised flows. However, for flows separated at the entrance of the venturi, the pressure drop could be higher than the homogenised flow. This effect is as result of the venturi acting as a mixer, enhancing re-entrainment of the liquid as droplets, that is accelerated to give a higher pressure drop (Falcone et al., 2014).

The best results for multiphase flow velocity measurement using venturi are mostly achieved by homogenizing the mixture. For homogenized two-phase flow, the volumetric flow rate through a venturi meter with mixture density (ρ_m) can be calculated by using the formula:

$$\mathbf{Q} = \boldsymbol{C_d}\frac{\boldsymbol{\pi}}{\mathbf{4}}\mathbf{D^2}\sqrt{\frac{\mathbf{2\Delta P}}{\boldsymbol{\rho_m}(\mathbf{1}-\boldsymbol{\beta^4})}} \tag{2-10}$$

and the associated mass flowrate (M) of multiphase flow is given as:

$$\boldsymbol{M} = \frac{\boldsymbol{C_d}}{\sqrt{\mathbf{1}-\boldsymbol{\beta^2}}}\frac{\boldsymbol{\pi}}{\mathbf{4}}\boldsymbol{D^2}\sqrt{\mathbf{2}\boldsymbol{\rho_m}\boldsymbol{\Delta P}} \tag{2-11}$$

where ΔP is the measured pressure drop, β is the diameter ratio between the venturi throat and the pipe, *D* is the diameter of the pipe, and C_d is the discharge coefficient which is dependent on the Reynolds number of the multiphase flow. In typical oil and gas field, the coefficient is usually in the range of 0.98 – 1. The values can be used confidently in the equation above without causing any significant error. However, for high viscous or heavy oil, the Reynolds number can be decreased so that the meter operates in an area significantly lower than 1. For this reason, it's a common practice to estimate the Reynolds number so as to provide accurate measurement of the flow rate (Meribout et al., 2020). The mass flowrate is a product of the volumetric flowrate and the mixture density of the flow. The mass flowrate is often preferred to the volumetric flowrate as it is considered to be more accurate and reliable as it does not vary with change in temperature and pressure unlike the volumetric flowrate. This measurement principle using the venturi has the advantages of being relatively less expensive, simple, and reliable measurements.

Positive displacement meter

This method employs the use of vanes, pistons, gears, and diaphragm to measure the volumetric flow rate of multiphase flow by separating the stream into known volumes and quantifying them over time. The volumetric flow rate is achieved by detecting the pulses of the rotor revolutions (Ibrahim & Yeung, 2009). The mass flow rate can be obtained by measuring the densities of the component mixtures and multiplying by the measured volume of the segregated streams. One major advantage of this flow meter over differential flow meters is the ability to measure reverse flow which can be required in many applications. For instance, in in an oil and gas field where a producing well is worked over or converted to an injection well, a positive displacement meter is preferred over a venturi meter as the latter is unidirectional.

Coriolis flow meter

Coriolis flow meter is regarded as the first meter to provide mass flow measurement for multiphase flow (Baker, 1991). The meters utilize the angle of deflection of the tube due to momentum change of the fluid as it passes through the meter, to measure the mass flow rate. This is achieved with the use of built-in electro-mechanical actuator that vibrates its flow tube with an angular velocity (w). The flow measurement is carried out by a magnetic detector that detects the vibrational amplitude of the angular deflection (Ibrahim & Yeung, 2009). The intensity of the Coriolis force perpendicular to the angular velocity *w* and the fluid velocity *v* is given as:

$$\boldsymbol{F = 2mwv} \qquad \textbf{(2-12)}$$

Where *m* is the combined mass of the fluid and the carrying probe. In Coriolis flow meter, two sensors, located at the edge of the flow tube are used to measure the mass flowrate and the density by measuring the phase shift and period from the two sensors respectively.

The meter was initially used for liquid flow measurement but have further developed for gas measurements. One advantage of this flowmeter is that it is

not affected by temperature and pressure variation as result of direct measurement of the mass flowrate.

Tomography method

The tomography is an image processing technology that is used to provide cross-sectional image of the multiphase flow in the pipe (Beck & Williams, 1996; Dyakowski, 1996; Li et al., 2013; Yang, 2010; Yang et al., 1995; York, 2001; Yu et al., 1993). Tomography methods are applied as they provide phase distribution of the component multiphase flow, thereby providing insight on flow regimes in the pipe. Since most multiphase flow meters are flow regime dependent, it is a common practice to have a tomography sensor installed in the pipeline to capture the phase distribution and consequently the flow pattern in the pipe. Different forms of tomography sensors are available for multiphase flow measurement such as electrical capacitance tomography (ECT), electrical impedance tomography (EIT), electrical resistance tomography (ERT), microwave tomography (MWT), and electromagnetic tomography (EMT).

The ECT is among the popular processing technology that has been investigated for multiphase flow measurements by various authors (Gamio et al., 2005; Jeanmeure et al., 2002; Li et al., 2013; Wang et al., 2010; Xie et al., 1992). The ECT sensor is usually suitable for oil-continuous flows but has some setbacks in measurement due to inversion problem that is induced by the imaging reconstruction algorithm (Hansen et al., 2019).

The ERT contrary to the ECT is preferable when the continuous phase is conducting i.e. water-continuous flow (Ismail et al., 2005). Generally, the ECT is suitable for vertical flows as the electrodes are almost always in constant contact with the conducting phase. In horizontal flows, certain flow regimes such as slug flow may have varying electrical properties as a conducting continuous phase may not be guaranteed for a slug cycle. Different approaches including the use of multi-modal tomography system on the basis of ECT and ERT technology to remedy these challenges have been proposed by various authors (Deng et al., 2011; Ma et al., 2001; Qiu et al., 2007; Sun & Yang, 2015; Xie et al., 1995).

EMT technology utilizes electromagnetic wave to determine the phase fractions of the flow based on the permittivity of the fluid. EMT sensor is made up of excitation coils that produces magnetic field. More details on the working principle of EMT is presented in the works of Han-liang & Ling-an (2000) and Wylie et al. (2006). Implementation of EMT techniques can be quite challenging especially in petroleum industry since the measurements relies on the electrical conductivity and magnetic permittivity of the medium, and will normally need high excitation frequency to boost the signal from the sensor (Hansen et al., 2019). A combination of magnetic induction tomography (MIT) and electromagnetic velocity tomography (EVT) - two EMT techniques, are implemented recently to improve multiphase flow measurements (Ma et al., 2017).

The MWT utilizes the measurement of the scattered microwave field to provide imaging of the flow in the pipe. The working principle of MWT is based on determining the complex permittivity distribution of the multiphase flow being imaged from the scattered microwave field measured around the periphery of the flow in the pipe. The MWT sensor usually consists of 4 major blocks (Wu, 2015): the source part that generates the microwave signal; a detection part that measures the microwave signals; a routing part that converts the signals into multi-views of the flow, and the antennae part for transmitting and receiving microwave signals. The one major limitation of this technology is with the reconstruction algorithm being too slow for real time imaging of the dynamic behaviour of the multiphase flow (Wu et al., 2009).

The EIT system is non-intrusive imaging technology that measures the electrical conductivity and permittivity of multiphase from the sensor electrodes. The electrodes are flushed to the pipe such that they are in contact with the flow but do not obstruct the flow pattern in the pipe. When current is sent through the cross section of the pipe, the electrode voltage is measured, which correspond to the electrical properties of the multiphase flow. The electrode voltage will therefore vary depending on the component mixture of the flow. The EIT

technology is described in the works of George et al. (2000) and Heikkinen et al. (2006).

Virtual flow metering

In recent decades, virtual flow meter (VFM) is becoming an attractive alternative to MPFM for estimation of multiphase flow rate as result of its low cost of operation and maintenance. (Bikmukhametov & Jaschke, 2020). Virtual flow meters involve the use of computational models which utilizes measurement data from existing sensors distributed along fluid system installations. It offers low costs, real-time monitoring capabilities, and easy integration with other software solutions for flow rate estimation. The two main type of VFM are physics-driven VFM and data-driven VFM (Ishak et al., 2022). The physics-driven approach employs first principles simulation based on law of physics and chemistry. This approach is based on modelling physical phenomena including thermal hydraulic, reservoir inflow, choke and/ or electric submersible pump models (Chaves et al., 2022). The physics-driven (first principles) approach is the most commonly used VFM tool, both as a standalone solution and as a backup for physical multiphase flow meters. Some of the published studies on first principles VFM system include (Amin, 2015; Couput et al., 2017, 2008; Lansangan, 2012; Tangen et al., 2017). The data-driven VFM utilizes historical production data to enable machine learning and generation of regression models without taking into account the physical phenomena of the flow (Ishak et al., 2022). Various machine learning models have been tested by various researchers including Azim (2020), Ahmadi et al. (2013), AL-Qutami et al. (2017) and Grimstad et al. (2021).

The prospect of combining physics-driven and data-driven VFM has been investigated by various authors. Bikmukhametov & Jaschke (2020) demonstrated that it is possible to create robust hybrid multiphase flow estimation solutions with enhanced accuracy, by combining machine learning with first principles model. Furthermore, the performance assessment, comparing physics-driven and data driven VFMs while running simultaneously has been evaluated by Ishak et al. (2020). Recently, Ishak et al. (2022)

describes a VFM method of flowrates estimation by combining two unique approaches of data-driven Ensemble Learning algorithm and first principles physics-based transient multiphase flow simulator. This approach generates a meta optimal estimator that combines both data-driven and physics driven predictions and tracks their respective performance over time.

Although VFM technology have been recommended in literature as an alternative solution to multiphase flow metering, they still possess significant limitations on the use of VFM model (Jadid, 2017). Most times, the VFM requires a specific data adjustment process which may appear in unique names or shapes. The purpose of this adjustment (tuning) is to adjust the model to the data. The tuning requires adequate knowledge of well operations and the software features. Regardless of the method applied to multiphase flow metering, systematic model tuning is one of the main reasons that VFM is not the main solution for multiphase flow metering. In the first place, accurate flowrates measurements for tuning is difficult to obtain, and as such, very challenging to establish a robust procedure for tuning VFM, particularly in subsea fields (Bikmukhametov & Jaschke, 2020). Another challenge is estimating the uncertainty of VFM predictions and taking that into account to make accurate predictions, which includes uncertainty of models, measurements, and reference flowrates, depending on the applied method.

2.2.2 Sand effect in multiphase flow metering

During production of oil and gas, the produced fluids may sometimes contain water depending on the field production condition. In addition to the water phase, sand particles may accompany produced fluids along the production strings. In late stage of life cycle of oil and gas well, the pore strength of the reservoir becomes weaker, leading to onset of increased sand production. The sand particle transportation and deposition in pipeline is an inherent problem in petroleum industry, that could lead to excessive pressure loss, equipment failure, pipeline erosion and production rate decline (Leporini et al., 2019). Correct and early design of sand control is deemed necessary to achieve remarkable and economic benefit. The two common methods for controlling

formation sand involves either reducing the production rate or using sand control techniques (Khamehchi et al., 2014). Details on sand control and management in wellbore is presented in the works of Daramola & Alinnor (2018); Dong et al. (2017); Khamehchi & Reisi (2015); O'hara (2019); Salahi et al. (2021). In recent decade, the MPFMs are implemented for measurement of formation sand as the 4th phase of the mixture with the produced fluids. The purpose of the formation sand measurement is for early detection and management of sand particles in the pipeline.

In certain field operations while formation sands are transported along with produced fluids in the flowline, the flowmeter like other pipeline components are susceptible to erosion or wears and tears that could affect its performance. For instance, the effect of sand on positive displacement multiphase flow meters has been reported to be most significant at process start-up and shut down (Pinguet, 2011). It is therefore important to take into consideration the sand effect on adequate MPFM that is least affected by formation sand especially in fields where sand productions are expected to be significant. For example, during cold heavy oil production with sand (CHOPS), enhance heavy oil production is achieved by creating large perforation in the reservoir's lower completion to increase the flowrate of heavy oil, therefore encouraging large volume of sand production. For such, it is recommended that more robust meters such as venturi is implemented as they are not significantly affected by sand particles (Pinguet, 2011). In recent decade, the MPFMs are implemented for measurement of formation sand in the mixture with the produced fluids. This is achieved by combining a venturi meter with a phase fraction meter that has the capacity of measuring 3 phases of the flow mixture. As the three measurements are taken at the same time and the same location, this allows to implement closure equation (where the sum of all the phases is equal to 1) without any correction, enabling high accuracy of the flowing phases (Bifout et al., 2014). The multi-energy gamma ray fraction using Barium 133 is usually employed for such measurement because of its several energy level. Additionally, acoustic sand detectors can be added to improve the phase fraction measurement of the produced sand. More details on this approach can

be found in the works of Bifout et al. (2014); Pinguet et al. (2007); Streeton et al. (2020).

2.2.3 Influences of flow behaviours on multiphase flow metering

The differential pressure meter (such as venturi and orifice plate) is the most widely used technology of all these metering technologies, because of their simple structure and no moving parts (Meng et al., 2010). It is reported that majority of the available commercial flow meter has venturi meter as one of its main component (Chinello et al., 2019). Almost all differential pressure flow meters for multiphase flow are based on semi empirical correlations, derived from single phase flow approach and the corresponding experimental data (Liu et al., 2020). One of early prominent works on multiphase flow was performed by Lockhart & Martinelli (1949), where the liquid holdup and frictional pressure drop in two-phase flow correlation for horizontal conduit was investigated. Based on this work, Lockhart and Martinelli parameter (X) was developed, which is widely regarded as the key to all differential pressure devices. Subsequently, various researchers have investigated the correlations between differential pressure and multiphase flow rate. Some of the correlations developed specifically for orifice plate include Murdock (1962), Bizon (1965), Chisholm (1967, 1973, 1977) and Zhang et al. (1992). The correlations for venturi meter were also investigated by De Leeuw (1997), Moura & Marvillet (1997), Steven (2002), Xu et al. (2003), Zhang et al. (2005), and He & Bai (2014), while their performance was tested by Steven (2002), Huang et al. (2005), Oliveira et al. (2009), Meng et al. (2010) and Gupta et al. (2016).

One of the drawbacks of differential pressure flowmeter is the influence of flow regime on flowmeter reading (Meng et al., 2010). Interest on the effect of flow regime on multiphase flow measurement has increased over the past decades (Meribout et al., 2020). It has been identified as one of the factors affecting multiphase flow measurement due to the impact of different flow patterns on metering (Reis & Goldstein, 2008; Silva et al., 2018). The uncertainties associated with flow regime prediction is compounded by the variety of flow patterns and their transitions in pipelines. To minimize the uncertainties in

prediction of flow parameters such as flow regime, implementation of methods which are more focused on the flow physics and the classification of flow regimes are recommended, as a result of the limitations in extrapolation of semi-empirical correlations with good certainty (Razali et al., 2021).

The relationship of MPFM and two-phase flow under different flow regimes have been investigated by different authors (Huang et al., 2005; Meng et al., 2010; Oliveira et al., 2009), who based on the results of their works concluded that flow regime has direct impact on multiphase flow measurement. Furthermore, the time averaged differential pressure (DP) and void fractions, which are some of the quantities of interest during measurement of multiphase flow are shown to be strongly connected to the flow regime (Shaban & Tavoularis, 2014; Taitel & Barnea, 1990; Tutu, 1982).

As the response of the MPFM varies with change in flow regime, it is common for these flowmeters to be tested and calibrated under different flow regimes in order to correlate their relationship. This is evidenced in some MPFM models, where different parameters are generated to account for flow regimes effect on measurement (Zhang et al., 2005). A common approach to reduce the influence of flow regime on measurement is to homogenize the flow by the installation of measurement sensors and meters vertically or implementation of blind-tees and inline mixers in the pipeline. However, achieving a satisfactory homogenisation can be quite difficult for flows with either high GVF or low GVF.

Flow quality (x_h) for determining mass flowrate has also been observed to depend on flow regime (Reis & Goldstein, 2008). The authors in their work on measurement of mass flowrate for horizontal flow observed that the flow quality depended on the flow regime and on the correlations used to calculate the flow quality and the mixture density. Also, the relative difference between the experimental and calculated data was observed to be small for low quality flows.

Investigations of multiphase flow behaviour for different pipe orientations have shown to have impact on logging and production sensors (Roesner et al., 1988). The authors observed different responses of production logging

instruments due to varying flow regimes. For two-phase bubble flow regime, a centralised instrument is observed to respond more accurately in vertical wells. Similarly in vertical wells, for slug flow regime, it was observed that flow characteristics such as slug frequency and the instrument's data could be used to calculate average flowrate and composition accurately. The instrument's reading was observed to be less accurate for slug flow regime in horizontal or deviated wells. The authors concluded therefore that it is paramount to understand multiphase flow behaviour in pipelines to adequately assess the MPFM performance and for choosing the right application for different flow conditions. However, this work was done primarily for horizontal and verticals wells in a view of choosing the right instruments for production logging purposes.

From the literature survey, it was observed that most of the work on multiphase flow and its measurements were mostly performed for horizontal/near horizontal and vertical/near vertical pipe orientation, but not much data is available for flows transitioning from the horizontal to vertical pipe. For such flow loop typically used in most industrial laboratories for validation of commercial flow meters, it is important to understand the flow regime or flow behaviour in such horizontal-to-vertical pipe configuration. As a result, part of the research is dedicated to the characterization of flow transitioning from the horizontal to the vertical section of the pipe.

Also, the literature review showed that understanding the behaviour of multiphase flow in pipeline/flow loop is important for adequate assessment of MPFM performance. However not much work has been carried out on multiphase flow behaviour and the response of the flow with varying upstream and downstream conditions (geometrical configurations) of the flow loop. There are sparse materials on effect of flow loop design on MPFM. As a result, this work is dedicated to the study of multiphase flow behaviour in flow loop, including the response of the flow to geometrical variances to provide insight on flow loop design for calibration and validation of multiphase flow meters.

2.3 Problem statement

During the validation process of MPFM which usually involves development of plan for the verification protocols, the MPFM is transferred and tested in different laboratories prior to its deployment to the field. As a testing provider, it is essential that the MPFM assessment results can be comparable, transferable and acceptable by other counterpart laboratories or institutions. This in turn would require the testing flow loop to be similar to ensure that test conditions are the same, as the test flowmeters' performances are deemed to be influence by those flow conditions. The flow loop used in calibration and validation of MPFM is made up of connections of pipe joints and instrumentation which may vary from one laboratory to another in terms of geometrical configuration such as the mixing distance of the fluids, nature of pipe connections, different pipe shapes and blind tee lengths. Since the flow behaviour especially flow regime is affected by pipe geometry and configuration, with the flow regime known to have effect on MPFM, it is therefore paramount to investigate the effect of flow loop design on multiphase flow behaviour to improve MPFM performance.

For most MPFM, vertical orientation installation is recommended by manufacturers to reduce the effect of flow regime on meter performance. As a result, most of these test laboratories usually have the flow/supply lines from the metering section connected to horizontal part of the flow loop with adequate mixing length to allow the flow to develop prior to moving into the MPFM test section in the vertical part of the flow loop. This type of flow loop configuration is usually achieved by connecting the horizontal section to the vertical sections using bends of various degrees or blind-tee junction. However, most of the work in literature on multiphase flow have always been devoted to the traditional horizontal or vertical configurations, and not many publications have been covered on flows transitioning from horizontal to vertical section. Since the flow loop in most test laboratories involves horizontal to vertical pipe configuration, it is important to understand the flow characteristics as it transitions from horizontal to vertical section.

As can be seen from the above, some of the knowledge gaps that will need to address include:

- Lack of understanding on flow characteristics as it transitions from the horizontal to the vertical section of the flow loop. Change in flow behaviour such as flow regime and void fraction are studied in this work. Part of the work will be devoted to characterization of flow transitioning from the horizontal to the vertical section.
- Lack of knowledge on effect of flow loop design on multiphase flow behaviour. The effect of variation of upstream configurations such as the mixing length of the fluids, swapping of sensor positions to investigate downstream effect, and effect of blind tee length are investigated in this work. This knowledge will help in improving the design of the flow loop for calibration and validation of MPFM.

To make the situation even worse, very limited experimental studies related to the above have been largely obtained from the industrial scale flow loop (i.e., tube diameter around 3 inch or above). However, the inline MPFM are mostly desirable at such scale.

2.4 Aims and Objectives

The aim of this research is to improve the understanding of the gas-liquid flow behaviour and its development in a typical laboratory testing flowline, and the effect of geometrical variances on flow behaviour. Based on this, guidelines can be derived to improve the design of MPFM performance test flow loop for better harmonization of results from different flow loops with similar design or set up guidelines.

Some of the individual objectives that will be addressed to achieve the overall aim include:

- Characterization of flow transition from the horizontal to the vertical section of the flow loop;
- Characterization of flow regime development in the flow loop with complex downstream geometries;

- Investigation of effect of blind tee pipe of different lengths on pressure fluctuation in the flow loop.

3 RESEARCH METHODOLOGY

3.1 Overview of research methodology

To achieve the aim and objectives of this work, the research was conducted experimentally at the Process Systems Engineering Laboratory at Cranfield University by studying the behaviour of gas-liquid flow in a dedicated flow loop consisting of pipe sections with an inner diameter (ID) of 3 inches.

Figure 3-1 Cranfield University's PSE Laboratory.

The 3-inch size flow loop is chosen for this research because it is a near industry scale flow loop, typical for MPFM testing in many industrial and national laboratories. This flow loop is part of the Three Phase Flow rig, an automated multiphase flow test facility that is able to supply individually controlled and metered air, water and oil flows from metering section to the test flow loop. The flow loop is made up of horizontal and vertical sections. The horizontal part is connected to the vertical part through a tee junction. Sensors and instrumentations are strategically placed in the flow loop (based on the research objectives) to study and measure some of the flow properties such as void fraction, flow regime, pressure and temperature in such pipe configuration. A simple schematic of the flow loop for the experimental studies is presented in Figure 3-2. More details on the flow loop dimensions and instrumentation positions can be seen in Section 3.2. The overall procedures related to the study are shown in Figure 3-3.

The experiment was performed with air and water under ambient temperature of around 20^{o}C and operating pressure of 1.2 barg respectively.

To achieve the research objectives, the relevant methods are as follows:

i. Characterisation of flow transition from the horizontal to vertical section

This research work was necessitated due to few studies on flow transitioning from the horizontal to vertical section as shown in the literature review. Experimental investigation was conducted to understand the behaviour of multiphase flow in such flow loop. In principle, this was achieved by experimentally testing two-phase flow in a horizontal pipe with conjoined vertical section, while observing and identifying the flow regimes in the horizontal section and its transition in the vertical section. Some flow properties such as the flow regime and void fraction are the variables that were studied to adequately characterize flow transitioning from the horizontal to vertical section of the flow loop. To achieve this, two WMS, each placed in the horizontal and vertical section of the flow loop, were implemented as measurement apparatus to study the behaviour of the flows in horizontal and vertical section. The flow regimes were identified using the combination of visual observation and PDF plot of the void fraction signal from WMS. The void fractions were obtained by processing the raw data file from the WMS using the Framework software. More details on data

acquisition and data processing of the WMS are explained in the experimental scheme section.

ii. Flow regime development in the flow loop with complex downstream geometries

Experimental studies on flow regime development are divided into two parts: flow regime development with different gas injection points at 100D and 200D, respectively; and the effect of downstream configuration on the flow behaviours such as flow regime and void fraction.

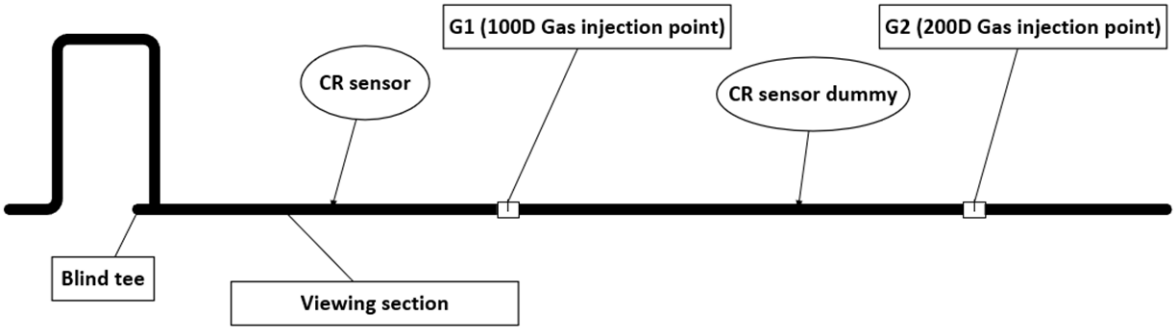

Figure 3-2 A simplified schematic of flow loop for the flow regime development studies.

The first part of the work was undertaken with the aid of two gas injections points at 100D and 200D in the flow loop which form 100D and 200D development lengths respectively (Figure 3.2). First, the 100D development length tests were performed with the gas injection point installed at G1 (100D) and the flow characteristics such as void fraction and flow regime recorded. The gas injection point was then moved to G2 (200D) with the same test conditions as in 100D tests repeated for 200D and flow parameters recorded as in previous tests. The results of the 100D and 200D tests were then compared and analysed (for change in flow patterns).

The associated flow patterns recorded for 100D and 200D tests were then plotted in flow regime map to analyse flow transitions and change in flow patterns for the two tests. Also, the PDF plots for similar test conditions of 100D and 200D tests were compared and analysed to assess the changes in the flow patterns based on the PDF signatures.

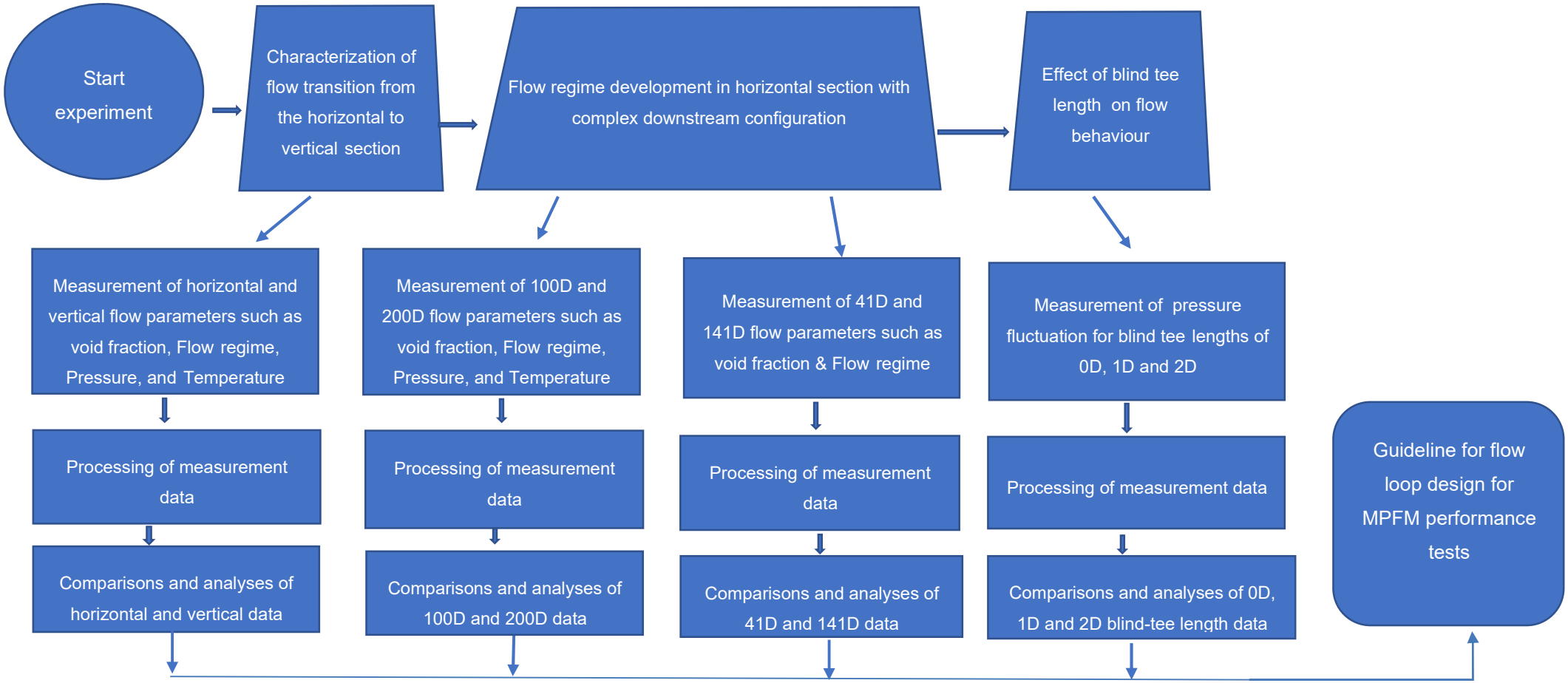

Figure 3-3 Research methodological procedure.

The second part of the experiment involves altering the downstream configuration by swapping the liquid hold up sensor (CR sensor). Due to the pipe configuration of the flow loop, backward flow resulting from backpressure from the blind tee junction (connection) is expected. The backward flow may have downstream effect on the sensor placed upstream of the blind-tee which could increase the measurement uncertainty of the sensor. Investigation of downstream effect on sensor measurement was conducted experimentally in the flow loop by testing and swapping the sensor position from 41D to 141D from the blind-tee while maintaining the same gas injection distance. The EMPIR 3in Flow loop is designed in such a way that it allows for the sensor spool to be swapped from 41D to 141D specifically for this experimental work.

First the test is performed with the sensor spool placed at 41D and the gas injection at 100D. The same test conditions are repeated this time with the sensor positioned at 141D and gas injection at 200D. The flow structure was analysed for downstream effect on measurement by comparing and analysing the signatures of the PDF plots for the 41D and 141D test cases. The void fractions of the 41D and 141D cases were also compared to understand the effect of change in downstream geometry on void fraction measurements.

iii. Effect of Blind-tee length on pressure fluctuation in the flow loop

Sitting in the riser base where the horizontal flow turns into vertical flow, blind tee hence plays a pivotal role for the flow loop and could have significant influence on both the horizontal and vertical flows. In this project the effect of blind tee length on multiphase flow behaviour was studied experimentally by designing a blind-tee with 3 different dead end lengths - 0D, 1D and 2D. The pressure fluctuation was monitored inside the blind tee and along the flow loop with the three blind tee lengths. The experiments were performed with the same test conditions on the 3in EMPIR flow loop with each of three different lengths of Blind-tee successively. For each of the three blind-tee lengths, a pressure transducer is attached to record the static pressure of the flow. The blind-tee design was achieved by attaching two 1D removable blanks to a flange using a screw. A pressure transducer is fixed at the dead-end of the blind-tee flange.

The 0D Blind-tee length test was first performed, then followed subsequently by 1D and 2D blind-tee length tests, respectively. The pressure fluctuation in the pipe were analysed and studied for the three different blind-tee lengths, including how the pressure fluctuation varies for different flow regimes.

3.2 Experimental setup

3.2.1 Description of tests facility

The experimental investigation was carried out in the Cranfield University's multiphase test facility shown in Figure 3-4. As part of the team involved in the EMPIR project, Cranfield university was tasked with the building of a metrological flow loop for small scale testing of multiphase flow. The 3" EMPIR flow loop was initially designed to match the prototype for the testing of Roxar flow meter in the project. To account for effect of other geometrical variances, downstream effect was incorporated in the design for our research purposes by changing the downstream configuration while maintaining the same injection distance (development length) as discussed in section 3.1. The effect of the blind tee length was also included in the design to assess its impact on pressure fluctuations in the flow loop and provide knowledge on best design for such flow loop. The development lengths and blind tee lengths for the flow loop were informed by literature survey and as well as existing structures and space constraints (length) in the laboratory.

Prior to construction of the flow loop, the total length of the flow loop design was first physically measured and positions of the instrumentation's marked on the nearest existing pipework for ease of building the flow loop. Flange aligners were used in connections of the pipes to ensure minimal disturbance of the flow along the flow loop.

The multiphase test rig is an automated facility designed to deliver a regulated and measured rate of multiphase flow fluid mixture from the flow metering section into the test flow loop, and finally into the phase separation section where the fluids are separated in the horizontal three-phase separator. The gas phase (air) is vented into the atmosphere while the liquid phase (water) is

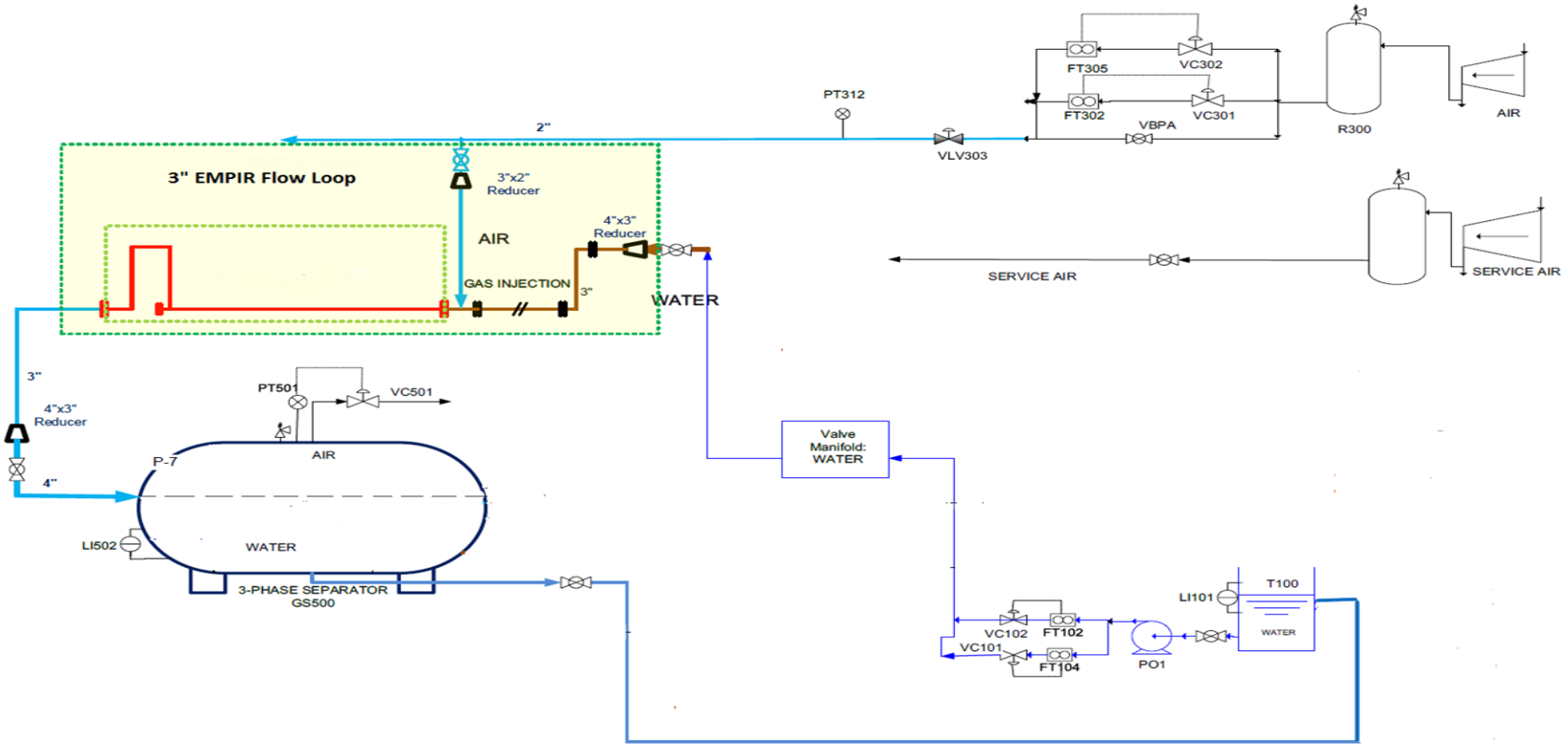

Figure 3-4 Schematics of Cranfield University's Three-phase Flow Test rig.

returned to the water storage tank. Water is supplied to the flow loop from 12.5 m3 capacity water tank with two multistage Grundfos CR90-5 pump, that has a capacity of 100 m^3/hr at 10 barg. The air is supplied to the loop from two compressors (AtlasCopco GA-55 and GA-75), which when connected in parallel can supply up to air flow rate of 1410 Sm^3/hr at a delivery pressure of 7 barg. Two flow meters (Rosemount magnetic flow meter for flowrates in range of 0 to 1 kg/s, and Foxboro CFT50 Coriolis meter for flowrates above 1 kg/s and up to a maximum flow rate of 10 kg/s) are used for metering of the water phase depending on the desired flow rate with uncertainties of ±0.2% and ±0.15% respectively.

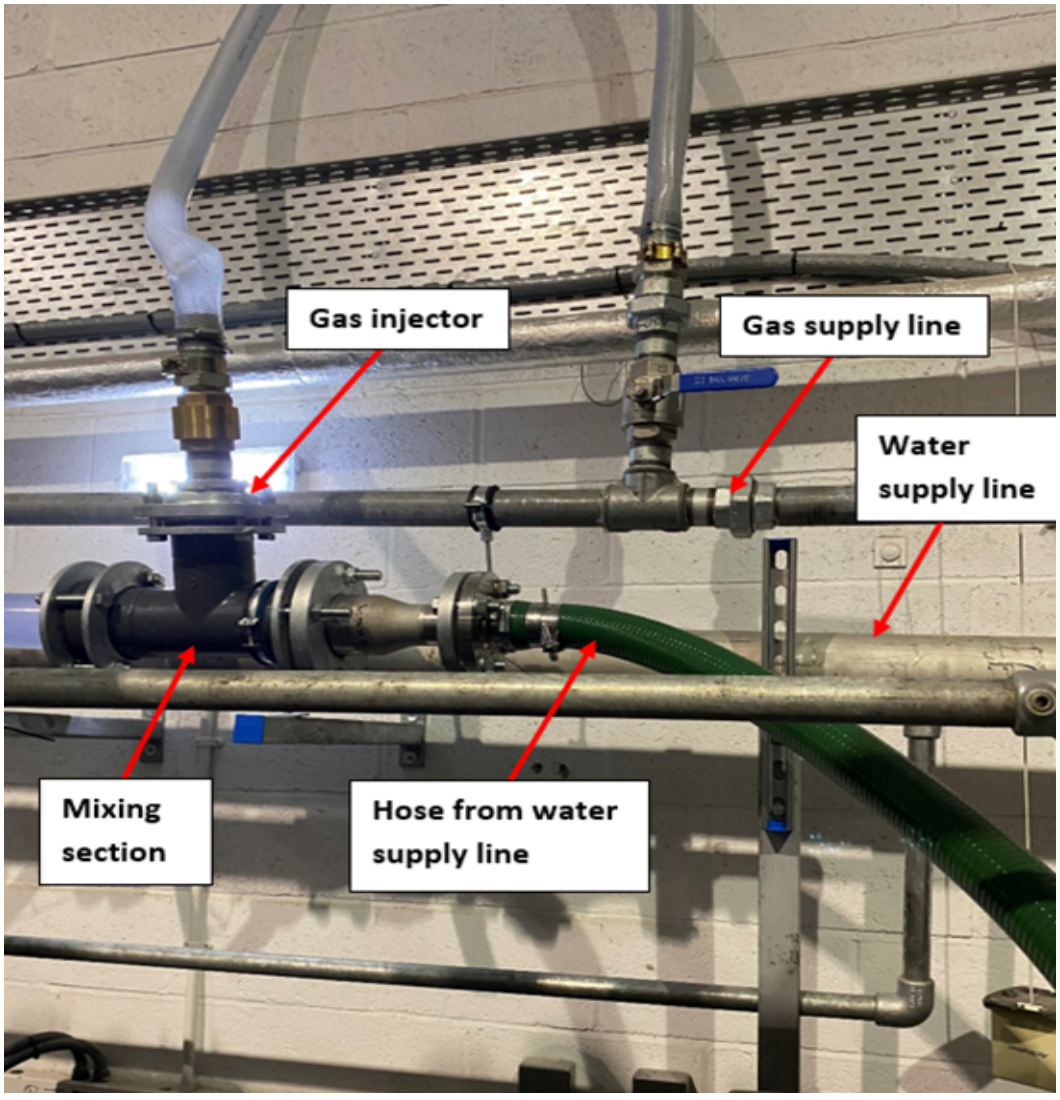

Figure 3-5 EMPIR flow loop fluid injection section.

Figure 3-6 EMPIR flow loop viewing section.

The air is metered by one of the two Rosemount Mass Probar flow meters (FT302 for flowrates in the range of 0 to 150 Sm3/hr, and FT305 for flowrates above 150 Sm3/hr) with uncertainty of ±1.4%.

The air is introduced into the flow loop through the gas injection point, where it mixes with the liquid (Figure 3-5) in the horizontal section before getting into the test section. The flow is allowed a stabilization time of 10 minutes before recording of the data. The test is motored from acquisition display monitors and from the viewing section of the EMPIR flow loop (Figure 3-6).

The Blind tee section of the flow loop is designed in such a way that allows for the length of the clearance between the dead end of the blind tee and the mid-section of the vertical pipe to be varied. A pressure transmitter is installed at the dead end (blank flange) of the blind tee section to monitor dynamic pressure response for different blind tee lengths (Figure 3-7). The two removable blanks of 1D length each are inserted inside the tee junction and screwed to the inner side of the dead end to form 0D blind tee length. To adjust the Blind tee length to 1D, the flange is loosened, and one of the 1D blanks is removed from the Blind tee and then installed back in the flow loop. Similarly, for 2D Blind tee length, the last blank is removed from the inside of the flange of the blind tee to create a 2D length.

3.2.2 Experimental scheme

The experiment was conducted in a 19.2 m long 0.077 m ID transparent PVC pipe flow loop with air and water as the working fluid. The flow loop consists of an inverted U-shaped vertical section that is preceded by the horizontal section (Figure 3-8). The horizontal section is joined to the inverted U-shaped section using a blind tee. A total of 5 pressure transducers are installed on the flow loop, with three pressure transducers P1, P2 and P3 placed in the horizontal section at 2.19 m, 6.10 m, and 9.92 mm respectively from the blind tee, while the fourth and fifth pressure sensors, P4 and P5 are located on the vertical section at 0.25 m and 1.58 m from the blind tee, respectively. Two WMS are installed in the flow loop to capture the phase distribution of the flow - one WMS at a horizontal distance of 1.39 m from the blind tee, while the other is placed at a 1.58 m vertically from the blind tee. The flow loop is equipped with two gas injection points at G1 and G2, which form the 100D and 200D flow regime development lengths respectively in the horizontal section of the flow loop.

Conductivity ring (CR) sensor

The CR sensor was used for liquid holdup measurement in the 0.077 m ID PVC flow loop. The mode of operation of the sensor is based on the concept of difference in electrical properties of the testing fluids.

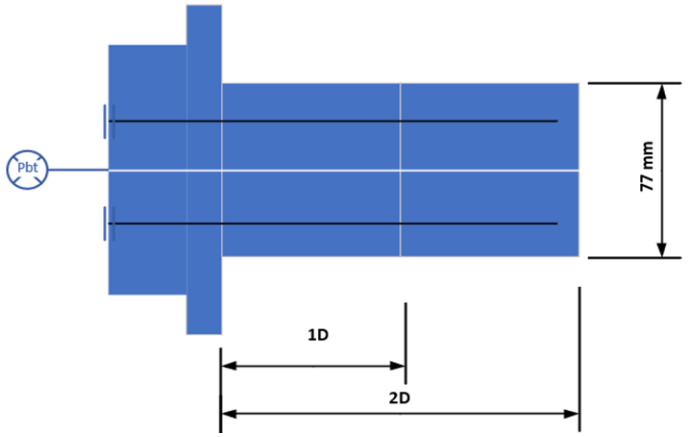

Dead end insertion of the blind tee

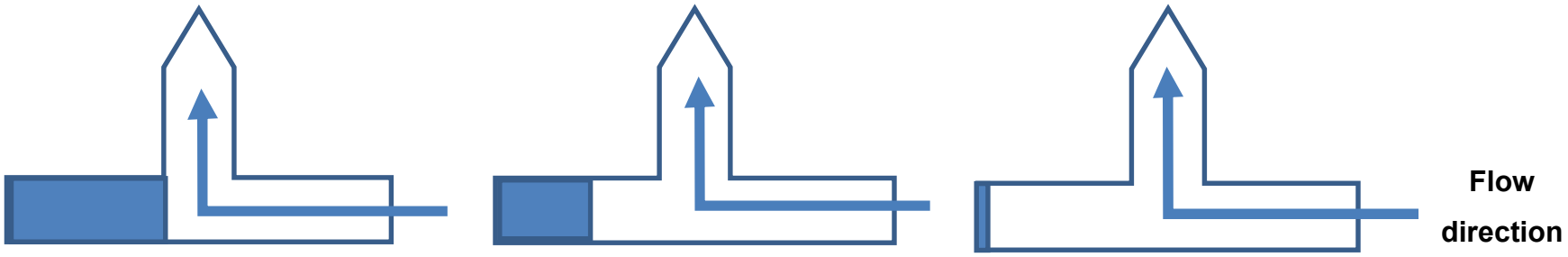

0D Blind tee (0D_Bt)

1D Blind tee (1D_Bt)

2D Blind tee (2D_Bt)

Figure 3-7 Blind tee design with insertable blanks for varying the blind tee length.

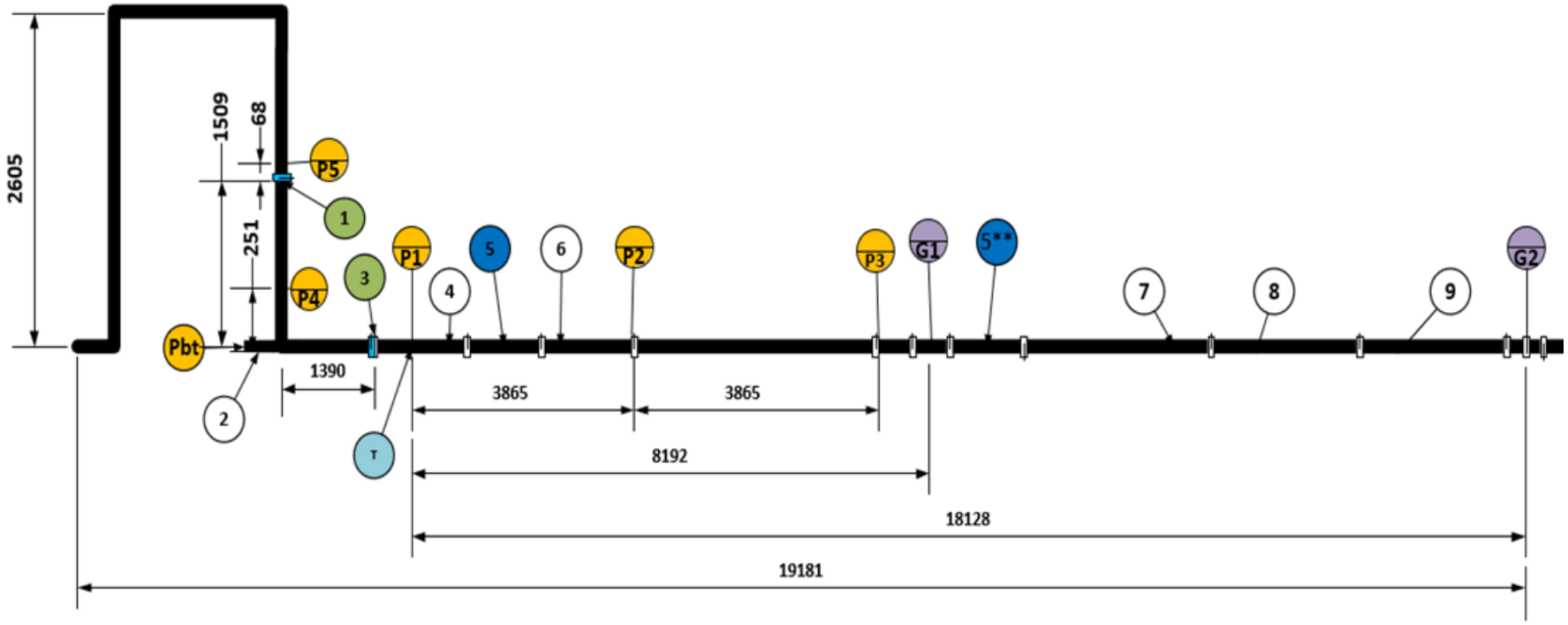

Figure 3-8 EMPIR flow loop test section diagram: 1-Vertical WMS; 2- Blind-tee; 3-Horizontal WMS; 4- Observation section; 5-Sensor spool; 5 -Sensor spool dummy; 6,7,8,9- blank dummy sections; P1, P2, P3, P4, P5- Pressure transducers; Pbt – blind tee pressure transducer; G1,G2,- gas injection points; T - Temperature sensor.**

The sensor measures the electrical property (impedance) of the fluid between the twin ring probes, as the fluid moves over the flushed mounted probes. The measured impedance between the two probes is dependent on the conductance and permittivity of the individual phases of the two-phase mixture, the fraction of the phases, the flow regime and sensor configuration. The sensor was designed (Figure 3-9) based on the recommendation of Fossa (1998). The geometry aspect ratio of the electrode spacing (De) and the pipe diameter (D) was obtained as 0.34, while the ratio of the probe thickness (S) and the pipe diameter yielded 0.13 both falling within ranges recommended by Fossa (1998).

The conductivity ring sensor used for this experiment is a 430 mm long cylindrical Perspex pipe of 77 mm diameter, on which twin ring electrodes are fitted internally to flush and align with the inner diameter of the pipe. This non-intrusive set up of the Conductivity ring allows for sensor not to obstruct or influence the flow pattern in the pipe. Each of the 2 pairs of the 10 mm probes are placed at both end of the sensors, 270 mm apart.

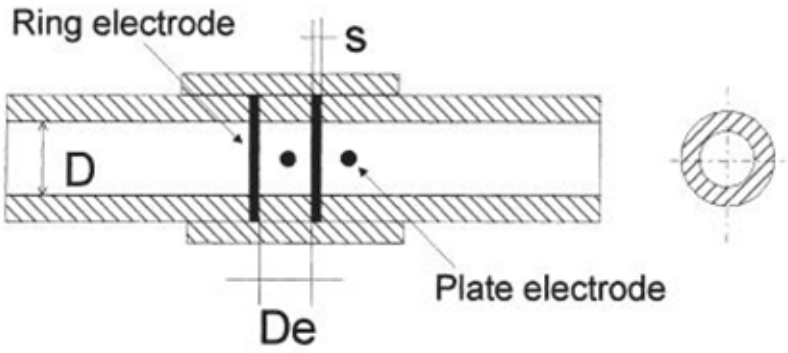

Figure 3-9 Conductivity ring probe's geometry ratio aspect parameters (Fossa, 1998).

Data available from literature survey shows that conductivity probe response is affected mainly by the probe geometry and the by the flow pattern (Fossa, 1998; Fossa et al., 2003). Fossa (1998) performed experimental investigation on design and performance of a conductivity probe for measuring the liquid fraction in multiphase flow. Based on performance of different geometry aspect ratios of the conductivity probes, the author recommended geometry aspect

ratio of De/D and S/D equal to 0.34-0.4 and 0.71-0.08 respectively. The conductivity ring sensor used in this work satisfies these conditions.

Calibration of conductivity ring sensor

Calibration of the Conductivity ring sensor is necessary prior to the test for establishing a relationship between the liquid holdup in the pipe and output voltage reading. The relationship is vital for approximating the liquid holdup during the actual tests/experiments.

The sensor was calibrated by connecting the twin ring pair electrodes to the electronic box electrode that is linked to the computer, where LabVIEW program is used for data acquisition. One end of the sensor was covered with blanked flange while the other end was covered with a special flange that has relief valve for air venting, and injection point funnel for introducing liquid into the sensor (Figure 3-10).

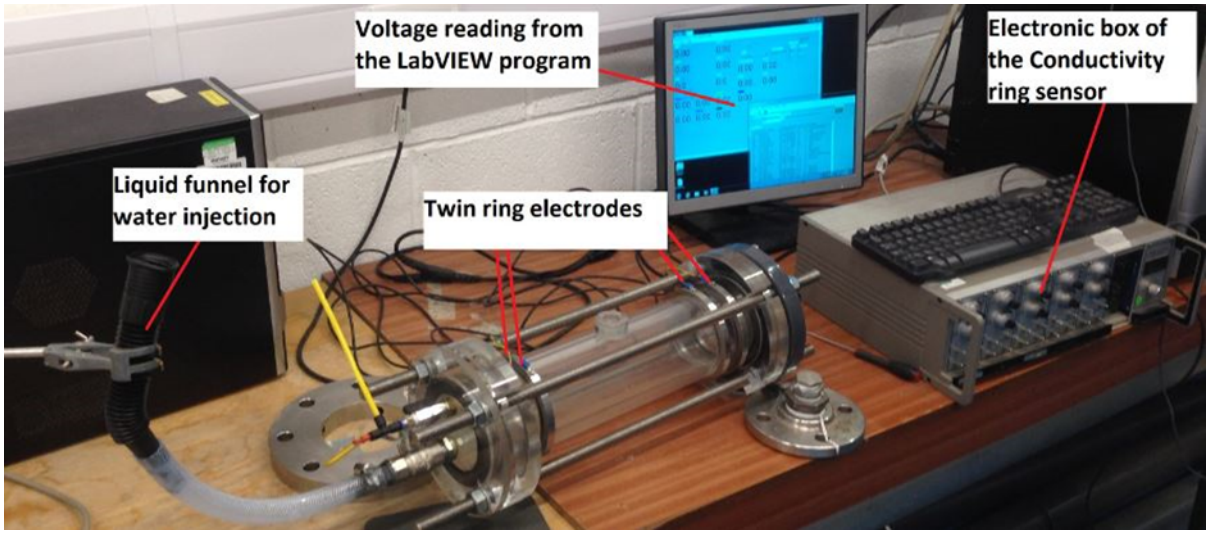

Figure 3-10 Calibration setup of the conductivity ring sensor.

First, the reading of the sensor in volts from LabVIEW program was taking when it was completely empty (only air). The sensor was then filled completely with water and the voltage reading of was taking as well. Then, a known volumes of water was gradually introduced into the sensor and the corresponding normalized voltage reading taking. 200ml of water was introduced successively and the corresponding voltage reading recorded. 10 readings were taking for

liquid volume of 0-2000ml. Both the liquid volume and the voltage reading were converted to fractions with 1 corresponding to full water pipe (100% liquid holdup) and 0 representing empty pipe.

A calibration curve was generated for the pair of twin ring electrodes C1 (Figure 3-11) and C2 (Figure 3-12). MS Excel was used to generate the polynomial relationship between the liquid holdup and the normalized voltage reading of the pairs of the twin ring electrodes which are presented in equations 3-1 and 3-2.

$$\boldsymbol{h_{L1} = 0.4543Y^4 - 1.7286Y^3 + 1.8542Y^2 + 0.4141Y + 0.0035} \quad \textbf{(3-1)}$$

$$\boldsymbol{h_{L2} = -1.6439Y^4 + 2.0859Y^3 - 0.0028Y^2 + 0.5602Y + 0.0008} \quad \textbf{(3-2)}$$

where *Y*, the normalized voltage is obtained from equation 3-3 below:

$$\mathbf{Y} = \frac{\boldsymbol{C_m - C_{min}}}{\boldsymbol{C_{max} - C_{min}}} \quad \textbf{(3-3)}$$

where C_m, C_{min}, and C_{max} are the measured voltages for the mixture, air (empty pipe), and water (full pipe).

The void fraction can be calculated using equation 3-4 below

$$\boldsymbol{\alpha} = 1 - h_L \quad \textbf{(3-4)}$$

The measurement uncertainty of the conductivity ring probe was observed to be within ±5% of indirect measurements. The error in the calibration measurement was recorded as ±2%. The Bench calibration was carried out under stratified flow condition. Since different flow regimes may occur during the experiments, the uncertainty of the averaged measurement of the liquid holdup could be up to ±5%.

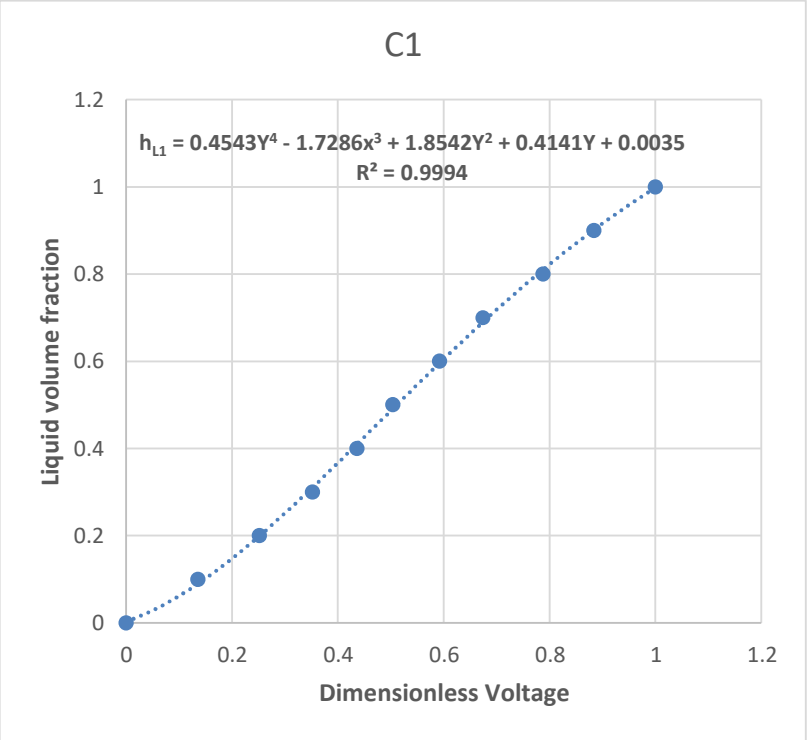

Figure 3-11 Calibration curve of conductivity ring pair 1.

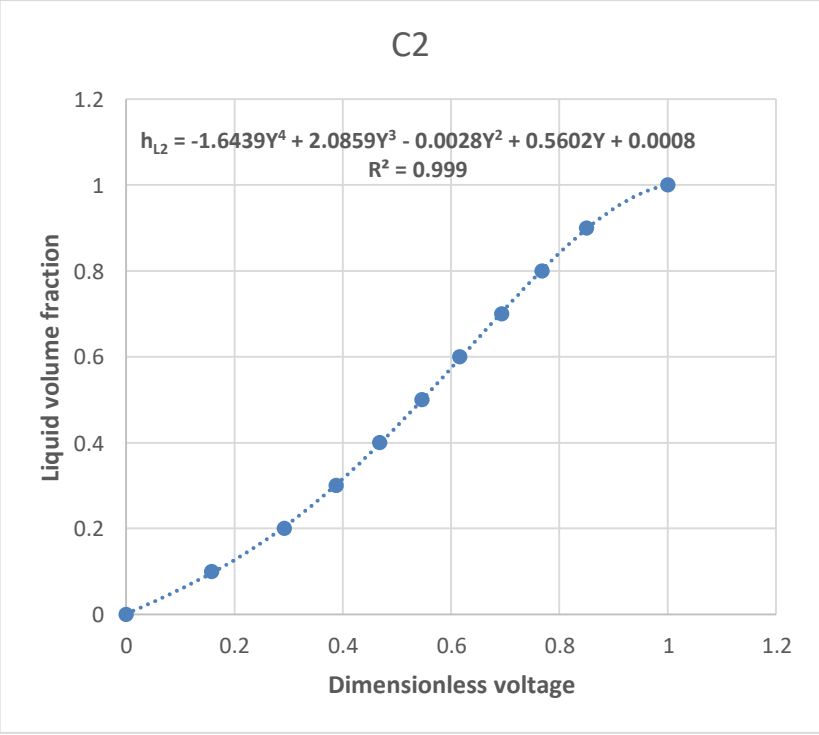

Figure 3-12 Calibration curve of conductivity ring pair 2.

Wire mesh sensor

The wire mesh sensor (WMS) shown in Figure 3-13 is a fast-imaging invasive multiphase sensor used for gas-liquid and liquid-liquid flows. The sensors are manufactured for measuring and visualizing multiphase flow when the phases have remarkable difference in electrical property. The WMS was first developed by Prasser et al. (1998). The sensor has since then been successfully utilized for multiphase flow measurements by various authors (Banowski et al., 2017; Beyer et al., 2012; Ito et al., 2011; Kanai et al., 2012; Kesana et al., 2017; Lee et al., 2017). The sensor is made of different matrix set size set of wires (i.e., 128, 64, 32, 24, and 16) that are placed perpendicular to each other in such a way that they form a set of cells or grids. For instance, the sensor size type used in this work is the 24x24 WMS which has 2 sets of 24 wires running perpendicular to each other. One set works as the transmitter, while the other set works as the receiver.

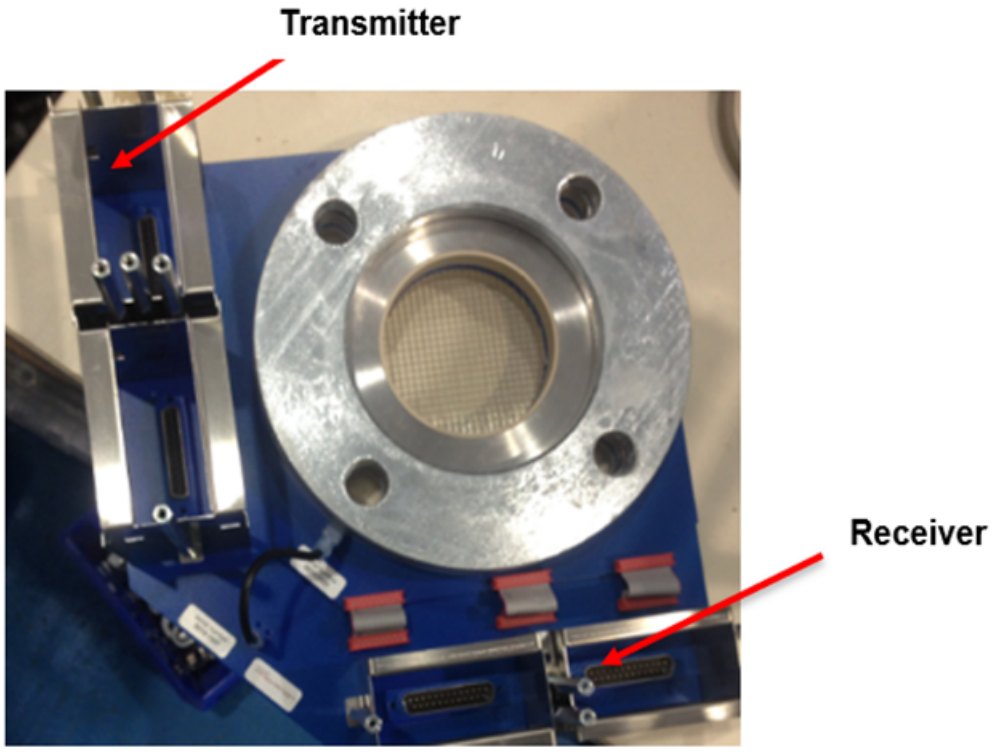

Figure 3-13 Wire mesh sensor.

The WMS is connected to the rest of the pipes at designated point of interest in the flow loop to measure permittivity of the flow. The sensor is connected between pipe joints of the flow loop in a way that that the wire mesh is placed directly in the flow path, such that the image of the flow is captured as the flow moves through the mesh of wires. The wires are thin (0.75 mm), that even though the sensor is intrusive, it does not necessarily obstruct flow structure/pattern. The WMS measures a value equivalent to the conductance/capacitance of the multiphase flow at multiple grids in a plane across the flow (Tompkins et al., 2018). The 24x24 wms sensor used in this work for void fraction calculation and phase distribution was acquired and processed using CAP200 and the WMS framework software, - products of Helmholtz-Zentrum Dresden-Rossendorf (HZDR).

Calibration of the wire mesh sensor

The WMS is calibrated prior to the main test/experiments with the same fluids that will be used in the experiments. Calibration process is based on the principle of obtaining the maximum contrast between the high permittivity fluid and low permittivity fluid used in the experiments.

The calibration is performed with the aid of the CAP200 WMS software. 2 calibration files, for the lowest and highest permittivity fluids are generated during the calibration of the sensor using the testing multiphase flow fluid. Starting with fluid with the lowest permittivity in the pipe, the offset slider was used to adjust the offset of value for the fluid by moving the Amplifier slider to maximum to get maximum gain for the low level of signal. The Offset is adjusted afterwards to values slightly above zero (approximately 5 %).

The fluid with the highest electrical permittivity is introduced into the flow loop until the wires of the sensor are completely covered with the fluid with highest permittivity. When all the wires are in sufficient contact with the fluid, the gain slider is slide to maximum, and then gradually lowered so as to obtain reading slightly below 90% to obtain sharp contrast between the low and high permittivity fluids.

After these adjustments to obtain maximum contrast, the calibration data for the lowest and highest permittivity fluid is acquired by taking separate measurements of the each of these fluids. The 2 files for the lowest and highest permittivity are used later with the measurements files of the experiments to estimate the local phase fraction.

The relationship between the permittivity for the calibration files and the estimated void fraction of the of the multiphase flow measurement as described by Da Silva (2008) is shown in equation below as

$$\boldsymbol{\alpha(i,j,k) = \frac{\varepsilon_H(i,j) - \varepsilon(i,j,k)}{\varepsilon_H(i,j) - \varepsilon_L(i,j)}} \quad \textbf{(3-4)}$$

where *i,j* are indices of the grid points (rows and columns) in the measurement plane and *k* is the number of the frame. H and L denote the high and low permittivity respectively, $\alpha(i,j,k)$ is the local estimated void fraction, and $\varepsilon(i,j,k)$ is the local sensor signal of the measured value of the permittivity of the mixture obtained from raw data of Cap200, $\varepsilon_H(i,j)$ is the permittivity for fluid with higher permittivity and $\varepsilon_L(i,j)$ is the permittivity for fluid with lower permittivity, $\varepsilon_H(i,j)$ and $\varepsilon_L(i,j)$ are the high and low fluid permittivity which are obtained from the calibration files for the high and low permittivity fluids using the WMS framework.

The output file with the void fraction estimation result is stored in a .epst file format, which could easily be imported into using MS Excel file. The WMS used in this work has measurement accuracy of ±2.5 %.

Pressure measurements

The pressure measurements form important part of these research for determining flow characteristics such as gas superficial velocities, test section pressure, and pressure fluctuation in the flow loop. The pressure measurements in the flow loop were recorded using pressure transducers manufactured by Druck GE. Three pressure transducers are installed in horizontal section of the flow loop while another three are installed in the vertical section to measure the static pressure in the flow loop. Additional pressure transducer is installed at the

blind tee to study the behaviour of two-phase flow with different blind tee lengths. All the pressure transducers are within the measurement range of 0-6 bar with an uncertainty of 0.15%.

Calibration of the pressure transducer

The GS-60 Calibration hand pump was used the calibration of the pressure transducers. The GS-60 calibration pump, which uses air as pressure media, has the capacity of generating air pressure withing the range of -1 to 60 barg. The transducers were calibrated under atmospheric pressure of 1 bara and ambient temperature of 17°C. To start calibration, the pressure transducer is connected to the GS-60 hand pump using 3 mm tube. The pressure is increased gradually by hand pumping of the device to the desired pressure and recording the corresponding output voltage. The offset of each of the pressure transducers are corrected for in the LABView program prior to start of the experimental testing. Figure 3-14 shows the plots of pressure against the output voltage for the pressure transducers during the calibration.

3.2.3 Data acquisition and processing

The flow rates for each condition are set up and started in the DeltaV program in the control room, while the test monitoring and recording is done at the workstation (Figure 3-15) in the test area. The LabView program is used for data acquisition in one computer. Additionally, another standalone computer equipped with WMS acquisition software (Cap200) is used for recording of WMS measurement data. The hardware of the CR sensor for data acquisition consists of the signal conditioning box for sending and receiving the electrical signals to and from the sensor; the sensor probe that is connected to the input channel in the signal conditioning box; the output cable for connecting the conditioning box to the data acquisition system (LabView). Similarly, data acquisition of pressure measurements is carried out with the help of pressure signal conditioning box that supplies 24 V power to the pressure transducers in

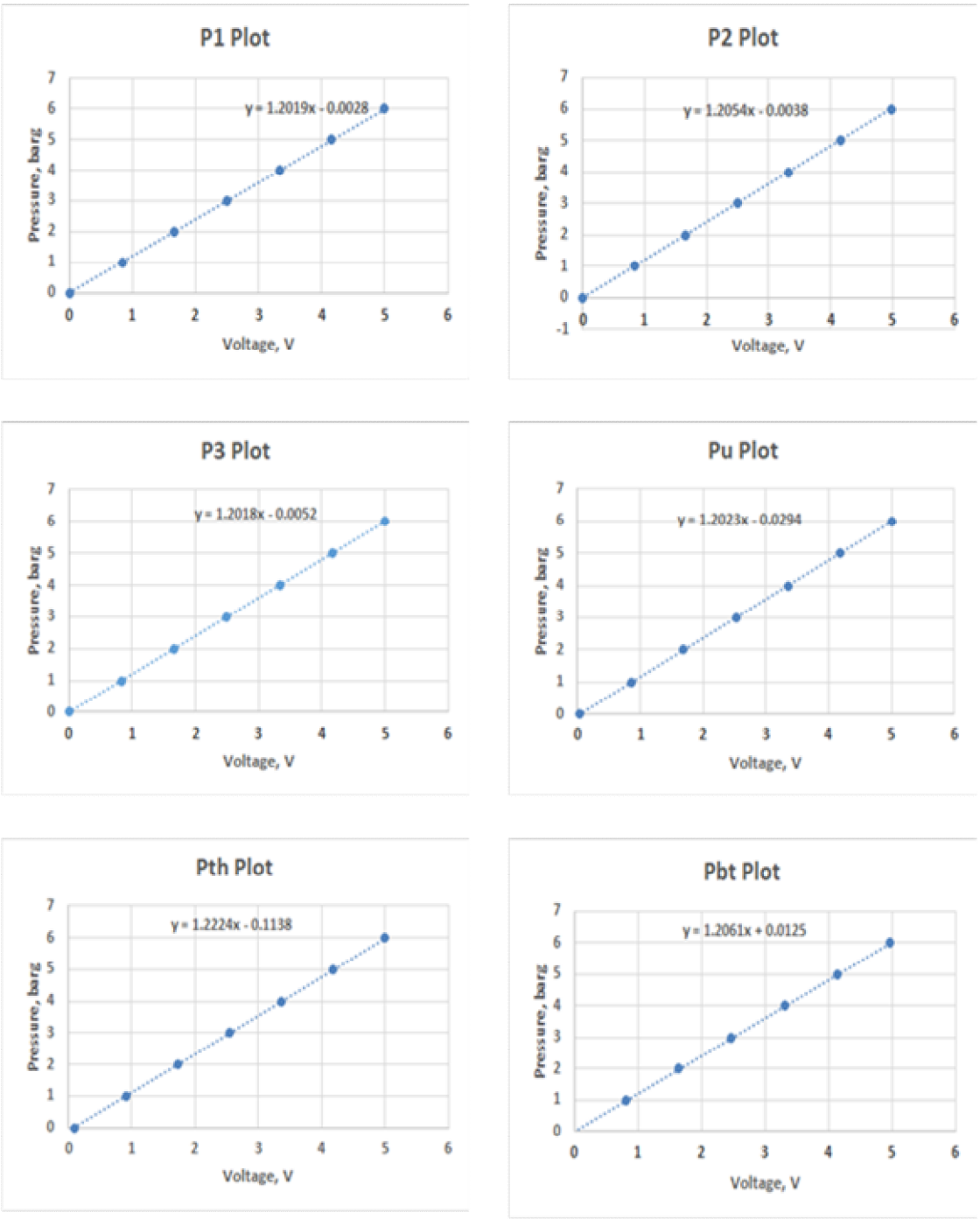

Figure 3-14 Plots of calibration of the pressure transducers.

the flow loop. The diaphragm in the pressure transducers is deflected due to the applied liquid/fluid pressure. The signals produced from the conversion of the deflection of the diaphragm in the pressure transducers due to applied fluid pressure are sent back to the DAQ system through ADC module.

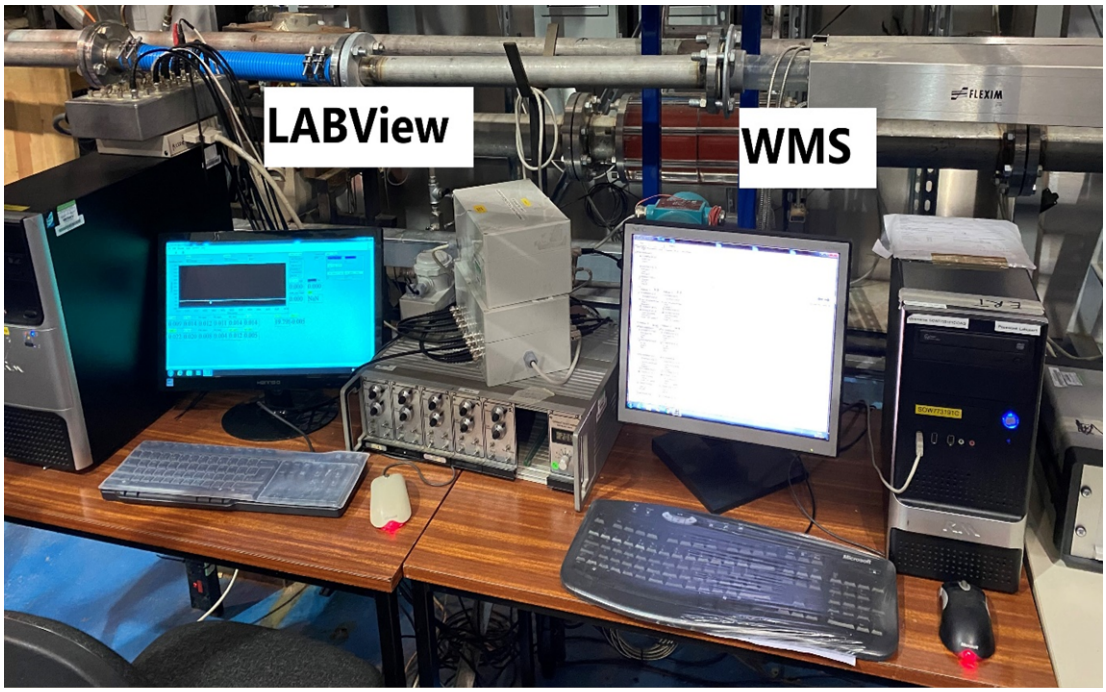

Figure 3-15 Workstation for data acquisition of LabView and WMS Cap200

The WMS acquisition system consists of the following hardware components: basic device for power supply, communication control and data storage; the transmitting modules as a source of transmitting voltage pulses for activation of the transmitter wires of the sensor; the receiving module which consists of the amplifier and control unit for receiving and measurement of the currents in the permittivity of the fluid in the pipe; and the USB for connecting the basic device to the computer. More details on the hardware components of the WMS can be found in the Cap200 manual by HZDR (2014).

Prior to the start of the data acquisition, 10 minutes stabilization period is allowed for the flow to stabilized before that is logged for 180 s, at a sampling frequency of 250 Hz for LabVIEW program, and 1000 HZ for WMS. Prior to the start of the testing, the sensors were calibrated for good data acquisition and data processing.

The LabVIEW program is used for the acquisition of pressure, temperature, superficial gas velocity (Usg), superficial liquid velocity (Usl) and conductivity ring data in the flow loop. The signals from the pressure and CR sensors are connected to the LABView PC through the adaptor module from the Pressure

excitation box and CR signal conditioning box respectively. The adaptor module links the signal from the sensors to the ADC, for digitization and processing of the signal in the computer.

The WMS Cap200 software is used to measure void fraction and phase distribution. The capacitance WMS utilizes sinusoidal alternating voltage for excitation of the transmitter and the receiver electrodes. The excitation voltage of the transmitter at selected frequency is produced by direct digital synthesizer circuit. The excitation voltage is multiplexed to each of the 24 wire electrodes, with the help of analogue switch. The current at any receiver electrode, due to the excitation of a given transmitter corresponds to the permittivity of the fluid at the crossing point of the wire grid. The AC current amplifier, connected to the receiver electrode, converts the current signal received from the crossing wire into voltage. The voltage signal is then processed and digitized in the computer with the aid of the USB cable.

The measured raw data from the WMS is processed using the wire mesh framework. The calibration files for air and water, together with the measured raw data are feed into the processing software to output the phase distribution and void fraction measurements. A statistical analysis using the probability density function (PDF) method together with visual observation of the flow and time trace of sensors are used for flow regime identification in this work. The PDF plot is obtained from the void fraction signal, which for WMS is stored in the output file of the WMS framework in ASCII format with. epst extension, while those of CR sensor from LABView are stored inform of .txt extension. For both WMS and CR data, the sensor measurements data are imported into Excel file for further processing (PDF and time series plots).

The PDF was determined by counting the number of data points in bins of width 0.02 based on void fraction range of 0.02 – 1.00. This was performed by using the Data analysis tool in Excel, where the void fraction measurements are fed into the “Input Range”, and the bins are selected in the “Bin Range” to create a new tab with table of the generated PDF.

Table 3-1 Sensors and meters specification and location on the rig

S/N	Sensors/meters	Specification (uncertainty)	Description	Location from blind tee (mm)
1	1 inch Rosemount Magnetic flow meter Foxboro CFT50 Coriolis meter	0 - 7.36 kg/s (±0.2%) 0 - 30 kg/s (±0.15)	Water flow rate	N/A (Metering section)
2	½ inch Rosemount mass flow meter 1 inch Rosemount mass flow meter	0 - 150 sm^3/hr (±1%) 100 - 4250 sm^3/hr (±1%)	Air flow rate	N/A (Metering section)
3	Pressure transducer (P1)	0 - 6 barg (±0.15%)	Pressure measurements in upstream of blind tee	2190
4	Pressure transducer (P2)	0 - 6 barg (±0.15%)	Pressure measurements in upstream of blind tee	6055
5	Pressure transducer (P3)	0 - 6 barg (±0.15%)	Pressure measurements in upstream of blind tee	9920
6	Pressure transducer (Pbt)	0 - 6 barg (±0.15%)	Pressure measurement in blind tee	-
7	Pressure transducer (P4)	0 - 6 barg (+0.15%)	Pressure measurement in downstream of blind tee	251
8	Pressure transducer (P5)	0 - 6 barg (+0.15%)	Pressure measurement in downstream of blind tee	1577
9	CR sensor	0 - 1 (±5%)	Liquid holdup	3190
10	WMS (Horizontal)	0 - 1 (2.5%)	Void fraction	1390
11	WMS (Vertical)	0 - 1 (2.5%)	Void fraction	1509

The PDF values are normalized by dividing each with the number of data points. The PDF plot is then generated by plotting the normalized PDF values against the bins.

4 CHARACTERIZATION OF FLOWS TRANSITIONING FROM THE HORIZONTAL TO THE VERTICAL SECTION

The characterization of multiphase flow in pipe networks is important for many industrial processes like petroleum, nuclear, and the aviation industry. Multiphase flows in some of these industries are usually in pipelines with different configurations. Most flow pipelines are usually a combination of pipes of different orientations (horizontal, vertical, or inclined) which form a zigzag or snake-like pipe network. Such pipe network is common in both upstream and downstream sections of the petroleum industry. For instance, some of deep offshore platforms have subsea tie-back pipes connecting the wellhead to surface production vessels via a series of pipes in different orientations. Furthermore, the manifolds of the oil well during the drilling and completion phase utilize sets of different pipe configurations for fluid supply and return from the oil well. Similarly, in the downstream sector, some of the processing and distribution lines consist of pipe network configurations with different orientations.

Although there have been many published works on multiphase flow dedicated to either horizontal flows (Barnea, 1987; Hubbard & Dukler, 1966; Kong & Kim, 2017; Taitel & Dukler, 1976; Thaker & Banerjee, 2017) or vertical flows (Barnea, 1987; Barnea et al., 1985; Griffith & Wallis, 1961; Hewitt & Roberts, 1969; Julia et al., 2011; Taitel et al., 1980; Wu et al., 2017), not much work has been done on two-phase flow in pipe configurations that include both horizontal and vertical flows. Since many of these industries have complex pipe networks that involve fluid transportation from horizontal pipe to vertical pipe and vice versa, it is therefore paramount to study the behaviour of the fluid as it transitions from one pipe configuration to a different pipe configuration. This work is devoted to study the characteristics of two-phase flow as it transitions from horizontal to vertical pipe to enable accurate flow characterisation and efficient pipeline design. Flow regime is considered as among the most important characteristic for multiphase flow (Jagan & Satheesh, 2016), and it is therefore important to identify and understand the response of flow pattern as it moves from a pipe of one orientation to another. The typical flow regimes found in horizontal and vertical pipes will be discussed briefly and then compared with resulting flow pattern witnessed in this work.

4.1 Flow regimes in horizontal and vertical sections

The flow regimes in the pipe were identified using the visualised flow structure images which were obtained by processing the raw measurement phase fraction data of the WMS using the FrameWork software by HZDR-Innovation GmbH, the device supplier. The FrameWork software allows a conversion of the cross-sectionally measured phase distributions into sideview of the phase fraction profiles along the pipe. The representative flow regimes observed in horizontal section are shown in Figure 4-1. Figure 4-1 represent the horizontal (side) views for the horizontal section of the two-phase flows in the flow loop. The pure liquid in the pipe is represented by blue colour while the pure gas is shown as white in the images.

In the horizontal section, the flow patterns are in agreement with most of the existing publication on air-water two-phase flow. However, it is noticed that the type of pipe configuration used in this work has reasonable effect on stratified flow regime due to backward flow and bottleneck effect from the tee joint that connects the horizontal to the vertical section. It is observed in this work that two-phase flows with low superficial velocities within the ranges of 0.14-1.36 m/s and 0.043-0.086 m/s for gas and liquid respectively are *unstable wavy-slug flow regime*, instead of the usual stratified flow regime associated with low superficial velocities in traditional horizontal pipes. The same unstable wavy slug (UWS) regime was observed for both cases of 100D and 200D injection points (see Chapter 5) for the same test conditions.

For such horizontal pipe with conjoined vertical pipe configuration, the bottleneck effect and backward flow lead to liquid accumulation in the pipe, which contributes to the occasional rise in liquid level that touches the top of the pipe. Furthermore, the liquid accumulation in the pipe also enhances the rise in the growing amplitude of the wave at the interphase of the gas and liquid in the pipe that forces the liquid to intermittently cover the pipe cross-section as can be seen in Figure 4-2.

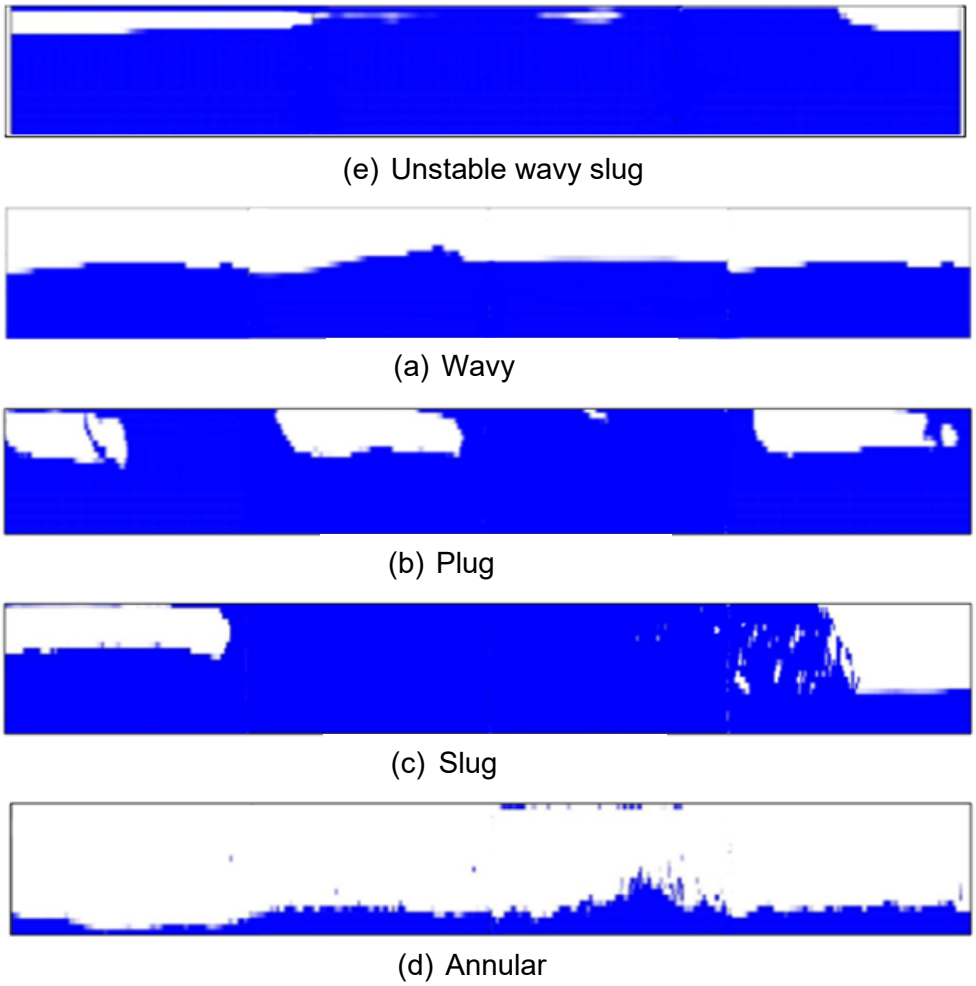

Figure 4-1 Axial slice images of the two-phase flow regimes in horizontal section at superficial gas and liquid velocities of (a) 0.14 m/s and 0.043 m/s (b) 2.73 m/s and 0.043 m/s (c) 0.14 m/s and 0.43 m/s (d) 2.73 m/s and 0.43 m/s and (e) 10.91 m/s and 0.043 m/s, respectively with 100D gas injection point.

Figure 4-2 Picture of unstable wavy-slug (UWS) flow regime for superficial velocities of 0.55 m/s and 0.043 m/s for gas and liquid respectively with 100D gas injection point.

The Probability density plot and time trace obtained under stratified flow condition supports this claim as the PDF signature and time series plot shown in Figure 4-3

indicate an unstable wavy-slug flow regime rather than the expected smooth stratified flow regime for flow with low superficial velocity.

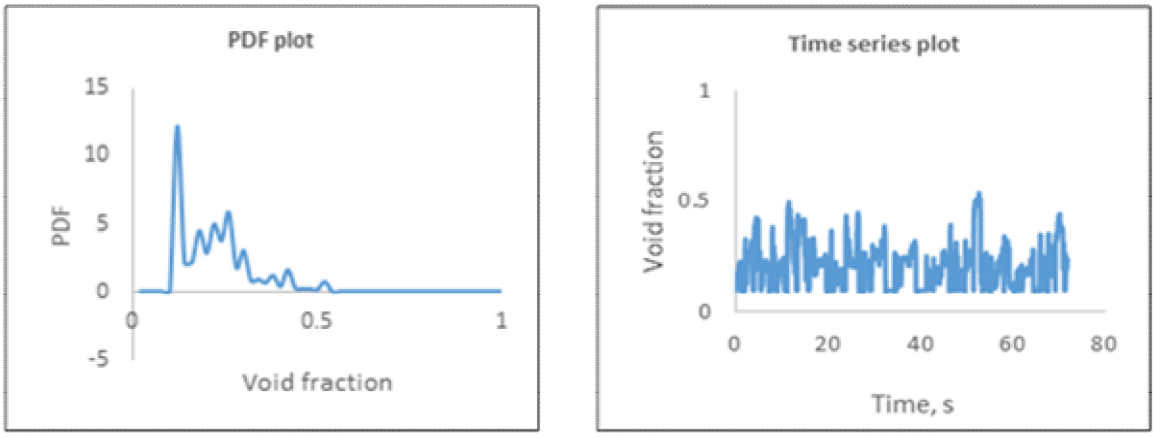

(a) (b)

(c)

Figure 4-3 plots of (a) PDF (b) time series and (c) axial slice images of the two-phase distribution profile for flow with low superficial velocities of 0.14 m/s and 0.043 m/s for gas and liquid respectively in the horizontal section with 100D injection point.

The unstable wavy-slug flow regime is usually associated with low superficial velocities and high liquid accumulation in the pipe. The flow is characterized by unstable intermittent flow with rippled surface. The PDF plot for such flow regime is represented by one or two peaks with at least one of the peaks having uneven surface due to the fluctuating liquid level in the pipe.

Increasing the gas superficial velocities to within the range of (2.73- 5.45 m/s) will lead to wavy flow regime. The increase in gas superficial velocity due to increased gas flow rate increases the hydraulic force in the pipe that pushes the liquid from the horizontal to the vertical section, thereby decreasing the liquid level in the pipe. This increase in gas superficial velocity sets in motion the Kelvin-Helmholtz instability as the suction due to local gas pressure drop, elevates the gas-liquid interface, while the force of gravity works in opposite direction to oppose the wave growth, leading to

the development of wavy flow regime (Kadri et al., 2009). When the liquid superficial velocity is increased in the range of 0.13 -1.2 m/s, the liquid layer also increases, enhancing the slug initiation by increasing the wave amplitude, which enables the liquid to bridge the pipe periodically. The increase in liquid layer in the pipe helps in rebuilding the liquid layer left behind by a newly formed slug and provides adequate liquid film to sustain the slug flow regime (Ujang et al., 2006).

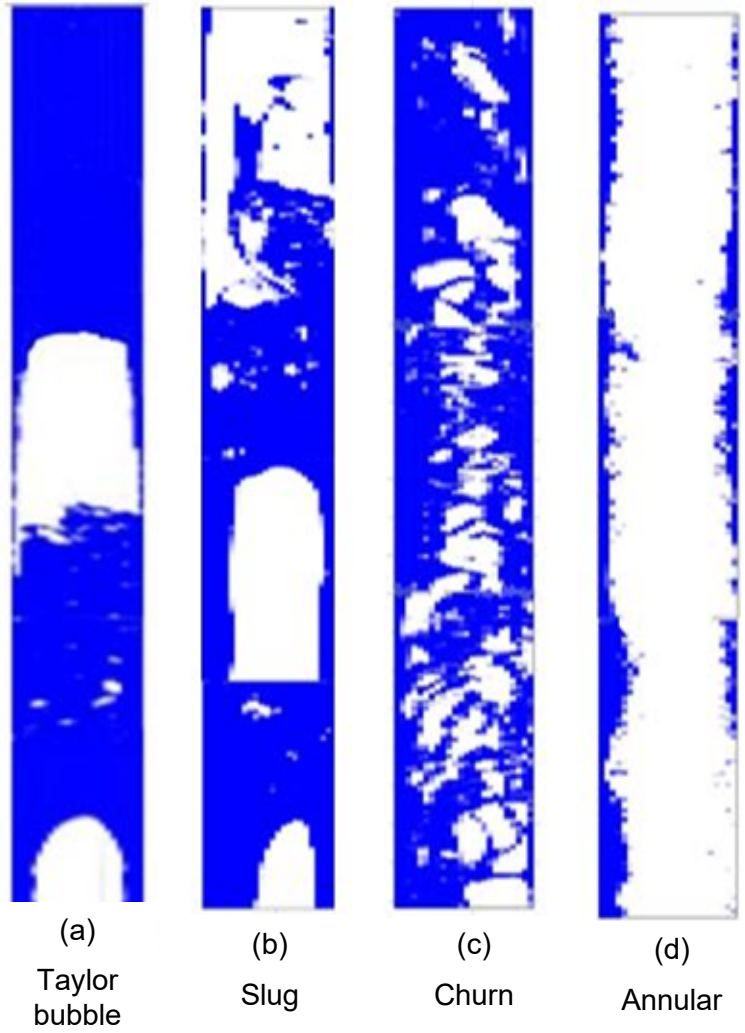

Figure 4-4 Axial slice images of the two-phase flow regimes in vertical section at superficial gas and liquid velocities of (a) 0.14 m/s and 0.043 m/s (b) 1.36 m/s and 0.043 m/s (c) 2.73 m/s and 0.43 m/s and (d) 10.91 m/s and 0.043 m/s.

If the superficial liquid velocity is further increased to the range of 0.4 – 2.0 m/s and the superficial gas velocity reduced slightly to 0.14 – 0.95 m/s, plug flow regime will develop. The velocity and size of the gas bubbles in the plug flow regime are observed to be smaller than those of slug flow regime.

At very high superficial gas velocity (10.91 – 27.26 m/s), and low liquid superficial velocity (0.043 - 0.22 m/s) annular flow regime was observed, with the gas phase occupying the core of the pipe while liquid film is forced to the top and the bottom of the pipe. The liquid film is observed to be thicker at the bottom of the pipe as results of gravity and slight liquid accumulation.

Almost all the flow regimes observed in horizontal section were also witnessed in the vertical section. The dominant flow regimes observed in the vertical section are shown in Figure 4-4. The flow regimes presented in Figure 4-4 are a selection of representative of the major flow regimes witnessed in the vertical section. Some of the images of corresponding flow regime transition from horizontal to vertical for the same flow conditions are presented in section 4.3. The images are obtained for the vertical flows in similarly manner as those of Figure 4-1. The unstable intermittent flows observed in the horizontal section transitioned to Taylor bubble flow regimes in the vertical section. The plug flow regime is grouped as slug flow regime in the vertical as the bubbles do not float at the upper part of the pipe as with the horizontal flow, but rather positioned slightly deeper in the pipe close to the centre of the pipe in the vertical section. The gas bubbles observed in the slug flow regime in vertical section were observed to move closer to the inward (right) part of the pipe. Slugs with relatively higher superficial gas velocities (2.2 m/s to 5.45 m/s) and superficial liquid velocities in the range of 0.043 - 1.2 m/s were observed to transition into churn flow in the vertical section.

For slug and annular flow regimes, biased axisymmetric flow was observed in the vertical section as the heavier fluid tends to settle at the outward part of the pipe, while the lighter fluid is pushed to inward part of the pipe (Figure 4-5). This phenomenon could be attributed to the net effect of the centrifugal force and force of gravity, that drives the liquid outward and the lighter fluid (air) inward in the pipe (Ma et al., 2021).

Breakage of some of the large bubbles was also observed due to the turbulence from mixing effect of the blind tee pipe. For annular flow, a thicker liquid film is observed in the outward part of the vertical pipe. The image obtained from the WMS for annular from regime in vertical section differs slightly with some of those shown in other works that was performed in traditional vertical pipes. For such vertical pipe that is conjoined with horizontal pipe, the thicker liquid layer observed in the bottom of the horizontal section tends to continue in the same direction of motion when

transitioning to the vertical section as the heavier fluid settles in the outward part of the part. With this observation, optimal sensor placement and orientation could be achieved in such pipe configuration, based on the metrological requirements. It is noted from the results that most of the flow regimes observed this work, comply with those found in the literature, except for the changes witnessed in flow structures for vertical flows due to the transition process.

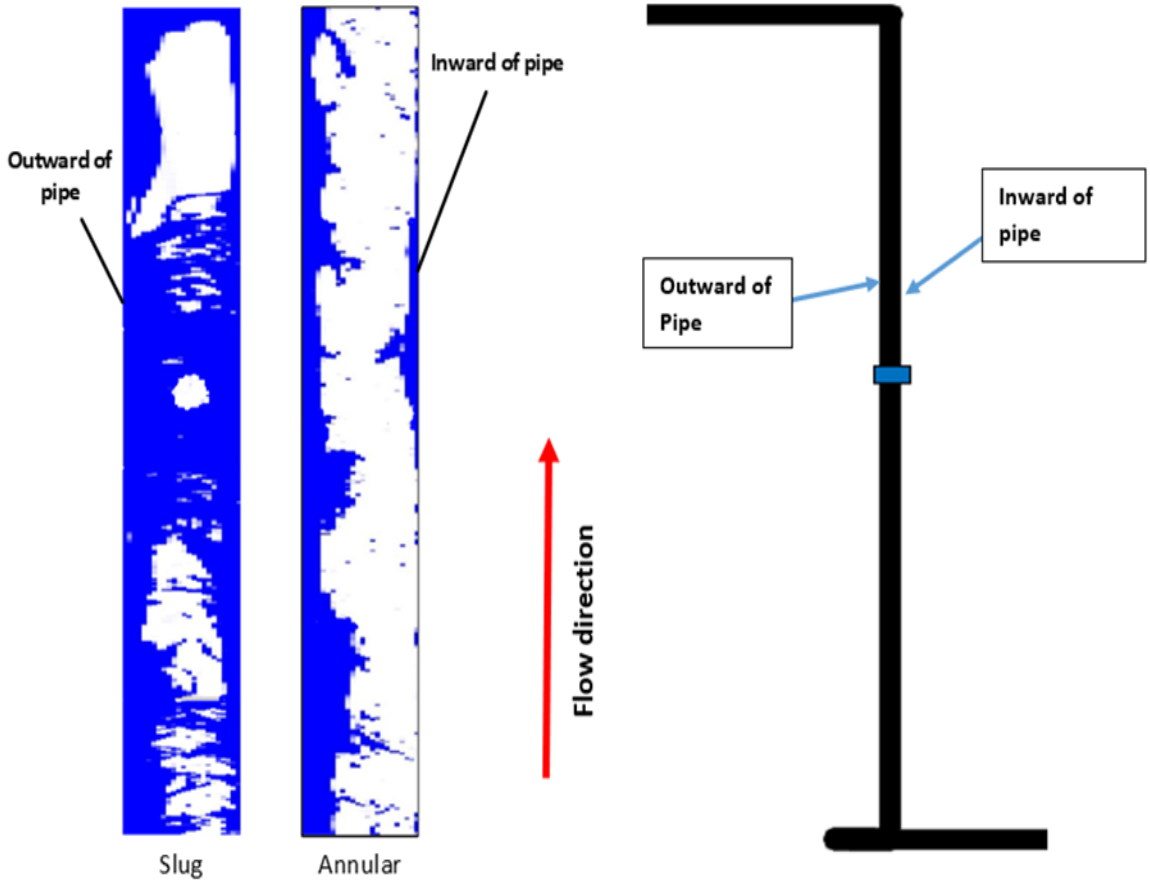

Figure 4-5 Slug and annular flow regimes in vertical section, the inward and outward sides of the pipe are regarding to the riser base elbow.

4.2 Flow regime map

The flow regimes identified in this experimental two-phase flow investigation are plotted in the existing and widely used flow regime maps to verify the transition boundaries. In the horizontal section, the combined flow regime maps of Mandhane et al. (1974) and Taitel & Dukler (1976), modified by Kong & Kim (2017) is used for the analyses of the two-phase flow (Figure 4-6). It can be seen from Figure 4-6 that none of the transition boundaries suggested by the authors in the maps correctly

predicted the unstable wavy-slug (UWS) flow regime. The transition boundaries suggested by the authors in Figure 4-6 were developed for two-phase flow in conventional straight horizontal pipe, while the present work is carried out in horizontal pipe with conjoined vertical pipe configuration.

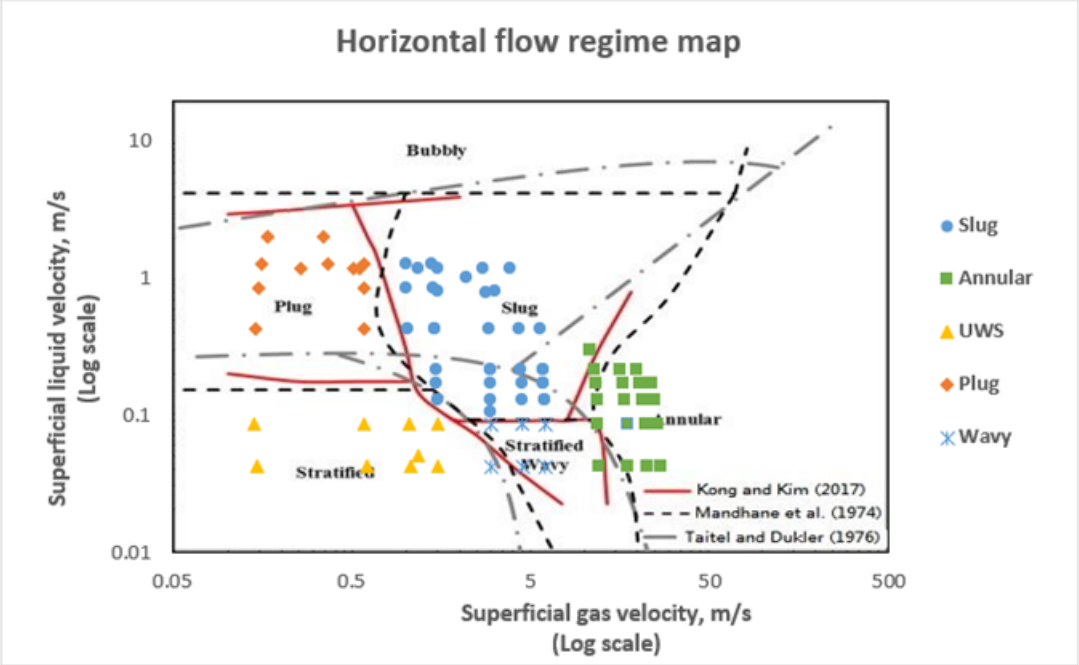

Figure 4-6 Combined flow regime maps of Mandhane et al. (1974) and Taitel & Dukler (1976) for horizontal flows (Kong & Kim, 2017).

As Figure 4-6 shows, the Kong & Kim (2017) flow regime map better described the flow regimes observed in this work. The improvement in Kong & Kim (2017) map is noticeable in the slug transition boundaries, which were overestimated by Mandhane et al. (1974), and slightly underestimated by Taitel & Dukler (1976). The better performance of Kong & Kim (2017) map could be attributed to having similar long development length with L/D ≥ 100D. The longer L/D allows for wave growth at the gas and liquid interface, which enhances slug flow regime development in the horizontal section. The flow regime map from The mandhane et al. (1974) was developed from the average compromise over a wide varying combination of physical properties of flows and pipe diameters, whose fit was observed to change with pipe size and fluid properties (Taitel & Dukler, 1976). This suggests that the transition boundaries should be viewed instead as transition regions, hence the possible reason for the overestimation of the transition boundaries. In constrast, The Taitel & Dukler (1976) flow regime map was formulated from a theoretical model for

the prediction of flow regime transition based on physical concepts. Their theoretical model, which strongly depends on the data being used to create the map is subject to uncertainty liability when extended to other flow conditions. The underestimation of the transition boundaries in Figure 4-6 could be as a result of the difference in flow conditions (especially the pipe size) in the present work, as the Taitel and Dukler map was developed for smaller pipe diameter flows.

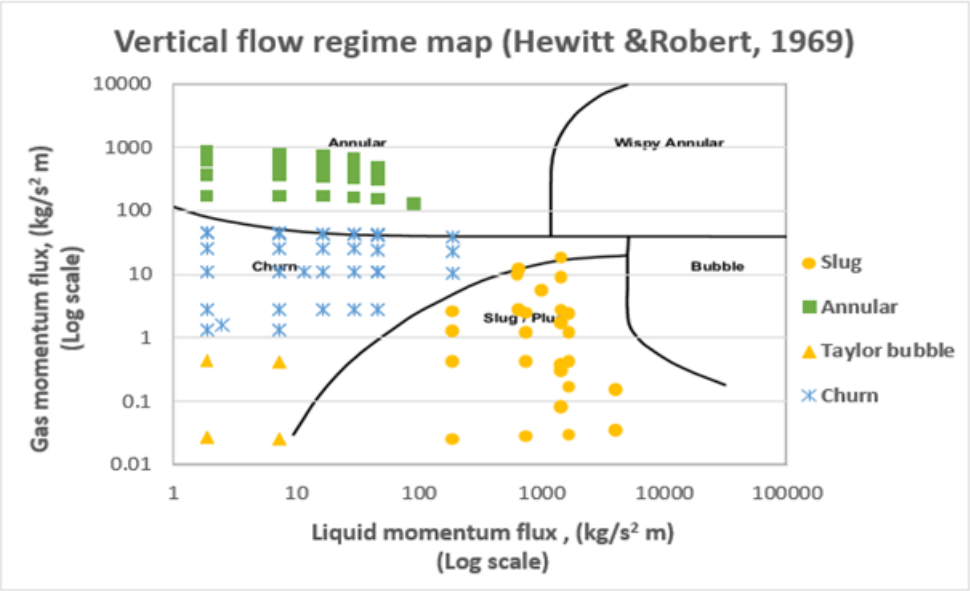

(a)

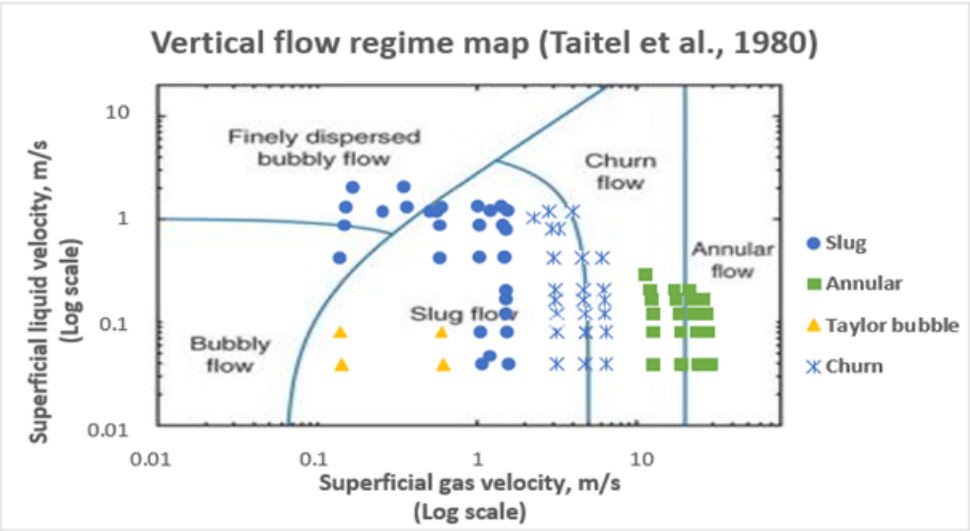

(b)

Figure 4-7 Vertical flow regime maps: (a) Hewitt & Roberts (1969) and (b) Taitel et al. (1980).

For vertical flows, the experimental data were plotted on both Hewitt & Roberts (1969) and Taitel et al. (1980) flow regime maps in Figures 4-7(a) and (b)

respectively. It was observed that the Hewitt & Roberts (1969) flow regime map gave a good estimate of the flow regime transition boundaries when compared with Taitel et al. (1980) flow regime map. This could be attributed to the relatively short development length in the vertical section for which the flow regime map was developed, as with the present work. Since the development length for both the present work and that of Hewitt & Roberts (1969) are brief (L/D ≤ 25D), most of the flow regimes observed in the vertical section may appear to be similar as they are still in the development stage, unlike the Taitel et al. (1980) flow regime map produced with longer flow regime development length (L/D≥ 100D). The Taitel et al. (1980) flow regime map underestimated the churn and annular flow regimes, with some of the intermittent flows with high superficial velocities being classified as dispersed bubble flow regime.

Churn flow regime was observed to be the dominant flow pattern in this section as result of the effect of gravity and the mixing effect of the blind tee on the flows. The unstable intermittent flow regime with low superficial velocities (0.14 – 1.36 m/s and 0.043 – 0.086 for gas and liquid respectively) observed in the horizontal section was witnessed to transition into Taylor bubble flow regime in vertical section. It was observed however that Hewitt & Roberts (1969) flow regime map did not correctly predict the Taylor bubble flow regime, while in Taitel et al. (1980) map, the Taylor bubble was observed to fall within the slug flow regime region. The Taylor bubble was distinguished from the typical slug flow regime due to the low superficial velocities (0.14 – 1.36 m/s and 0.043 – 0.086 m/s for gas and liquid) associated with such flow regime and the smooth curved shape of the leading large gas bubble.

New proposed flow regime map

As the previous section highlights, none of the typical flow regime maps used for characterisation of horizontal or vertical flows were able to accurately predict all the flow regimes observed in the present work. Pipe geometry, as discussed in the literature survey, is one of the factors influencing the flow morphology in pipelines. It is therefore most likely that the inability of the some of the existing flow regime maps to accurately predict some of the flow regimes observed in this work is mainly a result of the pipe configuration used in the present work. None of the transition boundaries proposed by Kong & Kim (2017), Mandhane et al. (1974), and Taitel &

Dukler (1976) were able to predict the UWS flow regime observed in the horizontal section. For slug and annular flows, the transition boundaries proposed by these authors either underestimated or overestimated the slug and annular flow regime transition boundaries for the present work.

New flow regime maps are proposed for air-water two-phase flow in a horizontal pipe with conjoined vertical pipe configuration using the liquid and gas superficial velocities as the axis coordinates (Figures 4-8 and 4-9). The liquid superficial velocity is used as the ordinate, and the gas superficial velocity as the abscissa. The transition boundary lines are drawn arbitrary based on the combination of visual observation of the flow patterns and the PDF plot of the void fraction measurements. One of the major distinctions between the new proposed horizontal flow regime map (Figure 4-8) and the majority of the typical horizontal flow regime maps found in literature is the replacement of smooth stratified flows with UWS for flows with low superficial velocities as result of the pipe configuration. The new proposed vertical flow regime map shown in Figure 4-9 shows a clear distinction between the Taylor bubble flow and slug flow regime, which was not indicated in any of the typical vertical flow regime maps compared in this work.

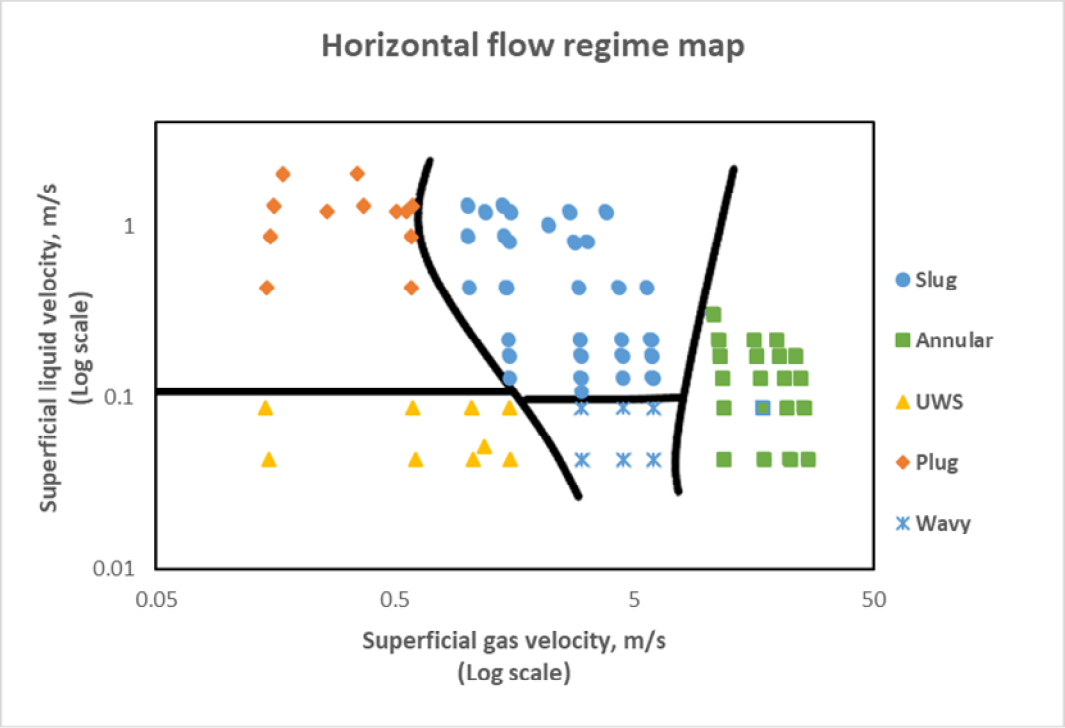

Figure 4-8 New proposed horizontal flow regime map.

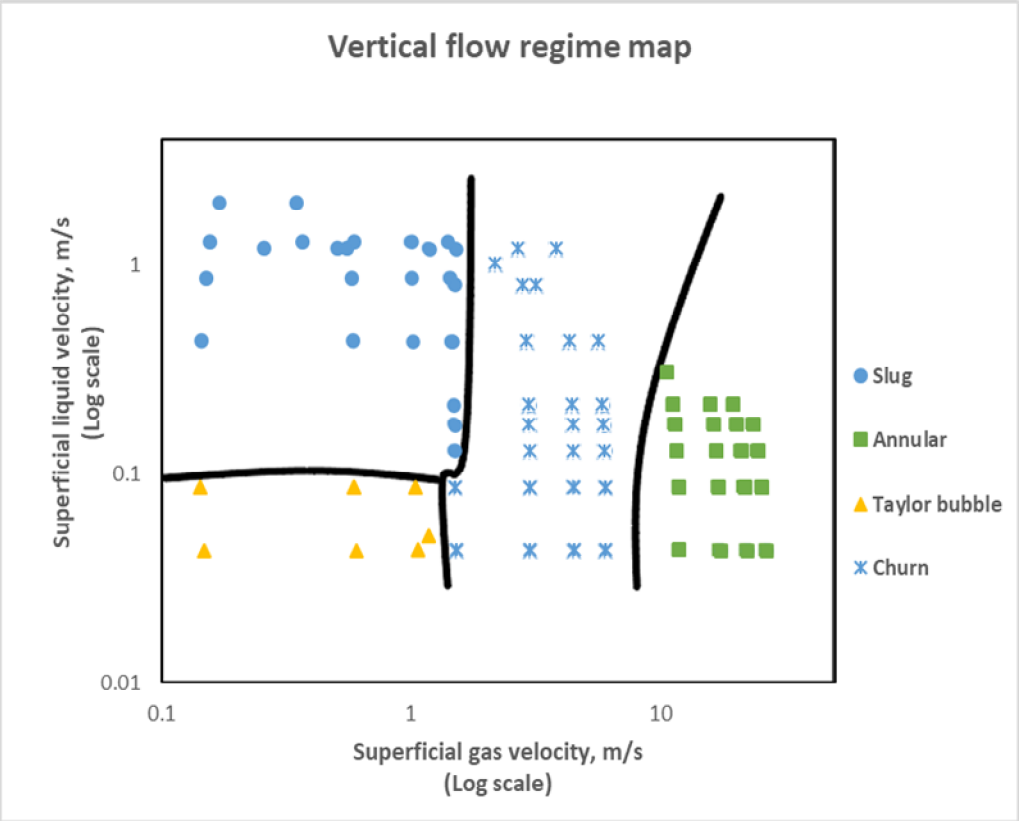

Figure 4-9 New proposed vertical flow regime map.

The gas bubbles in Taylor bubble flow regime are observed to move relatively slower than the gas bubble of slug flow regime. For such pipe configuration, the Taylor bubble flow regime is associated with low superficial velocities. In general, the flow regime transition boundaries in the new proposed maps fitted for all the flow regimes observed in present work unlike those compared in this work. The photos of the typical horizontal and vertical flow regimes indicated in the flow regime maps are illustrated in Figures 4-10 and 4-11, respectively.

4.3 Characterization of flow transition from horizontal to vertical section using local liquid hold up measurement.

Two WMS placed in the horizontal and vertical section of the flow loop are used to investigate the two-phase flow transition from the horizontal to the vertical section. A statistical analysis of the probability density function is applied to the void fraction measurements, and together with the time series plots, are used to describe the flow regimes and their transition in the loop.

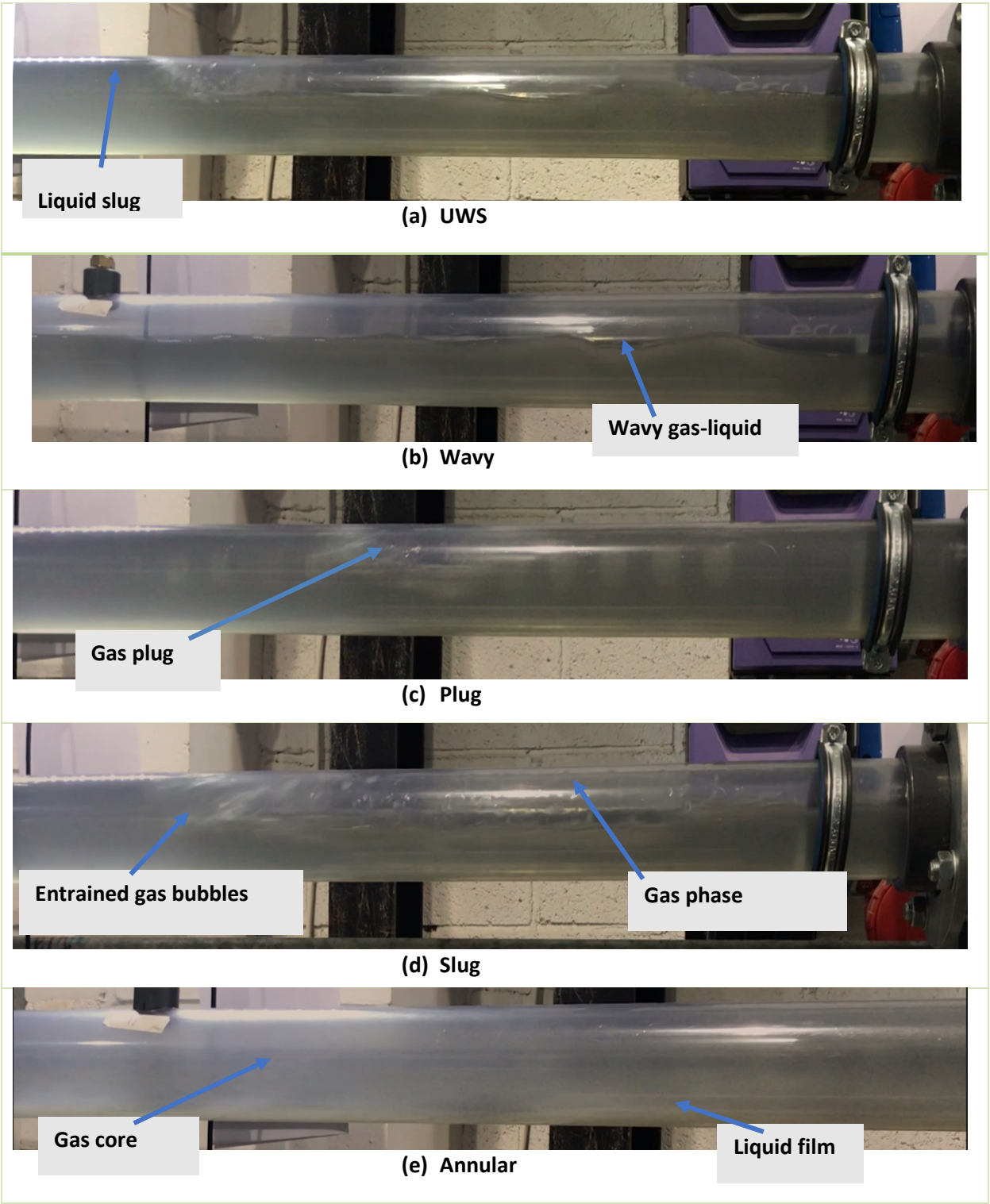

Figure 4-10 Experimental photos of typical flow regimes in horizontal section for superficial gas and liquid velocities of (a) 0.55 m/s and 0.043 m/s (b) 2.73 m/s and 0.043 m/s (c) 0.14 m/s and 0.43 m/s (d) 2.73 m/s and 0.43 and (e) 27.27 m/s and 0.043 m/s, respectively with 100D gas injection point.

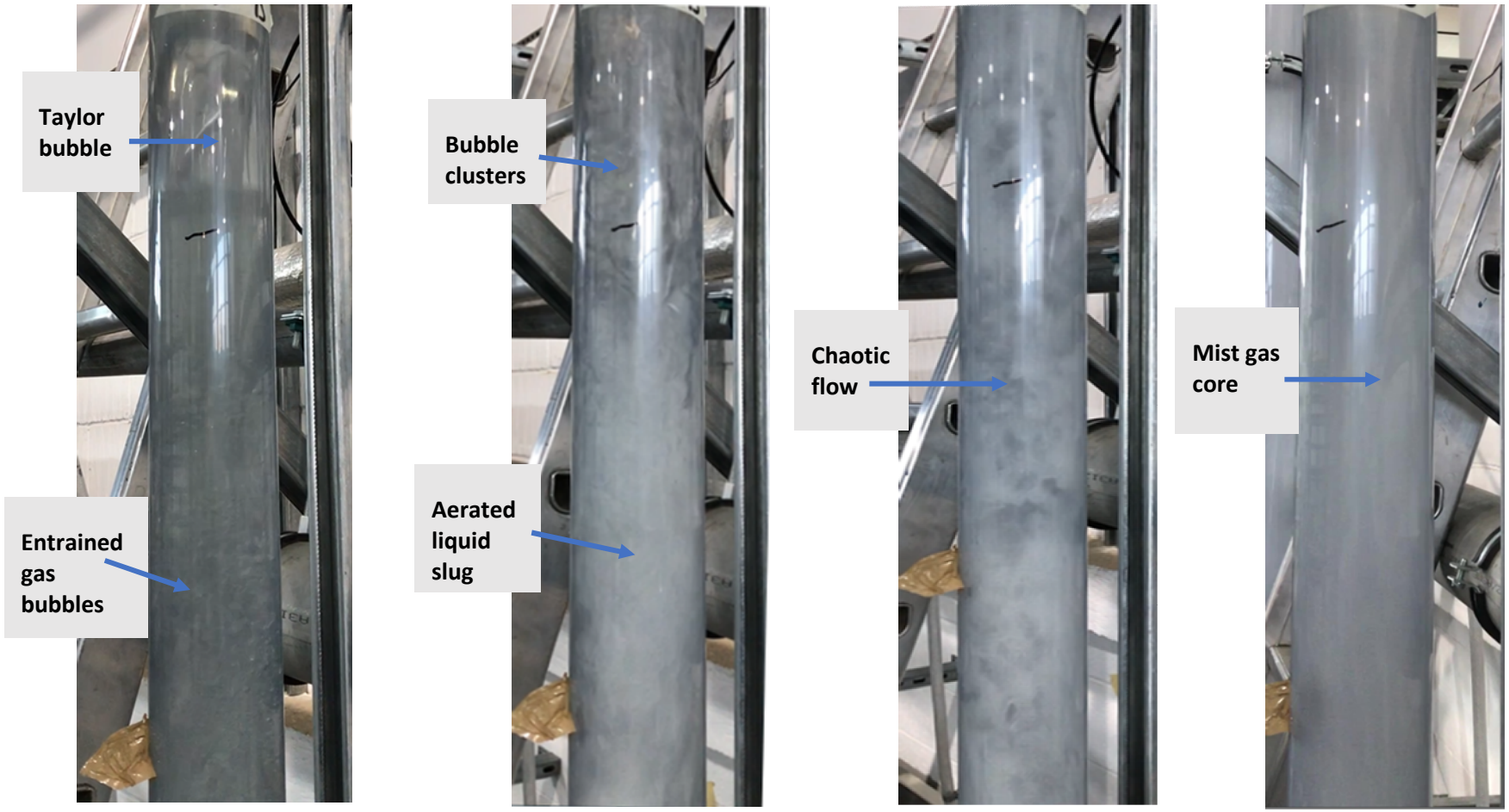

Figure 4-11 Experimental photos of flow regimes in the vertical section at superficial gas and liquid velocities of (a) 0.55 m/s and 0.043 m/s (b) 1.36 m/s and 0.43 m/s (c) 2.73 m/s 0.043 m/s and (d) 27.26 m/s and 0.043 m/s respectively at 100D.

For adequate characterization of the flow regime transitions, two sets of flow conditions are analysed: separated flows and intermittent flows. In this work, separated flow refers to wavy and annular flow regimes, while UWS, plug and slug flows are grouped as intermittent flows. The separated flows are tested with superficial liquid velocities of 0.043 and 0.086 m/s, and superficial gas velocities in range of 5.45 – 27.26 m/s. The intermittent flows are conducted with liquid superficial velocities of 0.086 and 1.3 m/s, and gas superficial velocities varied in the range of 0.14 – 1.36 m/s. The results, recorded at both the horizontal and vertical sections for the same flow conditions are compared in Figures 4-12 – 4-13 and Figures 4-14 – 4-15 for separated flows and intermittent flows respectively.

As expected for separated flows, a single peak is seen in all the PDF plot in Figures 4-12 – 4-13. It was observed that for the same test condition, the peak of the PDF plots is positioned at higher void fraction region for the horizontal section than those of the PDF plots for the vertical section, indicating increase of void fraction in the horizontal section.

Figure 4-12 shows gradual transition from stratified-annular to annular flow regime in the horizontal section, while transition of churn-annular to annular flow regime was observed in the vertical section. The PDF plots and time series plots in Figure 4-12(a) depict transition from stratified-annular flow in the horizontal section to churn-annular flow regime in the vertical section. Further increase in gas superficial velocity to 10.91 m/s leads to the liquid being pushed to the walls of the pipe, while the gas occupies the core of the pipe in the horizontal section. As the superficial gas velocity is steadily increased from 10.91 m/s to 27.26 m/s, more liquids are gradually displaced from the flow loop, leading to transition to annular flow regime in both horizontal and vertical section as can be seen in Figure 4-12(a) - (e).

When the superficial liquid velocity was increased to 0.086 m/s (Figure 4-13), similar trend of flow regime transition was observed in the horizontal section as in Figure 4-12. However, in the vertical section, churn flow regime was noticed to transition to annular flow regime. In Figure 4-13(a) the stratified annular flow regime in horizontal section was observed to develop into churn flow regime in the vertical section. With gradually increase in superficial gas velocity, annular flow regime was observed to develop in both horizontal and vertical section.

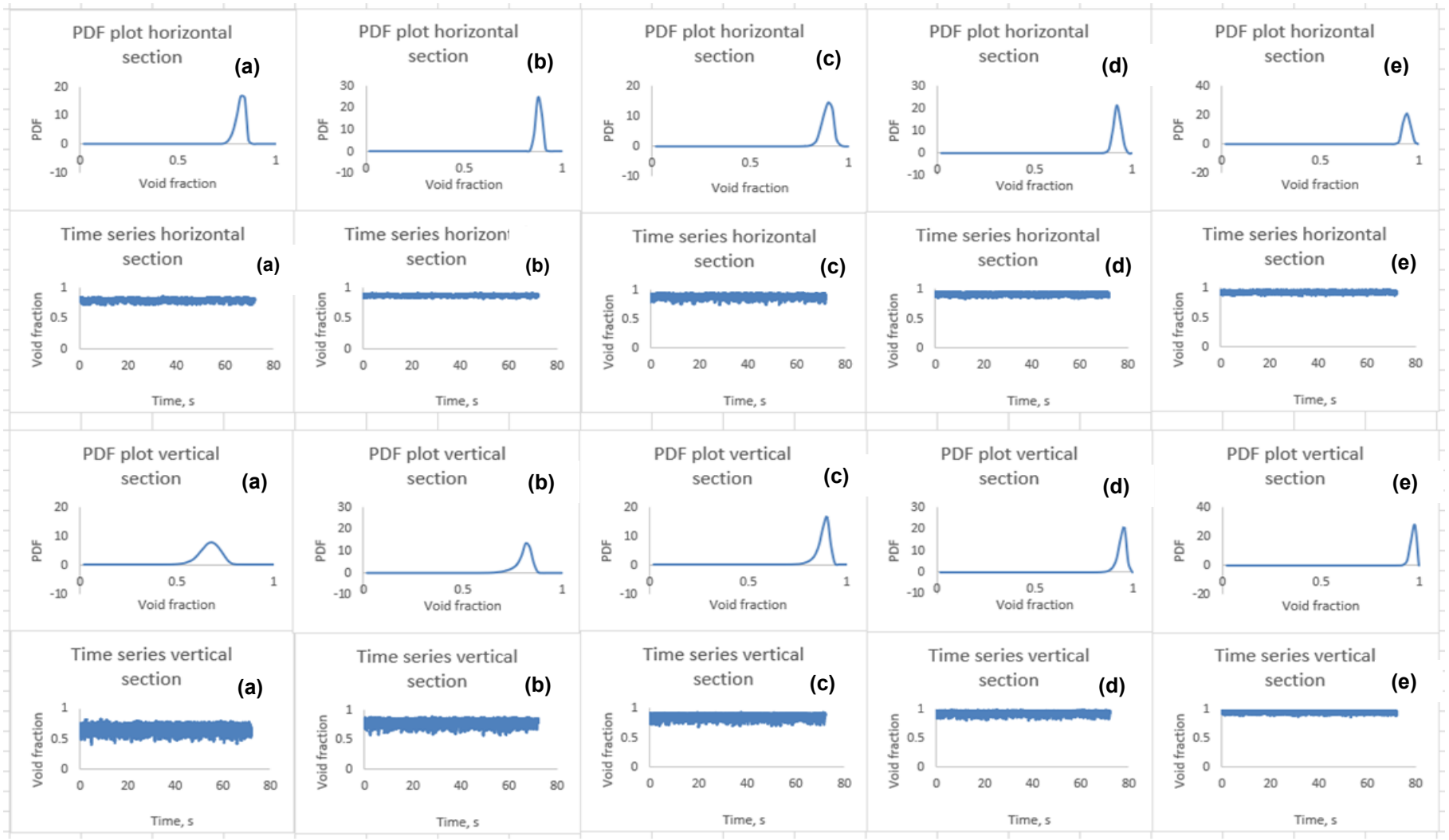

Figure 4-12 PDF and time series plots of horizontal and vertical flows for 100D with superficial liquid velocity of 0.043 m/s and superficial gas velocities of (a) 5.45 m/s (b) 10.91 m/s (c) 16.36 m/s (d) 21.81 m/s and (e) 27.26 m/s.

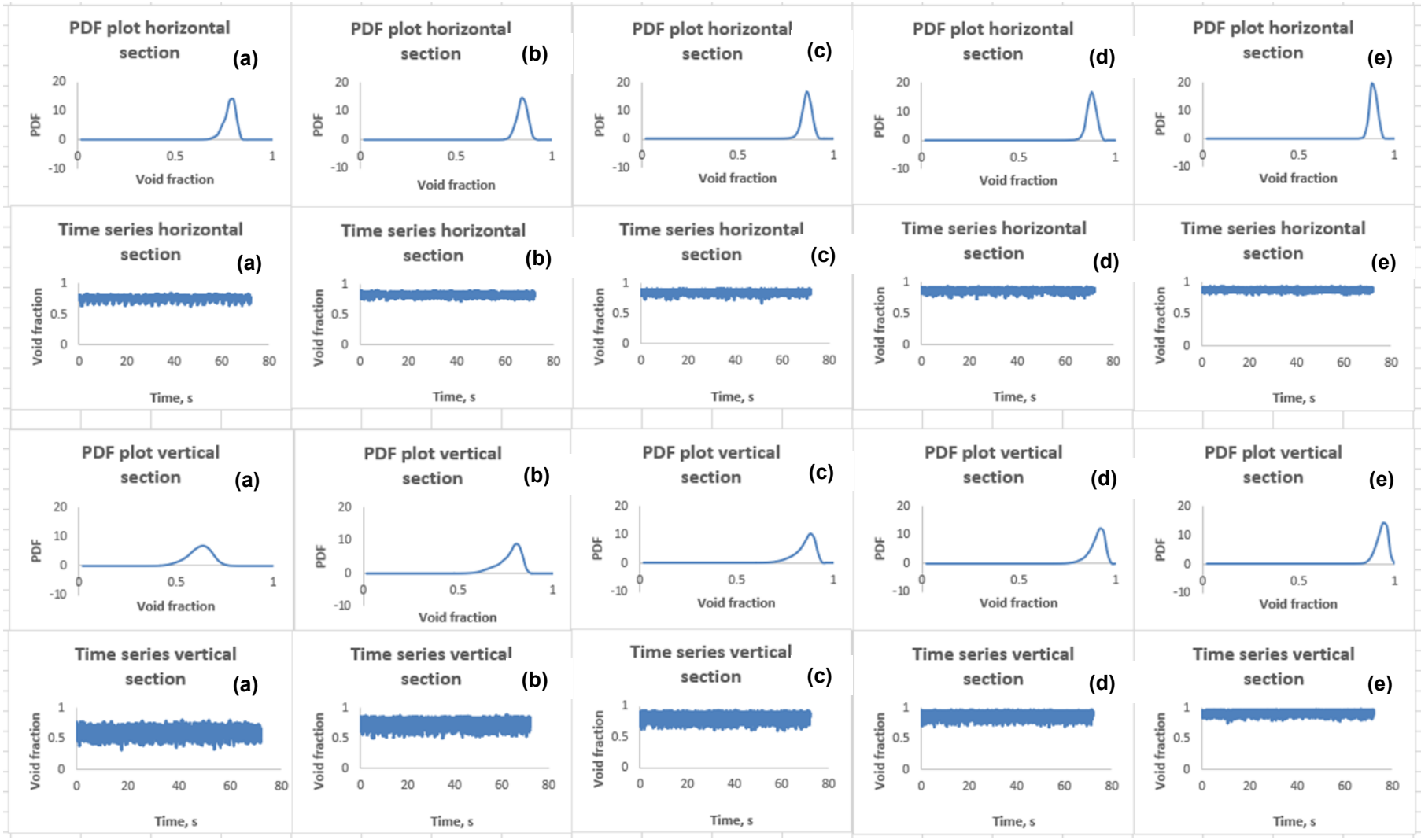

Figure 4-13 PDF and time series plots of horizontal and vertical flows for 100D with superficial liquid velocity of 0.086 m/s and superficial gas velocities of (a) 5.45 m/s (b) 10.91 m/s (c) 16.36 m/s (d) 21.81 m/s and (e) 27.26 m/s.

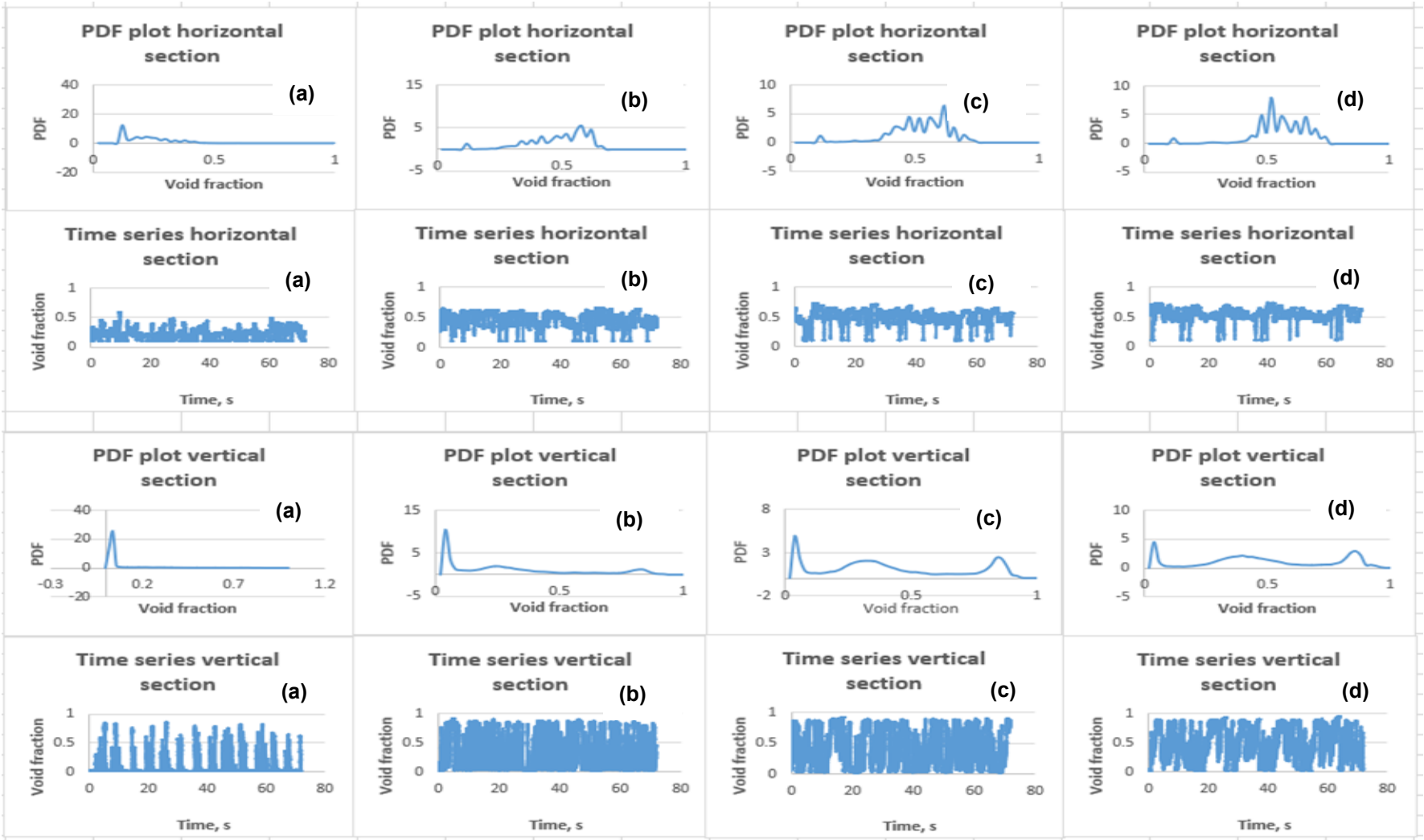

Figure 4-14 PDF and time series plots of horizontal and vertical flows for 100D with superficial liquid velocity of 0.086 m/s and superficial gas velocities of (a) 0.14 m/s (b) 0.55 m/s (c) 0.95 m/s and (d) 1.36 m/s.

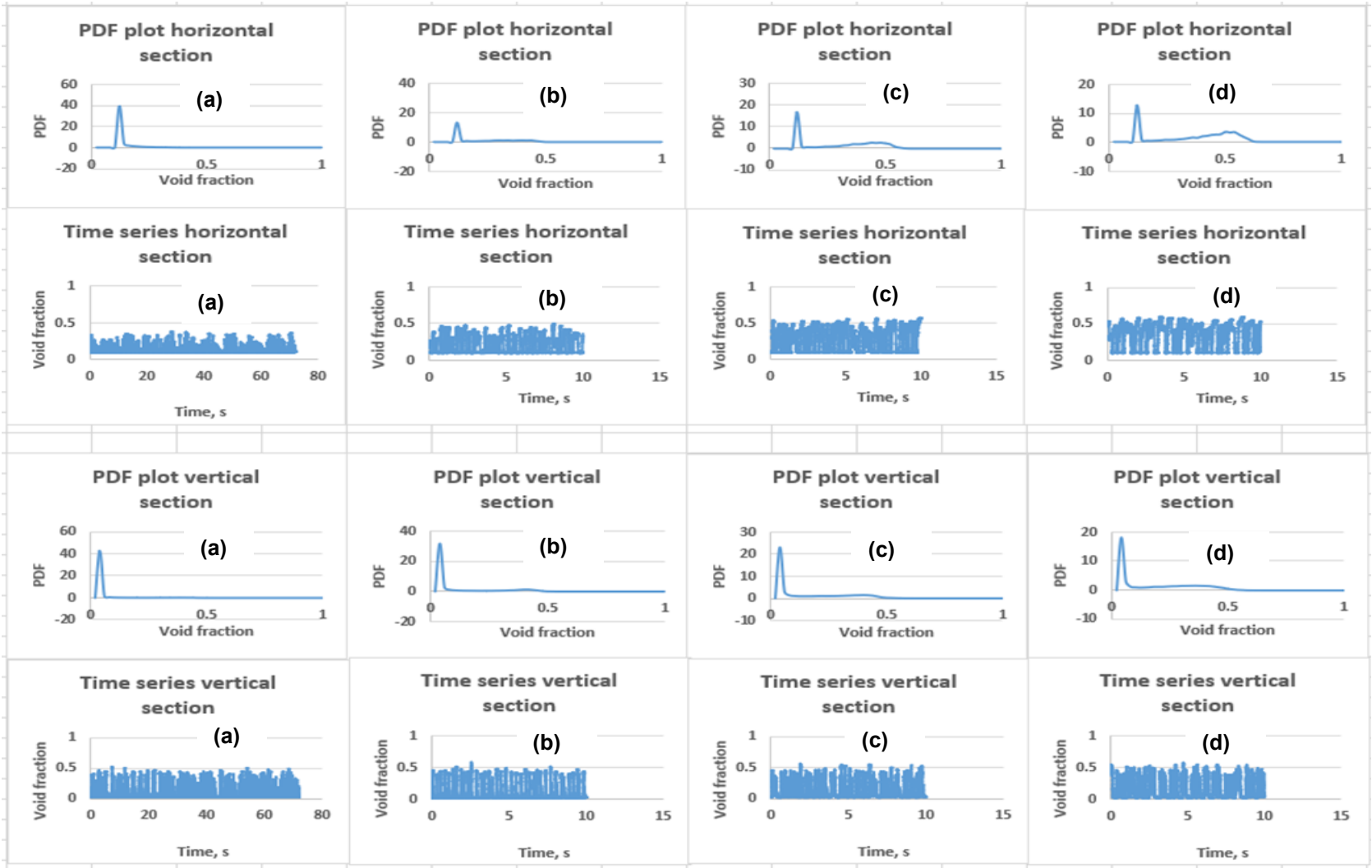

Figure 4-15 PDF and time series plots of horizontal and vertical flows for 100D with superficial liquid velocity of 1.3 m/s and superficial gas velocities of (a) 0.14 m/s (b) 0.55 m/s (c) 0.95 m/s and (d) 1.36 m/s.

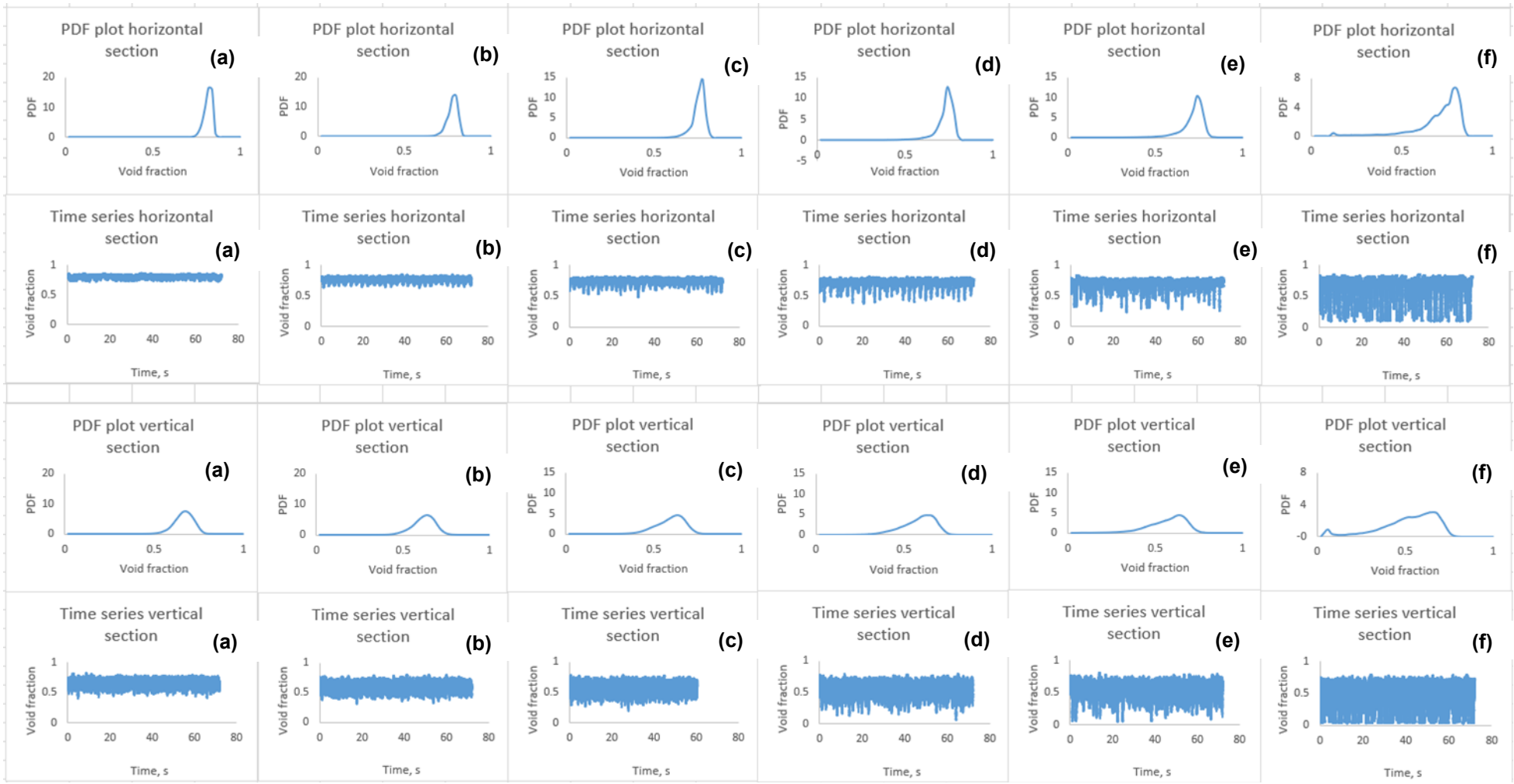

Figure 4-16 PDF and time series plots of horizontal and vertical flows for 100D with superficial gas velocity of 5.45 m/s and superficial liquid velocities of (a) 0.043 m/s (b) 0.086 m/s (c) 0.13 m/s (d) 0.17 m/s (e) 0.22 m/s and (f) 0.43 m/s.

In general, Figures 4-12 – 4-13 indicate that increase in gas superficial velocity (from 5.45 - 27.0 m/s) leads to increase in gas void fraction as can be seen in the gradual shift of the peak in the PDF plot to higher void fraction region in both horizontal and vertical section.

Figure 4-14 shows PDF and time series plots for unstable wavy slug (UWS) flow regimes. In the horizontal section, unstable elongated bubble was observed to gradually transition to unstable wavy-slug regime. While in the vertical section, the unstable Taylor bubble flow was witnessed to develop into underdeveloped slug flow regime. For such flow with low superficial fluid velocities, reverse liquid flow is witnessed in the vertical section. Due to the low hydraulic force associated with such flow with low superficial velocities, brief loss of momentum is usually expected in the vertical section. This loss of momentum will lead to momentary pauses in the flow (brief liquid loading) in the vertical section as the momentum is not enough to drive the liquid from the horizontal section through to the vertical section. This brief pauses in the flow of the liquid through the vertical section is recorded in the sensor and shows in the PDF plot as the additional peak in the high void fraction (Figure 4-14 (b) – (d)). Figure 4-15 reveals transition from plug flow to slug flow regime on increasing the gas superficial velocity in horizontal section. In the vertical section, increase in the gas superficial velocity causes breakages of large gas bubbles, leading to unstable slug flow regime in the vertical section. The PDF plot signature for intermittent flow is associated with two peaks or plateau. In Figure 4-15, the first peak, with the high PDF value at very low void fraction region represent the liquid body of the intermittent flow, while the second peak that appears as non-steep descending low plateau represent the gas phase of the flow. For the same flow condition, the PDF value of the 2nd peak or plateau for the horizontal section are slightly higher than the corresponding plateau for the vertical section, indicating higher relative length of the gas bubble in horizontal section as compared with the vertical section in Figure 4-15. The reverse is the case for the first peak representing the liquid slug, as the PDF value of the peak is observed to decrease in the vertical section. In general, on increasing the gas superficial velocity, the relative length of the gas bubble is observed to increase with in both the horizontal and vertical section as can be seen from the PDF plots in Figure 4-15.

The slices in Figures 4-12 – 4-15 show mainly the results from increase in superficial gas velocity. To observe the effect of liquid superficial velocity on two-phase flow as it transitions from the horizontal to vertical section, the liquid superficial velocity was steadily increased, and the data recorded. Figure 4-16 shows the effect of increase in superficial liquid velocity on flow transitioning from the horizontal to the vertical section when the superficial gas velocity was kept constant at 5.45 m/s and the superficial liquid velocity increased from 0.043 to 1.3 m/s. The result in Figure 4-16 shows flow regime transition from stratified-annular flow to slug flow regime in the horizontal section, while churn-annular flow was observed to transition to slug flow regime in the vertical section. Comparison of the PDF plot for each slide in Figure 4-16 for horizontal and vertical section shows that the peaks of the PDF plots in the high void fraction region appear to be steeper and higher in the horizontal section than in the vertical section. This is due to the change in the flow structure as it transitions to the vertical section where both the mixing effect of the blind tee and the gravitational force act on the flow in the vertical section. These effects lead to higher fluctuation of the void fraction reading in the vertical section as the peak of the PDF plots cover wider range (width) of void fraction as compared with the horizontal section. This claim is also supported by the time series plots where signals for vertical flow show higher fluctuation of void fraction measurements than that of the horizontal section.

Some of the results of the WMS images showing flow transition from horizontal to vertical section are shown in Figures 4-17 – 4-20, as the PDF plot alone may not show some flow phenomena such as air entrainment, droplet impact and break up. It is worthy to note that some flow features such as liquid film, bubble and droplet particles which do not make full contact with the crossing points of the WMS cell, may not be displayed on the WMS images. For instance, liquid film or droplet particles less than 3 mm may not be captured in the WMS images as they do not make full contact with crossing points of the WMS. Air entrainment, droplet impact and break up, associated with such transitional flow are discussed in this section.

Air (bubble) and droplet entrainment

During the flow transition from the horizontal to vertical pipe, air and bubble entrainment is observed in some of the flow regimes. Air entrainment occurs in the

form of bubbles trapped in impingement points of the flow. The results of the intermittent flows (UWS and slug flows) depicted in Figures 4-17 and 4-18 show that air entrainment is more prominent with the increase in the superficial gas velocity. In slug flow in horizontal section, the mixing zone, where the liquid shed from the rear of the liquid slug enters the next successive slug front, is characterised by high turbulence. The liquid shed from rear of liquid slug, forms part of the liquid film flowing around the nose of the long bubble, which entrains some of the gas on entering the next liquid slug. For such flow conditions, air bubbles are entrapped in the slug front as result of the shear layer developed between the high velocity slug front and the relatively slow proceeding liquid film. The rate of the air entrainment corresponds to the relative velocity between the advancing slug and the liquid layer (Nydal & Andreussi, 1991). The liquid film at slug front is observed to decrease with the increase in superficial gas velocity.

In the vertical section, the slow-moving elongated bubbles in UWS observed in horizontal section is seen to transition into Taylor bubble flow. Due to the low superficial velocities of the flow, part of the elongated bubble transitions into the vertical section developing into a slow-moving bullet-shaped bubble, which is followed by liquid slug region with entrained air bubbles (wake region). Air entrainment occurs as a result of the turbulence and swirling generated in the blind tee (mixing effect of blind tee) where part of elongated gas bubble is fragmented and entrained as the flow mixes around the blind tee region when transitioning into the vertical section. The bubble fragmentation is ascribed to the rate of turbulence generated in the flow that are developed in the Taylor bubble wake as the liquid film penetrates the slug front (Brauner & Ullmann, 2004). In slug flow regime with relatively higher superficial velocities and turbulence, the gas phase largely flows in a form of fragmented bubble trains or bubble clusters followed by liquid slugs which are aerated at the slug front. Some of the fragmented air bubbles (as result of interfacial instabilities as the flow transitions through the blind tee) are carried in the liquid slugs and tend to coalesce into larger bubble as the flow travel further in the pipeline.

Droplet entrainment is observed mostly in the churn and annular flows. Figures 4-19 shows that droplet entrainment decreases with the increase in superficial gas velocity. In Figure 4-19 (a) liquid bridge disintegration could be observed in churn

flow, leading to more droplets in the gas core, while few droplets are seeing in the core of annular flow (Figures 4-19 (b) – (c)). For high superficial gas velocity, it is noticed that droplet entrainment increases with increase in superficial liquid velocity especial in vertical flows (Figure 4-20). In general, more droplet entrainment is observed in the vertical flows as compared to horizontal flows due to effect of gravity as heavier fluid tends to segregate and quickly settle in the horizontal section. In vertical section, some of the droplets from the wall film are entrained instead in the gas core. The top-view images of the WMS (Figures 4-21 and 4-22) of vertical flows, shows that for medium and high superficial gas velocities, more droplets are entrained in the gas core with the increase in superficial liquid velocities. The top-view images also show that more droplets are entrained in churn flow (Figure 4-21 (a) – (b)) than in annular flow (Figure 4-21 (c)), with droplet entrainment decreasing with increase in superficial gas velocity.

Droplet impact

Droplet impact has been observed to produce small bubbles in a thin film which may contribute to bubble entrainment (Rodriguez & Shedds, 2004). In annular flow, where some of the liquid droplets entrained in the gas core are deposited back onto the liquid film, the impacting droplet is observed to create long and narrow furrow on the film surface. The Oblique impacts of droplets at base film leads to creation of bubbles which are accumulated by the disturbance waves (Hann et al 2018). Some of the bubbles are observed to be trapped in the film after the droplet have passed along the base film. Although the whole sequence of droplet impact could not be visualised in the present work, analyses of the WMS images for separated flows (annular flow) in Figure 4-20 show some trapped air bubble at base of liquid film which could be attributed to droplet impact on the liquid film.

Bubble or droplet breakup

A drop or bubble may split into two or more fragments of equal or unequal volumes, depending on the breakup mechanism, as the droplet or bubble is not only subject to turbulent field but also to both viscous and inertia forces. The two most important mechanism is assumed to be turbulent breakup and viscous shearing (Luo & Svendsen, 1996). Turbulent breakage is caused by fluctuating eddies that bombard the particle surface, causing oscillations (or deformations) of the particle surface.

Particle fragmentation occurs when the local turbulent energy dissipation of the flow is greater than the surface stabilizing energy (Krýsa & Šoóš, 2022). The bubbles are usually subjected to the velocity fluctuation of the turbulence behind the jet, which results in deformation forces that are much larger than the limiting forces due to surface tension, and subsequent bubble breakage. However the likelihood of this break up is dependent on the bubble size, and on the dissipation rate of the underlying turbulence (Lasheras et al., 1999).

For shear breakage, a droplet or bubble may break into multiple particles with varying volume due to viscous shear. However in a highly turbulent flow, the breakup of drop or bubble due to viscous forces can usually be ignored since the drop or bubble is normally much larger than the microscale of turbulence (Luo & Svendsen, 1996). Moreover, for air-water system, interfacial shear force can be ignored due to the low viscosity of water in air-water flow.

It is observed that more breakages of droplets or large bubbles increased significantly on transitioning to the vertical section due to the increased turbulence from the blind tee. Large or elongated bubbles from the horizontal section (Figures 4-17 and 4-18) can be seen to become unstable or broken on transition through the blind tee, leading to turbulent breakages of these bubbles. For separated flows, especially in annular flows, shearing off of the roll wave occurs as the high flowrate of the gas causes shearing on the gas-liquid interface. The crest of the roll wave becomes elongated and thin ligaments are torn from the liquid film. The ligaments are quickly broken down to droplet particles (Azzopardi, 1998). The phenomenon is shown in Figure 4-19 as the liquid ligaments are shredded off the gas-sheared liquid film.

4.4 Influence of pipe configuration on void fraction measurement

As noted in section 4.1 that liquid accumulation in the horizontal section is a common phenomenon for such pipe configuration, further investigation of downstream effect due to the conjoined vertical part of the flow loop was carried out in this work.

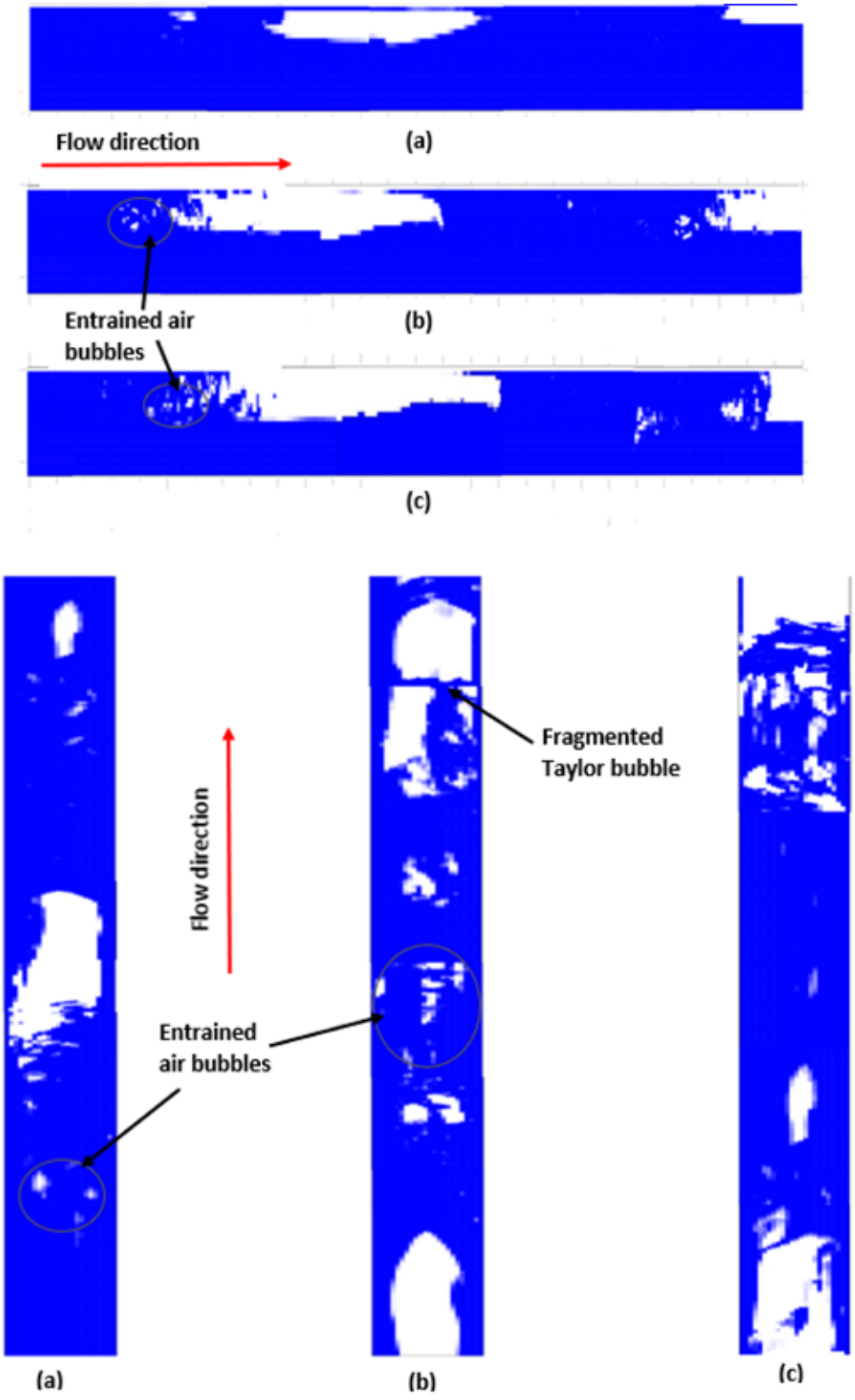

Figure 4-17 Axial slice images of flow regimes in horizontal and vertical section at superficial gas and liquid velocities of (a) 0.14 m/s and 0.086 m/s (b) 0.55 m/s and 0.086 m/s and (c) 1.05 m/s and 0.086 m/s respectively with 100D gas injection point.

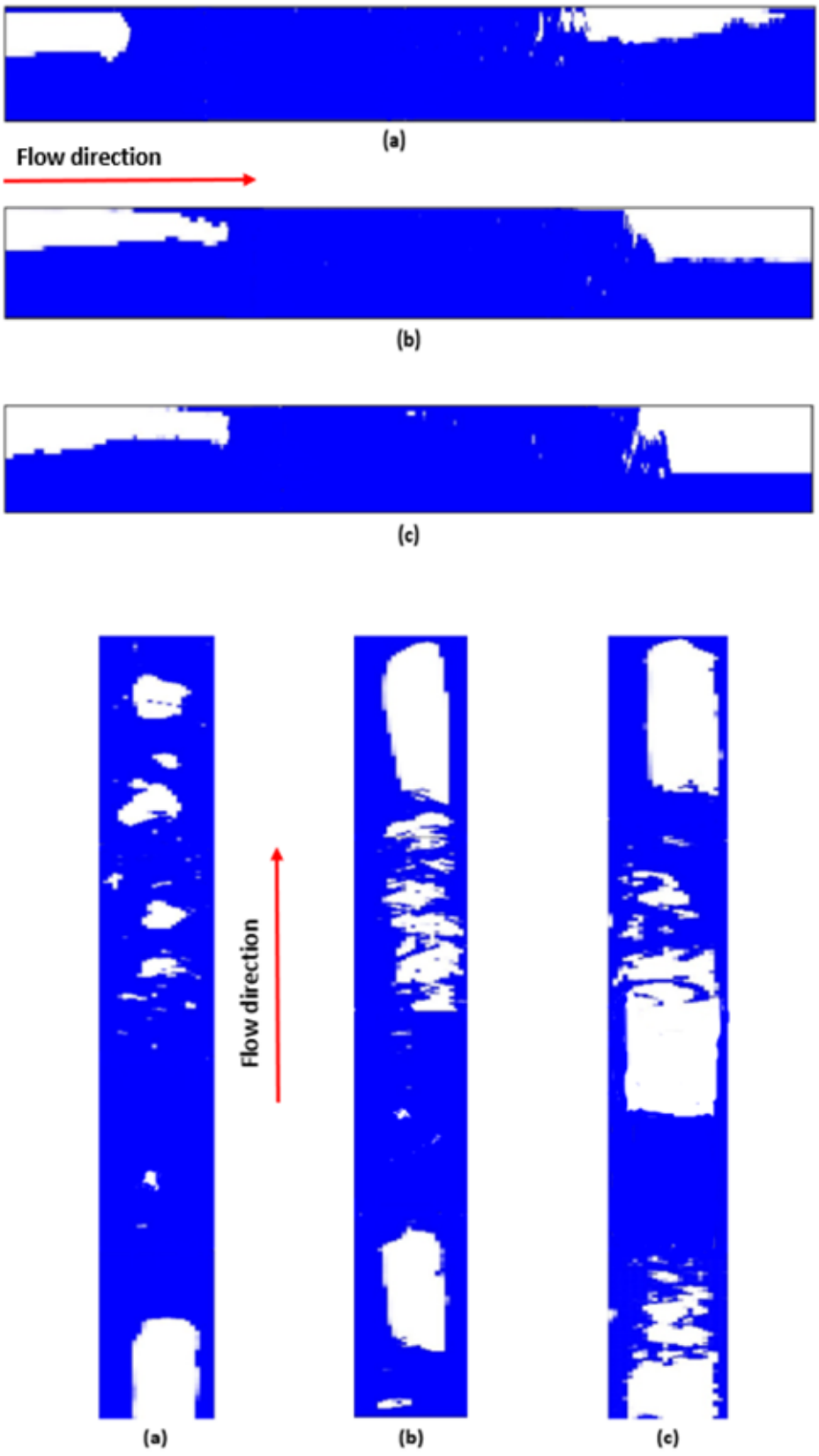

Figure 4-18 Axial slice images of flow regimes in horizontal and vertical section at superficial gas and liquid velocities of (a) 0.14 m/s and 0.43 m/s (b) 0.55 m/s and 0.43 m/s and (c) 1.05 m/s and 0.43 m/s respectively with 100D gas injection point.

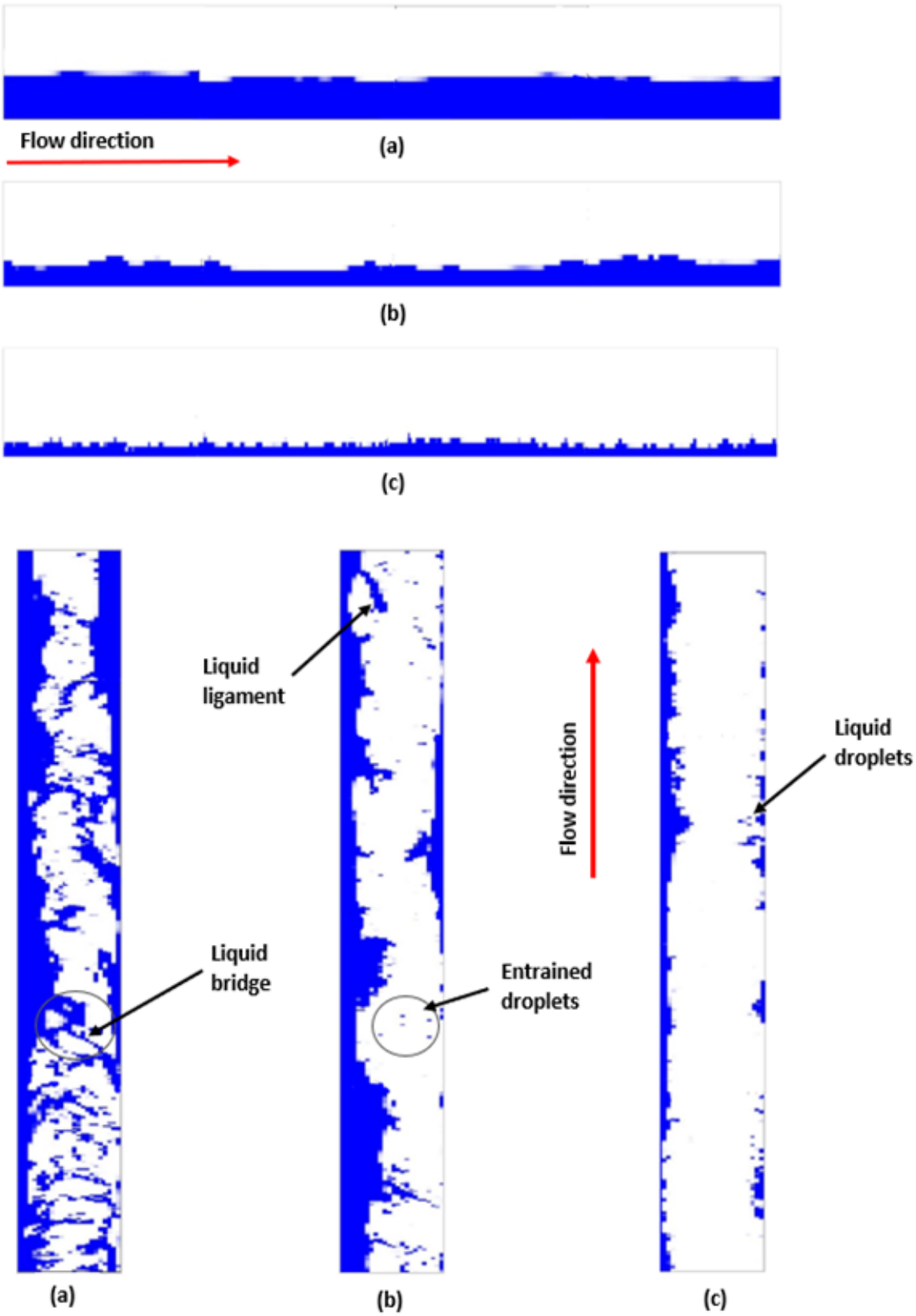

Figure 4-19 Axial slice images of flow regimes in horizontal and vertical section at superficial gas and liquid velocities of (a) 2.73 m/s and 0.43 m/s (b) 5.45 m/s and 0.43 m/s and (c) 10.91 m/s and 0.43 m/s respectively with 100D gas injection point.

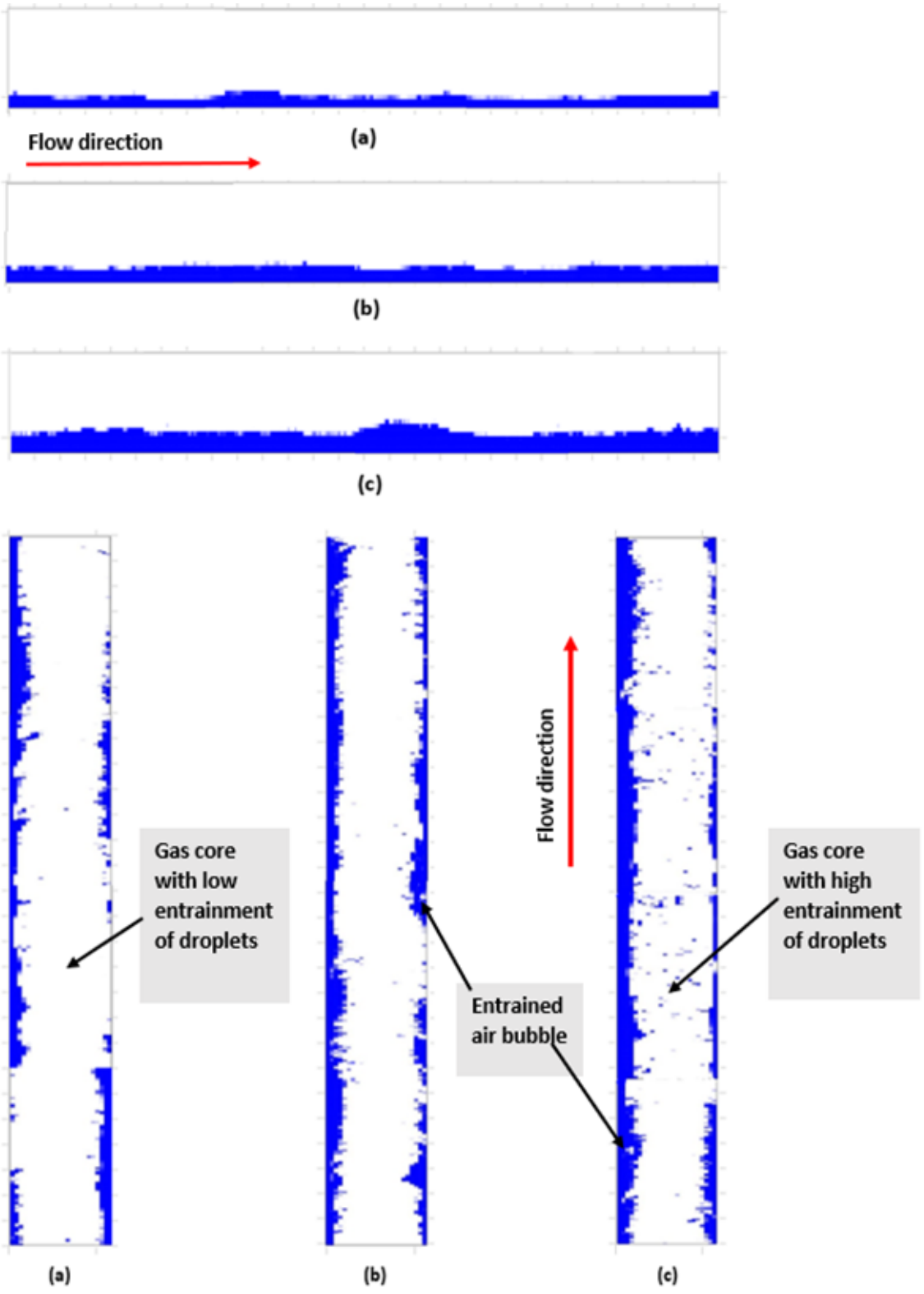

Figure 4-20 Axial slice images of flow regimes in horizontal and vertical section at superficial gas and liquid velocities of (a) 10.91 m/s and 0.043 m/s (b) 10.91 m/s and 0.086 m/s and (c) 10.91 m/s and 0.13 m/s respectively with 100D gas injection point.

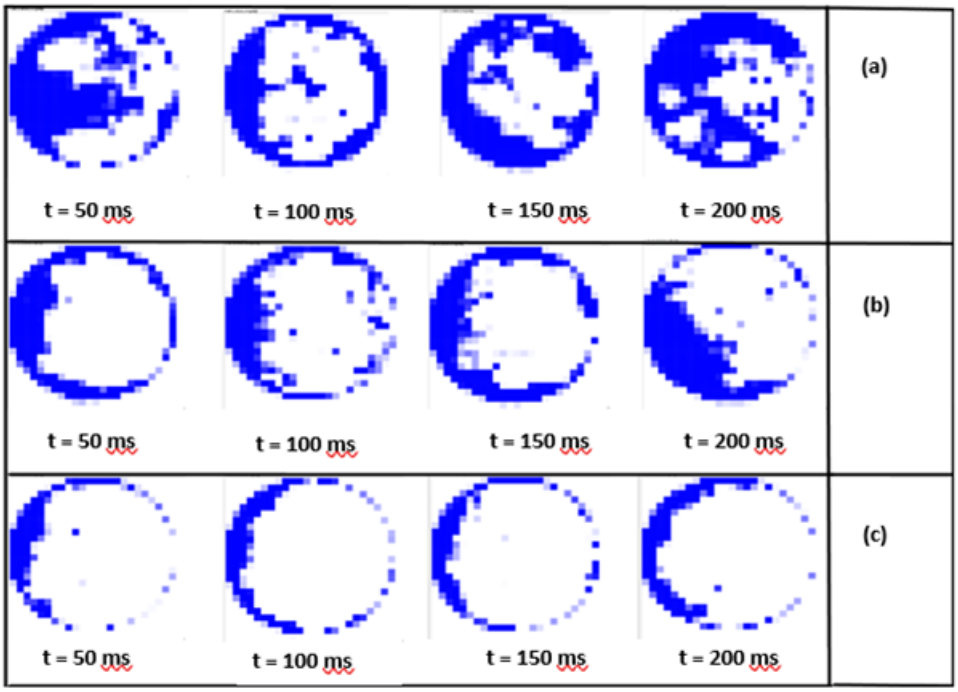

Figure 4-21 Top-view images of WMS for vertical flows with superficial gas and liquid velocities of (a) 2.73 m/s and 0.43 m/s (b) 5.45 m/s and 0.43 m/s and (c) 10.91 m/s and 0.43 m/s respectively with 100D gas injection point.

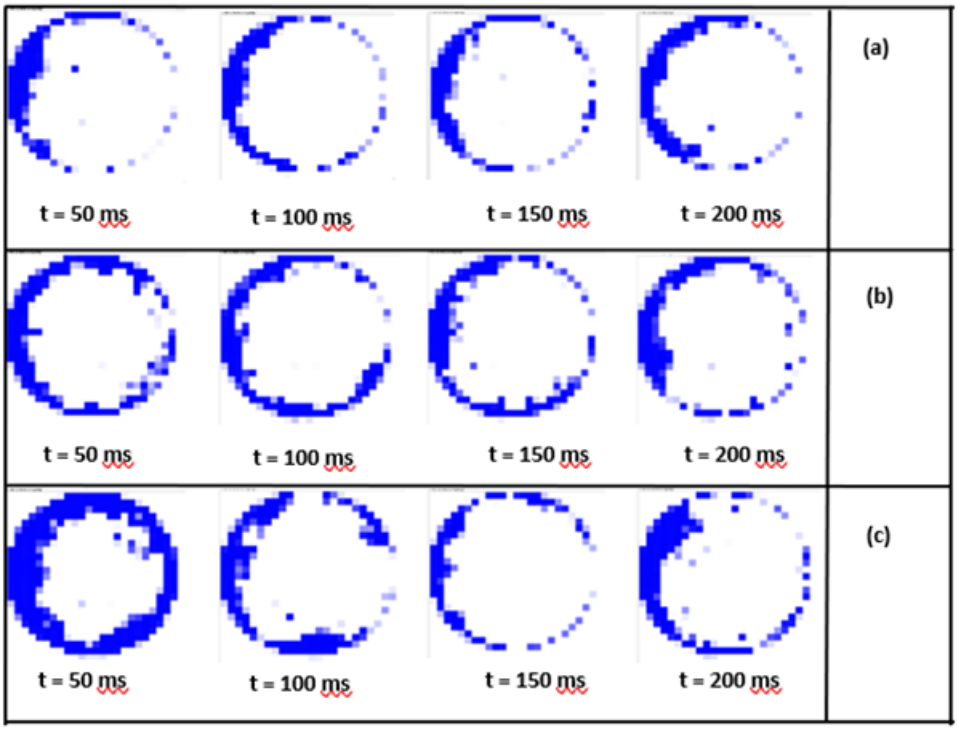

Figure 4-22 Top-view images of WMS for vertical flows with superficial gas and liquid velocities of (a) 10.91 m/s and 0.043 m/s (b) 10.91 m/s and 0.086 m/s and (c) 10.91 m/s and 0.13 m/s respectively with 100D gas injection point.

Table 4-1 Void fraction models for horizontal flow considered in the present work.

Models	Formular
Homogeneous	$\boldsymbol{\alpha = \alpha_H = \frac{1}{\left[1 + \left(\frac{1-x}{x}\right)\left(\frac{\rho_G}{\rho_l}\right)\right]}}$
$\boldsymbol{K\alpha_H}$	General form: $\boldsymbol{\alpha = K\alpha_H}$,
Armand (1946)	$\alpha = 0.833\alpha_H$
Slip ratio	General form: $\boldsymbol{\alpha = \frac{1}{\left[1+A\left(\frac{1-x}{x}\right)^a\left(\frac{\rho_G}{\rho_L}\right)^b\left(\frac{\mu_L}{\mu_G}\right)^c\right]}}$
Lockhart & Martinelli (1949)	$A = 0.28,\ p = 0.64,\ r = 0.36,\ s = 0.07$
Chisholm (1973)	$A = \sqrt{1 - x\left(\frac{\rho_L - \rho_G}{\rho_L}\right)},$ $p = 1, r = 1, s = 0$
Spedding & Chen (1984)	$A = 2.22,\ p = 0.65, r = 0.65, s = 0$
Hamersma & Hart (1987)	$A = 0.26,\ p = 0.67,\ r = 0.33,\ s = 0$
Drift Flux	General form: $\boldsymbol{\alpha = \frac{U_{SG}}{(C_o U_M + U_{GM})}}$
Gregory and Scott (1969)	$C_o = 1.19$ $U_{gm} = 0$
Toshiba (1989)	$C_o = 1.08$ $U_{gm} = 0.45$
Miscellaneous	
Cioncolini & Thome (2012)	$\alpha = \frac{hx^n}{(1 + (h-1)x^n)}$ $n = 0.3487 + 0.6513(\rho_G/\rho_L)^{0.515}$ $h = -0.2129 + 3.129(\rho_G/\rho_L)^{-0.2186}$

The effect of such pipe configuration on void fraction measurement was further investigated by comparing the void fractions obtained in this work with other known void fraction models that can be found in the literature. In the work of Jagan & Satheesh (2016) that was carried out to investigate air-water two-phase flow for pipe with different orientations, Toshiba model was observed to be the best void fraction correlation among the five different correlations compared in their work. Similarly, the

Toshiba model with other void fractions correlations shown in Table 4-1 are compared with the void fractions obtained in this work to highlight the effect of such pipe configuration on void fraction measurements. A total of 78 data points (Appendix B) were tested with the 5 categories of void fraction correlation.

The graph of the comparative analyses between the measured and predicted void fractions for the different correlations is shown in Figure 4-23. The result showed that majority of the data points are located around the upper region of the 20% error band of the void fraction. This indicates that most of the prediction models overestimate the void fractions measured in this work which could be as a result of the pipe configuration that leads to liquid accumulation in the pipe. This liquid accumulation, hence, leads to decrease in void fraction measured as compared with the predicted ones. The prediction models are compared by using logical functions in MS Excel to select the models with the most consistency in predicting the overall void fraction within the 20% error band (Figure 4-23). The comparison of the models shows that the Lockhart & Martinelli (1949) and Hamersma & Hart (1987) are the models with the highest number of data points (58 each) within 20% error band, and then followed by Spedding & Chen (1984) with 55. The homogenous model showed the least prediction performance with only 15 data points (19% of all the data points) within 20% error band. The graph shows that in high void fraction region, most of the data points of the models falls within the 20% error band except for the homogenous models. While Hamersma & Hart (1987), Lockhart & Martinelli (1949), and Spedding & Chen (1984) are dominant within 20% error band for low to medium void fraction (0.14 – 0.55) region in the graph.

In general, the graph in Figure 4-23 shows that the models are not adequate for predicting void fraction in such pipe configuration, with the most consistent models only have about 74% of the total data within 20% error band.

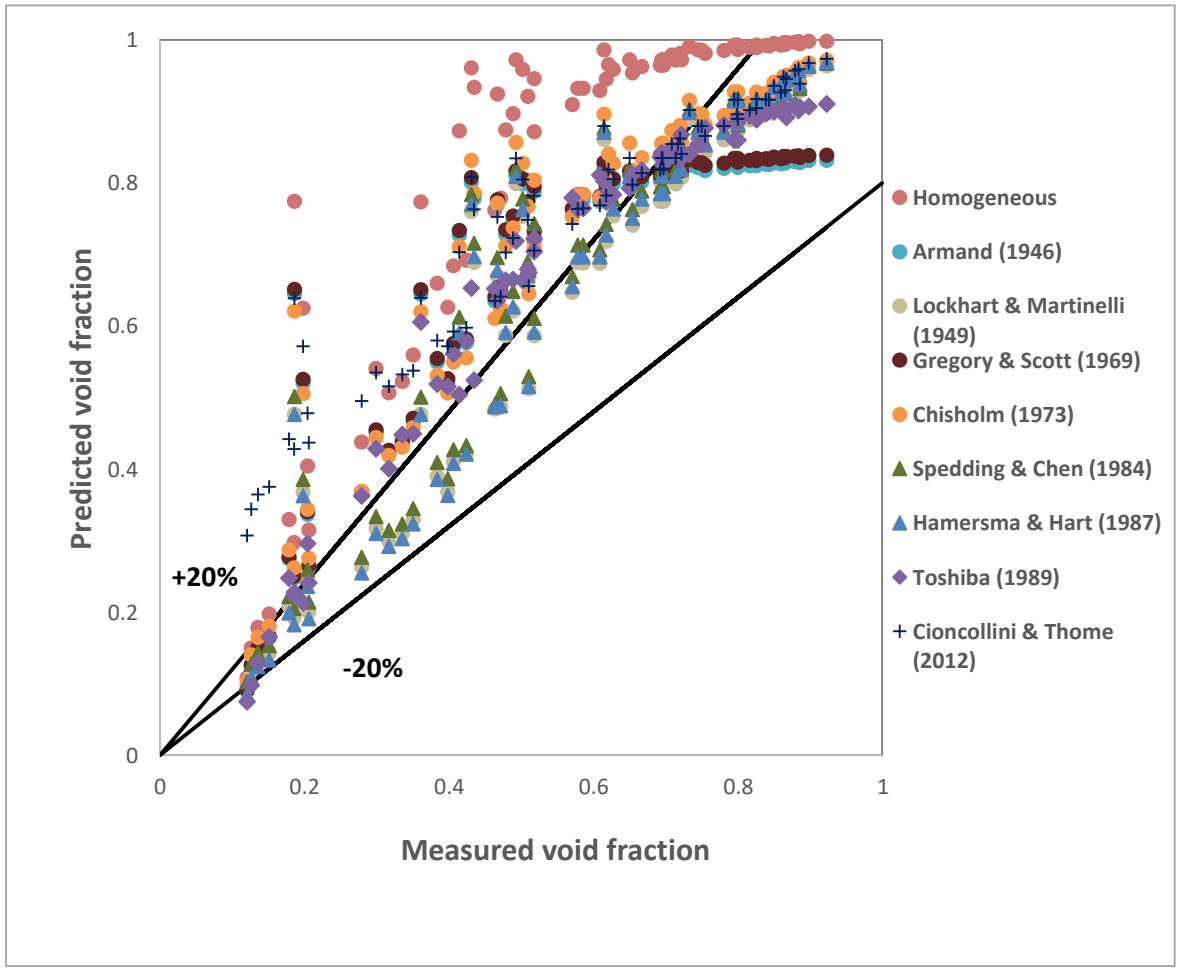

Models	Data points within 20% error band
Homogeneous	15
Armand (1946)	36
Lockhart & Martinelli (1949)	58
Gregory & Scott (1969)	36
Chisholm (1973)	27
Spedding & Chen (1984)	55
Hamersma & Hart (1987)	58
Toshiba (1989)	33
Cioncollini & Thome (2012)	30

Figure 4-23 Plot of comparative analyses between the measured and predicted void fractions.

Furthermore, the experimental data was compared with the void fraction models shown in Table 4-1 in view of comparing and selecting the best models for different flow regimes using the mean absolute percent error (MAPE) which is expressed as

$$\mathbf{MAPE} = \left[\frac{1}{n}\sum_{m=1}^{n}\left|\frac{Y_{exp.m} - Y_{pred.m}}{Y_{exp.m}}\right|\right] X\ 100 \quad \textbf{(4-1)}$$

where $Y_{exp.m}$ and $Y_{pred.m}$ are the average of the experimental and predicted values of void fraction respectively.

Table 4-2 Comparison of the accuracy of the void fraction models for different flow regimes.

Model	Error under different flow regimes (%)				
	UWS	**Wavy**	**Plug**	**Slug**	**Annular**
Homogeneous	49.8	30.9	27.9	37.4	13.7
Armand (1946)	39.7	17.0	24.0	26.0	5.7
Lockhart & Martinelli (1949)	35.0	19.7	13.6	**13.7**	7.8
Gregory & Scott (1969)	40.3	17.7	23.7	25.5	5.2
Chishom (1973)	41.4	23.4	23.3	25.3	9.3
Spedding & Chen (1984)	37.0	21.3	**10.9**	16.5	8.6
Hamersma & Hart (1987)	35.7	20.7	19.8	14.6	8.6
Toshiba (1989)	**28.6**	**16.9**	34.0	25.7	**4.8**
Cioncollini & Thome (2012)	39.8	21.9	58.6	24.3	8.9

The result of the comparison of the void fraction correlations for different flow regime is shown in Table 4-2. In general, the annular flow regime is observed to have the

least prediction error for all the models as compared with the other flow regimes. On the other hand, UWS flow regime is witnessed to have the worst prediction result for all the models in Table 4.2 which could be expected given the novelty of this flow regime. The Toshiba model gave the best void fraction prediction especially for separated flows. For Intermittent flows, Spedding & Chen (1984) and Lockhart & Martinelli (1949) gave the best results for plug and slug flow regimes respectively. These models are then selected and compared with the experimental data using the plot of void fraction against the mixture superficial velocity to show the effect of pipe configuration on void fraction measurements (Figures 4-24 & 4-25).

For intermittent flow regime, the void fraction of the present work appears to be lower than other selected models compared in Figure 4-24. The Lockhart & Martinelli (1949) and Spedding & Chen (1984) models as established earlier appear to be the closest to the present work especially when compared with the Toshiba model in the plot. Likewise in Figure 4-25 for separated flows, the present work is shown to have lower void fraction in comparison with the other four models in the plot. The Toshiba model for separated flow appears closest to the present work, while Spedding & Chen (1984) model is farthest from the present work.

From Figures 4-24 and 4-25, it can be seen that void fraction for this present work appears to be lower when compare with other void fraction models used in this work. The decrease in the void fraction for the present work could be connected to the liquid accumulation in the pipe due to the conjoined pipe configuration. The liquid accumulation in the pipe could contribute to error in estimation of two-phase flow in such pipe configuration due to the overestimation of the void fraction. The result of these plots in Figures 4-24 and 4-25 agrees with the earlier claim in previous section of the tendency of liquid accumulation in horizontal section, which decreases the void fraction for such pipe configuration. This indicates the need to develop a new model for predicting void fraction for two-phase flow in such pipe configuration.

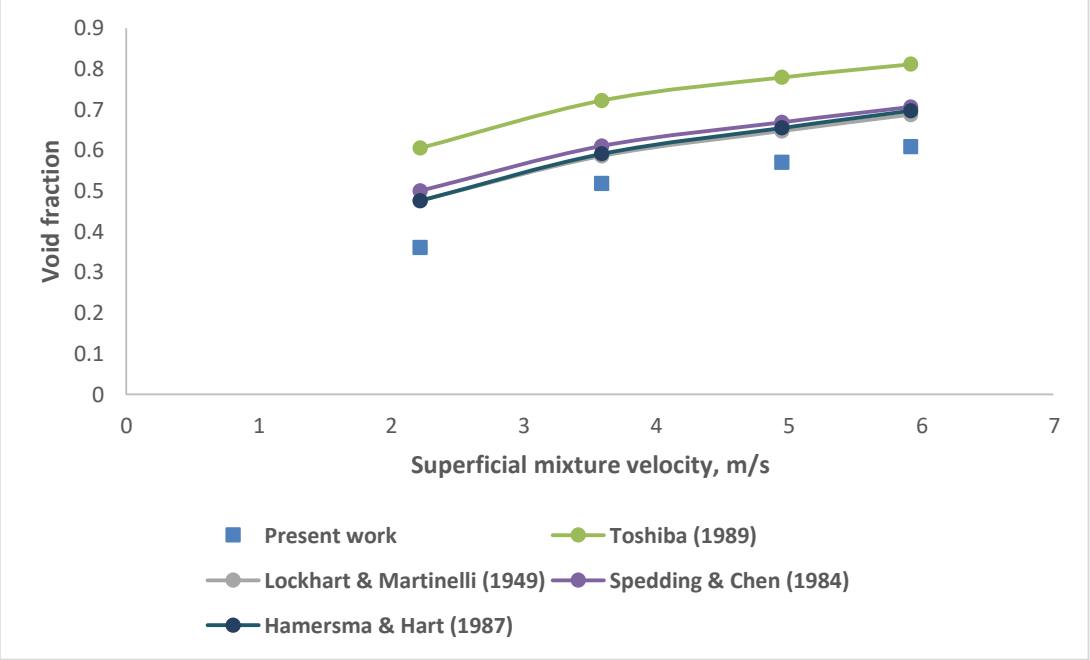

Figure 4-24 Plot of the relationship between void fraction and mixture superficial velocity to compare void fraction correlations used in conventional horizontal pipe with that of present work for flows with Usl= 0.43 m/s and Usg= 1.36 – 5.45 m/s.

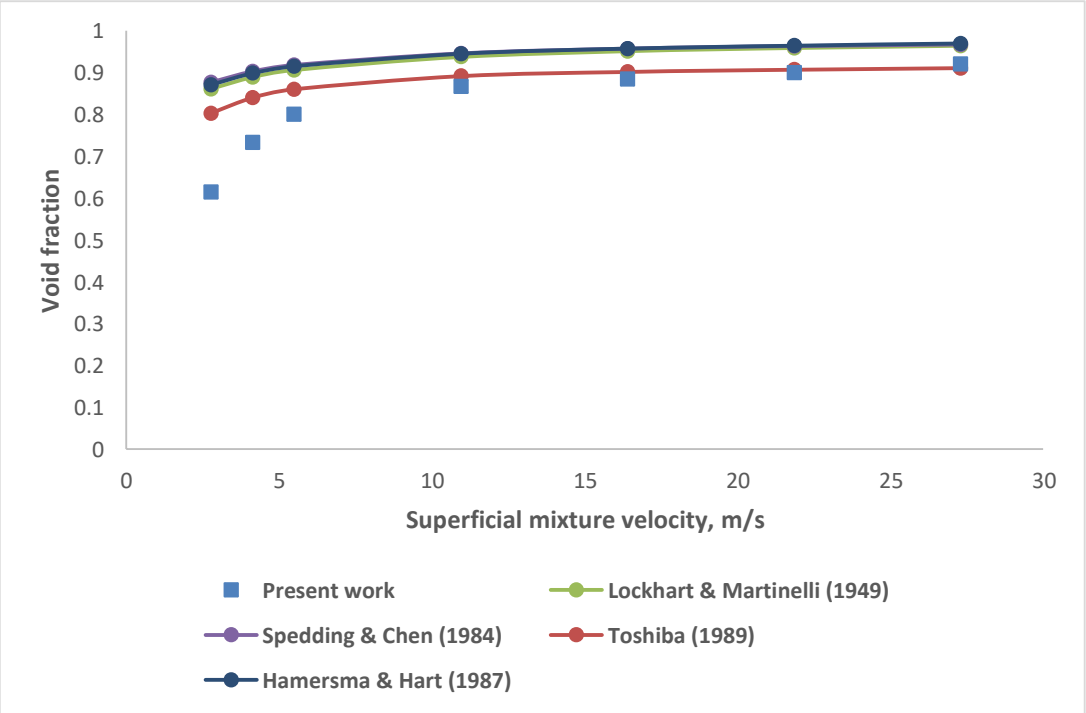

Figure 4-25 Plot of the relationship between void fraction and mixture superficial velocity to compare void fraction correlations used in conventional straight horizontal pipe with that of present work for flows with Usl= 0.043 m/s and Usg= 2.73 – 27.26 m/s.

4.4.1 New proposed (modified drift flux) model for void fraction estimation

Based on the experimental data, a new correlation for void fraction in such pipe configuration is developed for more accurate prediction of void fraction in horizontal section. The drift flux model is considered to be one of the most accurate methods for analyses of two-phase flow (Kataoka & Ishii, 1987). It accounts for the effects of non-uniform flow, void fraction profiles and the local relative velocity between both phases (Abdulkadir et al. 2018). The drift flux model utilizes the two drift-flux parameters, C_o and Ugm which addresses the effects of non-uniform distribution of the flow and relative velocity between the phases. The model correlates the gas velocity *Vg*, and the superficial mixture velocity, *Um*, which is represented below in equation (4-2)

$$\boldsymbol{V_g = C_o U_m + Ugm} \tag{4-2}$$

where C_o and Ugm are the distribution coefficient and drift velocity of gas respectively.

Zuber & Findlay (1965) presented that the linear form of the equation is dictated by continuity. This implies that the two-phase mixture is continuum, with the flow properties dependent on the thermodynamic and transport properties of each phase and their concentration (Zuber & Findlay, 1965). For two-phase flow, C_o is observed to typically fall within the range of 1.1 – 1.3 (Weber, 1981). Kokal & Stanislav (1989) observed this value to be 1.2, while Kataoka & Ishii (1987) proposed an equation for calculating C_o for round tubes as

$$\boldsymbol{C_o = 1.2 - 0.2\sqrt{\left(\frac{\rho_l}{\rho_g}\right)}} \tag{4-3}$$

On the other hand, the drift flux velocity (Ugm), which accounts for the local velocity difference between the gas and liquid phase could have a zero or non-zero value in the horizontal section (Weber 1981). Zuber & Findlay (1965) proposed that the drift velocity can be obtained using the expression below

$$\boldsymbol{U_{gm} = 0.35[\frac{g\Delta\rho D}{\rho_l}]^{\frac{1}{2}}} \tag{4-4}$$

where g, $\Delta\rho, D$, ρ_l are the acceleration due to gravity, density difference of the two-phases, pipe dimeter and the density of the liquid.

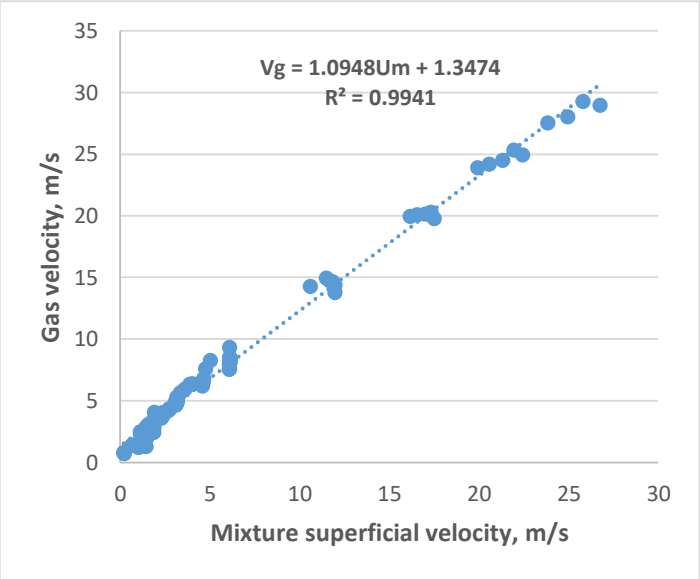

Figure 4-26 Plot showing relationship between gas velocity and mixture superficial velocity to obtain drift flux parameters.

The new model was obtained by fitting the present experimental data to the typical drift flux model to generate new set of drift flux parameters required for void fraction estimation in a horizontal pipe with conjoined vertical pipe configuration. Figure 4-26 shows the relationship between the gas velocity and superficial mixture velocity to obtain the drift flux parameters for void fraction estimation for such pipe configuration. A good correlation between the gas velocity and mixture velocity is observed with coefficient of determination of 0.994. The gas velocity was obtained by dividing the superficial gas velocity by the average void fraction of the flow, while the mixture superficial velocity is the sum of the superficial gas and liquid velocities. The plot in Figure 4-26 shows a generic correlation that could be used to calculate void fraction for two-phase flow in horizontal section for conjoined pipe configuration. The drift parameters (C_o and Ugm) is obtained by curve fitting the experimental data with straight line equation. From Figure 4-26, the C_o and Ugm is estimated to be 1.095 and 1.347 respectively. The void fraction can then be estimated by inserting

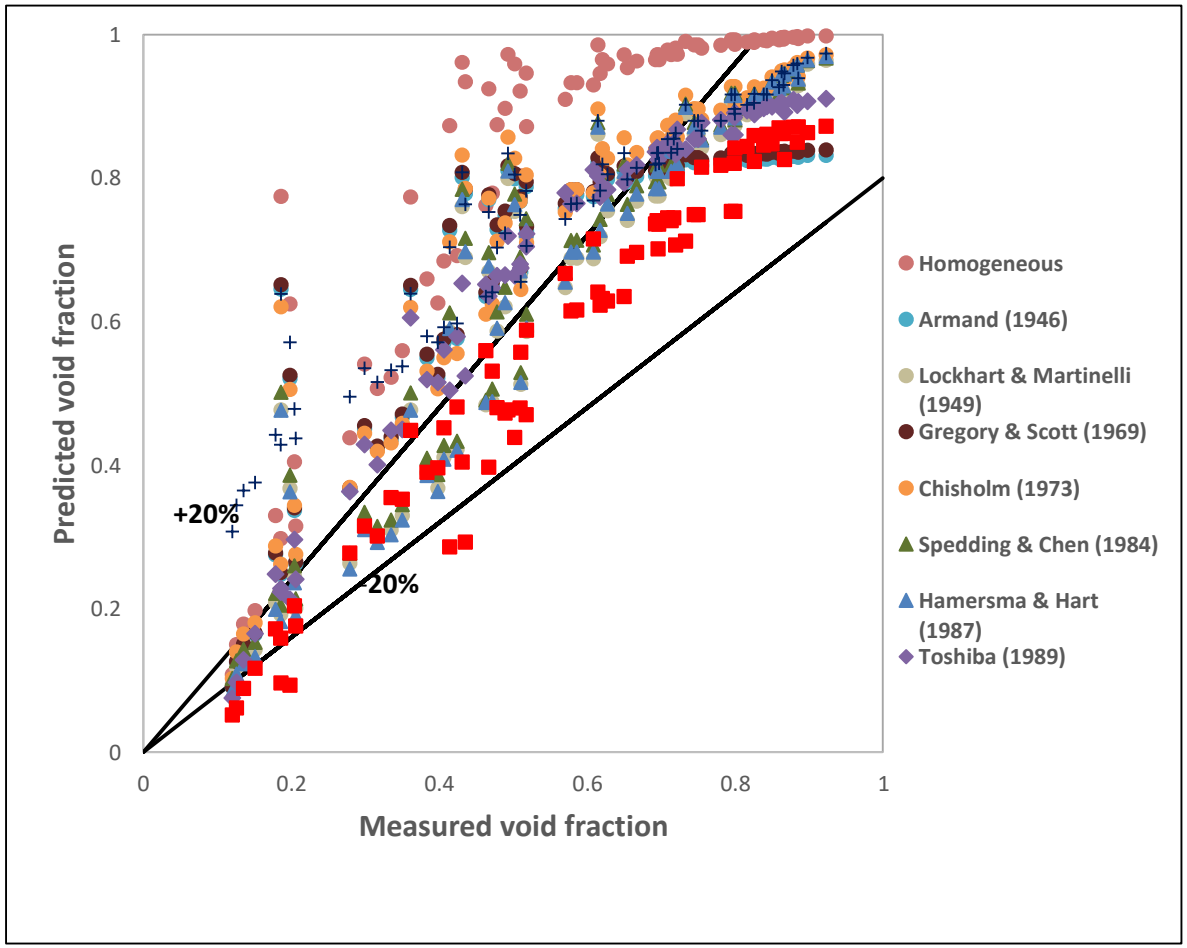

Models	Data points within 20% error band
Homogeneous	15
Armand (1946)	36
Lockhart & Martinelli (1949)	58
Gregory & Scott (1969)	36
Chisholm (1973)	27
Spedding & Chen (1984)	55
Hamersma & Hart (1987)	58
Toshiba (1989)	33
Cioncollini & Thome (2012)	30
Present work	68

Figure 4-27 Comparative analyses plot with the new proposed model.

Table 4-3 Comparison of the void fraction models with the new proposed models for different flow regimes.

Model	Flow regime related discrepancy, %				
	UWS	**Wavy**	**Plug**	**Slug**	**Annular**
Homogeneous	49.8	30.9	27.9	37.4	13.7
Armand (1946)	39.7	17.0	24.0	26.0	5.7
Lockhart & Martinelli (1949)	35.0	19.7	13.6	13.7	7.8
Gregory & Scott (1969)	40.3	17.7	23.7	25.5	5.2
Chishom (1973)	41.4	23.4	23.3	25.3	9.3
Spedding & Chen (1984)	37.0	21.3	10.9	16.5	8.6
Hamersma & Hart (1987)	35.7	20.7	19.8	14.6	8.6
Toshiba (1989)	28.6	16.9	34.0	25.7	4.8
Cioncollini & Thome (2012)	39.8	21.9	58.6	24.3	8.9
Present work	**5.8**	**2.8**	**8.8**	**11.2**	**2.3**

the values of the new drift parameters into the general drift flux void fraction model shown in Table 4-1. The C_o obtained in this work is observed to be slightly lower than the range suggested by Weber (1981) and the value proposed by Kokal & Stanislav (1989). Similarly, the correlation in equation (4-3) resulted to a C_o of 1.19, which falls within the typical range suggested by Weber (1981) but higher than the C_o, produced in the present work.

However, the drift velocity developed in the present work is a non-zero value which is significantly higher than that obtained when using the relationship in equation (4-4), which resulted to a Ugm of 0.304. The higher drift velocity in the present work could be a result of effect of pipe configuration that leads more liquid accumulation in

the pipe. Based on the experimental data, a new model for drift velocity estimation is proposed below as

$$U_{gm} = 1.552[\frac{g\Delta\rho D}{\rho_l}]^{\frac{1}{2}} \quad \textbf{(4-5)}$$

Equation (4-5) is a modification of drift velocity correlation of Zuber & Findlay (1965), using the data from present work.

The void fraction correlation developed in this work is compared with other models to assess its performance. The graph of comparative analyses between measured and predicted void fraction inclusive of the new proposed model is shown in Figure 4-27. The data points for the new proposed model are mostly located within the 20% error band unlike majority of the data points of other models that lie around the upper region of the error band.

The new model shows a better performance than the rest of the other models considered in this work as 87% of the data points fall within 20% error band. Moreover, only the new proposed model in present work appears more centralised within the 20% error band, which is an indication of effectiveness of the model in void fraction prediction for such two-phase flow system. The result of the comparison of the proposed new model with other selected models for different flow regimes in Table 4-3 shows the proposed new model has a better accuracy for prediction of void fraction for all the flow regimes observed in this work. With the new proposed model, it is noted that the least error is found in separated flows with 2.3% and 2.8% for annular and wavy flow respectively. The worst performance of the new model is observed in slug flow due to the complex nature of such flow regime.

From the results of the comparative analyses, it has been shown that the new model proposed has better prediction performance than most of the models compared in this work. Due to the liquid accumulation associated with such pipe orientation, most of the models compared in this work overpredicted the void fraction. As a result, a new model is proposed which gave a better prediction accuracy of void fraction in horizontal section for such pipe orientation.

4.5 Chapter summary

The summary of the work performed in this work and the key findings are presented below:

- Flow regime was identified in both horizontal and vertical section using combination of visual observation and signals from the WMS sensor.
- Flow regime maps were used to characterize horizontal and verticals air-water two-phase flow. The combined flow regime map of Mandhane et al. (1974) and Taitel and Dukler (1976) was used to characterize the flow in the horizontal section. The Hewitt & Robert (1969) and Taitel et al. (1980) flow regime maps were employed to compare flow regimes observed in this work in the vertical section.
- For such pipe configuration, the stratified flow regime observed in convectional straight pipes in horizontal section for flows with low superficial velocities was noticed to be absent in this work. Instead, a new flow regime (UWS) was observed due to the backward flow, and liquid accumulation associated with such pipe geometry.
- None of the flow regime maps were able to correctly predict the UWS flow regime.
- In general, the Kong and Kim (2017) flow regime map gave a relatively good estimate of the flow regimes observed in the horizontal section as compared with the Mandhane et al. (1974) and Taitel & Dukler (1976) flow regime maps. The Hewitt & Robert (1969) flow regime map gave a better estimate of the flow regime transition boundaries when compared with Taitel et al. (1980) flow regime map.
- Slug flow regime was the dominant flow regime observed in the horizontal section due to long length of flow regime development that enhances wave growth along the pipe. In the vertical section churn flow regime was observed to be the most dominant flow regime due to the effect of gravity and the mixing effect of the blind tee on the flows.
- Liquid accumulation was observed to be common in such pipe configuration especially for flows with low superficial velocities of the fluids which could contribute to error in multiphase flow rate estimation. The liquid accumulation is mainly due to bottle neck effect and back flow from the blind tee.

- Comparison of the flow regime structure in the horizontal and vertical section for the same flow condition using PDF plot and time trace plot shows a higher fluctuation in the void fraction reading in the vertical section. Increase in gas and liquid superficial velocities has shown to increase the void fraction fluctuation in the vertical section.
- Comparison of two-phase flow void fraction prediction models shows that most of the models found in the literature overpredicted the void fraction in the horizontal section of the flow loop. The effect of such pipe configuration is evidenced in the noticeable decrease in void fraction in the horizontal section due to liquid accumulation in the pipe.
- A new (modified drift flux) model was proposed for such air-water two-phase flow system for prediction of void fraction in horizontal pipe with conjoined vertical section.

5 FLOW REGIME DEVELOPMENT WITH COMPLEX DOWNSTREAM GEOMETRIES

Adequate understanding of multiphase flow regime and its development is crucial within the process industries. It is also already established that different flow patterns may emerge when multiphase flow are transported in pipeline or conduit, and are mainly influenced by the pipe geometry, fluid, and flow properties. Understanding how these flows transition and develop helps in more accurate prediction of multiphase flow characteristics which is important for optimized operation of these process industries. Some of these flow patterns such as slug flow are undesirable in many process industries. For instance, the intermittent nature of the slug flow could lead to pipe damages due to corrosion or induced vibration of the system because of slugging. For multiphase metering, it is important that the flow is fully developed for accurate measurement and assessment of the meters. Adequate development length is necessary to achieve this. Different development lengths have been proposed by different authors as shown in the literature review. In this section, 100D and 200D development lengths were used to investigate flow regime development in the flow loop by varying the gas injection from G1 to G2 (see experimental scheme).

Majority of the research on flow regime development have mostly focused on upstream effect, such as gas injection type, pipe orientation and development length. However, the effect of downstream structures such as valves, joints and bends which may cause backward flow of fluid in pipeline have not been widely studied. During transportation of fluids in pipe network, reversed flow maybe witnessed due to backpressure from the pipe configuration or pipe components such as valves, joints and bends. In plumbing systems for instance, backward flow is a common phenomenon that involves reversed flow of fluid in pipe due to backpressure or back siphonage. Such reversed flow is not desirable as it has the risk of contaminating the mains (potable) water when it comes in contact with contaminated water. For multiphase flow, such phenomenon occurs for flows with low superficial velocities especially when there is resistance to flow due to downstream configuration of the pipe (Biberg, 2005). The backpressure downstream will tend to oppose the desired flow especially for flows with low superficial velocities and directs the fluid backward, towards the test region of the pipe. It is therefore possible that this backward flow could have effect on flow regime development in the pipe. Moreover, the results in

Chapter 4 showed that pipe configuration has effect on flow characteristics, especially the void fraction. The result also highlighted the effect of back flow on typical stratified flow regime usually seem in conventional straight pipes in horizontal section. This suggests that downstream pipe configuration could have effect on flow regime development, and consequently, on multiphase flow metering.

In this section, experimental studies on upstream effect on flow regime development was performed using 100D and 200D development lengths as described in Chapter 3. For the downstream effect, the gas injection distance was kept constant while the downstream configuration was changed by varying the distance of CR sensor from blind tee from 41D to 141D. The flow characteristics were compared in both cases for the effect of variation in upstream and downstream conditions.

5.1 Flow regime development length

To investigate flow regime development, measurements taken at 100D and 200D development lengths with gas and liquid superficial velocities within the range of 0.14 – 27.26 m/s and 0.043 – 1.3 m/s respectively, were analysed and compared. Figures 5-1 – 5-6 show the results of the tests that were obtained from the WMS in the horizontal section. The tests are classified into 3 groups: (i) Flow with low superficial velocities (ii) Stable intermittent flow and (iii) Separated flow.

5.1.1 Horizontal flows

i. Flow with low superficial velocities (Unstable wavy slug flow)

The results of the flow with low superficial velocities of gas and liquid show that unstable intermittent flow is prevalent both in 100D and 200D development lengths as can be seen in Figure 5-1. As already established in section 4.1 of this work that flows with low superficial velocities for such pipe configuration enhances intermittent flow regime development in the pipe as result of bottleneck effect at blind tee joint and the intermittent blockage of the pipe cross-section due to liquid accumulation in the pipe. The liquid accumulation in the horizontal section causes the gas-liquid interface level to increase, covering top of the pipe occasionally. The bottleneck effect from the blind tee junction is as a result of the low hydraulic force in the pipe that causes backward flow and the heavier fluid in the vertical section to fall back (in opposite direction of flow) in the pipe. This reverse flow due to action of gravity and

low hydraulic force leads to temporary restriction of flow around the blind tee, and backward flow which subsequently leads to more liquid accumulation in the horizontal section that causes periodic blockage of the pipe cross section.

As it can be seen in Figure 5-1, as the superficial gas velocity is increased, more liquid is pushed out from the horizontal section as the liquid level decreases. This is as the unstable plug flow regime transitions into unstable slug flow regime. It is observed generally that the liquid accumulation increases with increase in flow regime development length. This is evidenced in the PDF plots as the peak in the low void fraction region is usually higher for the 200D development length. This implies that void fraction decreases with increase in the flow regime development length. The pattern observed in the 100D and 200D were fairly the same with the PDF plots showing only a slight change in signature of the plots.

ii. Stable intermittent flow

For stable intermittent flow, the PDF and time series plots shown in Figure 5-2 indicates the transition from plug to slug flow regime with increase in the superficial gas velocity (from 0.14 – 1.36 m/s).

As the plots show, the 100D and 200D flow regime development lengths have almost the same PDF signature for plug flow, while the slight change in the PDF signature was observed with increase in the superficial gas velocity as the flow transitions to slug flow regime.

The time series plots indicate some significant changes due to variation in the flow frequency. This is evidenced in the reduced number of sinusoidal curves/waves observed in 200D flow regime development length. In intermittent flows, as the flow travel down the pipe, gas bubbles tend to coalesce, forming larger bubbles further down the pipes, hence the decrease in flow structure frequency in the 200D flow regime development length.

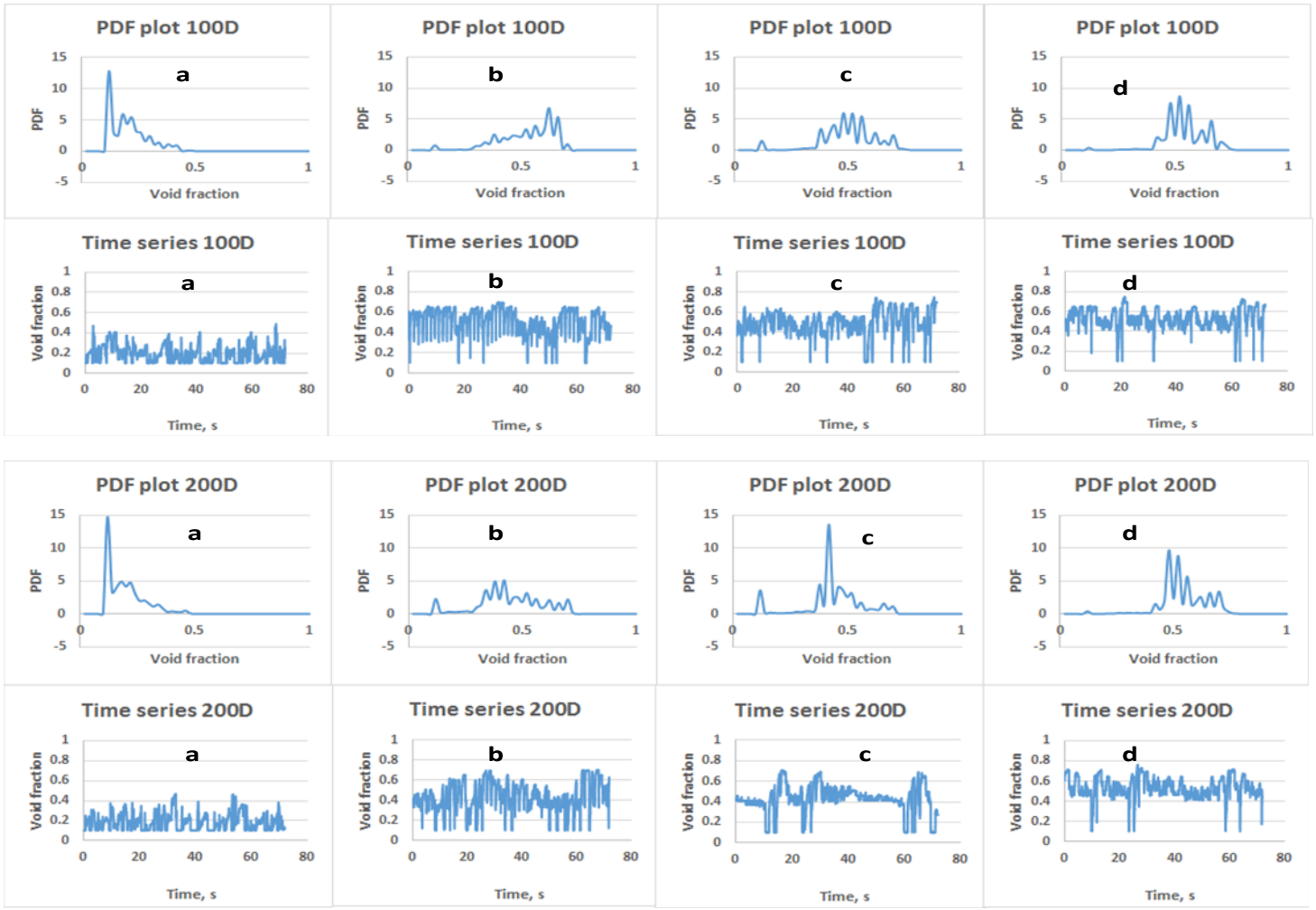

Figure 5-1 PDF and time series plots of flows with low superficial velocities for 100D and 200D with superficial liquid velocity of 0.043 m/s and superficial gas velocities of (a) 0.14 m/s (b) 0.55 m/s (c) 0.95 m/s and (d) 1.36 m/s.

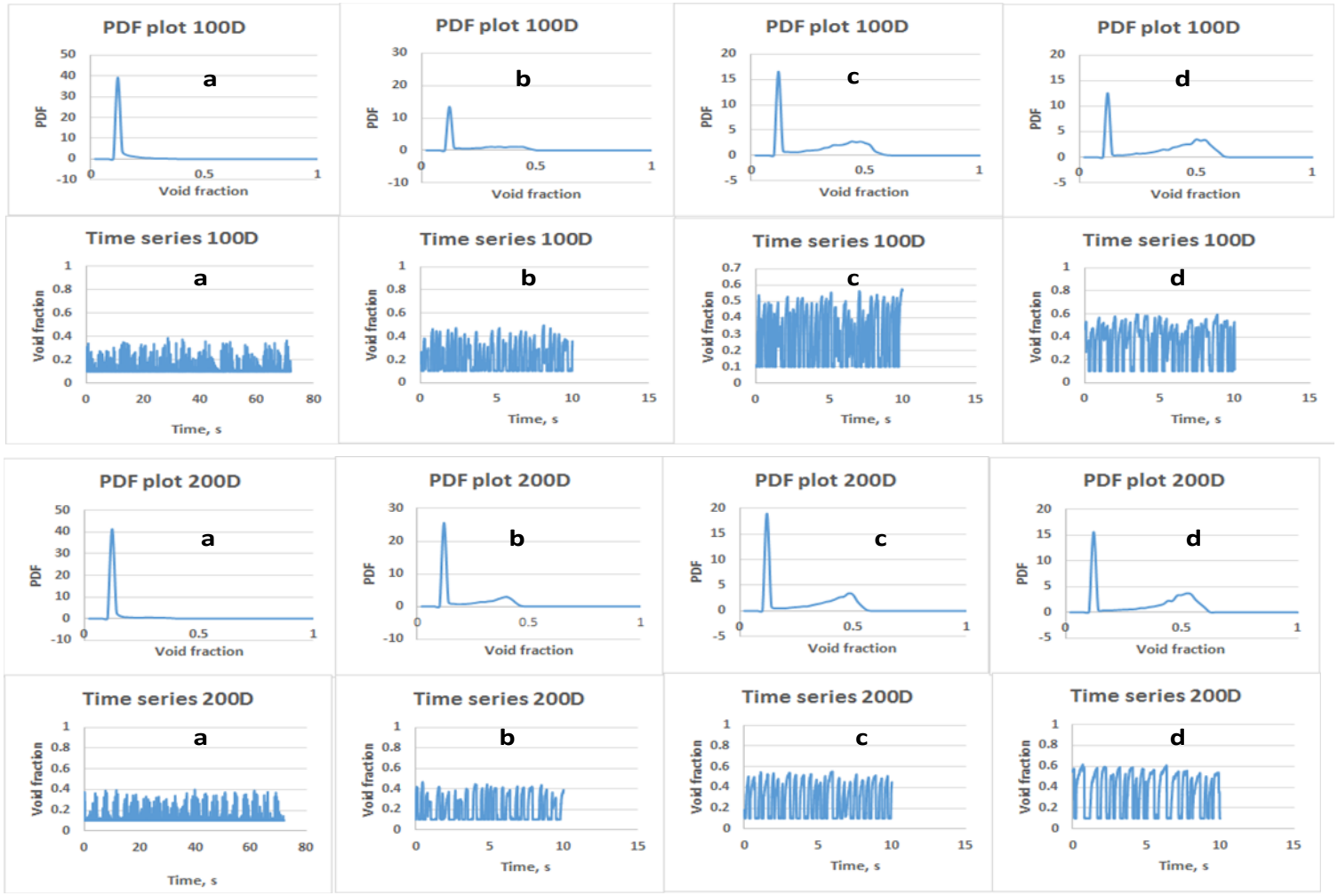

Figure 5-2 PDF and time series plots of stable intermittent flows for 100D and 200D with superficial liquid velocity of 1.3 m/s and superficial gas velocities of (a) 0.14 m/s (b) 0.55 m/s (c) 0.95 m/s and (d) 1.36 m/s.

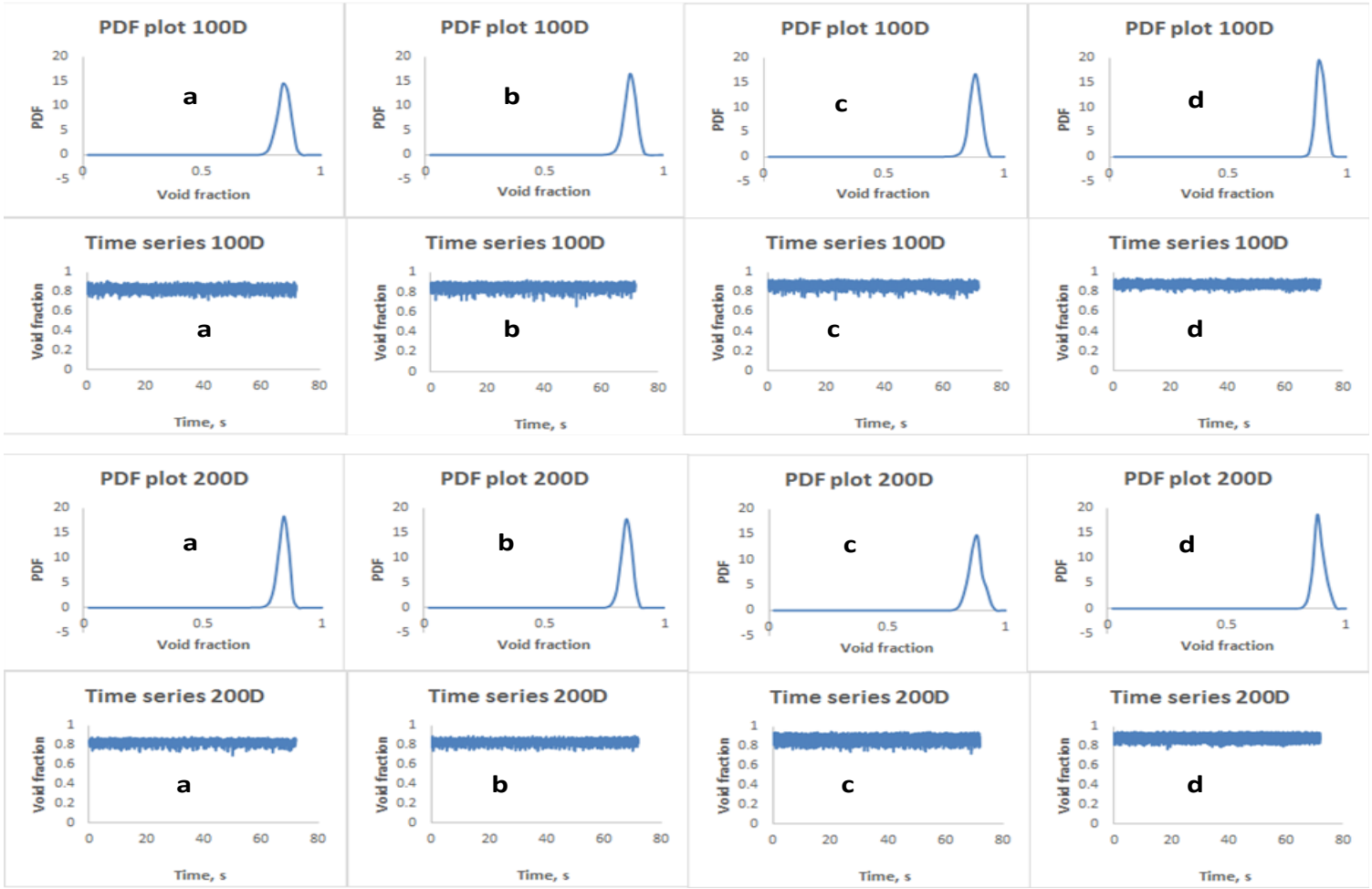

Figure 5-3 PDF and time series plots of separated flows for 100D and 200D with superficial liquid velocity of 0.086 m/s and superficial gas velocities of (a) 10.91 m/s (b) 16.36 m/s (c) 21.81 m/s and (d) 27.26 m/s.

iii. Separated flow

The results for the separated flow regime (Figure 5-3) show almost same flow patterns as can be seen from the PDF plots of 100D and 200D flow regime development length. The liquid accumulation is observed to reduce with increase in gas superficial gas velocity. This is evidenced by the amplitude (size) of the peak at high void fraction region. The plots show general increase in void fraction with the increase in superficial gas velocity, as can be seen with the gradual shift of the peak of the PDF to high void fraction region.

In general, liquid accumulation is noticed in almost all the flow regimes with the accumulation decreasing with increase in gas superficial velocity. It is therefore expected that the void fraction will decrease with the increase in flow regime development length due to higher liquid accumulation. This will be discussed further in section 5.3 on effect of flow regime development length on void fraction. Some of the experimental photos supporting the statistical analyses in this section are presented in Figures 5-4 – 5-7 to show no significant change in flow patterns for 100D and 200D development lengths. The 200D length photos can be differentiated from the 100D case based on the white plane paper covering part of the purple plastic device at the background of the pictures.

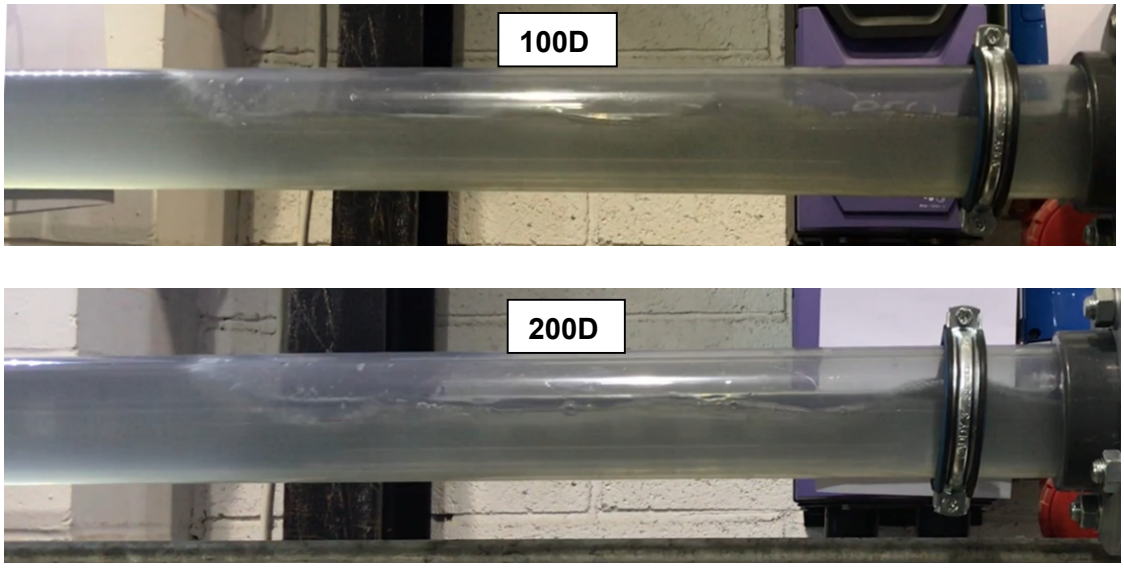

Figure 5-4 Photos from the experiments showing flow regime development with 100D and 200D gas injection points for flows with superficial gas and liquid velocities of (a) 0.55 m/s and 0.043 m/s respectively.

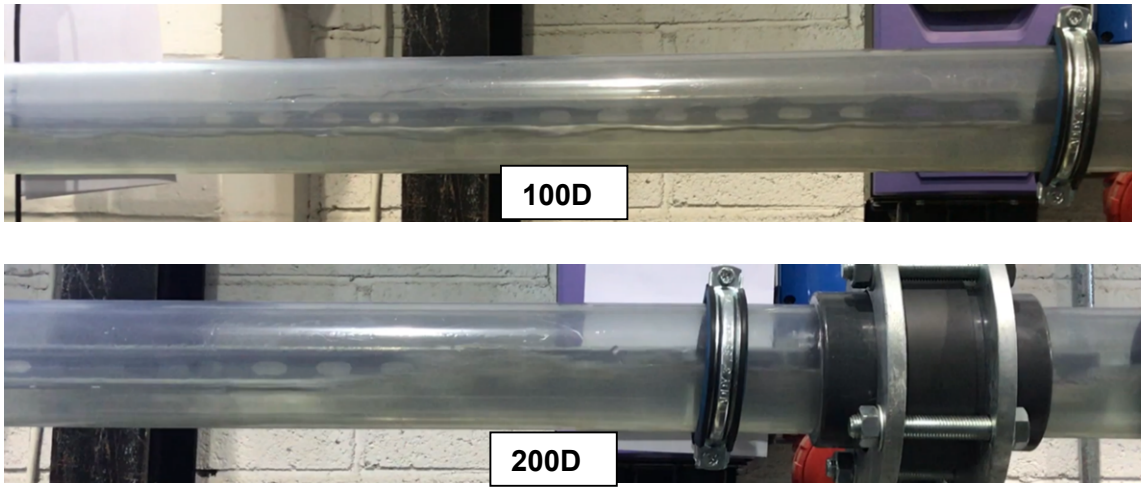

Figure 5-5 Photos from the experiments showing flow regime development with 100D and 200D gas injection points for flows with superficial gas and liquid velocities of (a) 4.09 m/s and 0.043 m/s respectively.

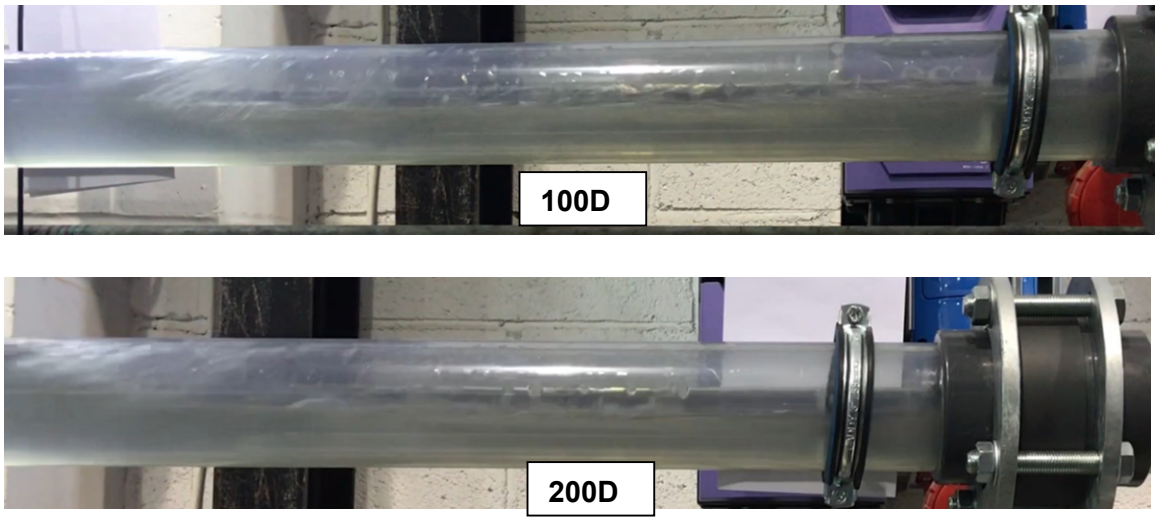

Figure 5-6 Photos from the experiments showing flow regime development with 100D and 200D gas injection points for flows with superficial gas and liquid velocities of (a) 2.73 m/s and 0.43 m/s respectively.

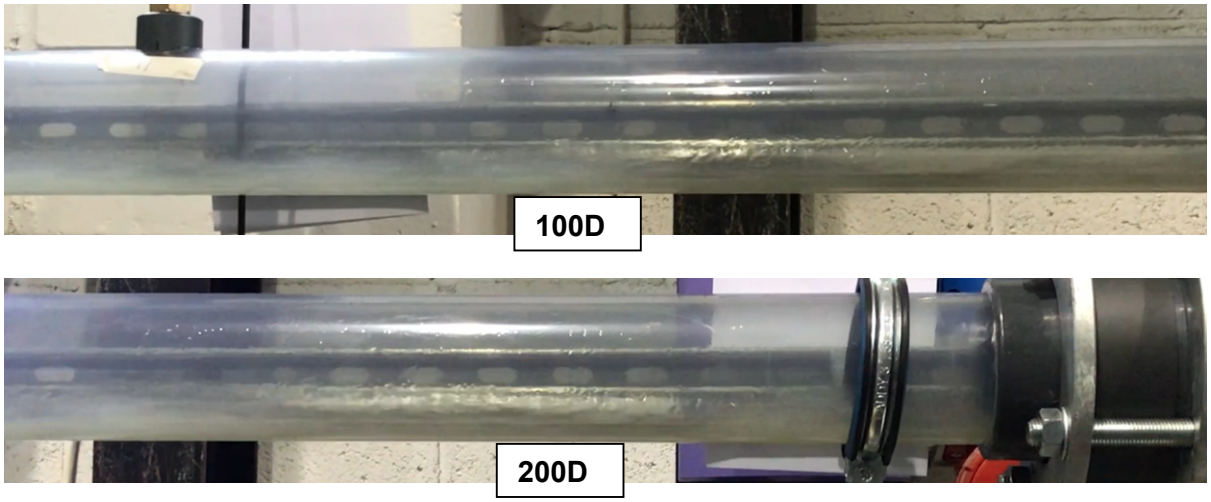

Figure 5-7 Photos from experiments showing flow regime development with 100D and 200D gas injection points for flows with superficial gas and liquid velocities of (a) 27.26 m/s and 0.043 m/s respectively.

5.1.2 Vertical flows

i. Flow with low superficial velocities

The results of flows with low superficial velocities are presented in Figure 5-8. Similar flow patterns are observed for 100D and 200D, with momentary pauses of the flow observed in both section. The momentary pauses of the liquid flow is as a result of the reasons stated in section (4.3) in the vertical section. The time series plot shows that the 200D has more occurence of such momentary pauses in liquid flow due to the reduced hydraulic force as a result of the longer development length of 200D. Such flow with low superficial velocities are usually associated with PDF signature of more than 2 peaks. Figure 5-8 shows a general transition from Taylor bubble flow to unstable slug flow regime.

In general, the flow patterns observed in flows with 100D development length are the same as those observed in 200D development length. The PDF of 100D and 200D cases have the similar signatures with more than 2 peaks (when the gas superficial velocity is increased above 0.14 m/s), which is peculiar for such flow pattern in the vertical section.

ii. Stable Intermittent flow

Figure 5-9 shows the result of intermittent flow regime for 100D and 200D development lengths. As the gas superficial velocity is increased steadily, gradual

development of the second peak of the PDF plot is witnessed due to the intermittent nature of the flow with the increase in the gas phase. The second peak of the PDF plot tends to shift to the right towards the high void fraction region with the increase in superficial gas velocity as a result of increase in void fraction in the pipe.

The first peak of the PDF plot in low void fraction region tends to decrease with increase in superficial gas velocity in both 100D and 200D tests in the vertical section.The first peak of the PDF plot at low void fraction region is observed to be higher in 100D than that of 200D development length case. This is as a result of higher volume of liquid that is pushed through the vertical section with 100D length, as compared with the 200D case where higher liquid accummulation is observed in the horizontal section due to the reduced hydraulic force.

As in the horizontal section, the flow patterns observed in the 100D and 200D development lengths are observed to be similar in the vertical section, as the PDF and time series plots show similar trend and signature. The observation above is an indication that 100D development length is sufficient as no significant change in flow pattern was observed over distance with 200D length.

iii. Separated flow

Gradual transition from churn to annular flow regime for both 100D and 200D development length tests is depicted in Figure 5-10. As the flow transitions to annular flow regime, the width of the peak of the PDF begins to shrink gradually with the increase in superficial gas velocity. A steady shift of the peak of the PDF plot from the mid void fraction region, towards the high void fraction is observed, which is as a result of the increase in void fraction with the increase in superficial gas velocity. The peak of the PDF plot is observed to be higher for 100D than 200D development length, indicating higher void fraction in 100D length.

In conclusion, it can be seen from results of the tests that the flow pattern observed in vertical section is almost the same for 100D and 200D development lengths. The results of the flows with low superficial velocities show that brief pauses are prevalent for such flow conditions.

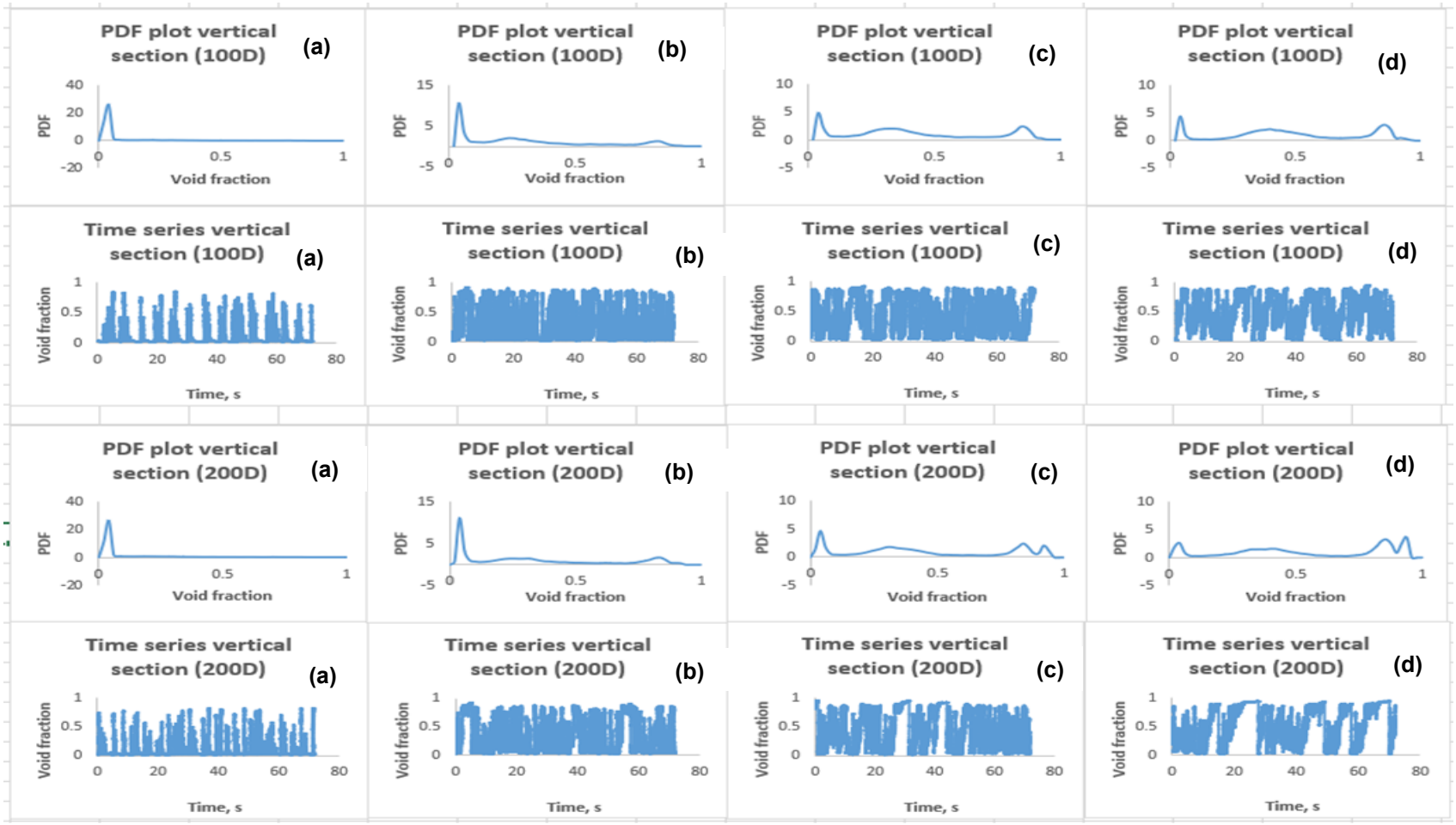

Figure 5-8 PDF and time series plots of flows with low superficial velocities for 100D and 200D with superficial liquid velocity of 0.086 m/s and superficial gas velocities of (a) 0.14 m/s (b) 0.55 m/s (c) 0.95 m/s and (d) 1.36 m/s.

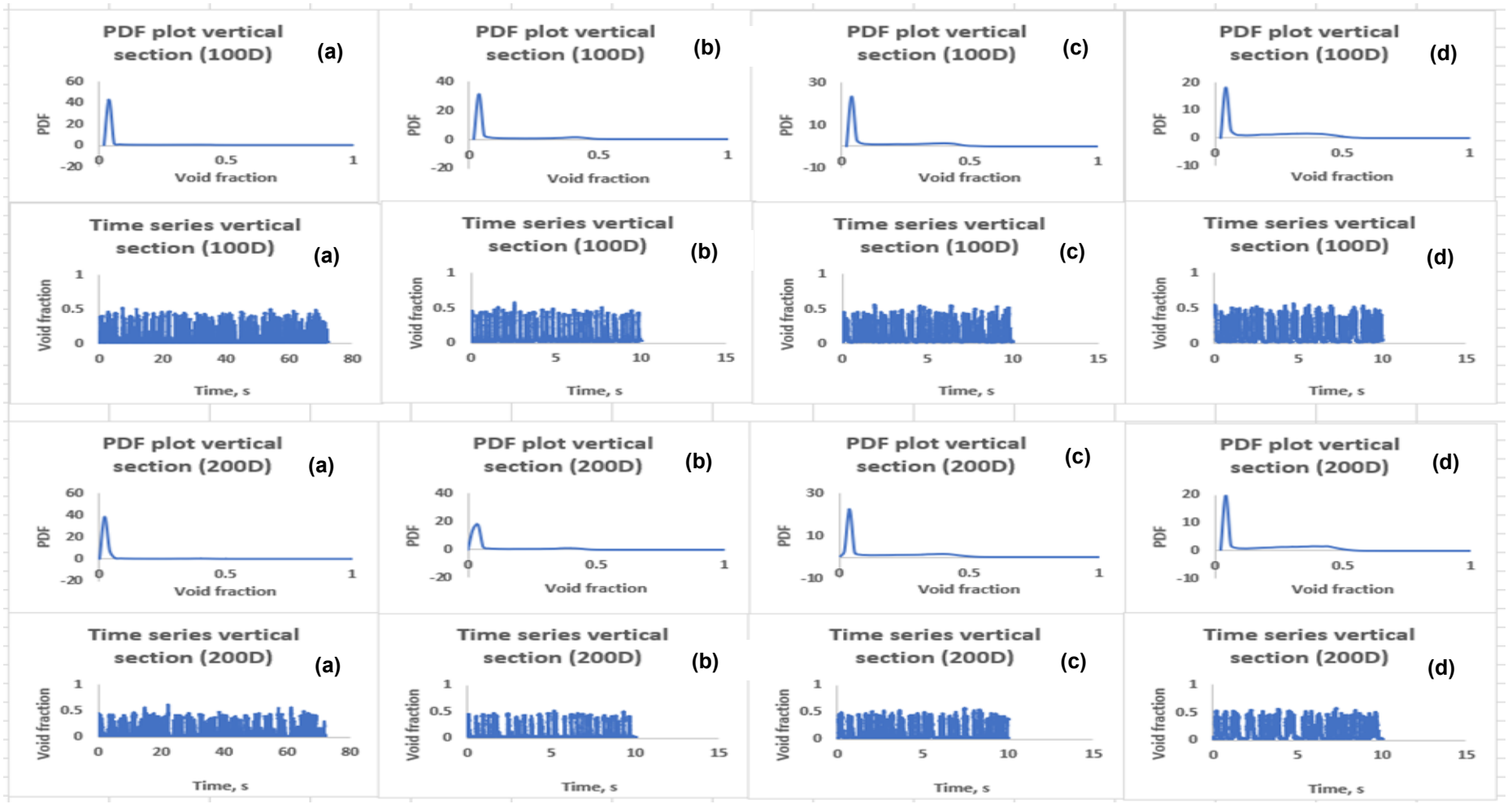

Figure 5-9 PDF and time series plots of stable intermittent flows for 100D and 200D with superficial liquid velocity of 1.3 m/s and superficial gas velocities of (a) 0.14 m/s (b) 0.55 m/s (c) 0.95 m/s and (d) 1.36 m/s.

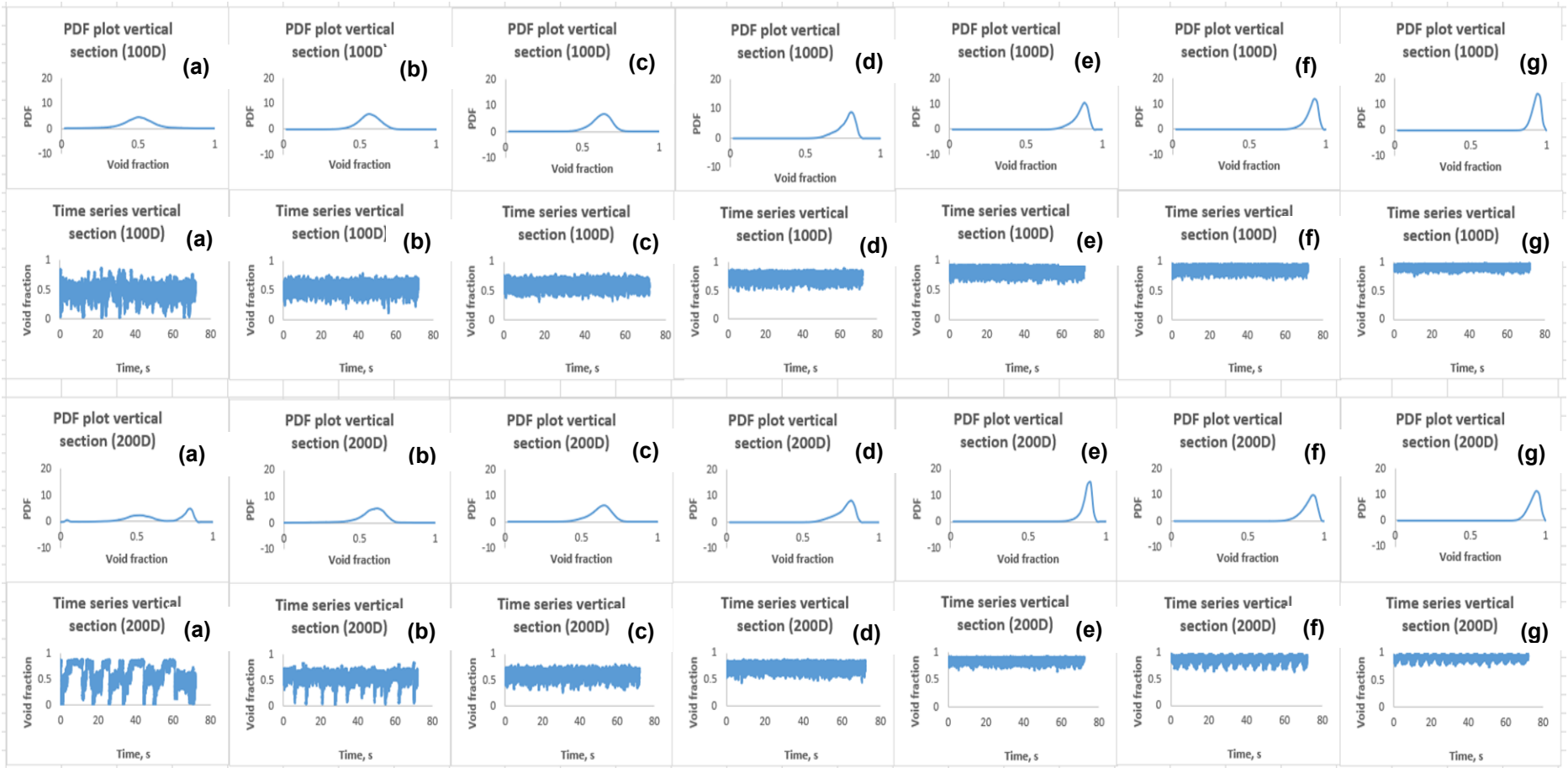

Figure 5-10 PDF and time series PDF and time series plots of separated flows for 100D and 200D with superficial liquid velocity of 0.086 m/s and superficial gas velocities of (a) 2.73 m/s (b) 4.09 m/s (c) 5.45 m/s (d) 10.91 m/s (e) 16.36 m/s (f) 21.81 m/s and (g) 27.26 m/s.

These brief pauses in the flows are due to the low hydraulic force associated with such flows with low superficial velocities. And as a result, the denser fluid will tend to fall back inside the pipe (flow reversal), resulting to increase in liquid accumulation in the pipe. Comparison of Figure 5-8 and Figure 5-10 shows that increase in superficial gas velocity helps to minimize the brief pauses of liquid flow in the vertical section. For flow with superficial liquid velocity of 0.086 m/s, it is noted that this phenomenon disappears when the superficial gas velocity is increased to up to 2.73 m/s. For 200D, higher superficial gas velocity of 4.09 m/s is required to eliminate this brief pause of liquid flow in the vertical section as a result of the longer travel distance of the flow. In gas wells, these brief pauses of liquid flow resulting in liquid accumulation could lead to production problems such as liquid loading due to excess pressure on the sandface. Moreover, such flow phenomenon is not desirable as it may contribute to error in measurement of flow characteristics for such pipe configuration.

5.2 Effect of flow regime development length on void fraction

5.2.1 Effect of flow regime development length on void fraction in horizontal section

The void fraction measurements taken in 100D and 200D development lengths for the same flow conditions with gas and liquid velocities within the range of 0.14 – 27.26 m/s and 0.043 – 1.3 m/s respectively, were analysed and compared. Comparison of the results of void fraction measurements are shown in Figures 5-11 – 5-12.

For flows with low superficial velocities (Figure 5-11), the void fraction for 100D was observed to be higher than that of 200D case for the same flow conditions in horizontal section. This occurrence is due to the higher liquid film accumulation for in 200D development length as highlighted in section 5.1. above. The higher liquid accumulation in the 200D cases lead to reduction in void fraction measurements as compared with the 100D cases. Figure 5-11 shows that the trend of the 100D is almost identical to 200D, suggesting a similar pattern. However, there appear to be slight variation in void fraction measurements in 100D and 200D development lengths, which could be contributed to the unstable nature of the flow.

When the superficial gas velocity was increased to 0.55 m/s, a sharp increase in void fraction was observed generally in Figure 5-11. However, further increase in gas superficial velocity resulted in fluctuation of the void fraction as can be seen in plot 5-11(a). This fluctuation in void fraction reading could be as a result of the effect of the backward flow from the downstream configuration of the flow loop. As a result of the proximity of the sensor to the blind tee, the backward flow due to the obstruction of flow will tend to easily reach the sensor position thereby affecting the sensor reading. The sharp increase in the void fraction reading in Figure 5-11 is as result of the change in flow structure from unstable elongated flow to unstable wavy flow when the superficial gas velocity was increased from 0.14 m/s to 0.55 m/s. Further increase of superficial gas velocity results to unstable intermittent flow pattern (unstable wavy and slug) which are unstable in nature. Therefore, the fluctuation of void fraction observed for such flow regime could be as result of the unstable nature of such flow regime and the backward flow from downstream configuration of the flow loop. When the superficial liquid velocity was increased to 0.086 m/s (Figure 5-11(b)), similar trend (as in Figure 5-11(a)) was observed when the gas superficial velocity was increased to 0.55 m/s. However, the fluctuations witnessed on further increase in superficial gas velocity appear to reduce slightly in Figure 5-11(b). This is due the increase in buoyancy and hydraulic force in the flow loop which helps to lift more fluid through the vertical section, and also counter the backward flow from the downstream configuration.

Although there was slight decrease in void fraction fluctuation in Figure 5-11(b), the combined plot shown in slide c of Figure 5-11, indicates that increase in liquid superficial velocity did not lead to decrease in void fraction generally due to influence of backward flow from downstream pipe configuration on the void fraction measurement. When the superficial gas velocity was increased steadily within the range of 2.73 – 27.26 m/s, the void fraction for 100D and 200D development lengths was also observed to follow similar trend. The variation in void fraction for 100D and 200D was quite minimal as both sets of measurement appear to align especially for the flows with high superficial gas velocities as can be seen from the Figure 5-12 (a) and (b).

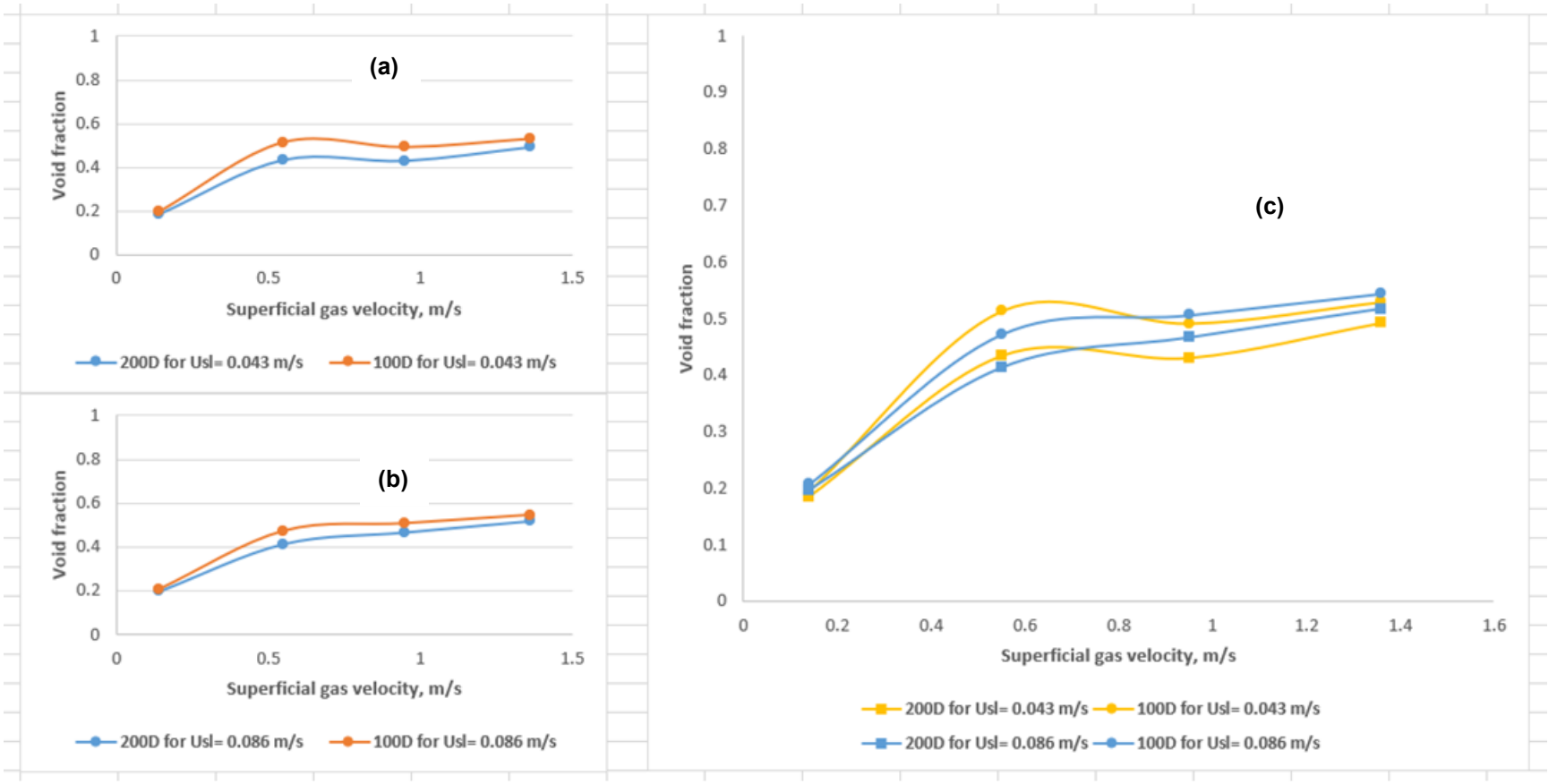

Figure 5-11 Plot of relationship between void fraction and superficial velocities to show the effect of development length on void fraction measurements in horizontal section for flows with low superficial gas velocities of 0.14 - 1.36 m/s and superficial liquid velocities of (a) 0.043 m/s and (b) 0.086 m/s with their combined plot (c).

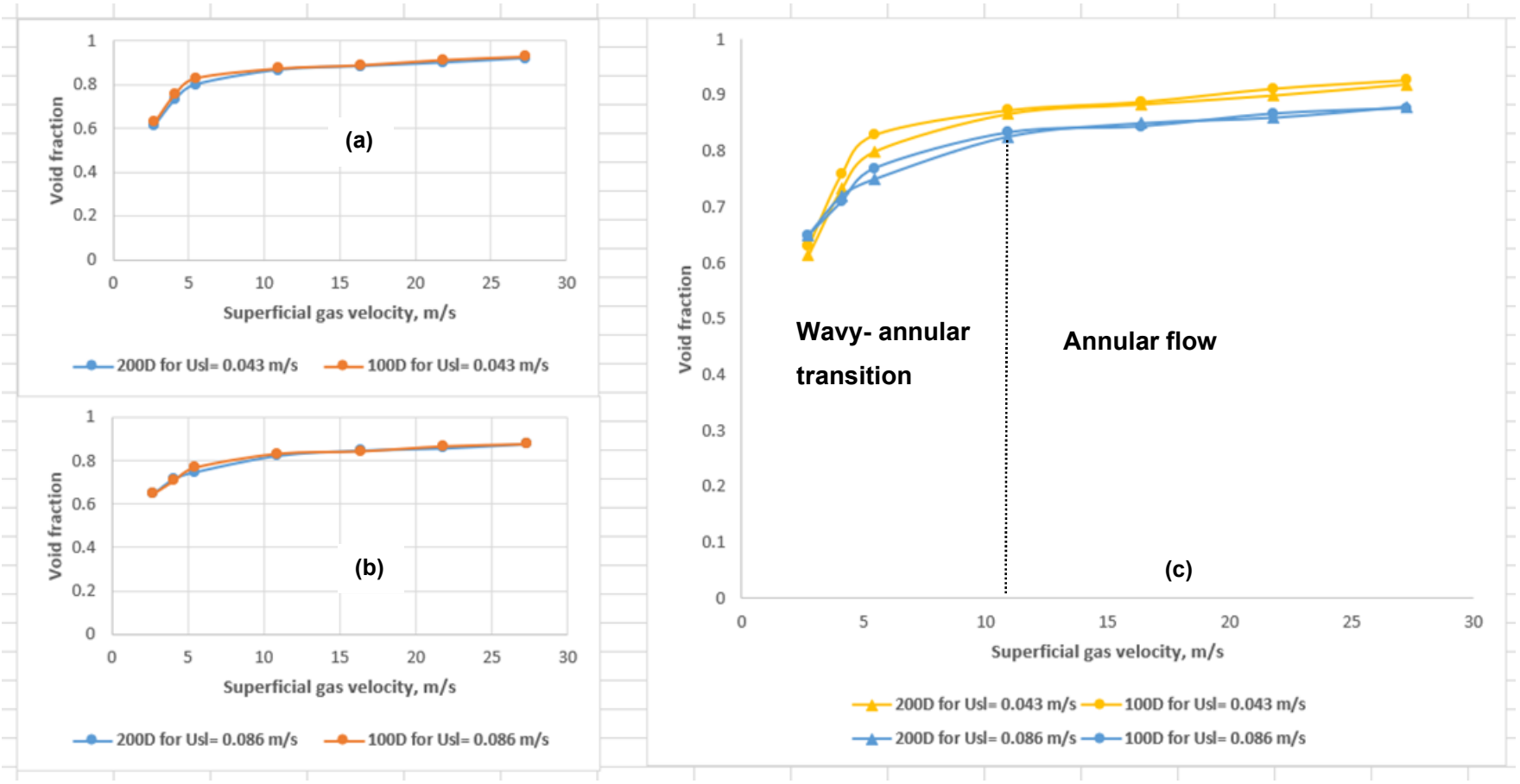

Figure 5-12 Plot of relationship between void fraction and superficial velocities to show the effect of development length on void fraction measurements in horizontal section for flows with superficial gas velocities of 2.73 – 27.26 m/s and superficial liquid velocities of (a) 0.043 m/s and (b) 0.086 m/s with their combined plot in (c).

The sharp increase in void fraction for 100D and 200D seen when the superficial gas velocity was increased to 5.45 m/s is due to change from wavy flow to stratified annular flow regime where the liquid film level was significantly reduced in the horizontal section. When the superficial velocity was increased to 10.91 m/s, annular flow regime was observed to ensue in the pipe. Further increase beyond this superficial gas velocity resulted to only a slight increase in void fraction reading due to the low liquid film level in the pipe. Generally, for flow with high superficial velocity, similar trend and void fraction reading was observed which indicates that the flow is fully developed.

In general, increase in superficial gas velocity leads to increase in average void fraction in the flow loop. The exception to this is for flows with low superficial liquid and gas velocities especially the UWS flow regime in the horizontal section. Due to the low hydraulic force of such flows, and as well as backward flow due to the bottleneck effect from the blind tee, fluctuation in liquid level is observed. This fluctuation in liquid level consequently leads to fluctuation in void fraction measurements. At medium to high superficial gas velocities (2.73 – 27.26 m/s), the backflow from blind tee becomes minimal, and as a result, increase in superficial gas velocity leads to increase in average void fraction in the pipeline. Sharp increase is witnessed when the flow transitions from wavy to stratified-annular flow (from superficial gas velocity of 2.73 m/s to 5.45 m/s). It is observed that the flow begins to transition to annular flow from superficial gas velocity of 5.45 m/s, with gradual increase in average void fraction in the pipe. The flow transitions fully to annular flow at superficial gas velocity of 10.91 m/s. At above this superficial gas velocity, for flows with low superficial liquid velocity (0.043 – 0.086 m/s), only slight increase in void fraction is observed as the flow fully develops to annular flow regime.

5.2.2 Effect of flow regime development length on void fraction in vertical section

The plots of effect of flow regime development length on void fraction in the vertical section is presented in Figures 5-13 and 5-14. For flows with low superficial gas velocity (Figure 5-13), the plots differ slightly with the corresponding plot in Figure 5-11 for horizontal section especially for the flow with superficial liquid velocity of 0.043 m/s. It is noticed that the void fraction increased with the increase in superficial gas

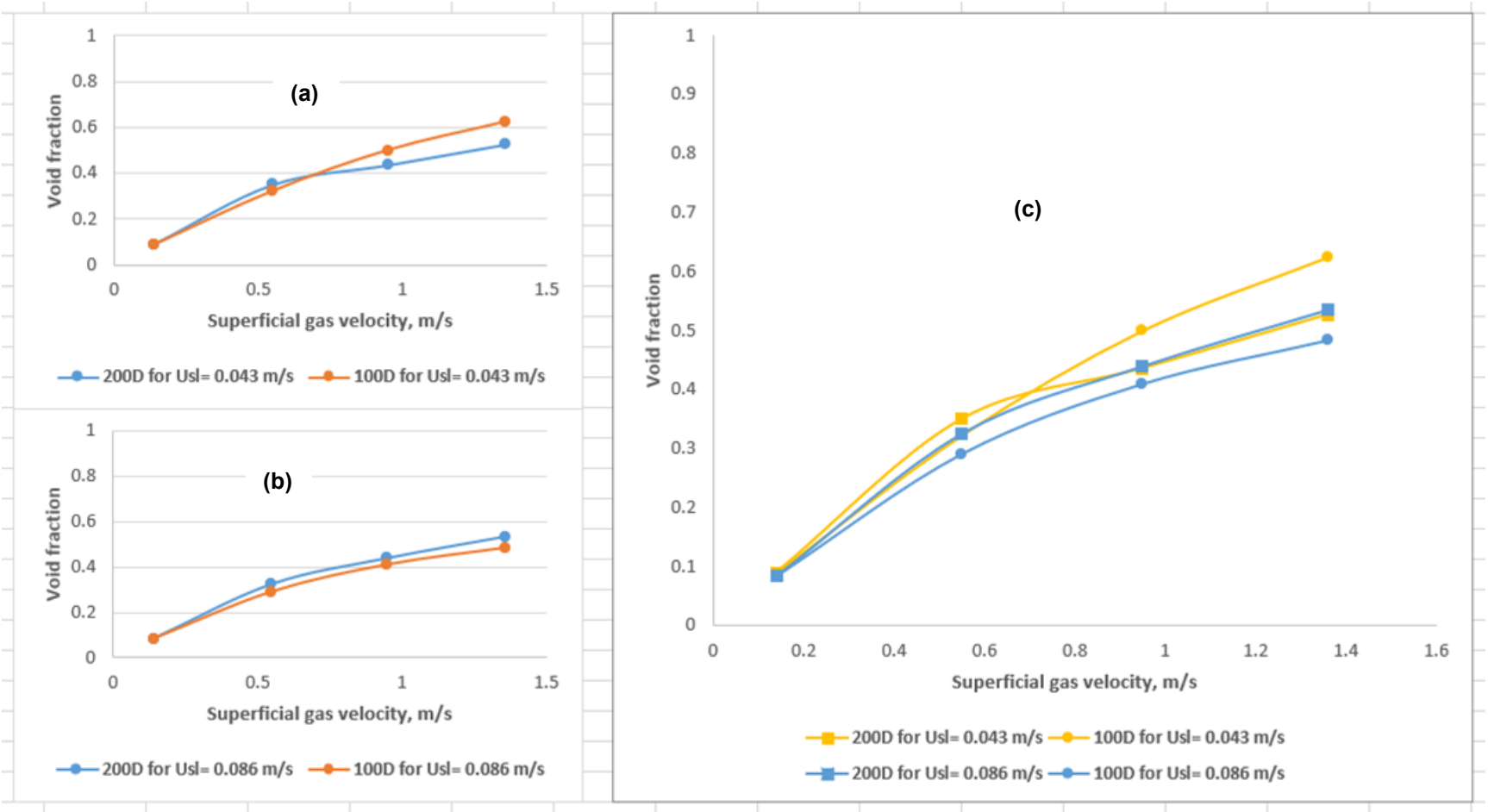

Figure 5-13 Plot of relationship between void fraction and superficial velocities to show the effect of development length on void fraction measurements in vertical section for flows with low superficial gas velocities of 0.14 - 1.36 m/s and superficial liquid velocities of (a) 0.043 m/s and (b) 0.086 m/s with their combined plot in (c).

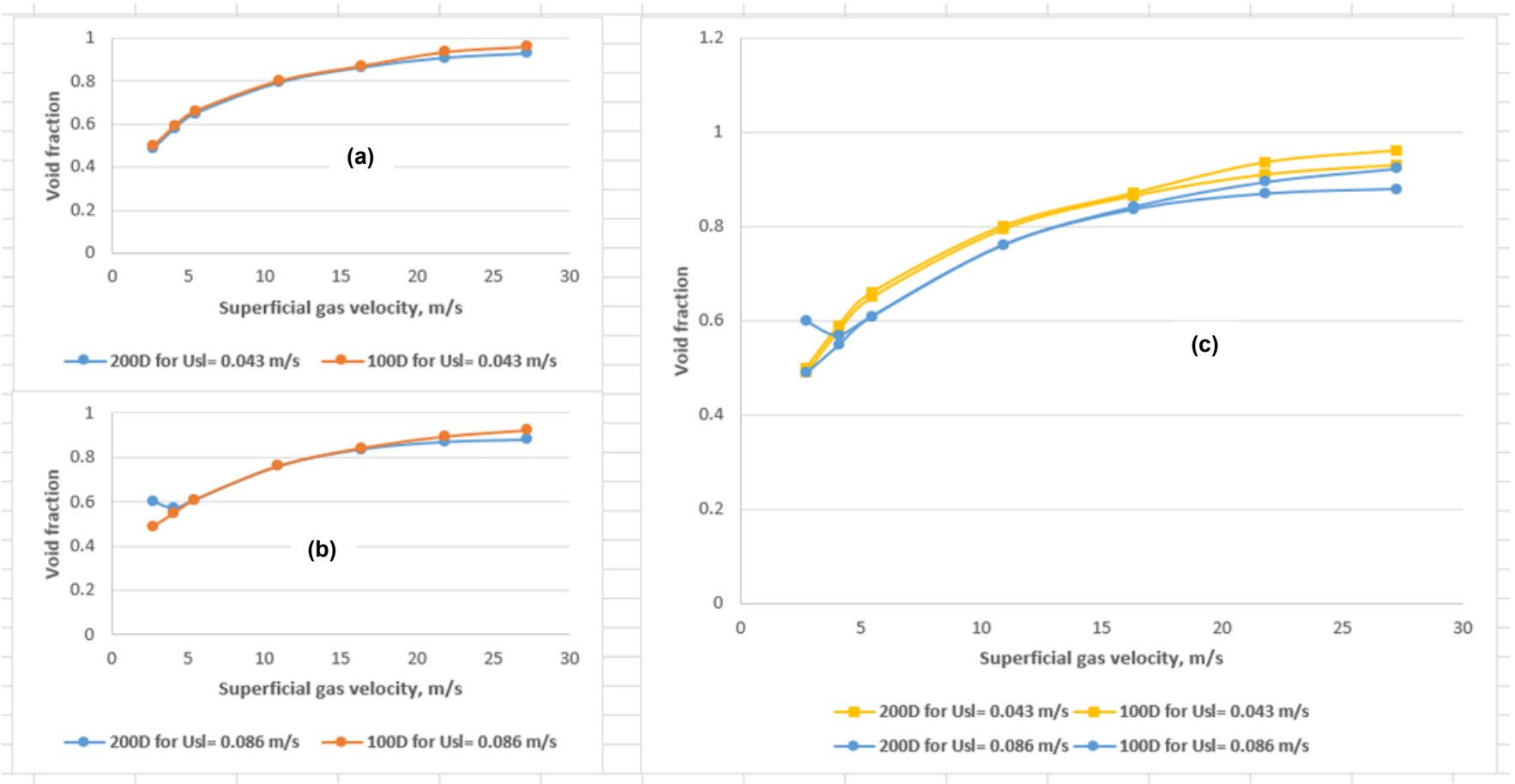

Figure 5-14 Plot of relationship between void fraction and superficial velocities to show the effect of development length on void fraction measurements in vertical section for flows with superficial gas velocities of 2.73 – 27.26 m/s and superficial liquid velocities of (a) 0.043 m/s and (b) 0.086 m/s with their combined plot (c).

velocity for both 100D and 200D development lengths. In Figure 5-13 (a), the void fraction plots tend to misalign at higher superficial gas velocity in the vertical section due to the irregular nature of such flow, shorter development length in vertical section, and the effect of blind tee that disrupts the flow on transitioning to the vertical section. It is noted that with the increase in superficial liquid velocity to 0.086 m/s, the void fraction in the vertical section for 100D and 200D tends to align more due to the increase in the buoyancy of the flow. As mentioned in section 5.1.2, such flows with low superficial velocities are associated with reverse liquid flow, with subsequent momentary pauses in the liquid flow upward of the pipe, which could also have contributed to the slight difference in the void fraction measurement for 100D and 200D in the vertical section.

For flows with medium to high superficial velocities (2.73 – 27.26 m/s), increase in superficial gas velocity leads to increase in void fraction as shown in Figure 5-14. The void fractions for 100D and 200D tends to align better for such flow conditions due the increase in superficial gas velocity. It can be seen in Figure 5-14(a) that a sharp increase in void fraction is witnessed when the superficial gas velocity is increased to 5.45 m/s as more liquid volume is removed from the flow loop. Further increase in superficial gas velocity results to gradual increase in void fraction for the annular flow condition in the vertical section. When the superficial liquid velocity is increased from 0.043 m/s to 0.086 m/s (Figure 5-14b), overall decrease in void fraction is observed.

The void fraction of 100D and 200D development tests tend to align as with the previous case above. However, an initial deviation in void fraction for 100D and 200D is observed when the superficial gas velocity is increased to 4.09 m/s due to transitioning of slug-churn to annular flow regime in 200D development case. As stated earlier in chapter 4 that increase in development length (100D to 200D) enhances wave growth which leads to development of intermittent fllow, hence the variation with the 200D case in vertical section. It is noted for such flow conditions with high superficial gas velocity, the variation in void fraction is observed to be minimal between 100D and 200D development length tests.

5.3 Downstream effect on flow behaviour

The effect of downstream configuration of pipelines on two-phase flow behaviour (i.e., flow regime and void fraction) was investigated by varying the distance of the CR sensor away from the blind tee from 41D to 141D. The PDF and time series plots of void fraction are used in identifying and analysing the flow behaviour. The results of the comparison of two downstream configuration are shown in Figures 5-15 – 5-20. In general, Figure 5-15 shows the transition from unstable elongated flow to a stable wavy flow regime, while in Figure 5-16, a transition from unstable elongated flow to wavy-slug flow regime is observed with the increase in superficial gas velocity. For flows with high superficial gas velocity (Figure 5-17 and Figure 5-18) a gradually transition from stratified-annular flow regime to annular flow regime is witnessed with the increase in superficial gas velocity. The PDF plots in Figure 5-15 show that for flows with low superficial velocities (0.14 – 1.36 m/s and 0.043 – 0.086 m/s for gas and liquid respectively), significant difference was observed in the PDF signature, which indicates a change in flow structure due to downstream effect. For such pipe configuration, flows with low superficial velocities are associated with backflow of liquid, as discussed in section 5.2. The backward flow of the liquid from the blind tee leads to more fluctuation in liquid level in the pipe. Figure 5-15 shows that the further away the sensor is from the blind tee, the less the effect of the downstream configuration on the measurements due to backward flow. The plots in Figure 5-15(a)-(d) indicate that the higher the gas superficial velocity, the less the fluctuation of the liquid level for such flow condition. This shows that the effect of the downstream configuration decreases with the increase in superficial gas velocity. When the superficial liquid velocity was increase to 0.086 m/s (Figure 5-16), more fluctuation was observed due to increase in liquid volume in the pipe, which enhances transition to intermittent flow regime. The fluctuation in the liquid level is observed to decrease when the sensor is moved to 41D to 141D. And like in Figure 5-15, for flows with low superficial velocity, a downstream effect was observed to be prominent. However, the downstream effect tends to decrease slightly with distance away from the blind tee.

For flows with high superficial gas velocity, the effect of downstream configuration is observed to be minimal. No significant fluctuation in liquid level was observed for 41D and 141D as shown in Figures 5-17 and 5-18. As expected, steady increase in superficial gas velocity leads to gradually transition from stratified-annular flow to annular flow regime. The plots of 41D and the corresponding 141D case were observed to be similar, indicating similar flow regime, which in turn shows that downstream configuration of the flow loop had no significant effect on the flow regime development for such flow conditions.

The results of the effect of increase in superficial liquid velocity on flow behaviour for 41D and 141D sensor distance from the blind tee for flows with low and high superficial velocities are shown in Figures 5-19 and 5-20 respectively. In Figures 5-19, the superficial liquid velocity was varied within the range of 0.043 m/s to 1.30 m/s, while the superficial gas velocity was kept constant at 1.36 m/s.

The result shows a gradual transition from UWS flow regime to slug flow regime. Backward flow due to the downstream configuration of the flow loop is shown to have slight effect on flows with low to medium superficial liquid velocity (0.043- 0.170 m/s) at constant superficial gas velocity of 1.36 m/s. More fluctuation of void fraction signal is observed for flows with sensor distance at 41D from the blind tee than that of 141D case. Further increase in superficial liquid velocity resulted to decrease in the effect of the backward flow as the difference in PDF plot signature of 41D and 141D flows becomes less significant.

Figure 5-20 depicts the effect of increase in superficial liquid velocity on downstream effect when the superficial gas velocity was kept constant at 5.45 m/s and the superficial liquid velocity increased steadily from 0.043 to 0.430 m/s. Overall, Figure 5-20 shows the transition from stratified-annular flow regime to a developing slug flow regime, with the fluctuation of the gas-liquid interphase level increasing with the increase in superficial liquid velocity.

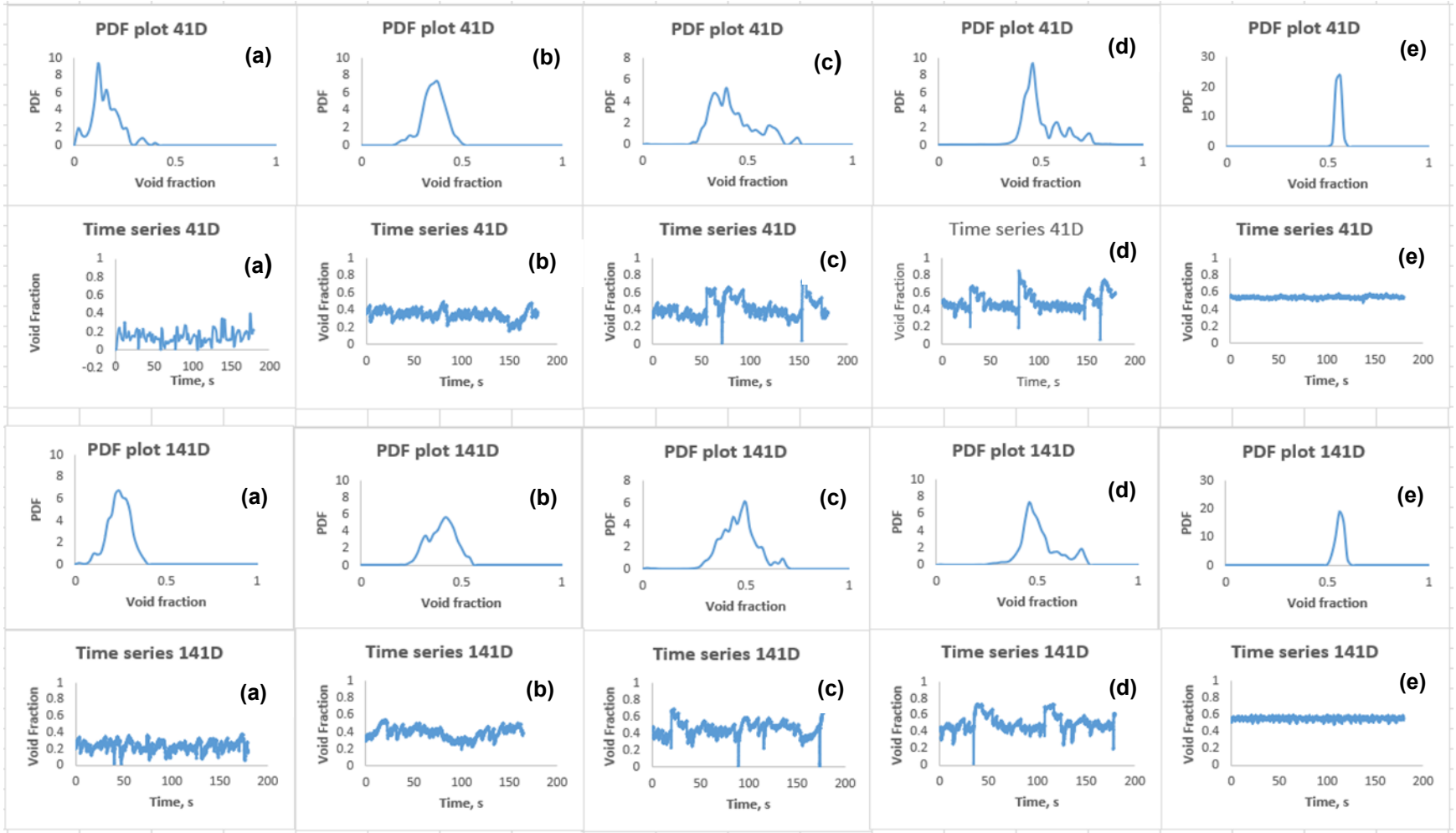

Figure 5-15. PDF and time series plots for flows with superficial liquid velocity of 0.043 m/s and superficial gas velocities of (a) 0.14 m/s (b) 0.55 m/s (c) 0.95 m/s (d) 1.36 m/s and (e) 2.73 m/s with sensor distance of 41D and 141D away from the blind tee.

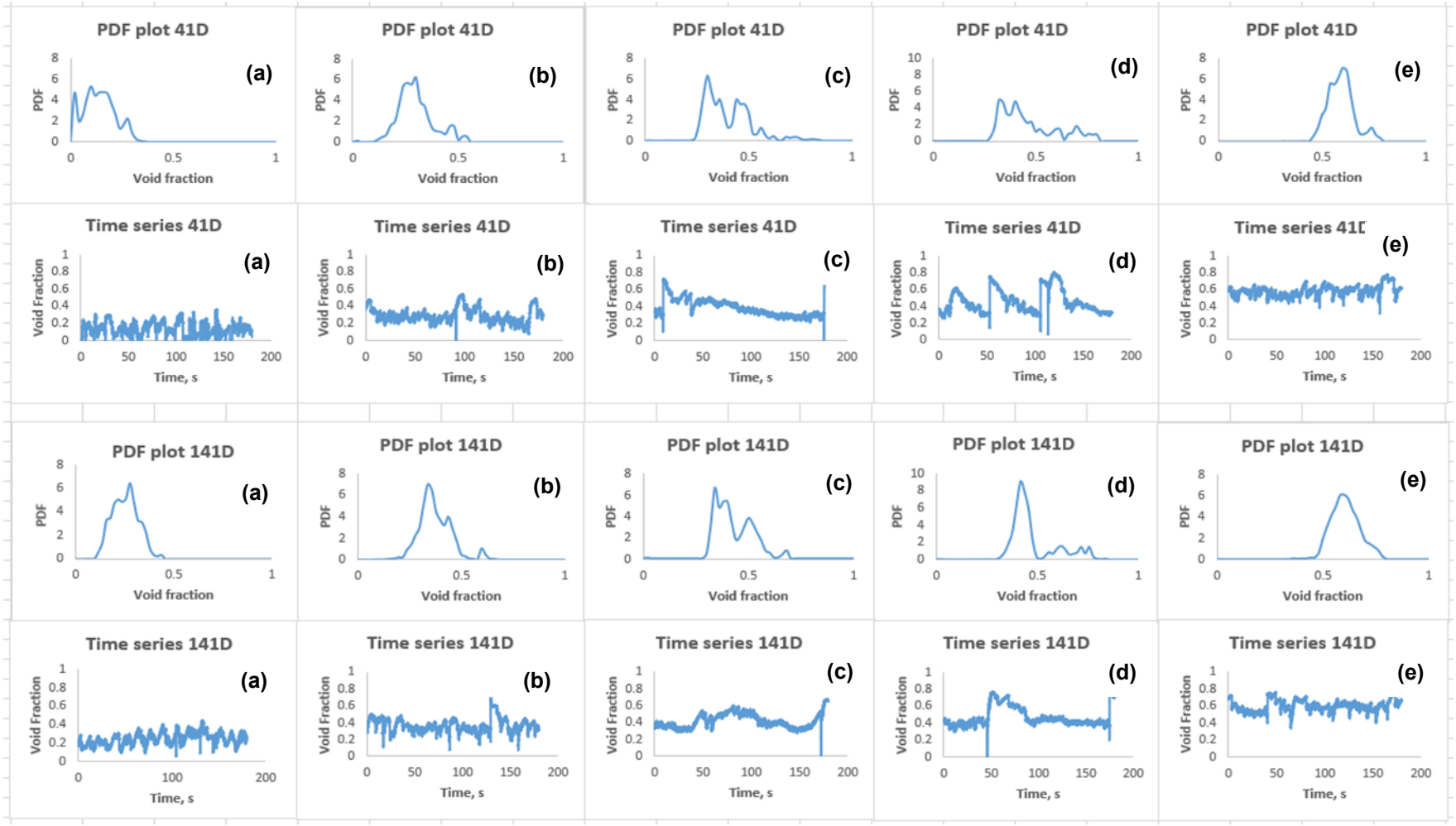

Figure 5-16. PDF and time series plots for flows with superficial liquid velocity of 0.086 m/s and superficial gas velocities of (a) 0.14 m/s (b) 0.55 m/s (c) 0.95 m/s (d) 1.36 m/s and (e) 2.73 m/s with sensor distance of 41D and 141D away from the blind tee.

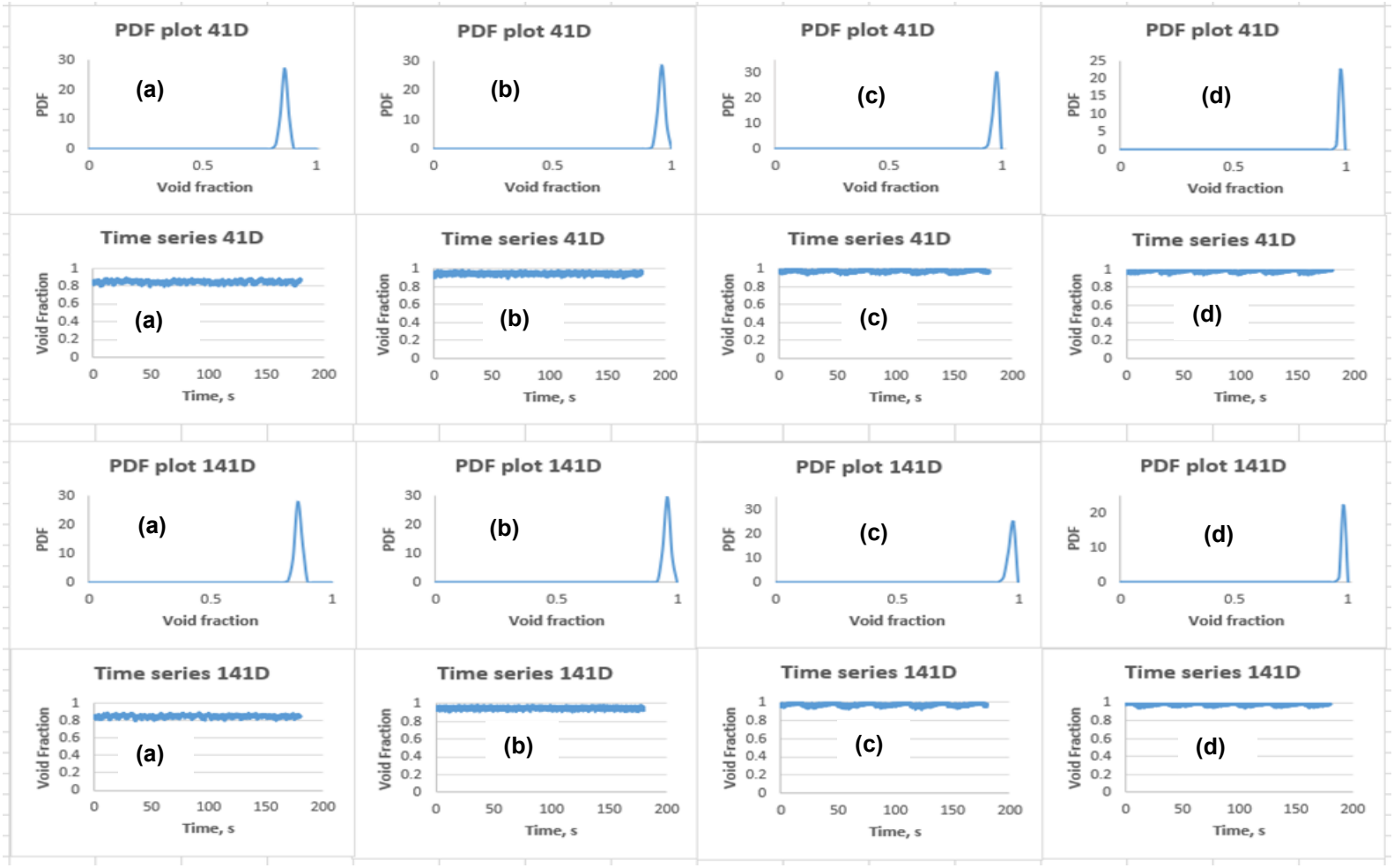

Figure 5-17. PDF and time series plots for flows with superficial liquid velocity of 0.043 m/s and superficial gas velocities of (a) 5.45 m/s (b) 10.91 m/s (c) 21.81 m/s and (d) 27.26 m/s with sensor distance of 41D and 141D away from the blind tee.

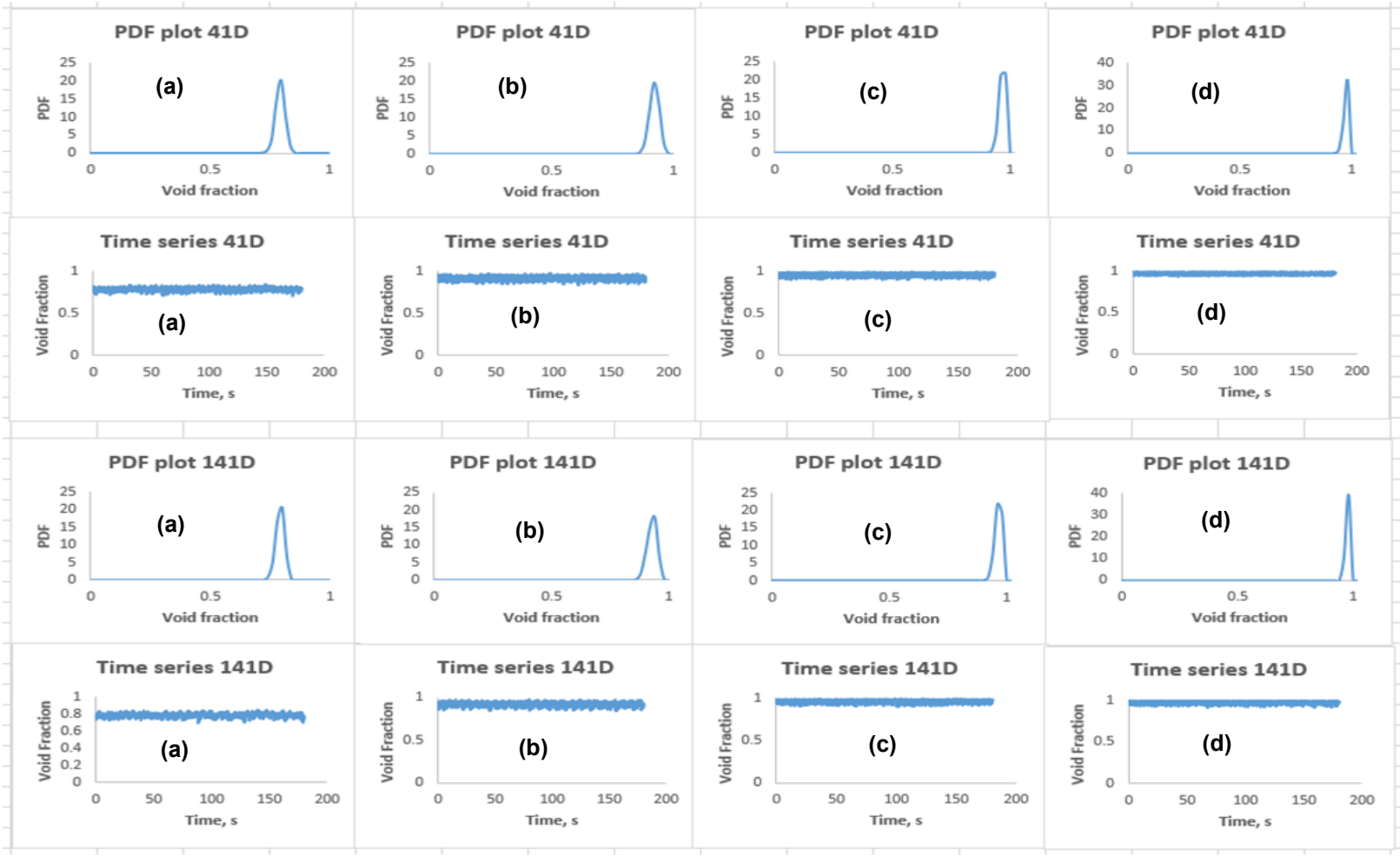

Figure 5-18. PDF and time series plots for flows with superficial liquid velocity of 0.086 m/s and superficial gas velocities of (a) 5.45 m/s (b) 10.91 m/s (c) 21.81 m/s and (d) 27.26 m/s with sensor distance of 41D and 141D away from the blind tee.

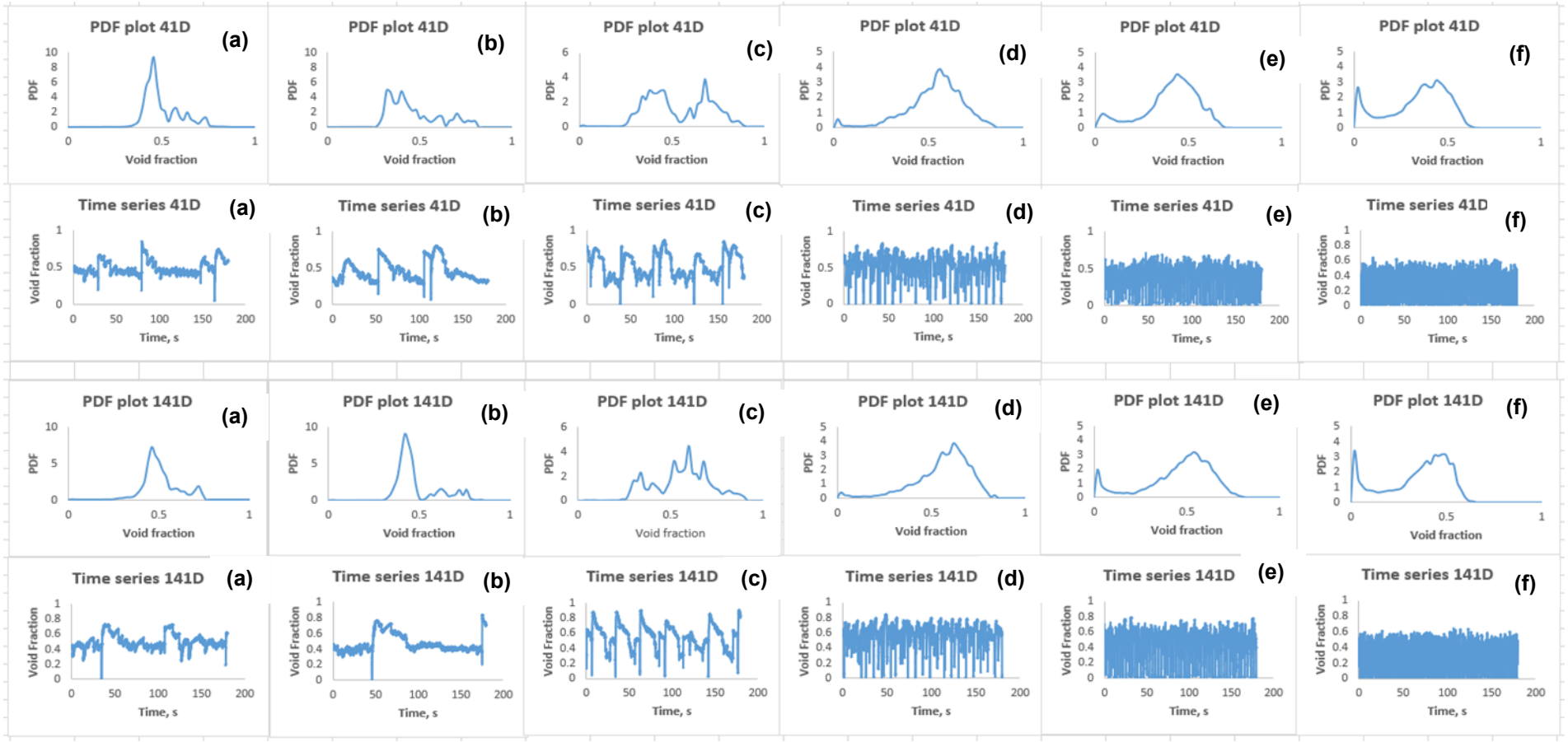

Figure 5-19 PDF and time series plots of flows with superficial gas velocity of 1.36 m/s and superficial liquid velocities of (a) 0.043 m/s (b) 0.086 m/s (c) 0.17 m/s (d) 0.43 m/s (e) 0.86 m/s and (f) 1.3 m/s with sensor distance of 41D and 141D from the blind tee.

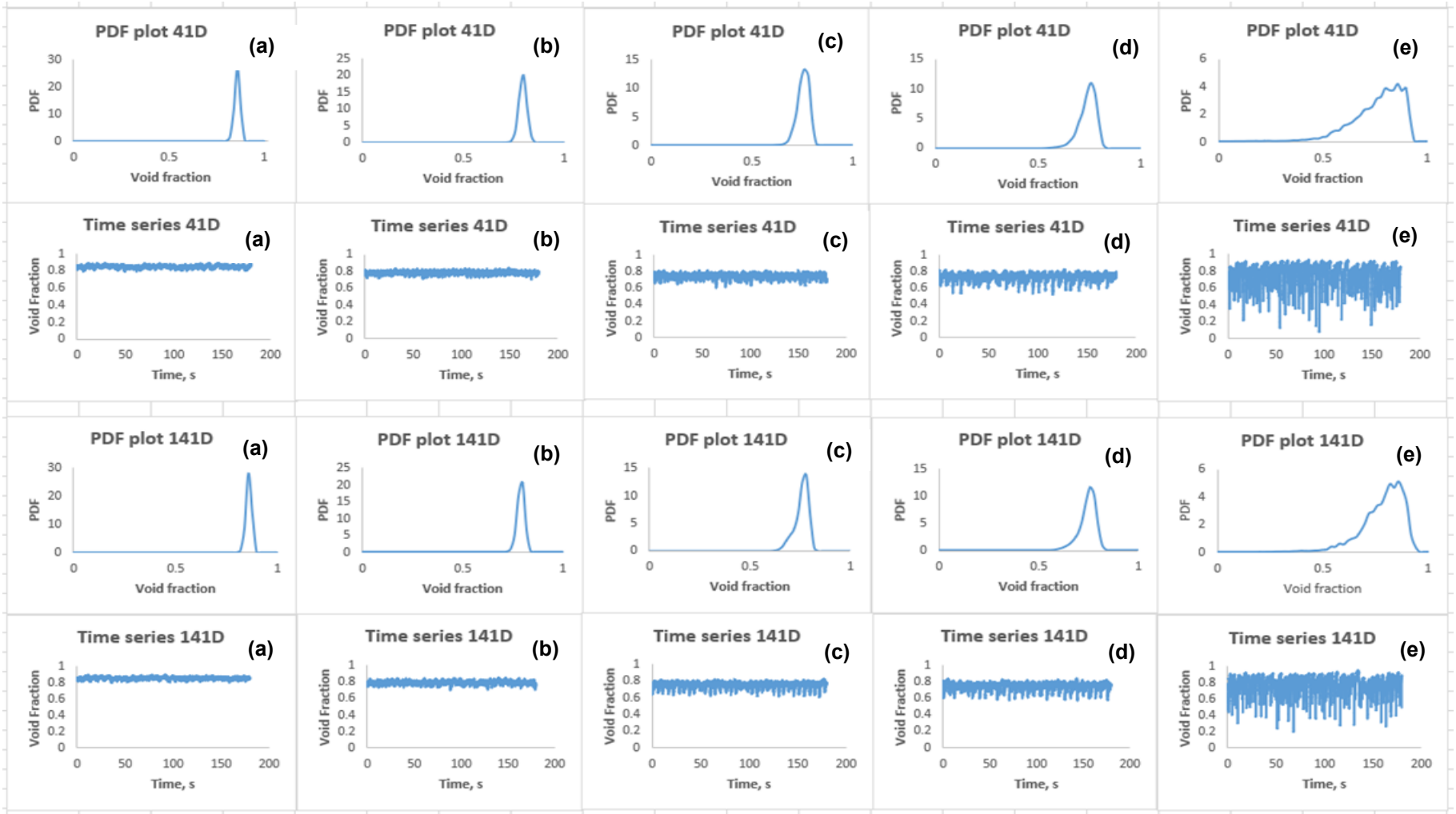

Figure 5-20. PDF and time series plots for flows with superficial gas velocity of 5.45 m/s and superficial liquid velocities of (a) 0.043 m/s (b) 0.086 m/s (c) 0.13 m/s (d) 0.17 m/s and (e) 0.43 m/s with sensor distance of 41D and 141D away from the blind tee.

The peak of the PDF plot at high void fraction region is observed to decrease with the increase in superficial liquid velocity (Figure 5-20), as the liquid volume increases steadily. The corresponding time series plots also show a gradual decrease in the average void fraction with the increase in superficial liquid velocity except for Figure 5-20 (d) and (e) where the flow transitioned to slug flow regime. For such flow conditions with relatively high superficial gas velocity, difference in the flow structure for flows with sensor distance of 41D and 141D from the blind tee was observed to be minimal when the liquid superficial velocity is increased gradually.

Comparison of the flows with the sensor at 41D and 141D distance away from the blind tee indicate that at high superficial gas velocity, increasing the superficial liquid velocity of the flow will not have significant effect on backward flow from the blind tee. However, at low superficial gas velocity, increasing superficial liquid velocity will result to slight impact on flow structure of the 41D cases especially for flows with low to medium superficial liquid velocities.

Downstream effect on void fraction

The result of the downstream configuration on void fraction measurement is presented in Figures 5-21 – 5-22 in order to highlight the influence of superficial gas velocity. For flows with low superficial velocities (0.14 – 1.36 m/s and 0.043 – 0.086 m/s for gas and liquid respectively) the void fraction is observed to be generally higher for 141D case as compared to the 41D case as shown in Figures 5-21. This could be contributed to less effect of the backward flow of liquid with distance of the sensor away from the blind tee. When the superficial gas velocity is increased to 1.36 m/s, the difference in void fraction for 41D and 141D appears to be insignificant as the two plots tends to align. However, for increase in superficial liquid velocity to 0.086 m/s, the difference in void fraction for 14D and 141D tends to be slightly higher generally due to higher fluctuation in liquid level in the pipe. It could also be seen from Figure 5-21 that the difference in void fraction of 41D and 141D decreases with increase in superficial gas velocity for such flow condition.

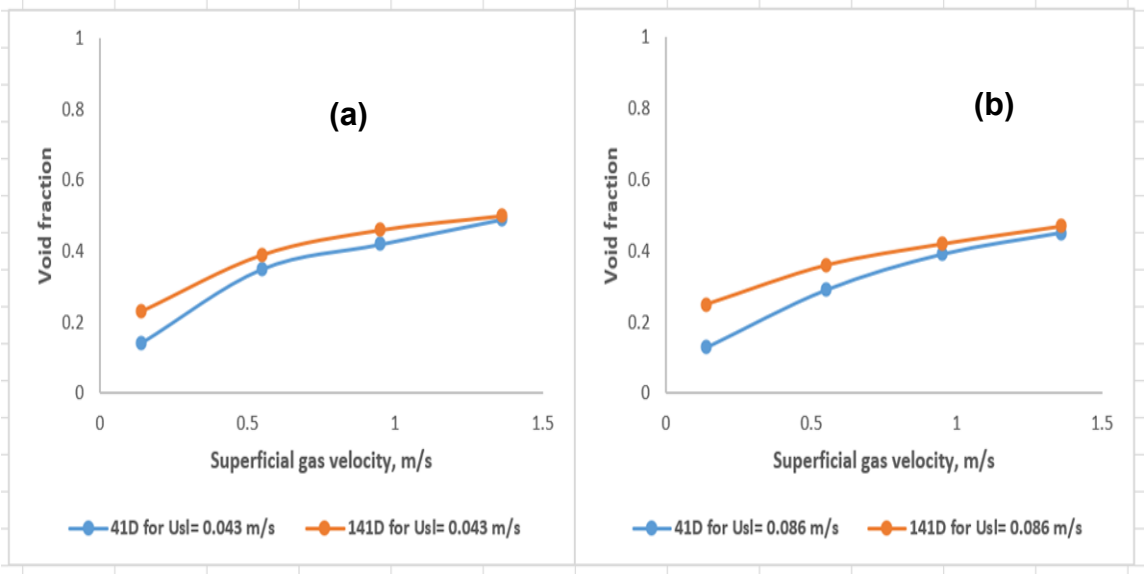

Figure 5-21 Plot of relationship between void fraction and superficial gas velocity to the show downstream effect on void fraction measurement in horizontal section for flows with superficial gas velocities of 0.14 – 1.36 m/s and superficial liquid velocities of (a) 0.043 m/s and (b) 0.086 m/s.

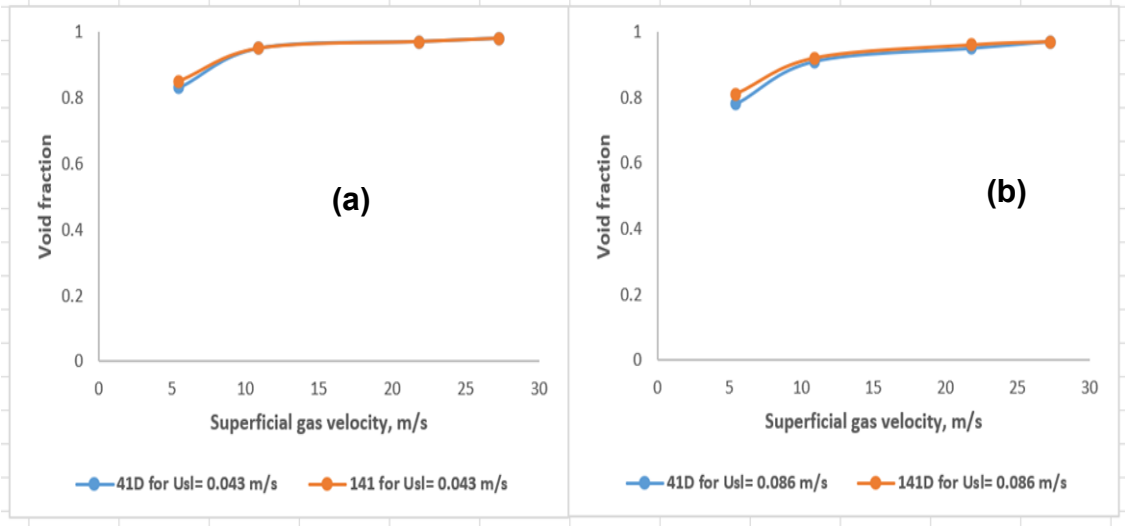

Figure 5-22 Plot of relationship between void fraction and superficial gas velocity to the show downstream effect on void fraction measurement in horizontal section for flows with superficial gas velocities of 5.45 – 27.26 m/s and superficial liquid velocities of (a) 0.043 m/s and (b) 0.086 m/s.

For flows with high superficial gas velocity (Figure 5-18), the void fraction is observed to be slightly higher for 141D as compared to 41D case for superficial gas velocity of 5.45 m/s. However, further increase in superficial gas velocity

resulted to no significance difference in void fraction measurements for 41D and 141D cases.

In general, it was observed that the void fraction was higher in 141D case as compared with the corresponding 41D. This suggests that the void fraction increases with distance away from the blind tee. This could be attributed to backward flow as a result of the effect of downstream configuration being more pronounced in proximity with the sensor especially for flows with low superficial gas velocity.

A comparison of the of the void fraction measurements from WMS and CR sensor placed at different positions (18D and 41D, 141D) from the blind tee in the horizontal section show that the backward flow leads to erratic reading in the WMS than CR sensor. It could be seen from the graph in Figure 5-11 that the void fraction did not increase statistically (in magnitude) with the increase in superficial gas velocity. For CR sensor in Figure 5-21, the void fraction is witnessed to increase with the increase in superficial gas velocity, which is an indication that backward flow is less pronounced, and no erratic reading of void fraction is observed at such sensor positions. Based on the observation above, it is noted that the sensor placement position of the WMS is affected significantly by the disturbance of the downstream configuration which causes the erratic reading for flows with low superficial velocities. It is therefore recommended that measurement sensors for multiphase flow should be placed more than 18D away from the blind tee to minimize disturbance from connection (blind tee) joint for such pipe configuration.

5.4 Chapter summary

The key findings covered in this chapter are as follows:

- Flow regime development was studied using two development lengths of 100D and 200D for flows with low superficial velocity, intermittent flows, and separated flows.
- Analyses of the PDF and time series plots indicate that liquid accumulation in the horizontal pipe increases with the increase in flow

regime development length. For flows with longer development length for the same flow condition, the reduced hydraulic force will result to less fluid being pushed out through the vertical section, and hence more liquid accumulation in the pipe.

- The liquid accumulation was observed to decrease with the increase in superficial gas velocity.
- The average void fraction was observed to generally decrease with the increase in flow regime development length as result of more liquid accumulation in the horizontal section.
- The void fraction plots show that the 100D and 200D measurements tend to align better in horizontal section than in vertical section due to the mixing effect of the blind tee and the shorter development in the vertical section.
- Analyses of the PDF and time series plots show similar flow pattern for 100D and 200D development lengths. This indicates that 100D length is sufficient for flow regime development as no significant change in flow pattern was observed for 100D and 200D development in the horizontal section.
- Downstream effect on flow behaviour was studied by placing the CR sensor at 41D and 141D away from the blind tee section.
- Downstream effect on two-phase flow behaviour was observed to be significant for flows with low superficial velocities, with this effect becoming less pronounced for flows with high superficial gas velocities (5.45 – 27.26 m/s).
- The void fraction was observed to increase with sensor distance away from the blind tee region, because of less effect of the backward flow with distance away from the blind tee section.

6 EFFECT OF BLIND TEE LENGTH ON PRESSURE FLUCTUATION

Pressure fluctuation abounds in many industrial process systems. Pressure fluctuation is undesirable for some of these industries as it leads to increase in measurement error, noise, structural vibration, wears or even total damage of pipeline parts (Kim, 1989). The understanding of the nature of pressure fluctuation is necessary to minimize or eliminate these problems. Different authors have investigated pressure fluctuations in straight pipes (Blake, 1970; Corcos, 1965; Kraichnan, 1956; Schewe, 1983; Willmarth, 1975). For multiphase flow, the four sources of pressure fluctuation include temporal change in average void fraction, difference in the convected pressure field surrounding a bubble in motion, turbulence produced from the wake of a bubble, and background turbulence in a continuous phase (Samways, 1992).

Fluctuating forces caused by internal two-phase flow in bends and tee pipe junctions have not been widely investigated. Most connections such as bends, elbows and tees used for changing fluid flow direction are often exposed to excitation forces (Riverin et al., 2006). One of the earliest work on this topic was conducted by Yih & Griffith (1968) for air-water two-phase flow in nuclear system, where the authors observed that internal fluctuating forces are proportional to the load induced by the steady component of the flow. These forces were correlated to the time variation of the fluid entering the pipe using momentum balance. Spectral analyses showed that dominant frequency emerged which was considered as rather too low in comparison with those usually associated with piping system. However, in the field of chemical and petroleum engineering, two-phase slug flow has shown that the measured forces are closely related to the dynamics of the slugs. The effect of liquid viscosity and liquid surface tension was noticed to be insignificant on pressure fluctuation in pipe connections (Tay & Thorpe, 2004; Tay & Thorpe, 2014). The magnitude of the forces may also be related to the local fluctuation of the void density (Riverin et al., 2006). Davis (1973) performed experimental studies on co-current upward two-phase gas-liquid flow in a small diameter pipe (0.019 m).

The result of the measurements of unsteady wall-pressure fluctuation showed, the strong attenuation of incidental disturbances by the flow, the generation of pressure fluctuations by the turbulence of the mixture, and the propagation of pressure disturbances associated with flow. The experiment however was restricted to low turbulent flow (mixture velocity < 5 m/s).

The blind tee length effect on pressure fluctuation in pipe is studied by using a blind tee junction of insertable blanks for different blind tee lengths of 2D, 1D and 0D (Figure 3-7). In this section, effect of blind tee length on pressure fluctuation along the flow loop and inside the blind tee are analysed. The pressure fluctuation is obtained by dividing the measured static pressure by the standard deviation of the static pressure measurements. The times series of the pressures in the flow loop with different blind tee lengths are presented in Appendix C. The standard deviation of the pressures is expressed as

$$SD = \sqrt{\frac{1}{n-1}\sum_{i=1}^{n}(x-\overline{x})^2} \quad \textbf{(6-1)}$$

where SD is the standard deviation; n is the total number of measurements in the data set; x is the i^{th} value in the data distribution, and $\overline{x}$ is the mean of the sample of the data set.

The pressure fluctuation along the flow loop is acquired using a total of five pressure transducers, P1- P5 (shown in Figure 3-8). Three pressure transducers, P1, P2, and P3 are placed at 28D, 78D, and 128D upstream of the blind tee, respectively. Additionally, two pressure transducers, P4 and P5 are located at 3.3D, and 20.4D downstream of the blind tee on the vertical section. The three blind tee lengths (0D, 1D and 2D) depicted in Figure 3.7, were tested under the same flow conditions and the pressure fluctuation then compared inside the blind tee and along the flow loop.

6.1 Pressure fluctuation in blind tee

When air-water two-phase flow transitions through the blind tee, the flow pattern becomes complicated due to the obstructions created by the blind tee's

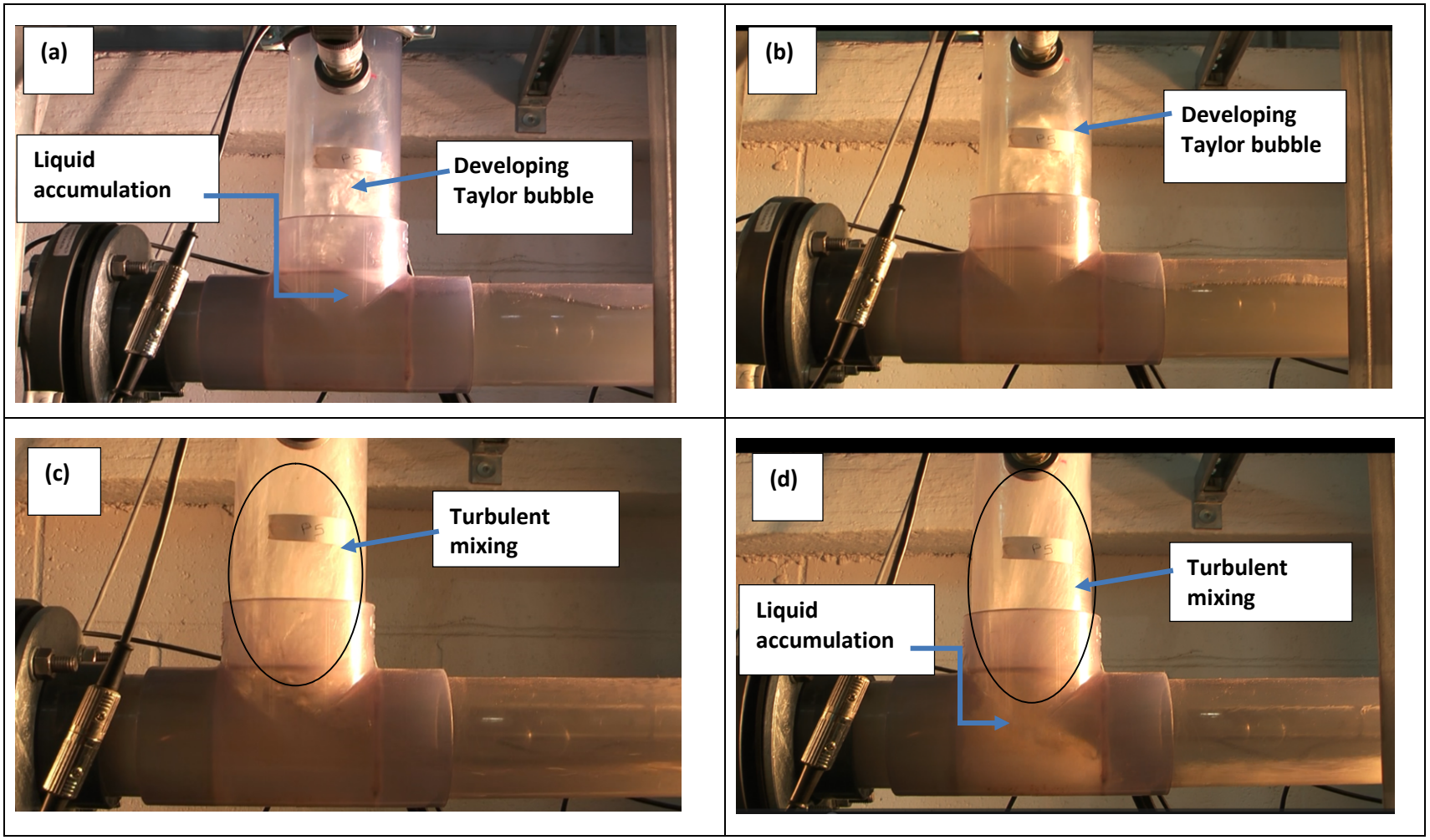

Figure 6-1 Photos of flows transitioning through the blind tee into the vertical section for flow with superficial gas and liquid velocities of (a) 0.14 m/s and 0.043 m/s (b) 0.55 m/s and 0.043 m/s (c) 5.45 m/s and 0.043 m/s and (d) 10.91 m/s and 0.043 m/s.

dead end (blanked off end of the horizontal section). As shown in Chapter 4, (Figures 4-17 and 4-18), that the bubble deformation and breakages are observed as the flow transitions through the blind tee into the vertical section are as result of effect of blind tee on hydrodynamic characteristics of the flow. In the blind tee, the net effect of centrifugal and gravitational force results to the lighter phase (air) being pushed to the inward of the pipe, while the heavier fluid (water) settles in the outward of the pipe. In the blind tee, significant air bubbles may be entrained in liquid that accumulates inside the blind tee. The liquid with some of the entrained air is circulated in the blind tee region depending on flow condition (superficial velocities of the gas and liquid). Flow circulation and vortices are produced in the blind tee as the incoming flow hits the dead-end of the blind tee or pipe wall (outward part), which consequently affect transitioning flow in the vertical section. The swirling motion of the flow generated in the blind tee region, enhances the turbulent mixing of the flow as it transitions into the vertical section.

For flows with low superficial velocities, the swirling effect from the blind tee is less pronounced as can be seen in Figure 6-1 (a) – (b). This is because the velocity of the flow is not high enough to displace most of the liquid that accumulates in the blind tee end. The high liquid accumulation in the blind tee acts as liquid cushion for part of the slow-moving gas bubbles to transition quickly into the vertical section without mixing or deforming significantly inside the blind tee. For flows with relatively high superficial gas velocities in Figures 6-1 (c) – (d), turbulent mixing of the flow is witnessed due to the swirling motion and turbulence generated in the blind tee. The relative high velocity of the flow displaces some of the liquid accumulation and reduces the liquid level in the blind tee as more incoming flow penetrates inside the blind tee. In general, increase in superficial gas velocity leads to decrease in the liquid level accumulation inside the blind, and consequently better mixing of the flow on transitioning to the vertical section.

The results of the analyses of pressure fluctuation inside the blind tee for different blind tee lengths of 0D, 1D and 2D are shown in Figures 6-2 – 6-7. The

tests, performed on the three blind tee lengths are grouped into intermittent and separated flows. The intermittent flows were tested with superficial liquid and gas velocities of 0.043 – 1.3 m/s and 0.14 – 1.36 m/s respectively. For separated flows, the superficial velocities were varied in the range of 0.043 – 0.086 m/s and 0.14 – 27.26 m/s for liquid and gas, respectively. The results for the intermittent flows are shown in the chart in Figure 6-2. For flows with low superficial liquid velocity, the overall magnitude of the pressure fluctuation was observed to increase generally, with the increase in gas superficial velocity. When the liquid superficial velocity is increased to 0.86 m/s, the magnitude of the pressure fluctuation is observed to show initial decrease with the increase in superficial gas velocity from 0.14 m/s to 0.55 m/s. The pressure fluctuation increased only slightly when the superficial gas velocity increased to 1.36 m/s. On further increase to high superficial liquid velocity of 1.3 m/s, initial decrease in pressure fluctuation was observed, which then increased gradually with the increase in superficial gas velocity as shown in Figure 6-2. The initial decrease in pressure fluctuation observed is due to the flow transition from elongated bubble to slug flow regime.

In Figure 6-2, the effect of blind tee length can be observed to generally decrease with increase in superficial gas velocity. The blind tee length of 2D is observed to have the least of pressure fluctuation while 0D has highest pressure fluctuation as can be seen in Figure 6-2. In general, the influence of the blind tee length is prominent for flows with very low superficial gas velocity (Usg= 0.14 – 0.55 m/s).

For separated flows, the increase in gas superficial velocity is shown to have weak effect on pressure fluctuation in blind tee as shown in Figure 6-3. Increase in superficial liquid velocity to 0.086 m/s is observed to increase the pressure fluctuation slightly in blind tee. Similar trend is also witnessed when the superficial liquid velocity is increased to 0.13 m/s, with the pressure fluctuation decreasing slightly with increase in superficial gas velocity. Furthermore, the effect of blind tee length is witnessed to be insignificant for such flow as no

major change in observed in magnitude of pressure fluctuation for the three blind tee lengths.

Comparison of the intermittent and separated flows shows that the magnitude of the pressure fluctuation is remarkably higher for intermittent flow due to the alternating nature of the flow structure. In general, the effect of the blind tee length on pressure fluctuation is observed to be more pronounced for flows with low superficial velocities.

The results of the effect of blind tee length on pressure fluctuation with the increase from low to high superficial gas velocities are shown in Figures 6-4 and 6-5. The liquid superficial velocity was varied from 0.043 m/s to 0.086 m/s for superficial gas velocities of 0.14 m/s – 27.26 m/s in Figure 6-3. Similar trend is observed for both flows with constant superficial liquid velocities of 0.043 m/s and 0.086 m/s.

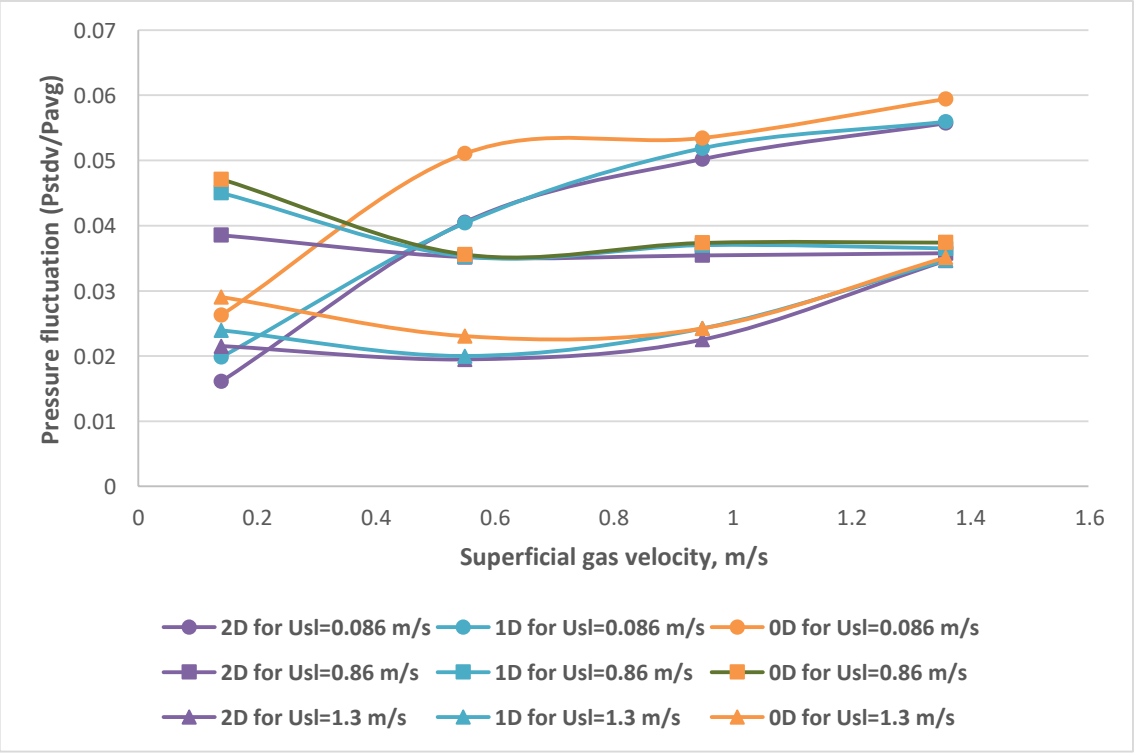

Figure 6-2 Effect of blind tee lengths (0D, 1D, and 2D) on pressure fluctuations in blind tee with increase in superficial gas velocity for intermittent flows.

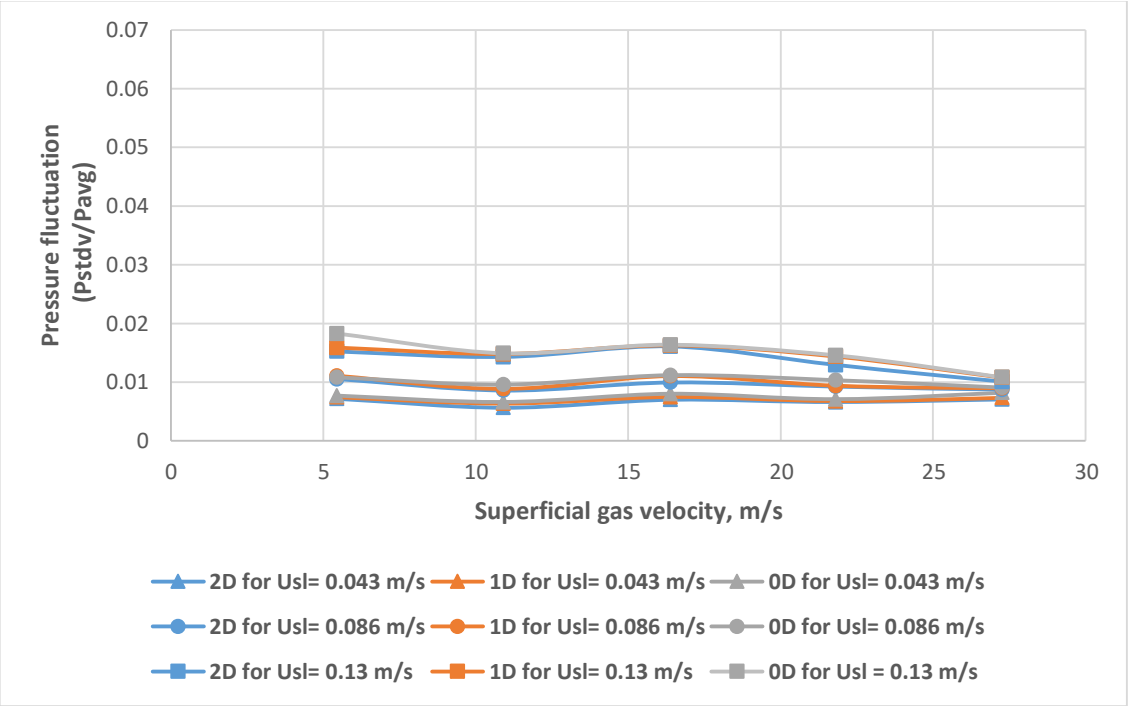

Figure 6-3 Effect of blind tee lengths (0D, 1D, and 2D) on pressure fluctuations in blind tee with increase in superficial gas velocity for separated flows.

For flows with constant liquid velocity of 0.043 m/s, an initial increase in pressure fluctuation is observed with the increase in gas superficial velocity to 0.55 m/s. The initial increase in pressure fluctuation observed, could be attributed to the change in flow structure from unstable elongated flow pattern to unstable slug flow pattern. For such flow conditions, increase in the superficial gas velocity results higher pressure fluctuation due to the chaotic and intermittent nature of such flow. The pressure fluctuation then reduced sharply with the gradual increase in superficial gas velocity from 0.55 m/s to 2.73 m/s. For such flow conditions, the decrease in the pressure fluctuation with the increase in superficial gas velocity is because of the flow transition from unstable slug flow regime to stratified-annular flow regime. The increase in superficial gas velocity leads to less liquid volume in the pipe and a transition to a more stable separated flow. Further gradual increase in gas superficial velocity from 2.73 m/s to 27.26 m/s results to no significant change in pressure fluctuation as the pressure fluctuation remained fairly stable. This could be ascribed to the nature of the flow – annular flow. The steady increase to a high

superficial gas velocity resulted to annular flow regime, in which the gas phase occupies the core of the pipe. For such flow regime, the morphology of the flow structure is fairly constant along the pipe, with no intermittency in the flow structure, hence less pressure fluctuation. The graph shows that annular flow regime has the lowest pressure fluctuation in the pipe. For the flow with increased superficial liquid velocity to 0.086 m/s, initial increase in pressure fluctuation was observed when the superficial gas velocity was increased 0.95 m/s. The increase in pressure fluctuation is as a result of the transition from unstable elongated flow to unstable slug flow regime. On increasing the superficial gas velocity gradually from 0.95 m/s to 5.45 m/s, steady decrease in pressure fluctuation was observed due to the transition from unstable slug flow to stratified annular flow regime. Unlike the flow with superficial liquid velocity of 0.043 m/s, the transition to stratified annular required a higher superficial gas velocity of 5.45 m/s due to higher liquid volume in the pipe. The gradual increase in superficial gas velocity leads to a fairly constant pressure fluctuation due to the occurrence of annular flow regime.

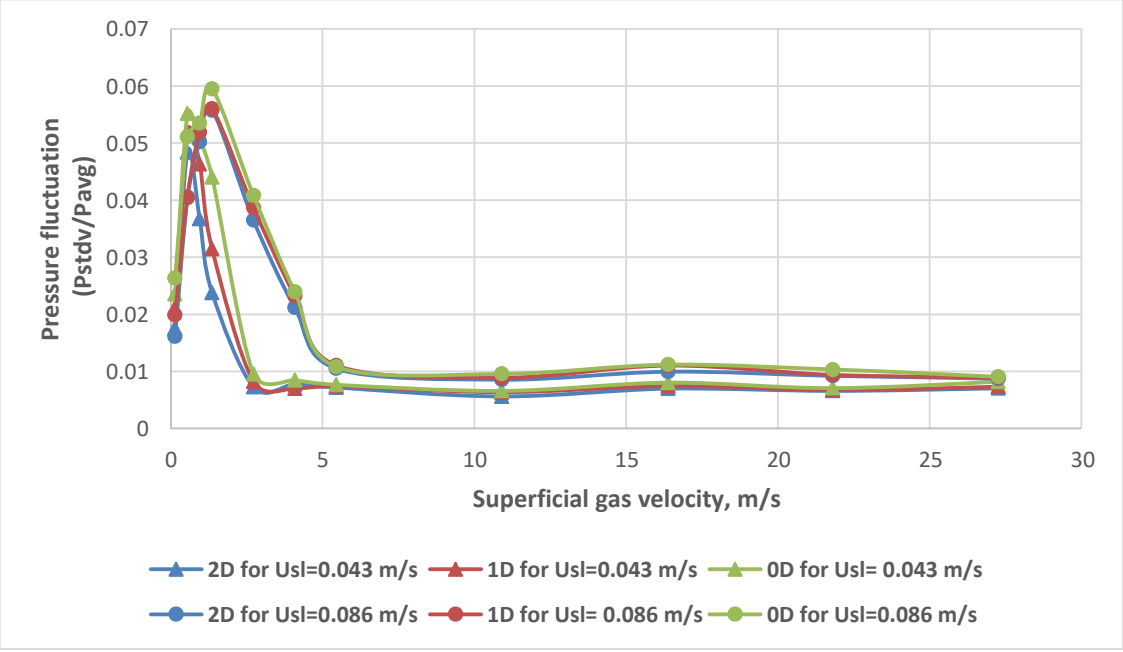

Figure 6-4 Plot of effect of blind tee lengths (0D, 1D, and 2D) on pressure fluctuations in blind tee with variation from low to high superficial gas velocity.

Figure 6-5 shows clear depiction of the effect of blind tee length on pressure fluctuation with the variation of superficial gas velocity. In general, the 2D blind tee length has the lowest pressure fluctuation while that of 0D length is observed to have highest pressure fluctuation for the same flow conditions. The effect of blind tee length on pressure fluctuation is observed to diminish with increase in superficial gas velocity.

The column plot in Figure 6-6 showing the effect of blind tee length with variation in superficial liquid velocity indicates that the major effect of blind tee length is witnessed for flows with low superficial liquid velocity. The effect of blind tee lengths becomes weaker with the increase in superficial liquid velocity.

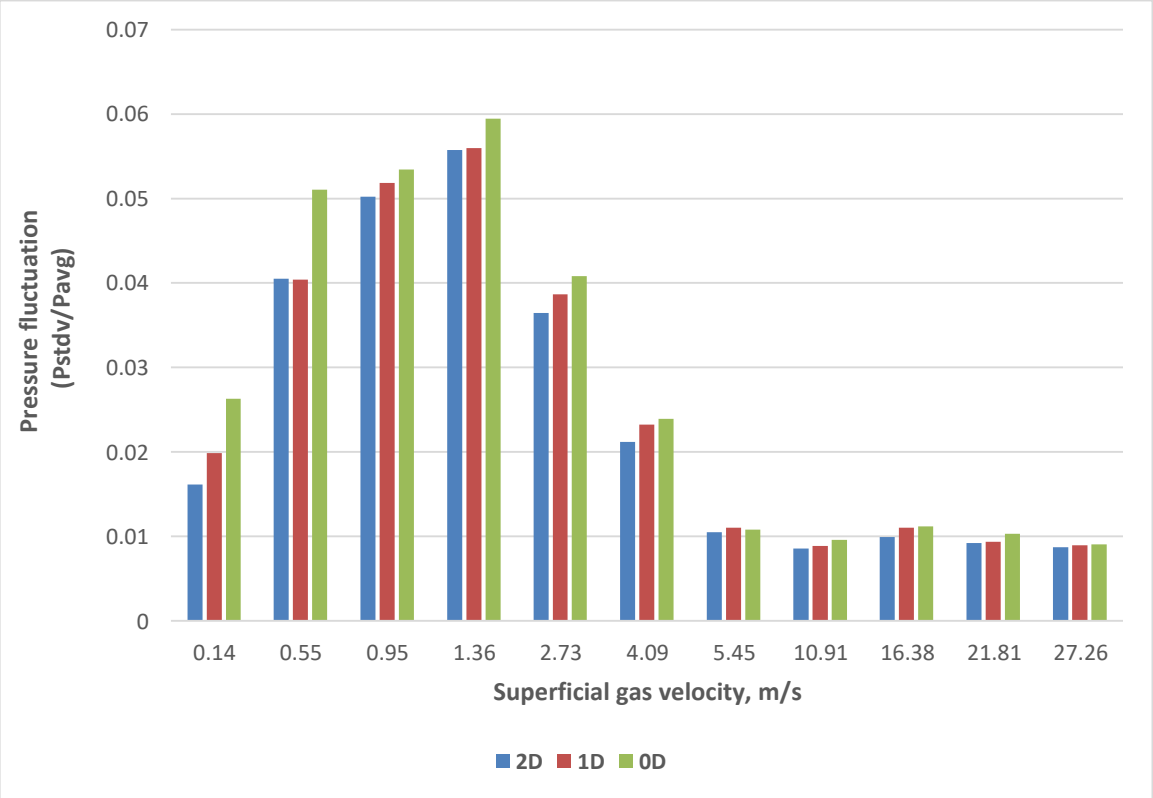

Figure 6-5 Plot of effect of blind tee lengths (0D,1D and 2D) on pressure fluctuations in blind tee with increase in superficial gas velocity for flows with superficial liquid velocity of 0.086 m/s.

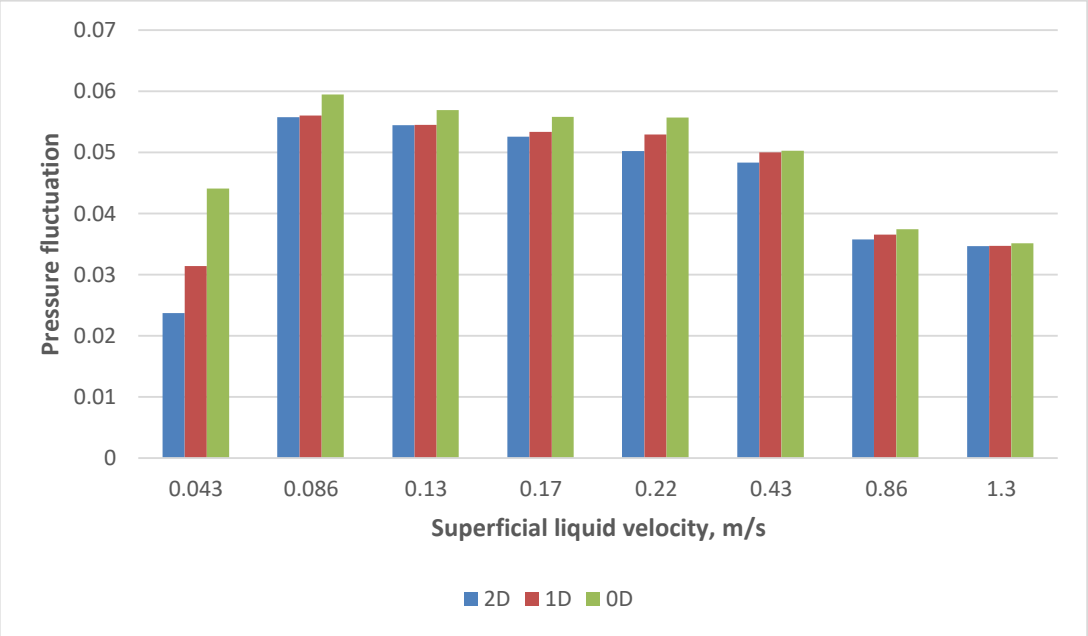

Figure 6-6 Effect of blind tee lengths (0D, 1D, and 2D) on pressure fluctuations in blind tee with increase in superficial liquid velocity for flows with superficial gas velocity of 1.36 m/s.

In general, the blind tee length is seen to have more influence on pressure fluctuation in intermittent flow than for separated flows. When the liquid superficial velocity is kept constant, the effect of the blind tee length on pressure fluctuation in the blind tee is observed to generally decrease with the increase in superficial gas velocity. This effect becomes almost insignificant at high superficial gas velocities of 5.45 – 27.26 m/s. Similar trend is observed when the superficial liquid velocity was varied at constant superficial gas velocity. The initial increase in pressure fluctuation at low superficial fluid velocity is as a result of the unstable nature of flow regime for such flow conditions.

6.2 Effect of blind tee length on pressure fluctuation in the flow loop

6.2.1 Effect of blind tee length on pressure fluctuation in the upstream section

The results of the effect of blind tee length on pressure fluctuation at 28D, 78D and 128D, upstream of the blind tee in the flow loop are shown in Figures 6-7 – 6.9. The three blind tees of length 0D, 1D and 2D are represented in the

Figures as 0D_Bt, 1D_Bt, and 2D_Bt, respectively. In Figure 6-7, for superficial liquid velocity of 0.043 m/s, the magnitude of the pressure fluctuation for each of the blind tee lengths did not change significantly across the flow loop generally. The magnitude of the pressure fluctuation along the flow loop were highest at flows with low superficial velocities. Just like in the blind tee in section 6.1, the pressure fluctuation decreases with increase in superficial gas velocity. The test conditions with 0D blind tee length are observed to predominantly have highest pressure fluctuation, while those of the 2D blind tee length showed the lowest pressure fluctuation in the flow loop. When the superficial liquid velocity is increased to 0.086 m/s (Figure 6-8), the pressure fluctuation in the flow loop appears to generally increase slightly. The degree of pressure fluctuation at 28D distance from the blind tee is observed to be the highest as compared with that of 78D and 128D cases. This could be attributed to the distance of the 28D case from the gas injection point that allows for a more developed flow with higher magnitude of slug length as compared with the 78D and 128D cases. Since 28D is closest to the blind tee region, it is possible that more turbulence could be generated from the flow due to the downstream effect of the blind tee, which could also have contributed to high pressure fluctuation at 28D. Similar to the flow condition with superficial liquid velocity of 0.043 m/s, the blind tee length of 0D is observed to have highest pressure fluctuation in the flow loop. The influence of blind tee length on pressure fluctuation is seen to reduce when superficial liquid velocity was increased from 0.043 m/s to 0.086 m/s. The flow conditions with low superficial gas velocities are observed to have highest pressure fluctuation as compared to those with high superficial gas velocities.

Similar pattern of pressure fluctuation is observed in the upstream section when the liquid superficial velocity was increased gradually from 0.043 m/s to 1.3 m/s for a constant superficial gas velocity of 1.36 m/s (Figure 6-9). An initial increase in pressure fluctuation is observed, which decreases generally with the increase in superficial liquid velocity.

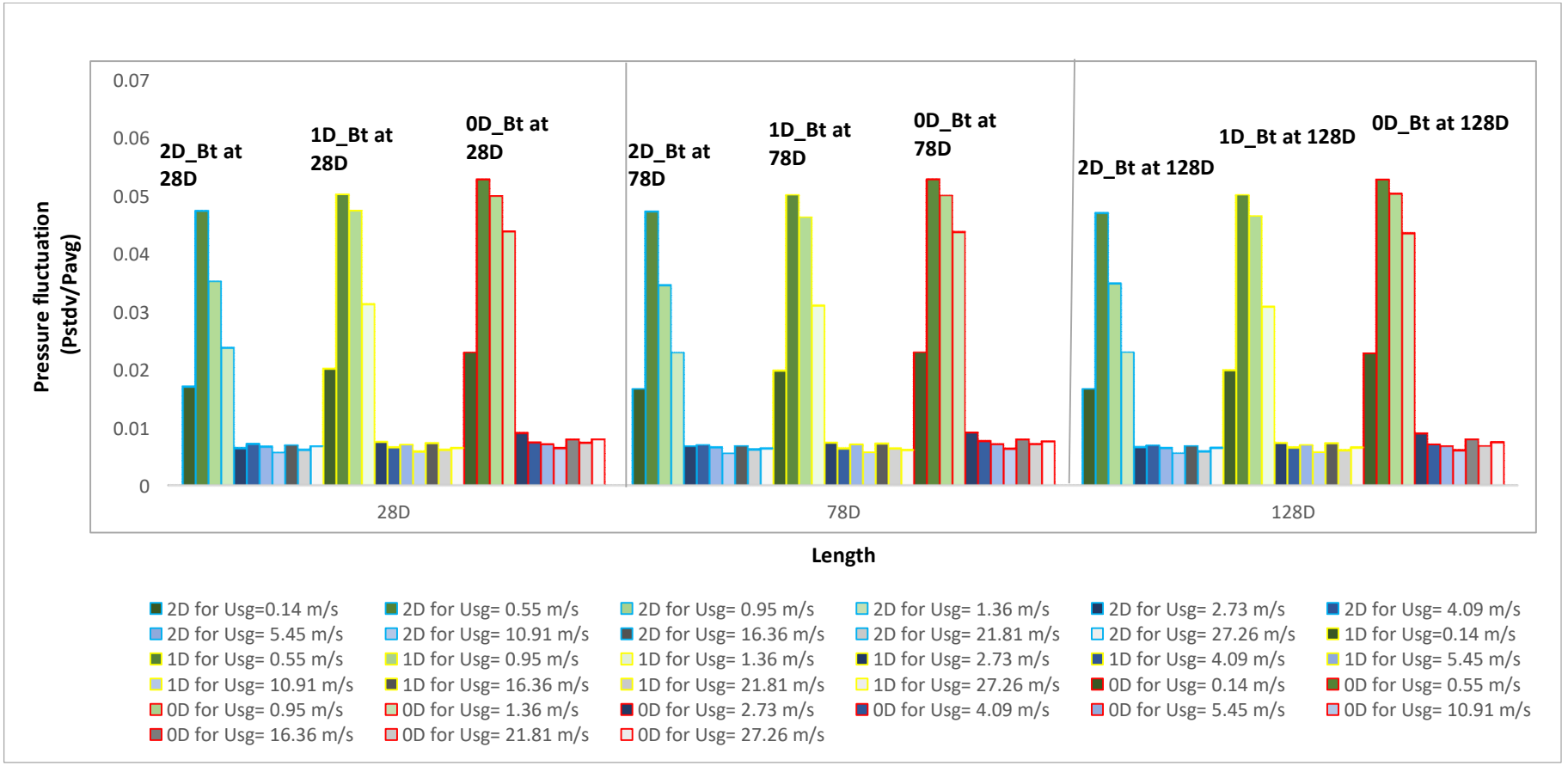

Figure 6-7 Effect of blind tee lengths (0D, 1D, and 2D) on pressure fluctuations in upstream section with increase in superficial gas velocity for flows with superficial liquid velocity of 0.043 m/s.

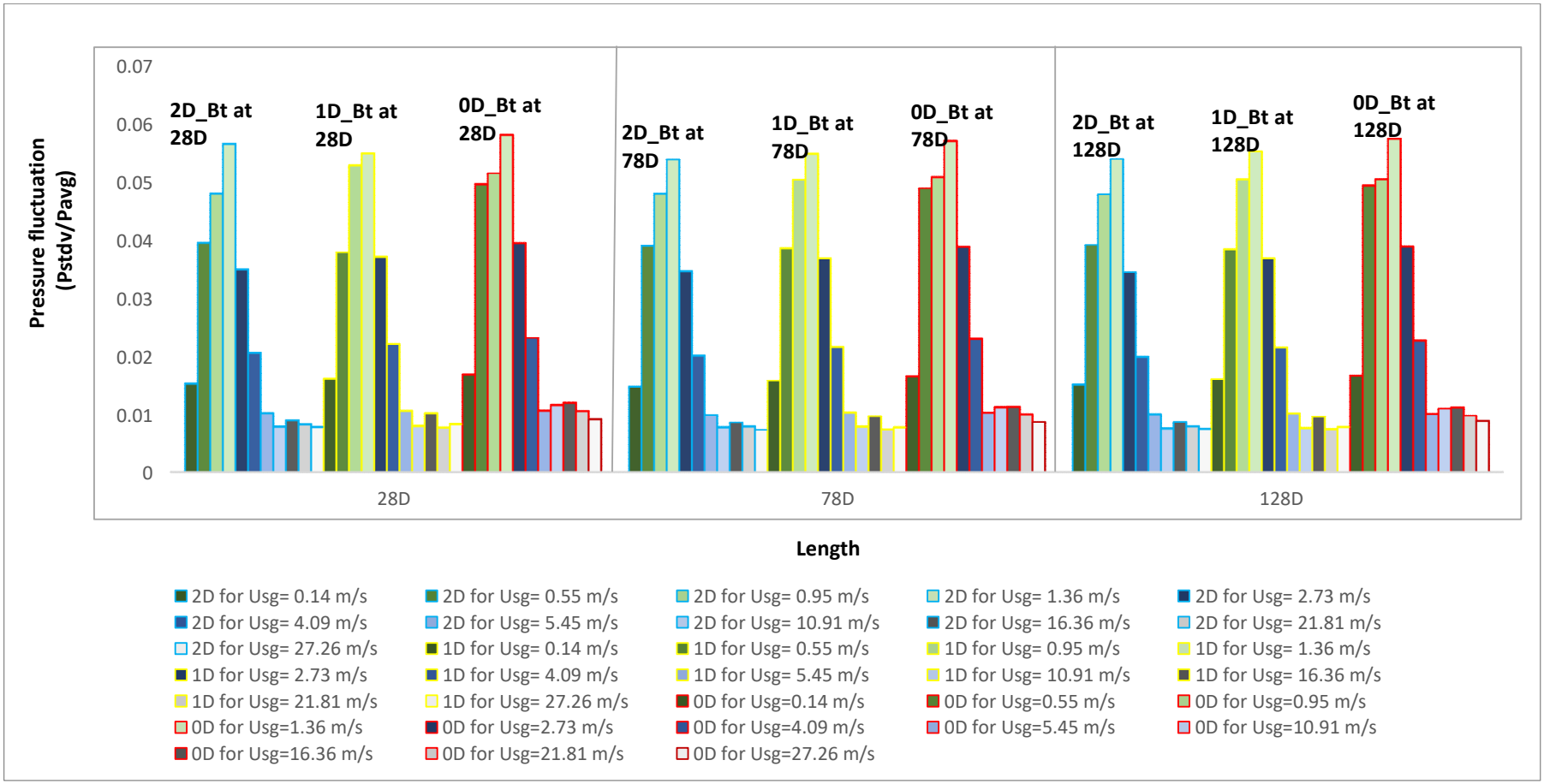

Figure 6-8 Effect of blind tee lengths (0D, 1D, and 2D) on pressure fluctuations in upstream section with increase in superficial gas velocity for flows with superficial liquid velocity of 0.086 m/s.

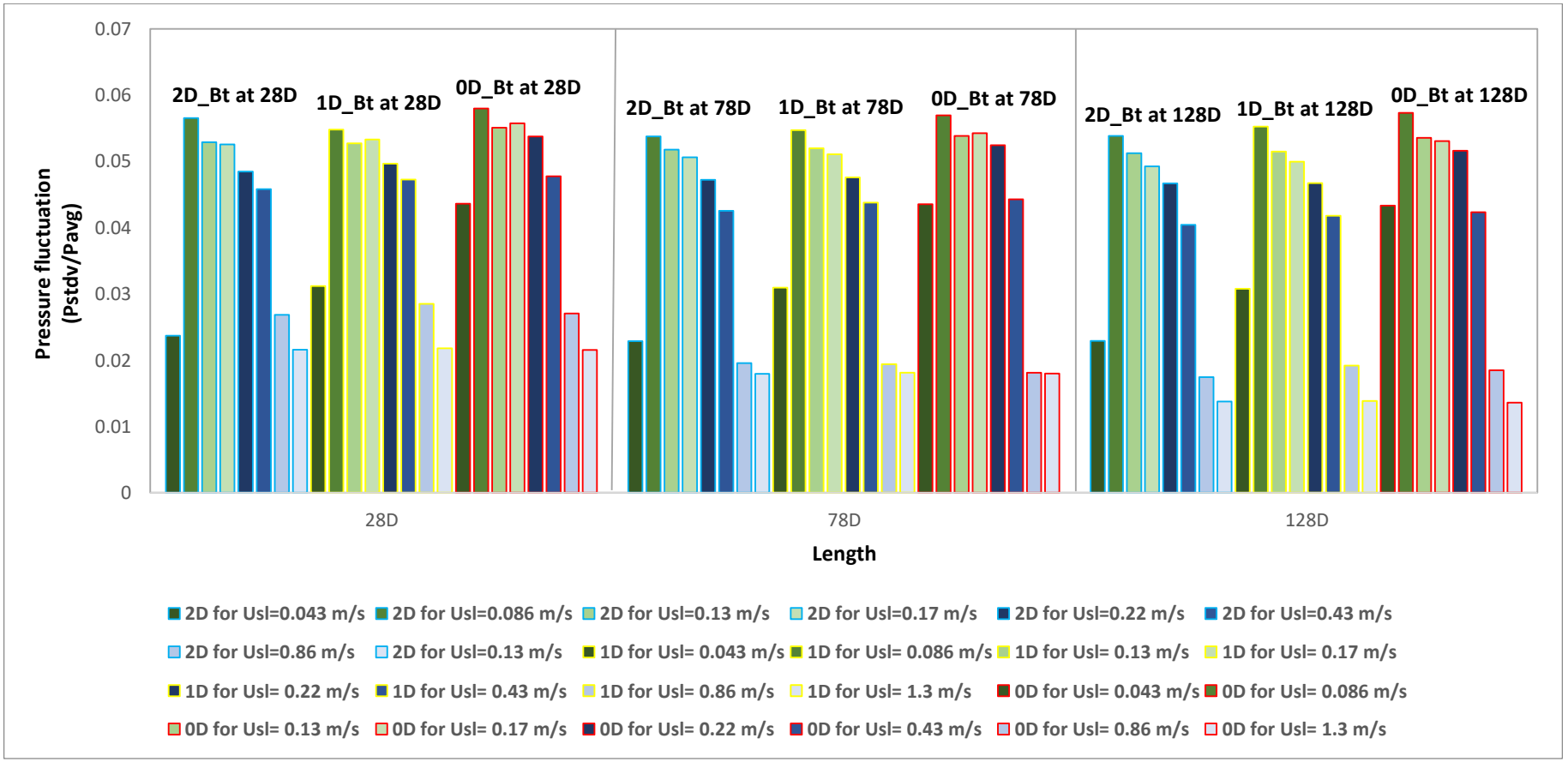

Figure 6-9 Effect of blind tee lengths (0D, 1D, and 2D) on pressure fluctuations in upstream section with increase in superficial liquid velocity for flows with superficial gas velocity of 1.36 m/s.

Although the pressure fluctuation across the upstream section of the flow loop did not change significantly, slightly higher pressure fluctuation is observed at 28D distance from the blind tee as with the previous results above. The effect of blind tee length is also observed to decrease significantly at high superficial liquid velocities (0.43 – 1.3 m/s), with highest pressure fluctuation observed for flows with 0D blind tee length.

From the results shown in Figures 6-7 and 6-8, it can be seen that increase in superficial velocities of the flow (and subsequently the superficial Reynolds number of the flow) do not necessarily lead to increase in pressure fluctuation. This means that the turbulence generated due to high flowrates (superficial velocities) of the flow do not always lead to increase in pressure fluctuation. Instead, the turbulence generated due to flow instability and the alternating nature of internal flow structures (Intermittent flows) gave the highest pressure fluctuation. In other words, the turbulence-induced pressure fluctuation is significantly lower than pressure fluctuation induced by the instability or alternating structure of flows. For flows superficial gas velocities of 5.45 m/s and above (separated flows), the amplitude of the pressure fluctuation is observed to be significantly lower than that of the flows with relatively low to medium superficial gas velocity (0.14 – 2.73 m/s). The higher fluctuation observed in the latter is as a result of flow instability (UWS) and the intermittency of the flow pattern associated with such flow conditions. In general, although increase in flowrate or superficial velocities may lead to increase in turbulence of the flow, however the magnitude of pressure fluctuation is dependent on the nature of the flow pattern.

6.2.2 Effect of blind tee length on pressure fluctuation in downstream section

The results for the downstream section are shown in Figures 6-10 – 6-12. In the downstream section, the pressure fluctuation is observed to be higher for flows with low superficial gas velocities, just as in the upstream section. However, the magnitude of the pressure fluctuation is observed to be slightly lower in the downstream section for flows with low superficial gas velocity due to the mixing

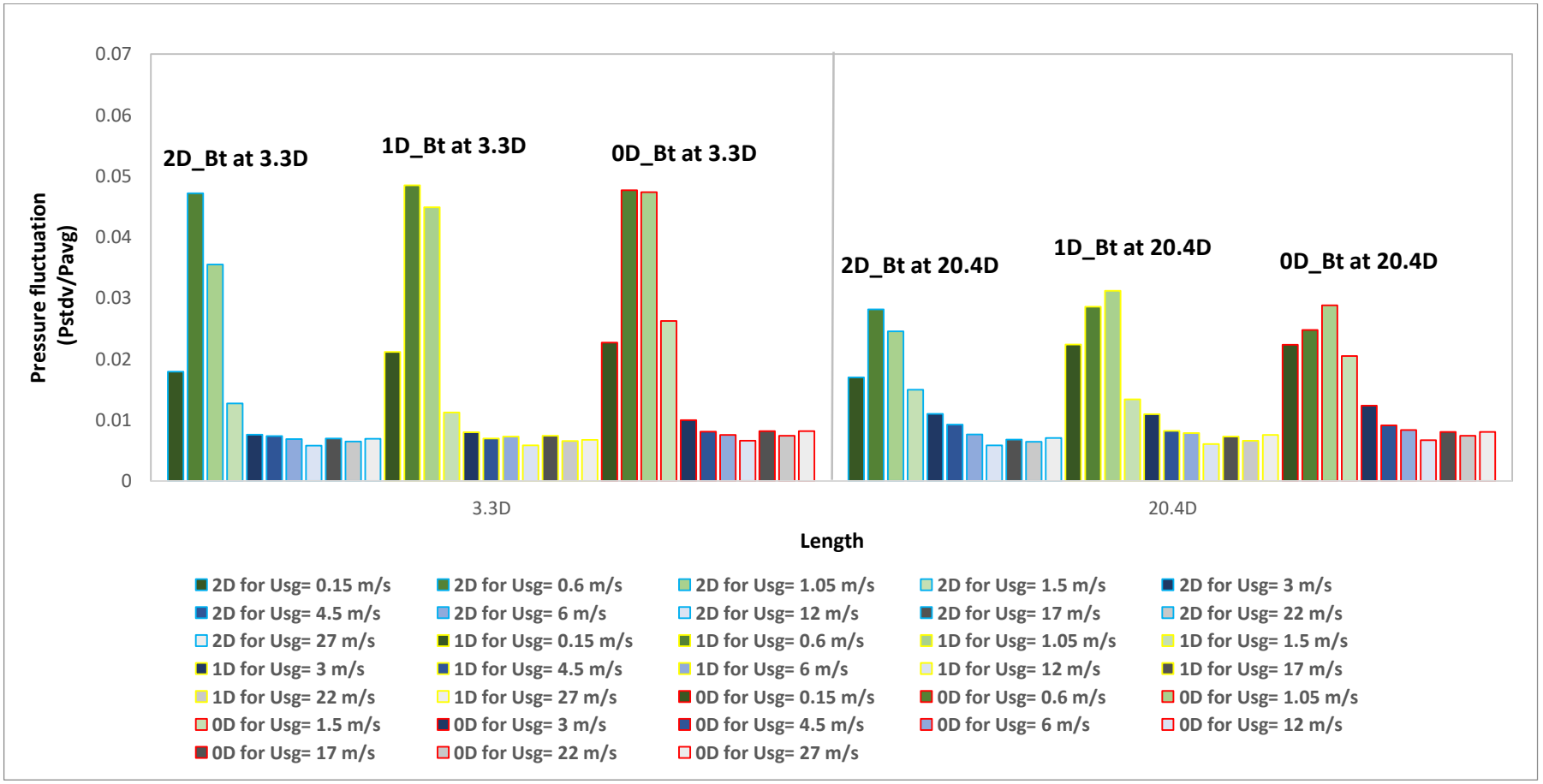

Figure 6-10 Effect of blind tee lengths (0D, 1D, and 2D) on pressure fluctuations in downstream section with increase in superficial gas velocity for flows with superficial liquid velocity of 0.043 m/s.

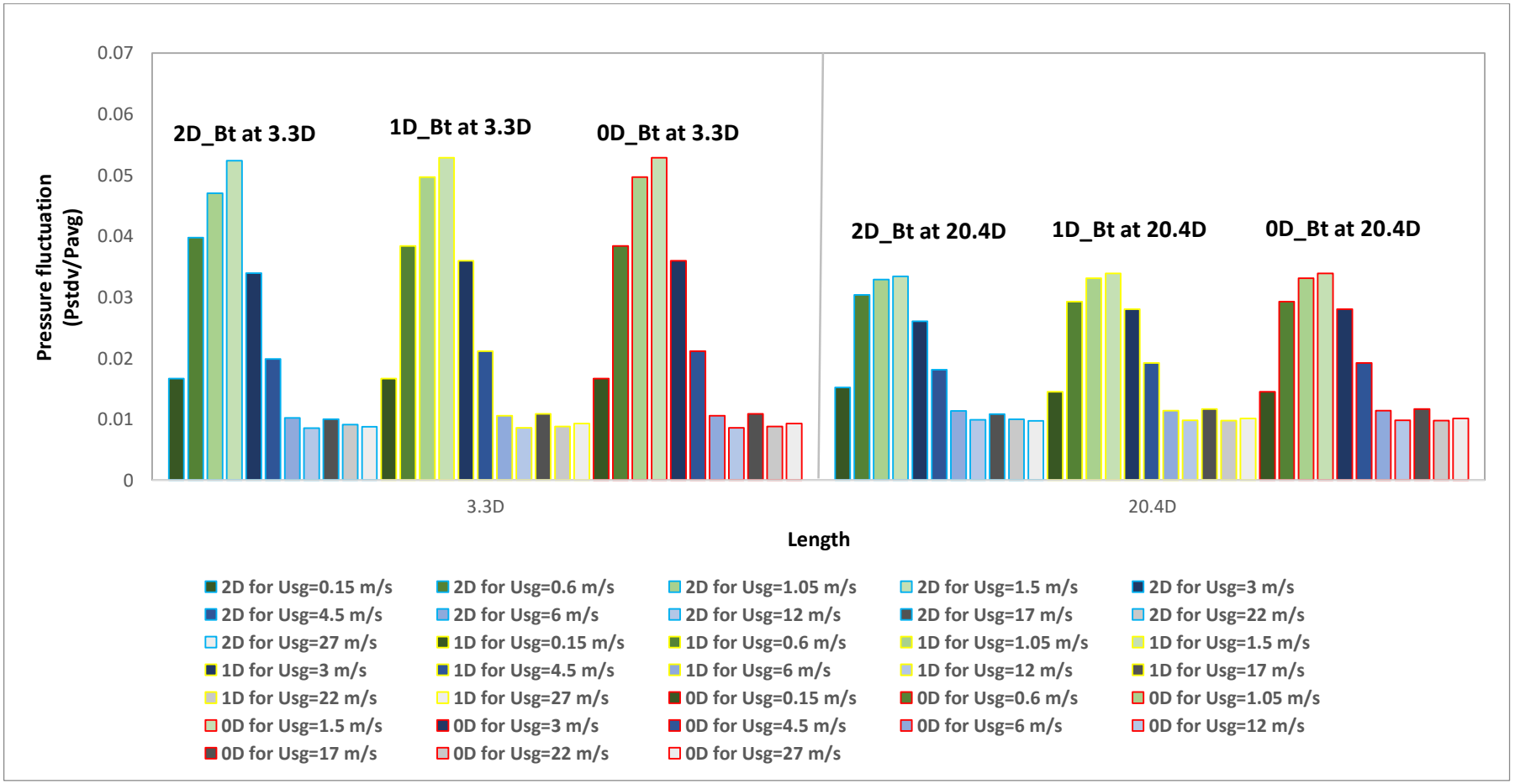

Figure 6-11 Effect of blind tee lengths (0D, 1D, and 2D) on pressure fluctuations in downstream section with increase in superficial gas velocity for flows with superficial liquid velocity of 0.086 m/s.

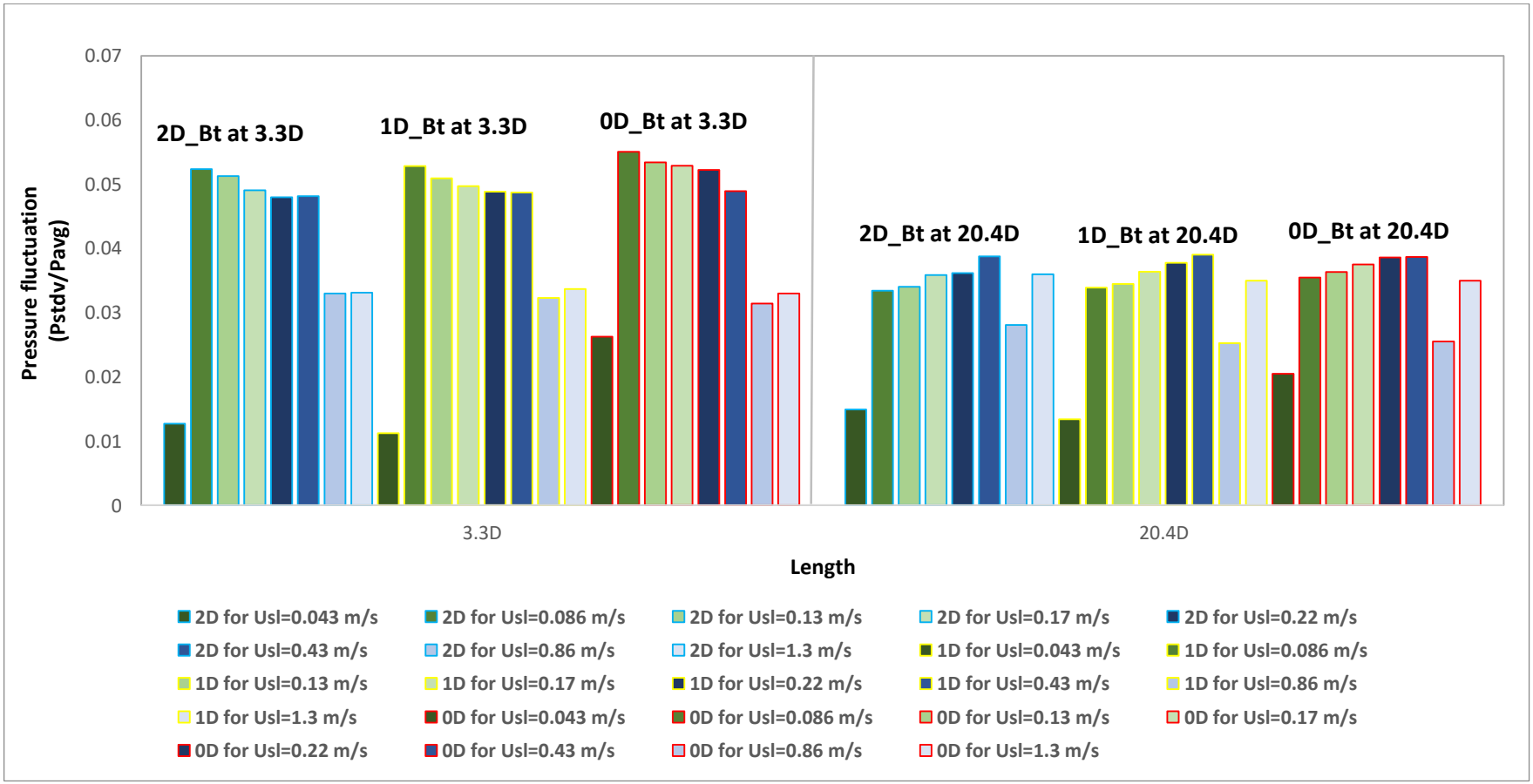

Figure 6-12. Effect of increase in superficial liquid velocity on pressure fluctuation for different blind tee lengths in downstream section of the flow loop for flows with superficial gas velocity of 1.36 m/s.

effect of the blind tee as the sensor positions are located closer to the blind tee region. At this position, the flow is still developing as the magnitude of the slugging or intermittency of the flow is relatively lower downstream of the blind tee. Furthermore, the mixing effect of the blind tee reduces the pressure fluctuation as the flow becomes slightly more homogenised especially for flows with low superficial velocity. The observation is also in agreement with the work of Hjertaker et al. (2018), as the authors observed that the flow is well mixed close to the blind tee. A related studies on pressure fluctuation in pipeline by Chinenye-Kalu et al. (2018) showed higher pressure fluctuation upstream of the blind tee compared to downstream section. Pressure transducers were placed 0.2 m upstream and downstream of the blind tee with the upstream section showing higher fluctuation. For flows with high superficial gas velocity, the pressure fluctuation remained relatively constant in both the upstream and downstream section as there is no intermittency in flow structures.

Figure 6-10 shows that the pressure fluctuation at 3.3D is higher than that at 20.4D distance away from the blind tee in the vertical (downstream) section. This could be as a result of the turbulence due to swirling and vortices that are generated around the blind tee section which reduces with distance away from the blind tee. Han et al. (2020) observed that the flow closer to the blind tee (2D downstream of the blind tee) has an uneven velocity profile, while those further away at 5D and 10D have more uniform velocity profiles, indicating better mixing of the flow around these regions. This implies that flows which are closer to the blind tee will have higher pressure fluctuation as observed in this work. Besides, Zeghloul et al. (2015) observed in their work that the flow tends to recover its flow pattern after 7 – 20 pipe diameters downstream of the blind tee. This suggests that mixing effect of the blind tee is predominant within close range of the blind tee. Overall, the pressure fluctuation with the 2D blind tee effect is observed to be slightly lower than those of 1D and 0D blind tee lengths due to better mixing of the flow with blind tee length of 2D. This finding agrees with the work of Han et al. (2020) which reported that better mixing of flow is observed with blind tee lengths of 2D and 3D. The authors further suggested that swirling strength inside the blind tee is dependent on the blind tee length

with blind tee length of 2D – 5D having better mixing of the flow than that of 1D length. Similarly in the present work, increase in blind tee length (2D) resulted to be better mixing of the flow as evidenced by the relative low pressure fluctuation of the flow.

When the liquid superficial velocity was increased to 0.086 m/s (Figure 6-11), the magnitude of the pressure fluctuation also increased, in similar trend as the corresponding upstream cases. The pressure fluctuation across the flow loop follows the same trend as those of flows with superficial liquid velocity of 0.043 m/s, with highest pressure fluctuation observed at region closest to the blind tee section. However, with further increase in superficial liquid velocity, the effect of blind tee length on pressure fluctuation is observed to decrease. When the superficial liquid velocity is varied from 0.043 m/s to 1.3 m/s (Figure 6-12), the pressure fluctuation is observed to decrease generally, after an initial first increase due to flow transition from unstable elongated flow to unstable slug flow regime. In similar manner as in upstream section, the effect of the blind tee length is observed to decrease significantly for flows with high superficial liquid velocities. Also, the effect of blind tee length is observed to be more prominent for flows with low superficial liquid velocities. Figure 6-12 shows that the magnitude of pressure fluctuation is observed to be highest at 3.3D than that of 20.4D from the blind tee for similar reason stated above for Figure 6-10.

6.3 Chapter summary

The experimental work and results of the effect of blind tee length on pressure fluctuation is summarized below

- Three blind tee lengths of 0D, 1D and 2D were tested with the same flow conditions to investigate their effect on pressure fluctuation in the flow loop.
- For straight pipes, pressure fluctuation is highest at blind tee, and regions closest to the blind tee (P1 and P4 for upstream and downstream section respectively).

- Blind tee length has highest influence on pressure fluctuation in the regions closest to the blind tee (P1 and P4) for upstream and downstream sections, respectively.
- The blind tee with 0D length is observed to have highest pressure fluctuation, while the lowest pressure fluctuation is predominantly witnessed with the 2D blind tee length.
- The magnitude of pressure fluctuation is observed to be higher in intermittent flows than that of separated flows.
- For intermittent flows, increase in superficial liquid velocity leads to decrease in both pressure fluctuation and influence of blind tee length on pressure fluctuation in the blind tee.
- For separated flows, increase in liquid superficial velocity leads to increase in pressure fluctuation.
- For separated flows, the effect of blind tee length is observed to be insignificant.
- In general, increase in superficial gas velocity is observed to lead to decrease both the effect of blind tee length and the pressure fluctuation in the flow loop.
- Influence of blind tee length on pressure fluctuation tends to decrease with distance away from the blind tee in straight pipes.

7 CONCLUSIONS AND RECOMMENDATIONS

7.1 Conclusions

A laboratory scale flow loop was designed to study multiphase flow behaviour and its development in a typical laboratory testing flowline and the effect of geometrical variances to improve the design of MPFM performance test flow loop. The experiments were conducted by using air and water as working fluids. The horizontal section was made up of the development section, equipped with three pressure transducers, Wire mesh sensor (WMS), and a Conductivity ring (CR) sensor with gas injection positions at 100D and 200D, and a sensor spool dummy for swapping sensor positions. Two pressure transducers and a WMS were installed in the vertical section for characterization of the flow. The research conclusions are presented below based on the key findings:

7.1.1 Characterization of flows transitioning from the horizontal to the vertical section

- The typical flow regime maps for conventional straight pipes were used to characterise the flow in the horizontal and vertical section.
- For the pipe configuration considered, the stratified flow regime observed in convectional straight pipes in horizontal section for flows with low superficial velocities was noticed to be absent in this work. Instead, a new flow regime (UWS) was observed due to the backward flow, and liquid accumulation associated with such pipe geometry.
- None of the typical flow regime maps were able to correctly predict the UWS flow regime.
- New flow regime map was developed for horizontal and vertical flows for horizontal pipe with conjoined vertical configuration.
- Slug flow regime was the dominant flow regime observed in the horizontal section due to long length of flow regime development that enhances wave growth along the pipe. In the vertical section churn flow regime was observed to be the most dominant flow regime due to the effect of gravity and the mixing effect of the blind tee on the flows.

- Liquid accumulation was observed to be common in horizontal pipes with conjoined vertical section especially for flows with low superficial velocities of the fluids which could contribute to error in multiphase flow rate estimation. The liquid accumulation is mainly associated to bottle neck effect and backward flow from the blind tee.
- Comparison of the flow regime structure in the horizontal and vertical section for the same flow condition using PDF plot and time trace plot shows a higher fluctuation in the void fraction reading in the vertical section than that of the horizontal section. Increase in gas and liquid superficial velocities has shown to increase the void fraction fluctuation in the vertical section.
- Comparison of two-phase flow void fraction prediction models shows that most of the models found in the literature overpredicted the void fraction in such pipe configuration. The effect of the system configuration is evidenced in the noticeable decrease in void fraction in the horizontal section due to liquid accumulation in the pipe.
- A new modified drift flux model was proposed for such air-water two-phase flow system for prediction of void fraction in horizontal pipe with conjoined vertical section.

7.1.2 Flow regime development with complex downstream geometries

- Analyses of the PDF and time series plots indicated that liquid accumulation in the pipe increased with the increase in flow regime development length. For flows with longer development length for the same flow condition, higher pressure drop will further reduce the fluid being pushed out through the vertical section, and hence more liquid can accumulate in the pipe.
- The liquid accumulation was observed to decrease with the increase in superficial gas velocity.

- The average void fraction was observed to decrease with the increase in flow regime development length as a result of more liquid accumulation for flows with longer flow regime development length.
- Analyses of the PDF and time series plots show similar flow pattern for 100D and 200D development lengths. This indicates that 100D length can be sufficient for flow regime development as no change in flow pattern was observed for 100D and 200D development lengths.
- Downstream effect on flow behaviour was studied by placing the CR sensor at 41D and 141D away from the blind tee section.
- Downstream effect on two-phase flow behaviour was observed to be significant for flows with low superficial velocities, with this effect becoming less pronounced for flows with high superficial gas velocities (Usg= 10.91 – 27.26 m/s).
- The void fraction was observed to increase with sensor distance away from the blind tee region, because of less effect of the backward flow with distance away from the blind tee section.

7.1.3 Effect of blind tee length on pressure fluctuation

- For straight pipes, pressure fluctuation was highest at blind tee, and regions closest to the blind tee (P1 and P4 for upstream and downstream section respectively).
- Blind tee length had significant influence on pressure fluctuation in the regions closest to the blind tee (P1 and P4) for upstream and downstream sections respectively).
- The blind tee with 0D length was observed to have predominantly highest pressure fluctuation, while the lowest pressure fluctuation was obtained with the 2D blind tee length.
- The magnitude of pressure fluctuation was higher in intermittent flows than in separated flows.
- For intermittent flows, increase in superficial liquid velocity led to both decrease in pressure fluctuation and a smaller influence of blind tee length on pressure fluctuation in the blind tee.

- For separated flows, increase in superficial liquid velocity led to increase in pressure fluctuation.
- For separated flows, the effect of blind tee was observed to be insignificant.
- In general, increase in superficial gas velocity decreased both the effect of blind tee length and the pressure fluctuation in the flow loop.
- Influence of blind tee length on pressure fluctuation decreased with distance away from the blind tee in straight pipes.

7.2 Recommendations

7.2.1 Proposed guidelines for flow loop design

Based on the results of the experimental studies, the following guidelines are suggested for a typical metrological flow loop:

- 100D length can be sufficient for air-water two-phase flow regime development in horizontal pipes with conjoined vertical pipe configuration.
- Although the flow regimes in 100D and 200D were observed to be fairly constant, 100D length may be preferable due to less liquid accumulation in horizontal section and less hydraulic energy required to push the fluids over the test section in the vertical section.
- Sensors and flowmeters should be placed at a distance of at least 18D (pipe diameters) upstream and 20.4D pipe diameters downstream of bends or other fitting to avoid flow disturbance.
- For oil and gas flow in pipeline, sensors or instrumentation that are susceptible to corrosion can be installed on the outward part of the pipe as thicker liquid film was observed for such pipe section. The Inward of pipe is prone to relatively higher rate of corrosion due gas bubbles that are pushed towards this part of pipe with less liquid film, which can speed up electrochemical reaction in the pipe.

- Due the tendency of liquid accumulation in the horizontal section which could lead to increased uncertainty in the phase measurement, it is recommended to place the MPFM in the vertical section.
- It is recommended that the test matrix is planned with a minimum superficial gas and liquid velocities of 2.73 & 0.043 m/s, and 4.09 m/s & 0.086 m/s for gas and liquid in 100D and 200D development length flows respectively to minimize the chaotic flow associated with the short pauses of liquid flow in the flow loop.
- For horizontal flow loop with conjoined vertical pipe configuration, a new void fraction model is proposed in this work to minimize the effect of overestimation of void fraction due to liquid accumulation in the horizontal section.
- Blind tee length of 2D is the recommended connection joint for such pipe configuration due to less pressure fluctuation associated with such connections.

7.2.2 Recommendations for future work

As a result of the experimental studies, the following recommendations can help to improve flow loop design and assessment of test performance of MPFM:

- Investigation of the effect of flow regime on MPFM performance in horizontal pipe with conjoined vertical pipe configuration by comparing the results of MPFM with the reference flow meter. This result will help provide insight on assessment of test performance of MPFM under different flow conditions for calibration and validation purposes of the MPFM.
- Comparing the results of the experiments with those of different scale flow loop to understand and determine the scaling rules.
- Further experimental studies on different injection design (orientation) on flow regime development in the flow loop.
- Further investigation of geometrical variance in the vertical section to investigate the mixing effect of different blind tee length on metering. This

could be achieved by varying the vertical distance of the MPFM and testing with different blind tee lengths.

- The experimental studies of this research can be considered as an initial step to address the research questions and research gap highlighted. Further numerical simulations are required to compare with the results obtained to provide more generic guidelines for flow loop design.

REFERENCES

Abdel Azim, R. (2020). Prediction of multiphase flow rate for artificially flowing wells using rigorous artificial neural network technique. *Flow Measurement and Instrumentation*, *76*, 1–9. https://doi.org/10.1016/j.flowmeasinst.2020.101835

Abdelsalam, A., Cem, S., & Eduardo, P. (2016). New dimensionless number for gas-liquid flow in pipes. *International Journal of Multiphase Flow*, *81*, 15–19. https://doi.org/10.1016/j.ijmultiphaseflow.2015.12.008

Abdulkadir, M., Hernandez-Perez, V., Kwatia, C. A., & Azzopardi, B. J. (2018). Interrogating flow development and phase distribution in vertical and horizontal pipes using advanced instrumentation. *Chemical Engineering Science*, *186*, 152–167. https://doi.org/10.1016/j.ces.2018.04.039

Abdulkadir, M., Hernandez-Perez, V., Lo, S., Lowndes, I. S., & Azzopardi, B. J. (2015). Comparison of experimental and Computational Fluid Dynamics (CFD) studies of slug flow in a vertical riser. *Experimental Thermal and Fluid Science*, *68*, 468–483. https://doi.org/10.1016/j.expthermflusci.2015.06.004

Abdulkadir, M., Hernandez-Perez, V., Lowndes, I. S., Azzopardi, B. J., & Sam-Mbomah, E. (2016). Experimental study of the hydrodynamic behaviour of slug flow in a horizontal pipe. *Chemical Engineering Science*, *156*(January 2018), 147–161. https://doi.org/10.1016/j.ces.2016.09.015

Abouelwafa, M. S. A., & Kendall, E. J. M. (1980). The measurement of component ratios in multiphase systems using γ-ray attenuation. *Journal of Physics E: Scientific Instruments*, *13*, 341. https://doi.org/10.1088/0022-3735/13/3/022

Acikgoz, M., Franca, F., & Lahey, R. T. (1992). An experimental study of three-phase flow regimes. *International Journal of Multiphase Flow*, *18*(3), 327–336.

Ahmadi, M. A., Ebadi, M., Shokrollahi, A., & Javad Majidi, S. M. (2013).

Evolving artificial neural network and imperialist competitive algorithm for prediction oil flow rate of the reservoir. *Applied Soft Computing Journal*, *13*(2), 1085–1098. https://doi.org/10.1016/j.asoc.2012.10.009

Al-Hadhrami, L. M., Shaahid, S. M., Tunde, L. O., & Al-Sarkhi, A. (2014). Experimental study on the flow regimes and pressure gradients of air-oil-water three-phase flow in horizontal pipes. *The Scientific World Journal*, *2014*(January). https://doi.org/10.1155/2014/810527

AL-Qutami, T. A., Ibrahim, R., Ismail, I., & Ishak, M. A. (2017). Development of soft sensor to estimate multiphase flow rates using neural networks and early stopping. *International Journal on Smart Sensing and Intelligent Systems*, *10*(1), 199–222. https://doi.org/10.21307/ijssis-2017-209

Amin, A. (2015). Evaluation of commercially available virtual flow meters (VFMs). *Proceedings of the Annual Offshore Technology Conference*, *2*(May), 1293–1318. https://doi.org/10.4043/25764-ms

Armand, A. A. (1946). The Resistance During the Movement of a Two-phase System in Horizontal Pipes. *Izvestiya Vsesoyuznogo Teplotekhnicheskogo Instituta*, *1*, 16–23.

Ashton, S. L., Cutmore, N. G., Roach, G. J., Watt, J. S., Zastawny, H. W., & McEwan, A. J. (1994). Development and trial of microwave techniques for measurement of multiphase flow of oil, water and gas. *All Days*, 681–689. https://doi.org/10.2118/28814-MS

Azzopardi, B. J. (1998). Drops in annular two-phase flow. *International Journal of Multiphase Flow*, *23*(97), 1–53.

Bachman, H. N., Lavigne, J., Leveridge, R., Heaton, N., Hürlimann, M. D., Looyestijn, W. J., & White, J. (2008). Nucear Magnetic Resonance Comes Out of Its Shell. *Oilfield Review*, *20*(4), 4–23.

Baker, R. C. (1991). Response of bulk flowmeters to multiphase flows. *Proceedings of the Institution of Mechanical Engineers, Part C: Journal of Mechanical Engineering Science*, *205*(4), 217–229.

https://doi.org/10.1243/PIME_PROC_1991_205_114_02

Banowski, M., Beyer, M., Szalinski, L., Lucas, D., & Hampel, U. (2017). Comparative study of ultrafast X-ray tomography and wire-mesh sensors for vertical gas–liquid pipe flows. *Flow Measurement and Instrumentation*, *53*, 95–106. https://doi.org/10.1016/j.flowmeasinst.2016.02.001

Barnea, D. (1987). A unified model for predicting transitions for the whole pipe inclinations. *International Journal of Multiphase Flow*, *13*(I), 1–12.

Barnea, D., Shoham, O., Taitel, Y., & Dukler, A. E. (1985). Gas-liquid flow in inclined tubes: Flow pattern transitions for upward flow. *Chemical Engineering Science*. https://doi.org/10.1016/0009-2509(85)85053-3

Beck, M. S., & Plaskowski, A. B. (1987). *Cross Correlation Flowmeters, Their Design and Application*.

Beck, M. S., & Williams, R. A. (1996). Process tomography: A European innovation and its applications. *Measurement Science and Technology*, *7*(3), 215–224. https://doi.org/10.1088/0957-0233/7/3/002

Beyer, M., Szalinski, L., & Schleicher, E. (2012). *Wire-Mesh Sensor Data Processing Software, User Manual and Software Description*. *10.01.2011*, 1–28.

Biberg, D. (2005). *Mathematical models for two-phase stratified pipe flow*. University of Oslo, Norway.

Bifout, S., Pinguet, B., & Rojas, C. (2014). How to cope with sand production without any additional sensor when using the right multiphase technology. *Society of Petroleum Engineers - 30th Abu Dhabi International Petroleum Exhibition and Conference, ADIPEC 2014: Challenges and Opportunities for the Next 30 Years*, *6*, 4210–4228. https://doi.org/10.2118/172096-ms

Bikmukhametov, T., & Jaschke, J. (2020). Machine learning and first principles modeling applied to multiphase flow estimation with a focus on the oil and gas industry. In *NTNU Grafisk senter*. Norwegian University of Science and

Technology.

Bizon, E. (1965). Two-phase flow measurement with sharp-edged orifices and venturis. In *Heat Transfer and Fluid Flow*. https://www.osti.gov/biblio/4598247

Blake, W. K. (1970). Turbulent boundary-layer wall-pressure fluctuations on smooth and rough walls. *Journal of Fluid Mechanics*, *44*(4), 637–660. https://doi.org/10.1017/S0022112070002069

Brauner, N., & Ullmann, A. (2004). Modelling of gas entrainment from Taylor bubbles. Part A: Slug flow. *International Journal of Multiphase Flow*, *30*(3), 239–272. https://doi.org/10.1016/j.ijmultiphaseflow.2003.11.007

Brauner, Neima. (2001). The prediction of dispersed flows boundaries in liquid-liquid and gas-liquid systems. *International Journal of Multiphase Flow*, *27*(5), 885–910. https://doi.org/10.1016/S0301-9322(00)00056-2

Brauner, Neima, & Barnea, D. (1986). Slug/churn transition in upward. *Chemical Engineering Journal*, *41*(1), 159–163.

Brennen, C. E. (2005). Fundamentals of multiphase flow. In *Fundamentals of Multiphase Flow*. Cambridge University Press. https://doi.org/10.1017/CBO9780511807169

Cai, J. Y., Gopal, M., & Jepson, W. P. (1999). Investigation of flow regime transitions in large-diameter inclined pipes. *Journal of Energy Resources Resources Technology*, *121*, 91–95.

Chaves, G. S., Karami, H., & Ferreira Filho, V. J. M. (2022). Design and evaluation of a virtual flowmeter for multiphase flow in production lines. *SPE Production & Operations*, *September 2021*, 1–8. https://doi.org/10.2118/206259-pa

Chen, L, Tian, Y., & Karayiannis, T. (2006). The effect of tube diameter on vertical two-phase flow regimes in small tubes. *International Journal of Heat and Mass Transfer*, *49*, 4220–4230.

https://doi.org/10.1016/j.ijheatmasstransfer.2006.03.025

Chen, Lejun. (2006). *Flow patterns in upward two-phase flow in small diameter tubes*.

Cheng, L., Ribatski, G., & Thome, J. R. (2008). Two-phase flow patterns and flow-pattern maps: fundamentals and applications. *Applied Mechanics Reviews*, *61*(5), 28. https://doi.org/10.1115/1.2955990

Chidamoio, J. F., Akanji, L., & Rafati, R. (2017). *Prediction of optimum length to diameter ratio for two-phase fluid flow development in vertical pipes*. *14*(1), 1–17. https://doi.org/10.3968/9886

Chidamoio, J. F., Akanji, L., & Rafati, R. (2018). Effect of length-to-diameter ratio on axial velocity and hydrodynamic entrance length in air-water twophase flow in vertical pipes. *Journal of Oil, Gas and Petrochemical Sciences*, *0*(0), 3–9. https://doi.org/10.30881/jogps.00003

Chinello, G., Graham, E., Reader-Harris, M., Clark, S., & Collins, A. (2019). Using venturi meters installed in vertical orientation for wet-gas flow measurement. *37th International North Sea Flow Measurement Workshop, NSFMW 2019*, *October*, 1–28.

Chinenye-Kalu, N. M., Hossain, M., Droubi, M. G., & Islam, S. Z. (2018). Numerical investigation of two-phase flow induced local fluctuations and interactions of flow properties through elbow. *International Conference on Numerical Modelling in Engineering*, 121–141.

Chisholm, D. (1967). flow of incompressible two-phase mixtures through sharp-edged orifices. *Journal of Mechanical Engineering Science*, *9*(1), 72–78. https://doi.org/10.1243/jmes_jour_1967_009_011_02

Chisholm, D. (1973). Pressure gradients due to friction during the flow of evaporating two-phase mixtures in smooth tubes and channels. *International Journal of Heat and Mass Transfer*, *16*(2), 347–358. https://doi.org/10.1016/0017-9310(73)90063-X

Chisholm, D. (1977). Two-phase flow measurement through sharp-edged orifices. *Journal of Mechanical Engineering Science*, *19*(3), 19–22. https://doi.org/10.1243/JMES

Cioncolini, A., & Thome, J. R. (2012). Void fraction prediction in annular two-phase flow. *International Journal of Multiphase Flow*, *43*, 72–84. https://doi.org/10.1016/j.ijmultiphaseflow.2012.03.003

Corcos, G. M. (1965). The structure of the turbulent pressure field in boundary-layer flows. *Journal of Fluid Mechanics*, *18*(3), 353. https://doi.org/10.1016/0011-7471(65)90880-6

Couput, J. P., Laiani, N., & Richon, V. (2017). Operational experience with virtual flow measurement technology. *35th International North Sea Flow Measurement Workshop, NSFMW 2017*, *October*.

Couput, J. P., Louis, A., & Danquigny, J. (2008). Transforming E&P data into knowledge: Applications of an integration strategy. *Intelligent Energy Conference and Exhibition: Intelligent Energy 2008*, 1171–1174. https://doi.org/10.2118/112517-ms

Da Hlaing, N., Sirivat, A., Siemanond, K., & Wilkes, J. O. (2007). Vertical two-phase flow regimes and pressure gradients: Effect of viscosity. *Experimental Thermal and Fluid Science*, *31*(6), 567–577. https://doi.org/10.1016/j.expthermflusci.2006.03.030

Da Silva. (2008). Impedance sensors for fast multiphase flow measurement and imaging [Technische Universität Dresden]. In *Elektrotechnik Und Informationstechnik*. http://d-nb.info/992681979/34

Daramola, B., & Alinnor, C. M. (2018). Optimising sand control and production strategies in a low permeability sandstone oil field. *Proceedings - SPE International Symposium on Formation Damage Control*. https://doi.org/10.2118/189556-ms

Davis, M. R. (1973). Pressure fluctuations in a vapour-liquid mixture flow. *International Journal of Heat and Mass Transfer*, *16*(11), 2043–2054.

https://doi.org/10.1016/0017-9310(73)90107-5

De Leeuw. (1997). Liquid correction of venturi meter readings in wet gas flow. *North Sea Flow Measurement Workshop*, *4*, 1–18.

Deng, X., Chen, D., & Yang, W. (2011). Study on electrodynamic sensor of multi-modality system for multiphase flow measurement. *Review of Scientific Instruments*, *82*(12). https://doi.org/10.1063/1.3665207

Dinaryanto, O., Prayitno, Y. A. K., Majid, A. I., Hudaya, A. Z., Nusirwan, Y. A., Widyaparaga, A., Indarto, & Deendarlianto. (2017). Experimental investigation on the initiation and flow development of gas-liquid slug two-phase flow in a horizontal pipe. *Experimental Thermal and Fluid Science*, *81*, 93–108. https://doi.org/10.1016/j.expthermflusci.2016.10.013

Dong, C., Gao, K., Dong, S., Shang, X., Wu, Y., & Zhong, Y. (2017). A new integrated method for comprehensive performance of mechanical sand control screens testing and evaluation. *Journal of Petroleum Science and Engineering*, *158*(February), 775–783. https://doi.org/10.1016/j.petrol.2017.08.043

Dukler, A. E., & Taitel, Y. (1986). Flow pattern transitions in gas-liquid systems: Measurement and Modeling. *Multiphase Sci and Tech*, *2*, 1–94. https://doi.org/10.1615/multscientechn.v2.i1-4.10

Dyakowski, T. (1996). Process tomography applied to multi-phase flow measurement. *Measurement Science and Technology*, *7*(3), 343–353. https://doi.org/10.1088/0957-0233/7/3/015

Falcone, G, Hewitt, G. F., Alimonti, C., & Harrison, B. (2014). Multiphase flow metering: current trends and future developments. *Journal of Petroleum Technology*, *54*(04), 77–84. https://doi.org/10.2118/74689-jpt

Falcone, Gioia. (2009a). Multiphase flow fundamentals. In *developments in petroleum science* (Vol. 54, pp. 1–18). https://doi.org/10.1016/S0376-7361(09)05401-6

Falcone, Gioia. (2009b). Chapter 1 Multiphase Flow Fundamentals. In *Developments in Petroleum Science* (Vol. 54, pp. 1–18). https://doi.org/10.1016/S0376-7361(09)05401-6

Fossa, M. (1998). Design and performance of a conductance probe for measuring the liquid fraction in two-phase gas-liquid flows. *Flow Measurement and Instrumentation*, *9*(2), 103–109. https://doi.org/10.1016/S0955-5986(98)00011-9

Fossa, M., Guglielmini, G., & Marchitto, A. (2003). Intermittent flow parameters from void fraction analysis. *Flow Measurement and Instrumentation*, *14*(4–5), 161–168. https://doi.org/10.1016/S0955-5986(03)00021-9

Fukano, T., & Kariyasaki, A. (1993). Characteristics of gas-liquid two-phase flow in a capillary tube. *Nuclear Engineering and Design*, *141*, 59–68.

Gamio, J. C., Castro, J., Rivera, L., Alamilla, J., Garcia-Nocetti, F., & Aguilar, L. (2005). Visualisation of gas-oil two-phase flows in pressurised pipes using electrical capacitance tomography. *Flow Measurement and Instrumentation*, *16*(2–3), 129–134. https://doi.org/10.1016/j.flowmeasinst.2005.02.011

George, D. L., Torczynski, J. R., Shollenberger, K. A., O'Hern, T. J., & Ceccio, S. L. (2000). Validation of electrical-impedance tomography for measurements of material distribution in two-phase flows. *International Journal of Multiphase Flow*, *26*(4), 549–581. https://doi.org/10.1016/S0301-9322(99)00029-4

Griffith, P., & Wallis, G. B. (1961). TWO-PHASE SLUG FLOW. *JOURNAL OF HEAT TRANSFER*, *83*(3), 307–318.

Grimstad, B., Hotvedt, M., Sandnes, A. T., Kolbjørnsen, O., & Imsland, L. S. (2021). Bayesian neural networks for virtual flow metering: An empirical study. *Applied Soft Computing*, *112*, 1–15. https://doi.org/10.1016/j.asoc.2021.107776

Gualtieri, C., & Chanson, H. (2007). Experimental analysis of Froude number

effect on air entrainment in the hydraulic jump. *Environmental Fluid Mechanics*, *7*(3), 217–238. https://doi.org/10.1007/s10652-006-9016-1

Guo, L., Bai, B., Zhao, L., Wang, X., & Gu, H. (2009). Online recognition of the multiphase flow regime and study of slug flow in pipeline. *Journal of Physics: Conference Series*, *147*. https://doi.org/10.1088/1742-6596/147/1/012047

Gupta, B., Nayak, A. K., Kandar, T. K., & Nair, S. (2016). Investigation of air-water two phase flow through a venturi. *Experimental Thermal and Fluid Science*, *70*, 148–154. https://doi.org/10.1016/j.expthermflusci.2015.07.012

Hall, A. R. W., & Reader-Harris, M. J. (1999). Use of Venturi Meters in Multiphase Flow Measurement. *North Sea Flow Measurement Workshop*, *17*, 85–105.

Hamersma, P. J., & Hart, J. (1987). A pressure drop correlation for gas/liquid pipe flow with a small liquid holdup. *Chemical Engineering Science*, *42*(5), 1187–1196. https://doi.org/10.1016/0009-2509(87)80068-4

Han-liang, X., & Ling-an, X. (2000). Electromagnetic tomography (EMT): Theoretical analysis of the forward problem. *Applied Mathematics and Mechanics*, *21*(9), 1034–1044. https://doi.org/10.1007/BF02459313

Han, F., Ong, M. C., Xing, Y., & Li, W. (2020). Three-dimensional numerical investigation of laminar flow in blind-tee pipes. *Ocean Engineering*, *217*(October 2019), 107962. https://doi.org/10.1016/j.oceaneng.2020.107962

Hansen, L. S., Pedersen, S., & Durdevic, P. (2019). Multi-Phase Flow Metering in Offshore Oil and Gas Transportation Pipelines: Trends and Perspectives. *Sensors*, *19*(9), 2184. https://doi.org/10.3390/s19092184

Hapanowicz, J. (2010). Phase inversion in liquid–liquid pipe flow. *Flow Measurement and Instrumentation*, *21*, 284–291. https://doi.org/10.1016/j.flowmeasinst.2010.03.001

Hassan, I., Vaillancourt, M., & Pehlivan, K. (2005). Two-phase flow regime transitions in microchannels: A comparative experimental study. *Microscale Thermophysical Engineering*, *9*(2), 165–182. https://doi.org/10.1080/10893950590945049

Hazuku, T., Takamasa, T., & Matsumoto, Y. (2008). Experimental study on axial development of liquid film in vertical upward annular two-phase flow. *International Journal of Multiphase Flow*, *34*(2), 111–127. https://doi.org/10.1016/j.ijmultiphaseflow.2007.10.008

He, D., & Bai, B. (2014). A new correlation for wet gas flow rate measurement with Venturi meter based on two-phase mass flow coefficient. *Measurement: Journal of the International Measurement Confederation*, *58*, 61–67. https://doi.org/10.1016/j.measurement.2014.08.014

Heikkinen, L. M., Kourunen, J., Savolainen, T., Vauhkonen, P. J., Kaipio, J. P., & Vauhkonen, M. (2006). Real time three-dimensional electrical impedance tomography applied in multiphase flow imaging. *Measurement Science and Technology*, *17*(8), 2083–2087. https://doi.org/10.1088/0957-0233/17/8/005

Hewitt, G. F., Parry, S. J., & Shires, G. L. (1995). Development and testing of the “mixmeter” multiphase flow meter. *North Sea Flow Measurement Workshop*.

Hewitt, G. F., & Roberts, D. N. (1969). Studies of two-phase flow patterns by simultaneous x-ray and flash photography. In *Atomic Energy Research Establishment*. https://doi.org/a953138.pdf

Hjertaker, B. T., Tjugum, S. A., Hallanger, A., & Maad, R. (2018). Characterization of multiphase flow blind-T mixing using high speed gamma-ray tomometry. *Flow Measurement and Instrumentation*, *62*(October), 205–212. https://doi.org/10.1016/j.flowmeasinst.2017.10.001

Huang, Z., Xie, D., Zhang, H., & Li, H. (2005). Gas-oil two-phase flow measurement using an electrical capacitance tomography system and a Venturi meter. *Flow Measurement and Instrumentation*, *16*(2–3), 177–182.

https://doi.org/10.1016/j.flowmeasinst.2005.02.007

Hubbard, M. G., & Dukler, A. E. (1966). The characterization of flow regimes for horizontal two-phase flow. *Proceedings of the Heat Transfer and Fluid Mechanics Institute*, 100–121.

Ibrahim, A. A., & Yeung, H. (2009). Intelligent multiphase flow measurement. In *Cranfield University*. http://hdl.handle.net/1826/4082

Imada, F. H. J., Saltara, F., & Baliño, J. L. (2013). Numerical study of the churn-slug transition dynamics in vertical upward air-water flows. *WIT Transactions on Engineering Sciences*, *79*(October 2016), 101–114. https://doi.org/10.2495/MPF130091

Ishak, M. A., Al-Qutami Hasan, T. A., Ellingsen, H., Ruden, T., & Khaledi, H. (2020). Evaluation of data driven versus multiphase transient flow simulator for virtual flow meter application. *Offshore Technology Conference Asia 2020, OTCA 2020*, 1–9. https://doi.org/10.4043/30422-ms

Ishak, M. A., Al-qutami, T. A. H., & Ismail, I. (2022). Virtual Multiphase Flow Meter using combination of Ensemble Learning and first principle physics based. *International Journal on Smart Sensing and Intelligent Systems*, *15*(1), 1–21. https://doi.org/10.2478/ijssis-2022-0010

Ismail, I., Gamio, J. C., Bukhari, S. F. A., & Yang, W. Q. (2005). Tomography for multi-phase flow measurement in the oil industry. *Flow Measurement and Instrumentation*, *16*(2–3), 145–155. https://doi.org/10.1016/j.flowmeasinst.2005.02.017

Ito, D., Prasser, H. M., Kikura, H., & Aritomi, M. (2011). Uncertainty and intrusiveness of three-layer wire-mesh sensor. *Flow Measurement and Instrumentation*, *22*(4), 249–256. https://doi.org/10.1016/j.flowmeasinst.2011.03.002

Jadid, M. (2017). Performance evaluation of virtual flow metering models and its application to metering backup and production allocation. In *LSU Doctoral Dissertations*.

https://digitalcommons.lsu.edu/gradschool_dissertations/4303

Jagan, V., & Satheesh, A. (2016). Experimental studies on two phase flow patterns of air–water mixture in a pipe with different orientations. *Flow Measurement and Instrumentation*, *52*(September), 170–179. https://doi.org/10.1016/j.flowmeasinst.2016.10.006

Jeanmeure, L. F. C., Dyakowski, T., Zimmerman, W. B. J., & Clark, W. (2002). Direct flow-pattern indentification using electrical capacitance tomography. *Experimental Thermal and Fluid Science*, *26*(6–7), 763–773. https://doi.org/10.1016/S0894-1777(02)00186-3

Julia, J. E., Ozar, B., Jeong, J. J., Hibiki, T., & Ishii, M. (2011). Flow regime development analysis in adiabatic upward two-phase flow in a vertical annulus. *International Journal of Heat and Fluid Flow*, *32*(1), 164–175. https://doi.org/10.1016/j.ijheatfluidflow.2010.09.003

Kadri, U., Mudde, R. F., Oliemans, R. V. A., Bonizzi, M., & Andreussi, P. (2009). Prediction of the transition from stratified to slug flow or roll-waves in gas–liquid horizontal pipes. *International Journal of Multiphase Flow*, *35*(11), 1001–1010. https://doi.org/10.1016/j.ijmultiphaseflow.2009.07.002

Kaji, R., Azzopardi, B. J., & Lucas, D. (2009). Investigation of flow development of co-current gas-liquid vertical slug flow. *International Journal of Multiphase Flow*, *35*(4), 335–348. https://doi.org/10.1016/j.ijmultiphaseflow.2009.01.004

Kanai, T., Furuya, M., Arai, T., Shirakawa, K., & Nishi, Y. (2012). Three-dimensional phasic velocity determination methods with wire-mesh sensor. *International Journal of Multiphase Flow*, *46*, 75–86. https://doi.org/10.1016/j.ijmultiphaseflow.2012.06.006

Kataoka, I., & Ishii, M. (1987). Drift flux model for large diameter pipe and new correlation for pool void fraction. *International Journal of Heat and Mass Transfer*, *30*(9), 1927–1939. https://doi.org/10.1016/0017-9310(87)90251-1

Kesana, N. R., Parsi, M., Vieira, R. E., Azzopardi, B., Schleicher, E., McLaury,

B. S., Shirazi, S. A., & Hampel, U. (2017). Visualization of gas-liquid multiphase pseudo-slug flow using Wire-Mesh Sensor. *Journal of Natural Gas Science and Engineering*, *46*, 477–490. https://doi.org/10.1016/j.jngse.2017.08.010

Keskin, C., Zhang, H. Q., & Sarica, C. (2007). Identification and classification of new three-phase gas/oil/water flow patterns. *Proceedings - SPE Annual Technical Conference and Exhibition*, *4*, 2363–2375. https://doi.org/10.2118/110221-ms

Khamehchi, E., Kivi, I. R., & Akbari, M. (2014). A novel approach to sand production prediction using artificial intelligence. *Journal of Petroleum Science and Engineering*, *123*, 147–154. https://doi.org/10.1016/j.petrol.2014.07.033

Khamehchi, E., & Reisi, E. (2015). Sand production prediction using ratio of shear modulus to bulk compressibility (case study). *Egyptian Journal of Petroleum*, *24*(2), 113–118. https://doi.org/10.1016/j.ejpe.2015.05.002

Khan, U., Pao, W., & Sallih, N. (2023). Gas-liquid two-phase flow regime identification in a horizontal pipe using dynamic pressure data. *Applied Science*, *13*(2), 1–17.

Khor, S. H. (1998). *Three-phase liquid-liquid-gas stratified flow in pipelines* (Issue January). Imperial College of Science, Technology and Medicine.

Kim, J. (1989). On the structure of pressure fluctuations in simulated turbulent channel flow. *Journal of Fluid Mechanics*, *205*(December), 421–451. https://doi.org/10.1017/S0022112089002090

Kjølaas, J., Belt, R., Wolden, M., Schümann, H., & Richon, V. (2022). Experiments and modelling of three-phase vertical pipe flow. *Chemical Engineering Science*, *247*. https://doi.org/10.1016/j.ces.2021.117091

Kokal, S. L., & Stanislav, J. F. (1989). An experimental study of two-phase flow in slightly inclined pipes-II. Liquid holdup and pressure drop. *Chemical Engineering Science*, *44*(3), 681–693. https://doi.org/10.1016/0009-

2509(89)85043-2

Kong, R., & Kim, S. (2017). Characterization of horizontal air–water two-phase flow. *Nuclear Engineering and Design*, *312*, 266–276. https://doi.org/10.1016/j.nucengdes.2016.06.016

Kraichnan, R. H. (1956). Pressure fluctuation in turbulent flow over a flat plate. *Journal of the Acoustical Society of America*, *28*(3), 378–390.

Krýsa, P., & Šoóš, M. (2022). Modelling of bubble breakage and coalescence in stirred and sparged bioreactor using the Euler-Lagrange approach. *International Journal of Heat and Mass Transfer*, *199*, 123466. https://doi.org/10.1016/j.ijheatmasstransfer.2022.123466

Lansangan, R. M. (2012). A study on the impact of instrument measurement uncertainty, degradation, availability and reservoir and fluid properties uncertainty on calculated rates of virtual metering systems. *30th International North Sea Flow Measurement Workshop, NSFMW 2012*, *October*, 1–30.

Lasheras, J. C., Martínez-Bazán, C., & Montañés, J. L. (1999). On the breakup of an air bubble injected into a fully developed turbulent flow. Part I: Breakup frequency. *30th Fluid Dynamics Conference*, *401*, 157–182. https://doi.org/10.2514/6.1999-3642

Lee, Y. G., Won, W. Y., Lee, B. A., & Kim, S. (2017). A dual conductance sensor for simultaneous measurement of void fraction and structure velocity of downward two-phase flow in a slightly inclined pipe. *Sensors (Switzerland)*, *17*(5). https://doi.org/10.3390/s17051063

Leporini, M., Marchetti, B., Corvaro, F., di Giovine, G., Polonara, F., & Terenzi, A. (2019). Sand transport in multiphase flow mixtures in a horizontal pipeline: An experimental investigation. *Petroleum*, *5*(2), 161–170. https://doi.org/10.1016/j.petlm.2018.04.004

Li, Y., Yang, W., Xie, C., Huang, S., Wu, Z., Tsamakis, D., & Lenn, C. (2013). Gas/oil/water flow measurement by electrical capacitance tomography.

Measurement Science and Technology, *24*(7), 074001. https://doi.org/10.1088/0957-0233/24/7/074001

Li, Z., Wang, G., Yousaf, M., Yang, X., & Ishii, M. (2018). Flow structure and flow regime transitions of downward two-phase flow in large diameter pipes. *International Journal of Heat and Mass Transfer*, *118*, 812–822. https://doi.org/10.1016/j.ijheatmasstransfer.2017.11.037

Lin, P. Y., & Hanratty, T. J. (1987). Effect of pipe diameter on flow patterns for air - water flow in horizontal pipes. *International Journal of Multiphase Flow*, *13*(4), 549–563.

Liu, X., Lao, L., & Falcone, G. (2020). A comprehensive assessment of correlations for two-phase flow through Venturi tubes. *Journal of Natural Gas Science and Engineering*, *78*, 1–11. https://doi.org/10.1016/j.jngse.2020.103323

Lockhart, R., & Martinelli, R. (1949). Proposed correlation of data for isothermal two-phase, two-component flow in pipes. *Chemical Engineering Progress*, *45*(1), 39–48.

Luo, H., & Svendsen, H. F. (1996). Theoretical model for drop and bubble breakup in turbulent dispersions. *AIChE Journal*, *42*(5), 1225–1233. https://doi.org/10.1002/aic.690420505

Ma, L., McCann, D., & Hunt, A. (2017). Combining magnetic induction tomography and electromagnetic velocity tomography for water continuous multiphase flows. *IEEE Sensors Journal*, *17*(24), 8271–8281. https://doi.org/10.1109/JSEN.2017.2758601

Ma, Yixin, Zheng, Z., Liu, X., & Wu, Y. (2001). Application of electrical resistance tomography system to monitor gas/liquid two-phase flow in a horizontal pipe. *Flow Measurement and Instrumentation*, *12*(4), 259–265. https://doi.org/10.1016/S0955-5986(01)00026-7

Ma, Yugao, Li, C., Pan, Y., Hao, Y., Huang, S., Cui, Y., & Han, W. (2021). A flow rate measurement method for horizontal oil-gas-water three-phase

flows based on Venturi meter, blind tee, and gamma-ray attenuation. *Flow Measurement and Instrumentation*, *80*(May), 101965. https://doi.org/10.1016/j.flowmeasinst.2021.101965

Mandhane, J. M., Gregory, G. A., & Aziz, K. (1974). A flow pattern map for gas-liquid flow in horizontal pipes. *International Journal of Multiphase Flow*, *1*(4), 537–553.

Mayor, T. S., Ferreira, V., Pinto, A. M. F. R., & Campos, J. B. L. M. (2008). Hydrodynamics of gas-liquid slug flow along vertical pipes in turbulent regime-An experimental study. *International Journal of Heat and Fluid Flow*, *29*(4), 1039–1053. https://doi.org/10.1016/j.ijheatfluidflow.2008.02.013

McQuillan, K. W., & Whalley, P. B. (1985). Flow patterns in vertical two-phase flow. *International Journal of Multiphase Flow*, *11*(2), 161–175.

Meng, Z., Huang, Z., Wang, B., Ji, H., Li, H., & Yan, Y. (2010). Air-water two-phase flow measurement using a Venturi meter and an electrical resistance tomography sensor. *Flow Measurement and Instrumentation*, *21*(3), 268–276. https://doi.org/10.1016/j.flowmeasinst.2010.02.006

Meribout, M., Azzi, A., Ghendour, N., Kharoua, N., Khezzar, L., & AlHosani, E. (2020). Multiphase flow meters targeting oil & gas industries. *Measurement*, *165*, 108111. https://doi.org/10.1016/j.measurement.2020.108111

Mishima, K., & Ishii, M. (1984). Flow regime transition criteria for upward two-phase flow in vertical tubes. *International Journal of Heat and Mass Transfer*, *27*(5), 723–737. https://doi.org/10.1016/0017-9310(84)90142-X

Morgado, A. O., Miranda, J. M., Araújo, J. D. P., & Campos, J. B. L. M. (2016). Review on vertical gas–liquid slug flow. *International Journal of Multiphase Flow*, *85*(July), 348–368. https://doi.org/10.1016/j.ijmultiphaseflow.2016.07.002

Moura, L. F. M., & Marvillet, C. (1997). Measurement of two-phase mass flow

rate and quality using venturi and void fraction meters. *American Society of Mechanical Engineers, Fluids Engineering Division FED*, *244*, 363–368.

Murdock, J. W. (1962). Two-phase flow measurement with orifices. *Journal of Fluids Engineering, Transactions of the ASME*, *84*(4), 419–432. https://doi.org/10.1115/1.3658657

Neogi, A., Mohanta, H. K., & Sande, P. C. (2022). Particle image velocimetry investigations on multiphase flow in fluidized beds: A review. *SSRN Electronic Journal*, *89*(January), 102309. https://doi.org/10.2139/ssrn.4272172

Netto, J. R. F., Fabre, J., & Peresson, L. (1999). Shape of long bubbles in horizontal slug flow. *International Journal of Multiphase Flow*, *25*, 1129–1160.

Nikolopoulos, N., Strotos, G., Nikas, K. S., & Bergeles, G. (2012). The effect of Weber number on the central binary collision outcome between unequal-sized droplets. *International Journal of Heat and Mass Transfer*, *55*(7–8), 2137–2150. https://doi.org/10.1016/j.ijheatmasstransfer.2011.12.017

Nydal, O. J., & Andreussi, P. (1991). Gas entrainment in a long liquid slug advancing in a near horizontal pipe. *International Journal of Multiphase Flow*, *17*(2), 179–189. https://doi.org/10.1016/0301-9322(91)90014-T

Nyfors, E. (2000). Industrial microwave sensors—a review. *Subsurface Sensing Technologies and Applications*, *1*(1), 23–43. https://doi.org/10.1023/A:1010118609079

O'hara, M. (2019). *Method and apparatus for characterising sand control*. https://patents.google.com/patent/US9750555B2/en

Oliveira, J. L. G., Passos, J. C., Verschaeren, R., & Geld, C. van der. (2009). Mass flow rate measurements in gas-liquid flows by means of a venturi or orifice plate coupled to a void fraction sensor. *Experimental Thermal and Fluid Science*, *33*(2), 253–260. https://doi.org/10.1016/j.expthermflusci.2008.08.008

Olsvik, K., & Widerse, T. (1995). Fluenta multiphase flow meter, tested and marinised. *North Sea Flow Measurement Workshop*, 250–270.

Paglianti, A., Giona, M., & Soldati, E. (1996). Characterization of subregions in two-phase slug flow. *International Journal of Multiphase Flow*, *22*(4), 783–796.

Pietro Fiorentini. (2021). *Multiphase flow metering* (pp. 1–18). Pietro Fiorentini.

Pietrzak, M., Płaczek, M., & Witczak, S. (2017). Upward flow of air-oil-water mixture in vertical pipe. *Experimental Thermal and Fluid Science*, *81*, 175–186. https://doi.org/10.1016/j.expthermflusci.2016.10.021

Pinguet, B. G. (2011). Worldwide review of 10 years of the multiphase meter performance based on a combined nucleonic fraction meter and venturi in heavy oil. *29th International North Sea Flow Measurement Workshop*.

Pinguet, B., Roux, G., Brocoletti, A., & Hopman, N. (2007). *Analysis of a full gamma ray spectrum in combination with a Venturi to monitor Salinity & Sand*. *March*, 1–15.

Pleshko, A. R., & Sharma, M. P. (1990). *An experimental study of vertical three-phase (oil-water-air) upward flows*. University of Wyoming.

Prasser, H. M., Böttger, A., & Zschau, J. (1998). A new electrode-mesh tomograph for gas-liquid flows. *Flow Measurement and Instrumentation*, *9*(2), 111–119. https://doi.org/10.1016/S0955-5986(98)00015-6

Qiu, C., Hoyle, B. S., & Podd, F. J. W. (2007). Engineering and application of a dual-modality process tomography system. *Flow Measurement and Instrumentation*, *18*(5–6), 247–254. https://doi.org/10.1016/j.flowmeasinst.2007.07.008

Razali, M. A. Bin, Xie, C. G., & Loh, W. L. (2021). Experimental investigation of gas-liquid flow in a vertical venturi installed downstream of a horizontal blind tee flow conditioner and the flow regime transition. *Flow Measurement and Instrumentation*, *80*(January), 1–16.

https://doi.org/10.1016/j.flowmeasinst.2021.101961

Reis, E. dos, & Goldstein, L. (2008). On the measurement of the mass flow rate of horizontal two-phase flows in the proximity of the transition lines which separates two different flow patterns. *Flow Measurement and Instrumentation*, *19*(5), 269–282. https://doi.org/10.1016/j.flowmeasinst.2008.01.002

Reis, E., & Goldstein, L. J. (2010). Characterization of slug flows in horizontal piping by signal analysis from a capacitive probe. *Flow Measurement and Instrumentation*, *21*(3), 347–355. https://doi.org/10.1016/j.flowmeasinst.2010.04.006

Riverin, J. L., de Langre, E., & Pettigrew, M. J. (2006). Fluctuating forces caused by internal two-phase flow on bends and tees. *Journal of Sound and Vibration*, *298*(4–5), 1088–1098. https://doi.org/10.1016/j.jsv.2006.06.039

Roach, G. J., Watt, J. S., Zastawny, H. W., Hartley, P. E., & Ellis, W. K. (1994). Multiphase flowmeter for oil, water and gas in pipelines based on gamma-ray transmission techniques. *Nuclear Geophysics*, *8*(3), 225–242.

Robert, A., & Hall, W. (1992). *Multiphase Flow of Oil , Water and Gas* (Issue October). Imperial College of Science, Technology and Medicine, University of London.

Rocha, D. M., de Carvalho, C. H. M., Estevam, V., & Rodriguez, O. M. H. (2017). Effects of water and gas injection and viscosity on volumetric fraction, pressure gradient and phase inversion in upward-vertical three-phase pipe flow. *Journal of Petroleum Science and Engineering*, *157*(March), 519–529. https://doi.org/10.1016/j.petrol.2017.07.055

Roesner, R. E., LeBlanc, A. J., & Davarzani, M. J. (1988). Effects of flow regimes on production logging instruments' responses. *Society of Petroleum Engineers of AIME, (Paper) SPE*, *PI*, 253-266 18206. https://doi.org/10.2118/18206-ms

Rouhani, S. Z., & Sohal, M. S. (1983). Two-phase flow patterns: A review of research results. *Progress in Nuclear Energy*, *11*(3), 219–259. https://doi.org/10.1016/0149-1970(83)90012-4

Saffari, H., Moosavi, R., Nouri, N. M., & Lin, C. X. (2014). Prediction of hydrodynamic entrance length for single and two-phase flow in helical coils. *Chemical Engineering and Processing: Process Intensification*, *86*, 9–21. https://doi.org/10.1016/j.cep.2014.10.005

Salahi, A., Dehghan, A. N., Sheikhzakariaee, S. J., & Davarpanah, A. (2021). Sand production control mechanisms during oil well production and construction. *Petroleum Research*, *6*(4), 361–367. https://doi.org/10.1016/j.ptlrs.2021.02.005

Samways, A. L. (1992). *Pressure fluctuations in shear flows*. University of Plymouth.

Schafer, L. (2017, January). Multiphase flowmeter advances. *P.I. Process Instrumentaton*. https://www.piprocessinstrumentation.com/instrumentation/flow-measurement/article/15563453/multiphase-flowmeter-advances

Schewe, G. (1983). On the structure and resolution of wall-pressure fluctuations associated with turbulent boundary-layer flow. *Journal of Fluid Mechanics*, *134*(September 1983), 311–328. https://doi.org/10.1017/S0022112083003389

Shaban, H., & Tavoularis, S. (2014). Identification of flow regime in vertical upward air-water pipe flow using differential pressure signals and elastic maps. *International Journal of Multiphase Flow*, *61*, 62–72. https://doi.org/10.1016/j.ijmultiphaseflow.2014.01.009

Shao, H., Jiang, L., Liu, L., & Zhao, Q. (2018). Modeling of multiphase fl ow through chokes. *Flow Measurement and Instrumentation*, *60*(April 2017), 44–50. https://doi.org/10.1016/j.flowmeasinst.2018.02.015

Shean, A. R. (1976). Pressure drop and phase fraction in oil-water-air vertical

pipe flow. *Mechanical Engineering*, 128.

Silva, E., Chacon, I. T., Garcia, D. A., Rosendahl, M., Teixeira, R. S., & Farias, M. H. (2018). Metrological concerns in multiphase flow measurement. *Journal of Physics: Conference Series*, *1044*, 012046. https://doi.org/10.1088/1742-6596/1044/1/012046

Spedding, P. L., Benard, E., & Crawford, N. M. (2008). Fluid flow through a vertical to horizontal 90° elbow bend III three phase flow. *Experimental Thermal and Fluid Science*, *32*(3), 827–843. https://doi.org/10.1016/j.expthermflusci.2007.10.002

Spedding, P. L., Benard, E., & Donnelly, G. F. (2006). Prediction of multiphase horizontal pipe flow: A reassessment. *Developments in Chemical Engineering and Mineral Processing*, *14*(3/4), 567–584.

Spedding, P. L., & Chen, J. J. J. (1984). Holdup in two phase flow. *International Journal of Multiphase Flow*, *10*(3), 307–339. https://doi.org/10.1016/0301-9322(84)90024-7

Spedding, P. L., Donnelly, G. F., & Cole, J. S. (2005). Three phase oil-water-gas horizontal co-current flow: I. Experimental and regime map. *Chemical Engineering Research and Design*, *83*(4 A), 401–411. https://doi.org/10.1205/cherd.02154

Steven, R. N. (2002). Wet gas metering with a horizontally mounted Venturi meter. *Flow Measurement and Instrumentation*, *12*(5–6), 361–372. https://doi.org/10.1016/S0955-5986(02)00003-1

Streeton, R., Sanchis, A., Helgaker, J. F., & Piotrowski, P. (2020). Erosion and sand detection testing of a subsea multiphase meter with integrated erosion monitoring system. *Society of Petroleum Engineers - SPE Asia Pacific Oil and Gas Conference and Exhibition 2020, APOG 2020*. https://doi.org/10.2118/202376-ms

Sun, J., & Yang, W. (2015). A dual-modality electrical tomography sensor for measurement of gas-oil-water stratified flows. *Measurement: Journal of the*

International Measurement Confederation, *66*, 150–160. https://doi.org/10.1016/j.measurement.2015.01.032

Taitel, Y., & Barnea, D. (1990). Two-phase slug flow. In *Advances in Heat Transfer* (Vol. 20, pp. 83–132). https://doi.org/10.1016/S0065-2717(08)70026-1

Taitel, Y., Bornea, D., & Dukler, A. . (1980). Modelling flow pattern transitions for steady upward gas-liquid flow in vertical tubes. *AIChE*, *26*(3), 345–354.

Taitel, Y., & Dukler, A. E. (1976). A model for predicting flow regime transitions in horizontal and near horizontal gas-liquid flow. *AIChE Journal*, *22*(1), 47–55. https://doi.org/10.1002/aic.690220105

Tan, C., Jia, J., Xu, C., Sun, Z., & Ding, F. (2018). Multiphase flow measurement : techniques and applications. *IEEE Access Special Section Editorial*, *6*, 32673–32675. https://doi.org/10.1109/ACCESS.2018.2844479

Tangen, S., Nilsen, R., & Holmås, K. (2017). Virtual flow meter - Sensitivity analysis part one. *35th International North Sea Flow Measurement Workshop, NSFMW 2017*.

Tay, B. L., & Thorpe, R. B. (2004). Effects of liquid physical properties on the forces acting on a pipe bend in gas-liquid slug flow. *Chemical Engineering Research and Design*, *82*(3), 344–356. https://doi.org/10.1205/026387604322870453

Tay, Boon Li, & Thorpe, R. B. (2014). Hydrodynamic forces acting on pipe bends in gas-liquid slug flow. *Chemical Engineering Research and Design*, *92*(5), 812–825. https://doi.org/10.1016/j.cherd.2013.08.012

Tengesdal, J. Ø., U, P. S., Kaya, A. S., & Tulsa, U. (1999). Flow-pattern transition and hydrodynamic modeling of churn flow. *SPE Journal*, *4*(4), 342–348.

Thaker, J., & Banerjee, J. (2017). Transition of plug to slug flow and associated fluid dynamics. *International Journal of Multiphase Flow*, *91*, 63–75.

https://doi.org/10.1016/j.ijmultiphaseflow.2017.01.014

Thorn, R., Johansen, G. A., & Hammer, E. A. (1997). Recent developments in three-phase flow measurement. *Measurement Science and Technology*, *8*(7), 691–701. https://doi.org/10.1088/0957-0233/8/7/001

Thorn, R., Johansen, G. A., & Hjertaker, B. T. (2013). Three-phase flow measurement in the petroleum industry. *Measurement Science and Technology*, *24*, 1–17. https://doi.org/10.1088/0957-0233/24/1/012003

Tompkins, C., Prasser, H., & Corradini, M. (2018). Wire-mesh sensors : A review of methods and uncertainty in multiphase fl ows relative to other measurement techniques. *Nuclear Engineering and Design*, *337*(July), 205–220. https://doi.org/10.1016/j.nucengdes.2018.06.005

Troniewski, L., & Ulbrich, R. (1984). The analysis of flow regime maps of two-phase gas-liquid flow in pipes. *Chemical Engineering Science*, *39*(7–8), 1213–1224. https://doi.org/10.1016/0009-2509(84)85082-4

Tutu, N. K. (1982). Pressure fluctuations and flow pattern recognition in vertical two phase gas-liquid flows. *International Journal of Multiphase Flow*, *8*(4), 443–447. https://doi.org/10.1016/0301-9322(82)90053-2

Ujang, P. M., Lawrence, C. J., Hale, C. P., & Hewitt, G. F. (2006). Slug initiation and evolution in two-phase horizontal flow. *International Journal of Multiphase Flow*, *32*(5), 527–552. https://doi.org/10.1016/j.ijmultiphaseflow.2005.11.005

Van Santen, H., Kolar, Z. I., & Scheers, A. M. (1995). Photon energy selection for dual energy γ- and/or X-ray absorption composition measurements in oil-water-gas mixtures. *Nuclear Geophysics*, *9*(3), 193–202. https://doi.org/10.1016/0969-8086(95)00012-G

Waltrich, P. J., Falcone, G., & Barbosa, J. R. (2013). Axial development of annular, churn and slug flows in a long vertical tube. *International Journal of Multiphase Flow*, *57*, 38–48. https://doi.org/10.1016/j.ijmultiphaseflow.2013.06.008

Wang, F., Marashdeh, Q., Fan, L. S., & Warsito, W. (2010). Electrical capacitance volume tomography: Design and applications. *Sensors*, *10*(3), 1890–1917. https://doi.org/10.3390/s100301890

Wang, M., Jia, J., Faraj, Y., Wang, Q., Xie, C. gang, Oddie, G., Primrose, K., & Qiu, C. (2015). A new visualisation and measurement technology for water continuous multiphase flows. *Flow Measurement and Instrumentation*, *46*, 204–212. https://doi.org/10.1016/j.flowmeasinst.2015.06.022

Wang, W., Liang, X., & Zhang, M. (2015). Measurment of gas-liquid two-phase slug flow with a Venturi meter based on blind source separation. *Chinese Journal of Chemical Engineering*, *23*(9), 1447–1452. https://doi.org/10.1016/j.cjche.2015.05.008

Wang, X., Guo, L., & Zhang, X. (2006). Development of liquid slug length in gas-liquid slug flow along horizontal pipeline: Experiment and simulation. *Chinese Journal of Chemical Engineering*, *14*(5), 626–633. https://doi.org/10.1016/S1004-9541(06)60125-0

Wang, Z. Y., Jin, N. D., Gao, Z. K., Zong, Y. B., & Wang, T. (2010). Nonlinear dynamical analysis of large diameter vertical upward oil-gas-water three-phase flow pattern characteristics. *Chemical Engineering Science*, *65*(18), 5226–5236. https://doi.org/10.1016/j.ces.2010.06.026

Warren, B. A., & Klausner, J. F. (1995). Developing lengths in horizontal two-phase bubbly flow. *Journal of Fluids Engineering, Transactions of the ASME*, *117*(3), 512–518. https://doi.org/10.1115/1.2817292

Weber, M. E. (1981). Drift in intermittent two-phase flow in horizontal pipes. *The Canadian Journal of Chemical Engineering*, *59*, 398–399.

Willmarth, W. W. (1975). Pressure fluctuations beneath turbulent boundary layers. *Fluid Mech.*, 13–38.

Wolf, A., Jayanti, S., & Hewitt, G. F. (2001). Flow development in vertical annular flow. *Chemical Engineering Science*, *56*(10), 3221–3235. https://doi.org/10.1016/S0009-2509(00)00546-7

Woods, G. S., Speddeng, P. L., Watterson, J. K., & Raghunathan, R. S. (1998). Three-phase oil/water/air vertical flow. *Chemical Engineering Research and Design*, *76*(5 A5), 571–584. https://doi.org/10.1205/026387698525252

Wu, B., Firouzi, M., Mitchell, T., Rufford, T. E., Leonardi, C., & Towler, B. (2017). A critical review of flow maps for gas-liquid flows in vertical pipes and annuli. *Chemical Engineering Journal*, *326*, 350–377. https://doi.org/10.1016/j.cej.2017.05.135

Wu, Z., McCann, H., Davis, L. E., Hu, J., Fontes, A., & Xie, C. G. (2009). Microwave-tomographic system for oil- and gas-multiphase-flow imaging. *Measurement Science and Technology*, *20*(10), 1–8. https://doi.org/10.1088/0957-0233/20/10/104026

Wu, Zhipeng. (2015). Developing a microwave tomographic system for multiphase flow imaging: Advances and challenges. *Transactions of the Institute of Measurement and Control*, *37*(6), 760–768. https://doi.org/10.1177/0142331214546523

Wylie, S. R., Shaw, A., & Al-Shamma'a, A. I. (2006). RF sensor for multiphase flow measurement through an oil pipeline. *Measurement Science and Technology*, *17*(8), 2141–2149. https://doi.org/10.1088/0957-0233/17/8/013

Xie, C. G., Chizelle, K. De, & Jundt, J. (2011). *SYSTEMS AND METHODS FOR MEASURING MULTIPHASE FLOW IN A HYDROCARBON TRANSPORTNG PIPELINE*.

Xie, C. G., Huang, S. M., Hoyle, B. S., Thorn, R., Lenn, C., Snowden, D., & Beck, M. S. (1992). Electrical capacitance tomography for flow imaging: System model for development of image reconstruction algorithms and design of primary sensors. *IEE Proceedings, Part G: Circuits, Devices and Systems*, *139*(1), 89–98. https://doi.org/10.1049/ip-g-2.1992.0015

Xie, C. G., Reinecke, N., Beck, M. S., Mewes, D., & Williams, R. A. (1995). Electrical tomography techniques for process engineering applications. *The Chemical Engineering Journal*, *56*, 127–133. https://doi.org/10.1016/0923-

0467(94)02907-5

Xu, L., Xu, J., Dong, F., & Zhang, T. (2003). On fluctuation of the dynamic differential pressure signal of Venturi meter for wet gas metering. *Flow Measurement and Instrumentation*, *14*(4–5), 211–217. https://doi.org/10.1016/S0955-5986(03)00027-X

Yan, Y., Wang, L., Wang, T., Wang, X., Hu, Y., & Duan, Q. (2018). Application of soft computing techniques to multiphase flow measurement: A review. *Flow Measurement and Instrumentation*, *60*(February), 30–43. https://doi.org/10.1016/j.flowmeasinst.2018.02.017

Yang, W. (2010). Design of electrical capacitance tomography sensors. *Measurement Science and Technology*, *21*(4), 042001. https://doi.org/10.1088/0957-0233/21/4/042001

Yang, W. Q., Stott, A. L., Beck, M. S., & Xie, C. G. (1995). Development of capacitance tomographic imaging systems for oil pipeline measurements. *Review of Scientific Instruments*, *66*(8), 4326–4332. https://doi.org/10.1063/1.1145322

Yaqub, M. W., & Pendyala, R. (2018). CFD simulations of gas-liquid-liquid three-phase co-current flow in horizontal pipe by tracking volume fractions using VOF model. *IOP Conference Series: Materials Science and Engineering*, *458*(1). https://doi.org/10.1088/1757-899X/458/1/012078

Yaqub, M. W., Rusli, R., & Pendyala, R. (2020). Experimental study on gas-liquid-liquid three-phase flow patterns and the resultant pressure drop in a horizontal pipe upstream of the 90° bend. *Chemical Engineering Science*, *226*, 115848. https://doi.org/10.1016/j.ces.2020.115848

Yih, T. S., & Griffith, P. (1968). Unsteady momentum fluxes in two-phase flow and the vibration of nuclear reactor components. In *Technical report (Massachusetts Institute of Technology, Heat Transfer Laboratory)* (Vol. 5). https://doi.org/10.1038/scientificamerican03261870-208a

York, T. (2001). Status of electrical tomography in industrial applications.

Journal of Electronic Imaging, *10*(3), 608. https://doi.org/10.1117/1.1377308

Yu, Z. Z., Peyton, A. T., Beck, M. S., Conway, W. F., & Xu, L. A. (1993). Imaging system based on electromagnetic tomography (EMT). *Electronics Letters*, *29*(7), 625. https://doi.org/10.1049/el:19930418

Zargar, M., Johns, M. L., Aljindan, J. M., Noui-Mehidi, M. N., & O'Neill, K. T. (2021). Nuclear magnetic resonance multiphase flowmeters: Current status and future prospects. *SPE Production and Operations*, *36*(2), 423–436. https://doi.org/10.2118/205351-PA

Zeghloul, A., Azzi, A., Saidj, F., Azzopardi, B. J., & Hewakandamby, B. (2015). Interrogating the effect of an orifice on the upward two-phase gas-liquid flow behavior. *International Journal of Multiphase Flow*, *74*, 96–105. https://doi.org/10.1016/j.ijmultiphaseflow.2015.04.013

Zhang, H. J., Lu, S. J., & Yu, G. Z. (1992). An investigation of two-phase flow measurement with orifices for low-quality mixtures. *International Journal of Multiphase Flow*, *18*(1), 149–155. https://doi.org/10.1016/0301-9322(92)90013-7

Zhang, Hong Jian, Yue, W. T., & Huang, Z. Y. (2005). Investigation of oil-air two-phase mass flow rate measurement using Venturi and void fraction sensor. *Journal of Zhejiang University: Science*, *6 A*(6), 601–606. https://doi.org/10.1631/jzus.2005.A0601

Zuber, N., & Findlay, J. A. (1965). Average volumetric concentration in two-phase flow systems. *Journal of Heat Transfer*, *87*(4), 453–468.

APPENDICES

Appendix A Gas-liquid-liquid three-phase flow regime

A.1 Gas-liquid-liquid three-phase flow regime in horizontal pipes

There is relatively less amount of published works on three-phase flow as compared to two-phase flow. In general, three-phase gas-liquid-liquid flow is more complex than its corresponding two-phase gas-liquid flow, because of an additional oil-water interface (Spedding et al., 2008). Different forms of gas-liquid-liquid three-phase flow have been identified by different authors over the past decades. In a bid to classify horizontal three phase flow regimes, Acikgoz et al. (1992) distinguished between plug and slug flows. Plug flow was observed when the liquid phases were driving the gas phases, while in contrast, the slug flow regime was observed when the gas phase was driving the liquid phases. The authors grouped the flow regimes into two category- oil-based flow regimes and water-based flow regimes. A total of 10 different flow regimes were distinguished as shown in Figure A-1 and Figure A-2. *Oil-based dispersed plug* flow is observed for relatively low water and air superficial velocities. This flow regime is characterised by the foamy appearance in the liquid phases due to the mixing of the oil and water. Plug flow indicates that the liquid phases are driving the air phase in such flow regime. *Oil-based dispersed slug* flow is observed when the superficial air velocity is increased. As in previous flow regime, the oil-based liquid phase is also foamy, however, the tail of the large gas bubbles is not sharply defined, in contrast to plug flow. *Oil-based dispersed stratified/wavy* flow is observed when stratification and gravitational separation is prevalent in the flow. The water film layer is observed at the bottom of the pipe while the oil-based mixture, containing droplets of dispersed water, settles between the gas and water layer. The air-oil-based liquid interface takes a wavy form. When the three-phase fluid is completely stratified, with no dispersed phase within the liquid stream, *oil-based separated stratified/wavy* flow is observed. The *oil-based separated wavy stratifying annular* flow is similar to oil-based separated stratified/wavy flow. However, for oil-based separated wavy

stratifying annular flow, increase in the oil film thickness at the upper part of the pipe means continuous wetting of the pipe.

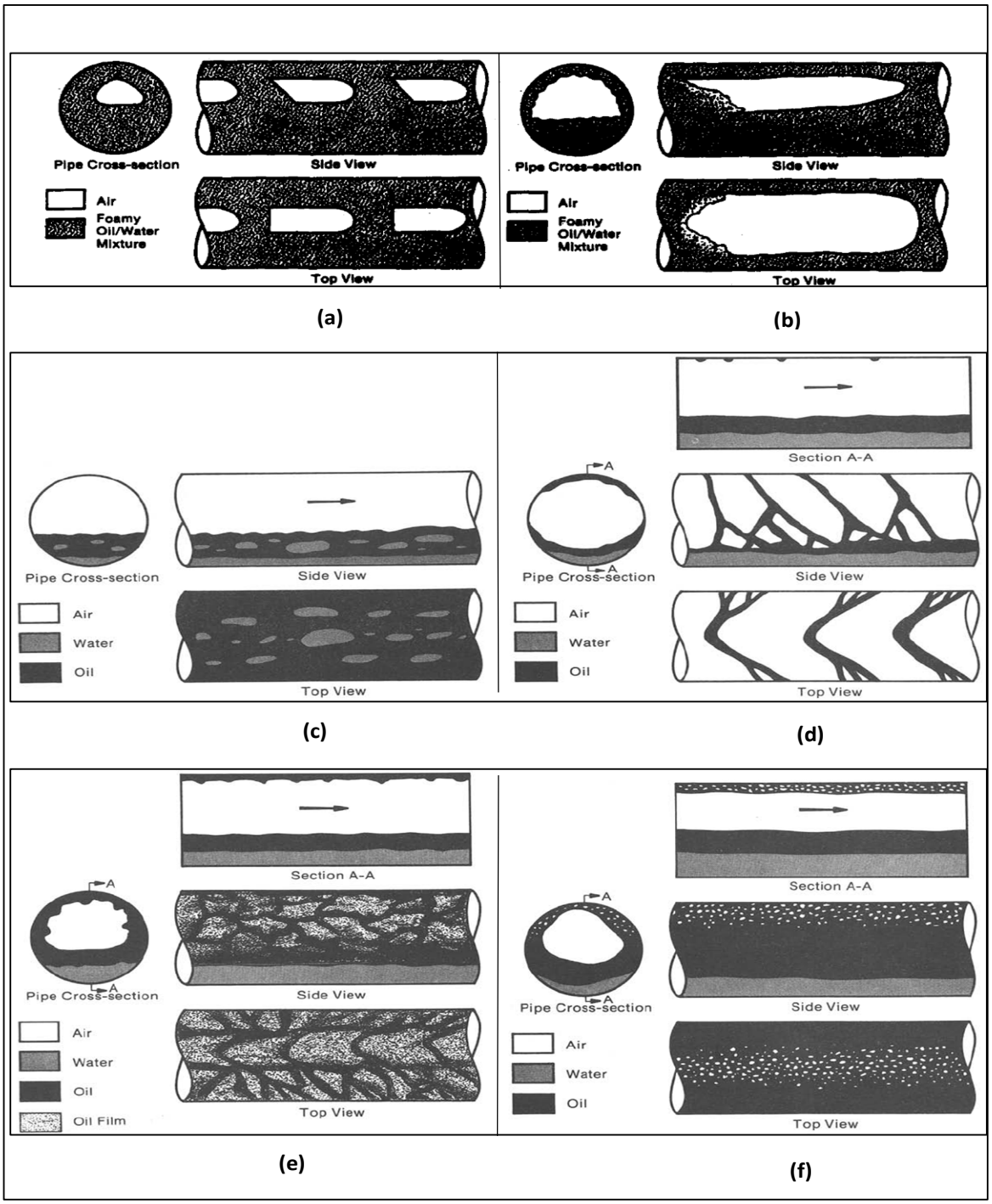

Figure A-1 Oil-based three-phase flow regime group (a) Oil-based dispersed plug flow, (b) Oil-based dispersed slug flow, (c) Oil based dispersed stratified/wavy flow, (d) Oil based separated stratified/wavy flow, (e) Oil-based separated wavy stratifying-annular flow, (f) Oil-based separated/dispersed stratifying-annular flow (Acikgoz et al., 1992).

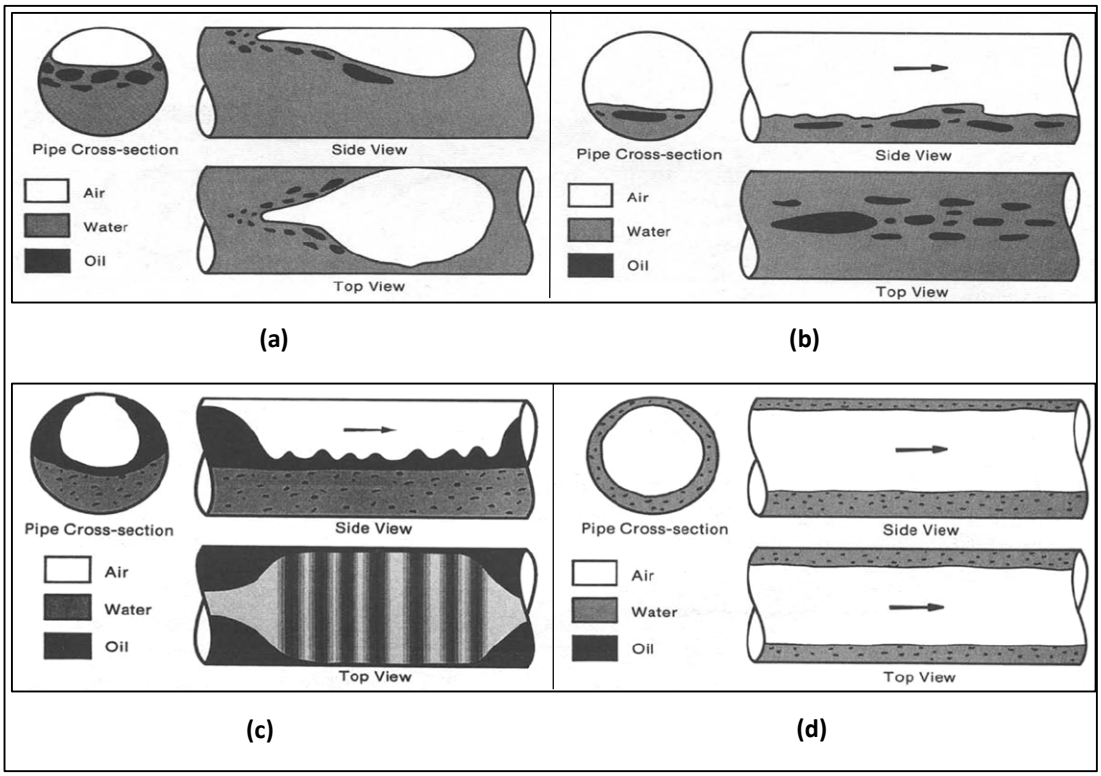

Figure A-2 Water-based three-phase flow regime group (a) water-based dispersed slug flow, (b) Water-based dispersed stratified/wavy flow, (c) water-based separated dispersed incipient stratifying-annular flow, and (d) water-based dispersed stratifying-annular flow (Acikgoz et al., 1992).

Oil-based separated/dispersed stratifying-annular flow is observed with the increase in the gas flowrate, which leads to change in the oil film thickness at the top of the pipe with more gas-bubble entrained in liquid film at the upper part of the pipe wall.

Water-based dispersed slug flow is observed for relatively low air and high liquid flowrates, with the large gas bubbles having distinct tails. Significant concentrations of oil droplets are found around the tail of the gas bubble. *Water-based dispersed stratified/wavy* flow observed with increase in air flowrate is similar to the common two-phase stratified/wavy flow, with the exception of the dispersed oil droplets. *Water-based separated/dispersed incipient stratifying-annular flow* (Figure A-2 (c)) is observed with further increase in the air flowrate. The low amplitude waves observed in Figure A-2 (b) is replaced by roll waves. *Water-based dispersed stratifying-annular* flow is characterised by the

continuous wetting of the perimeter of the pipe by a water-based film with dispersed oil droplets. The water film thickness at the upper and lower part of the pipe is more noticeable at lower air flowrates. This flow regime is similar to the typical two-phase stratifying-annular flow.

Table A-1 Three phase flow regime (Spedding et al., 2005)

Group	No.	Flow regime
Oil dominated (OD)	1	Plug separated
	2	Plug dispersed
	3	Slug separated
	4	Slug dispersed
	5	Blow through slug
	6	Smooth stratified separated
	7	Stratified wavy separated
	8	Stratified roll wave dispersed
	9	Stratified roll wave dispersed droplet
	10	Annular separated
	11	Annular dispersed
Inversion	12	Broken film
Water dominated (WD)	13	Plug dispersed
	14	Slug dispersed
	15	Blow through slug
	16	Smooth stratified separated
	17	Stratified ripple dispersed
	18	Stratified roll wave dispersed
	19	Stratified roll wave droplet
	20	Annular water annular oil
	21	Annular froth
	22	Annular dispersed

Similar flow regimes as above was observed by Lahey et al. (1992) in their experimental work on three-phase gas-oil-water flows. The authors observed that there was significant variation in the drift flux parameters for the different flow regimes-which is an indication that flow regime has effect on multiphase flow phase fraction measurement. Spedding et al. (2005) showed another common flow regime classification in literature, where the flows are grouped either as oil dominated (OD) or water dominated (WD), with the dominant liquid phase forming the continuum in which the liquid phase is dispersed. The flow regimes are then further classified for stratified, annular or intermittent type regime (Table A-1). The three-phase flow regimes are shown in Figure A-3 for oil dominated flow and Figure A-4 for water dominated flow.

A simplified three-phase flow regime classification based on the gas-liquid interface interactions was adopted by Kee et al. (2015) in distinguishing the 5 flow regimes observed in the gas-oil-water three phase flow experimental work. The authors indicated that the flow patterns are mostly influenced by the spatial distribution of the gas and the liquid phases, and to a lesser extent by phase distribution within the two-liquid phases. The five flow regimes observed their work is described and shown in Figure A-5

- Stratified (ST) flow is distinguished by the flow of the two liquid streams at the bottom, and a gas steam at the top of the pipe. The liquid phases are often separated or slightly dispersed at the oil-water interface. The gas-liquid interface maybe smooth or wavy based on the flow condition.
- Elongated bubble (EB) flow sometimes referred to plug flow, exhibits an intermittent flow structure which occur at relatively low gas velocity. It gas phase forms a long gas pockets trapped at the top of the pipe, moving alternatively in between continuous sections of liquid that occupy the pipe.

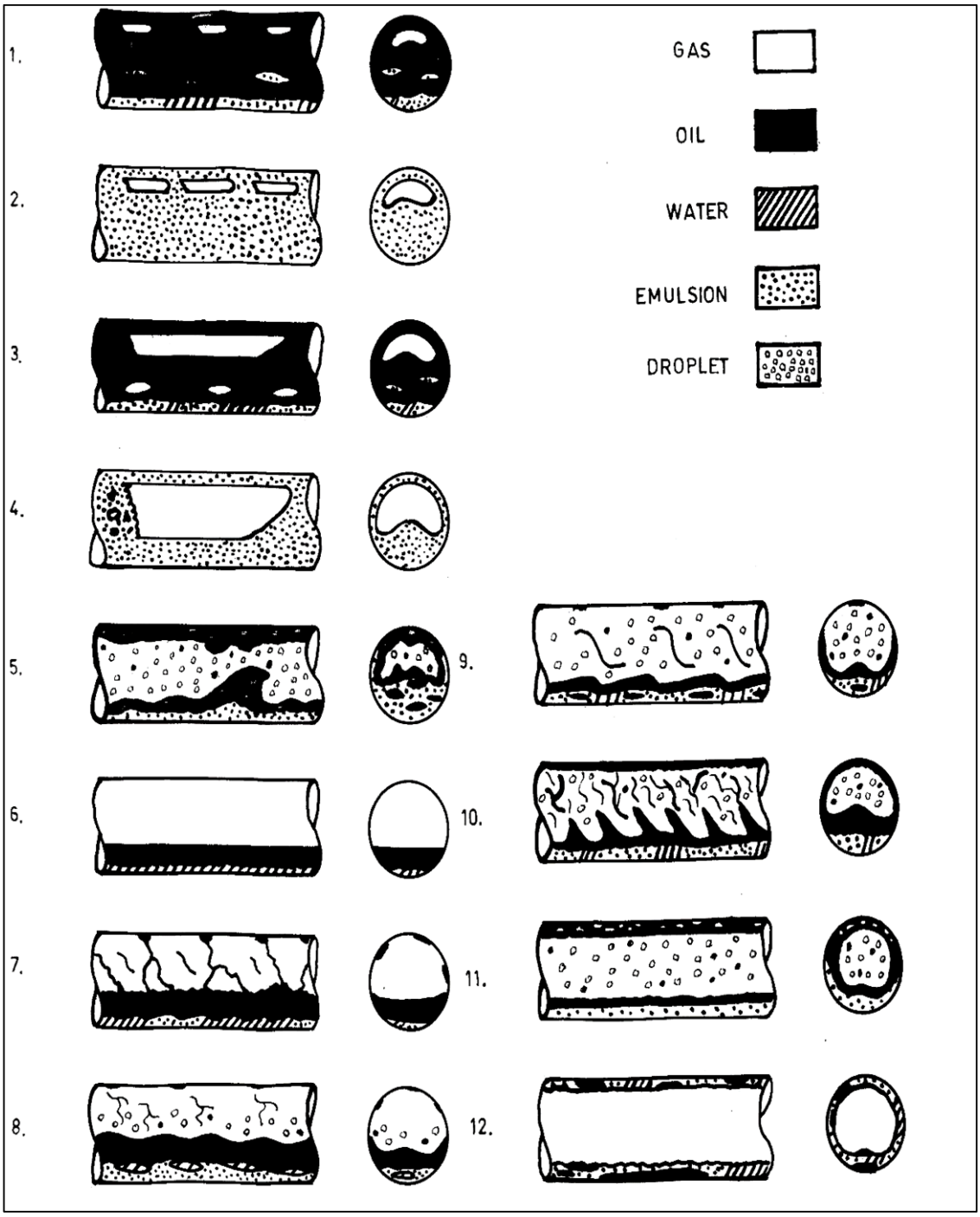

Figure A-3 Oil dominated flow regimes and inversion for three phase horizontal co-current pipe flow (Spedding et al., 2005)

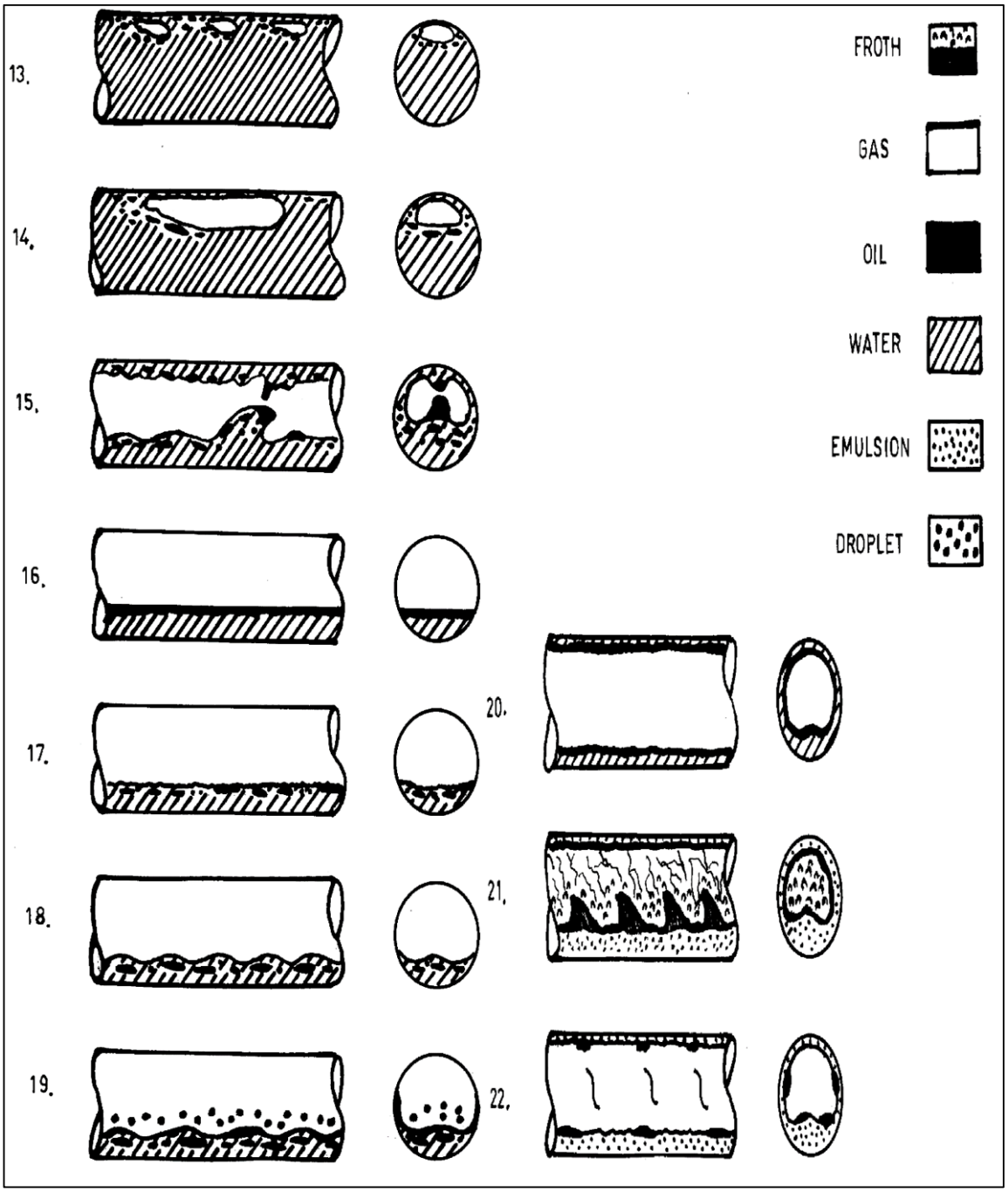

Figure A-4 Water dominated flow regimes for three phase horizontal co-current pipe flow (Spedding et al., 2005)

- *Slug (SL)* flow is another form of intermittent flow that occurs when the liquid bridges the entire pipe cross section forming a liquid slug, while the gas flows as a large bubble in between the train of liquid slugs. The large gas bubble flows over the slower moving stratified liquid layer. The liquid slug wetting the entire of the pipe section moves with higher velocity and overruns the slow flowing liquid film ahead. Turbulent liquid mixing region, occupied largely by small gas bubbles is observed at the slug front.
- Wavy annular (WA) flow is observed at the transition between slug and annular flow. The high amplitude waves between the gas and liquid interface is observed temporarily but do not cover the pipe top. Droplet entrainment is observed as a result of breakup of the unstable waves. The water phase is usually dispersed, mostly distributed along the pipe cross section.
- Annular-mist (AM) flow is characterised by high gas velocity, where the gas occupies the core of the pipe, and liquid moves as thin films around the pipe wall. The high gas flow contributes to turbulence and rough gas-liquid interfaces with interfacial waves of varying amplitudes. Some liquid films are entrained as mist in the gas core. The liquid film is usually thicker at the bottom than at the top due to gravity.

Similar method of flow regime classification was adopted by Yaqub et al. (2020) who classified the gas-liquid-liquid based on the typical gas-liquid flow, with further subclass for each of this typical flow regime based on the liquid-liquid interaction.

In summary, different authors have distinguished several varying flow regimes using different naming nomenclature. The initial approach of using both the gas-liquid and liquid-liquid interface flow structure to classify three-phase flow regime results to several flow regimes which could be impractical (Keskin, 2007). Therefore, more simplified approach involving generic grouping of similar flow pattern is assumed to be more practical.

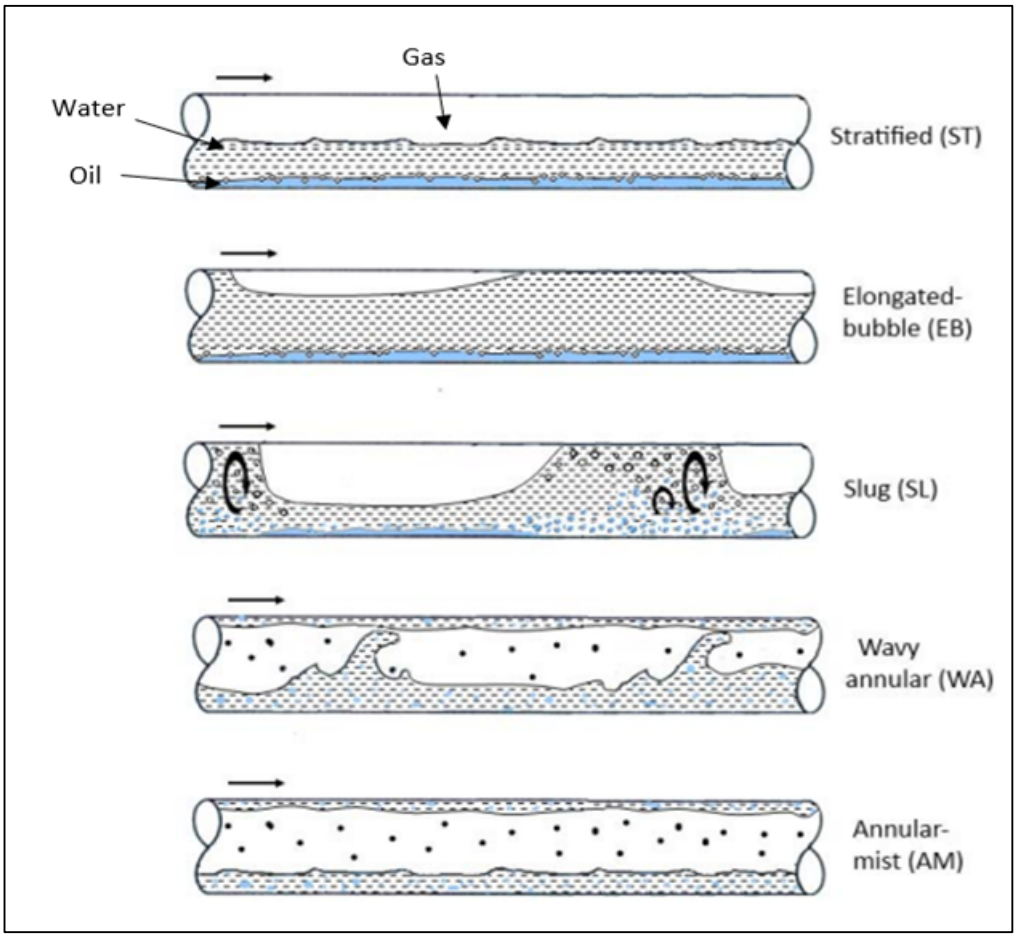

Figure A-5 Horizontal three phase flow regime (Kee et al., 2015)

A.2 Gas-liquid-liquid three-phase flow regime in vertical pipes

Some of the earliest work on vertical three-phase flow was performed on the basis of extending two-phase flow correlations to three -phase flow (Shean, 1976). However, the result of experimental studies by Pleshko & Sharma (1990) shows that two-phase flow models are not always well suited for predicting three-phase flows. This claim is supported by Spedding et al. (2006), who reported that two-phase correlations extended to three phase were only successful in prediction of intermittent slug type flows in certain cases

A detailed work on vertical three phase flow was performed by Woods et al. (1998). The authors identified flow regimes by visual and pressure drop techniques. The two major kind of flow patterns observed were either oil dominated (OD) or water dominated (WD). The following flow regimes were

observed : 1- OD oil annulus/dispersed annulus; 2- OD broken annulus; 3- OD dispersed churn; 4- OD dispersed slug; 5- WD water annulus/oil annular; 6- WD Dispersed annulus/oil annular; 7- WD dispersed churn; 8- WD dispersed slug. The flow regimes are described and presented in Figure A-6.

- OD oil annulus/dispersed annulus is observed when the oil film covering the walls of the pipe is overlaid by an oil-based stream with dispersed water droplets within the oil stream, that is interfaced with gas core. The flow sometimes could be considered semi annular flow, which is associated often with surface waves.
- OD broken annulus flow is witnessed when the water superficial velocity is increased to a point where the system moves from OD to WD (inversion point). For such flow condition, the OD annulus closest to the pipe wall begins to break and are gradually replaced by a WD annulus. The pipe wall has a marble-like appearance with significant liquid entrainment in the gas phase.
- OD Dispersed churn flow is almost the same as the typical two-phase churn flow regime, where water droplets are dispersed in the oil, that has a vertical oscillatory motion.
- Oil dispersed slug flow has similar flow structures as the two-phase slug flow, where water droplets are dispersed in oil. The liquid film around the large gas bubble is thicker than the two-phase slug flow regime.
- WD water annulus/oil annular flow is observed when the superficial velocity is increased beyond the inversion point, where the conversion to WD flow occurs with the formation of a water annulus next to the pipe wall, which is overlaid by the annular oil film. The interface of the annular oil film may appear rippled depending on the flow condition (gas flowrate).
- WD dispersed annulus/oil annular flow is associated with significant degree of mixing of the liquid phases that forms a partial dispersion of oil droplets in the water annulus. The interface of the liquid and gas may appear as roll waves or ripples depending on the gas flow condition.

- WD dispersed churn flow has the same flow features as the two-phase churn flow where the oil droplets are dispersed in water with a vertical oscillatory motion.
- WD dispersed slug flow has similar flow characteristics as the two-phase slug flow, where oil droplets are dispersed in water.

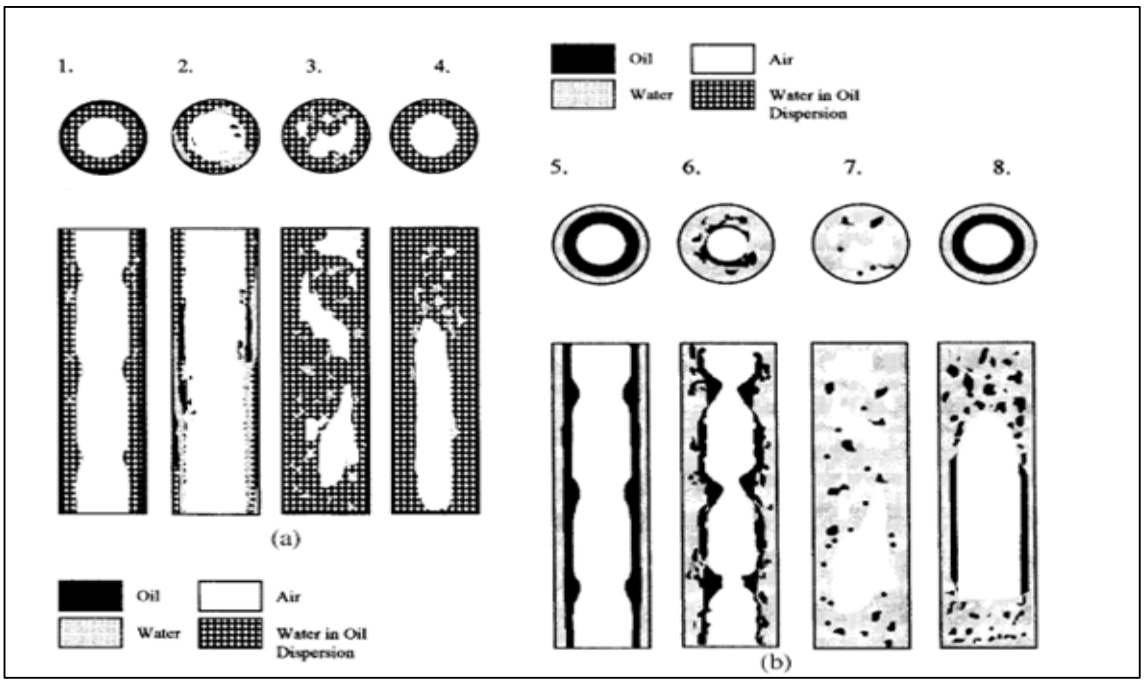

Figure A-6 Vertical three-phase flow (Woods et al., 1998)

In an experimental study of gas-oil-water flow conducted by Wang et al. (2010) using signals measured from mini-conductance probe and vertical multi-electrode array, the authors identified three-phase flow regimes (Figure A-7) as follows: oil in water type bubble flow, oil in water type bubble slug transitional flow, oil in water type slug flow, emulsion type bubble-slug transitional flow, emulsion type slug flow and water in oil type slug flow.

Pietrzak et al. (2017) performed experimental studies on three phase gas-oil-water flow in vertical pipes. In attempt to investigate the influence of gas injection on oil-water two-phase flow, the authors measured the mean in situ phase fraction and pressure drop, which was accompanied by flow pattern observation. The flow patterns observed in the experiments is shown in Figure A-8, and the flow patterns are described in Table A-2. From the result of the

experiments, the authors suggested that the characteristic feature of gas and two immiscible liquids flow is exhibited by the nature of the complex changes in pressure drop values, which on its own, is dependent on water, oil and gas flow rates, and the flow patterns present in the pipe.

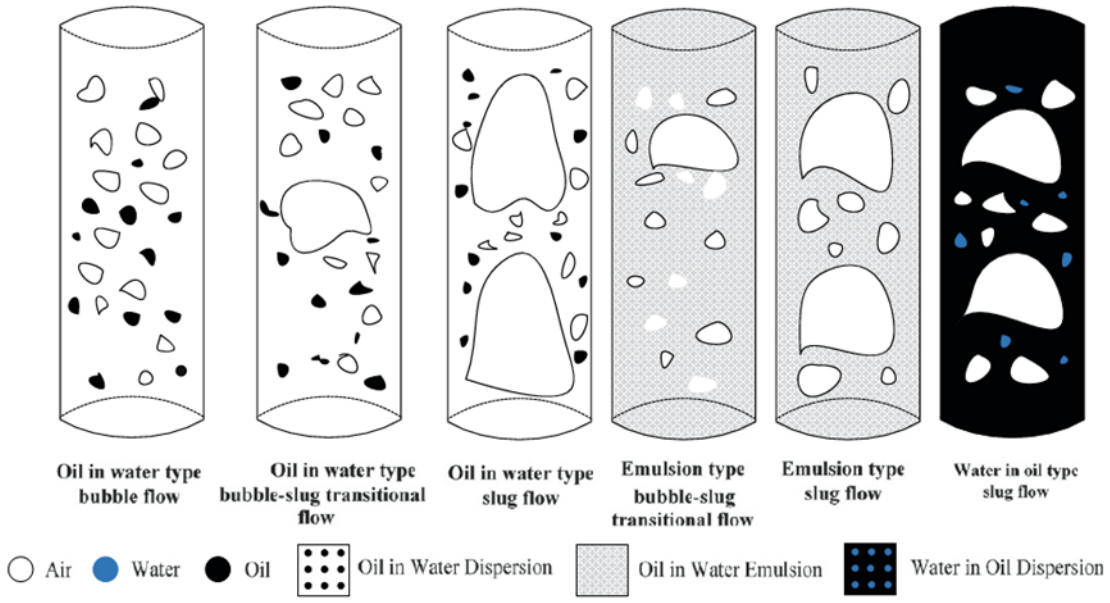

Figure A-7 Vertical three-phase flow (Wang et al., 2010)

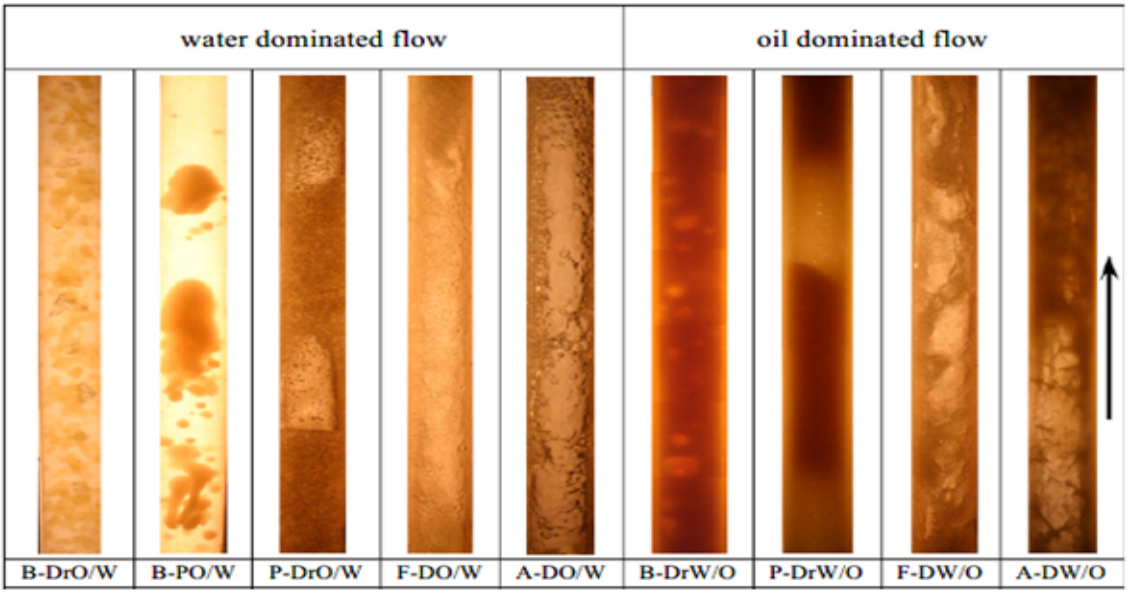

Figure A-8 Vertical three-phase flow (Pietrzak et al., 2017)

Table A-2 Description of the three phase gas-oil-water flow regime (Pietrzak et al., 2017)

Name	Flow description
B-DrO/W	Gas bubbles (B) and drops of oil (DrO) in water continuum (W)
B-PO/W	Gas bubbles (B) and plugs of oil (PO) in water continuum (W)
P-DrO/W	Plugs of gas (P) and discrete oil droplets (DrO) in water continuum (W)
F-DO/W	Breaking up and coalescence of gas bubbles; irregularly shaped gas bubbles flowing with high velocity; an oscillating fluid flow contributes to the formation of multi-phase mixture with foam characteristics (F); oil is dispersed (DO) in water continuum (W)
A-DO/W	Annular (A) air-liquid mixture flow; oil dispersed (DO) in water (W)
B-DrW/O	Gas bubbles (B) and drops of water (DrW) in oil continuum (O)
P-DrW/O	Gas plugs (P) and drops of water (DrW) in oil continuum (O)
F-DW/O	Breaking and connecting gas bubbles with irregularly shape flowing at a high velocity, with an oscillating fluid flow contributes to the formation of multi-phase mixture with foam characteristics (F); water dispersed (DW) in oil continuum (O)
A-DW/O	Annular (A) air-liquid mixture flow; water dispersed (DW) in oil (O)

In summary, as with two-phase flow, the vertical three-phase flow tends to have reduced number of flow regimes than the horizontal three-phase flow regimes. The common flow regimes observed in the literature were mostly classified based dominant(continuous) liquid phase and the gas-liquid interface features.

Appendix B Experimental test points

The tests points used for the experimental work is presented in the below

Table B-1 Test points of the experimental studies

Test Point	Gas flow rate (m^3/hr)	Gas flow rate (m^3/s)	Liquid flow rate (l/s)	Liquid flow rate (m^3/s)	Superficial gas velocity (m/s)	Superficial liquid velocity (m/s)	Superficial gas Reynold's number	Superficial Liquid Reynold's number
1	457.014	0.1269	0.20	0.0002	27.262	0.043	1.38E+05	3.30E+03
2	457.014	0.1269	0.40	0.0004	27.262	0.086	1.38E+05	6.60E+03
3	457.014	0.1269	0.60	0.0006	27.262	0.129	1.38E+05	9.90E+03
4	457.014	0.1269	0.80	0.0008	27.262	0.172	1.38E+05	1.32E+04
5	365.611	0.1016	0.20	0.0002	21.809	0.043	1.11E+05	3.30E+03
6	365.611	0.1016	0.40	0.0004	21.809	0.086	1.11E+05	6.60E+03
7	365.611	0.1016	0.60	0.0006	21.809	0.129	1.11E+05	9.90E+03
8	365.611	0.1016	0.80	0.0008	21.809	0.172	1.11E+05	1.32E+04
9	365.611	0.1016	1.00	0.0010	21.809	0.215	1.11E+05	1.65E+04
10	274.208	0.0762	0.20	0.0002	16.357	0.043	8.31E+04	3.30E+03
11	274.208	0.0762	0.40	0.0004	16.357	0.086	8.31E+04	6.60E+03
12	274.208	0.0762	0.60	0.0006	16.357	0.129	8.31E+04	9.90E+03
13	274.208	0.0762	0.80	0.0008	16.357	0.172	8.31E+04	1.32E+04
14	274.208	0.0762	1.00	0.0010	16.357	0.215	8.31E+04	1.65E+04

Test Point	Gas flow rate (m^3/hr)	Gas flow rate (m^3/s)	Liquid flow rate (l/s)	Liquid flow rate (m^3/s)	Superficial gas velocity (m/s)	Superficial liquid velocity (m/s)	Superficial gas Reynold's number	Superficial Liquid Reynold's number
15	182.805	0.0508	0.20	0.0002	10.905	0.043	5.54E+04	3.30E+03
16	182.805	0.0508	0.40	0.0004	10.905	0.086	5.54E+04	6.60E+03
17	182.805	0.0508	0.60	0.0006	10.905	0.129	5.54E+04	9.90E+03
18	182.805	0.0508	0.80	0.0008	10.905	0.172	5.54E+04	1.32E+04
19	182.805	0.0508	1.00	0.0010	10.905	0.215	5.54E+04	1.65E+04
20	91.403	0.0254	0.20	0.0002	5.452	0.043	2.77E+04	3.30E+03
21	91.403	0.0254	0.40	0.0004	5.452	0.086	2.77E+04	6.60E+03
22	91.403	0.0254	0.60	0.0006	5.452	0.129	2.77E+04	9.90E+03
23	91.403	0.0254	0.80	0.0008	5.452	0.172	2.77E+04	1.32E+04
24	91.403	0.0254	1.00	0.0010	5.452	0.215	2.77E+04	1.65E+04
25	91.403	0.0254	2.00	0.0020	5.452	0.429	2.77E+04	3.30E+04
26	68.552	0.0190	0.20	0.0002	4.089	0.043	2.08E+04	3.30E+03
27	68.552	0.0190	0.40	0.0004	4.089	0.086	2.08E+04	6.60E+03
28	68.552	0.0190	0.60	0.0006	4.089	0.129	2.08E+04	9.90E+03
29	68.552	0.0190	0.80	0.0008	4.089	0.172	2.08E+04	1.32E+04
30	68.552	0.0190	1.00	0.0010	4.089	0.215	2.08E+04	1.65E+04
31	68.552	0.0190	2.00	0.0020	4.089	0.429	2.08E+04	3.30E+04
32	45.701	0.0127	0.20	0.0002	2.726	0.043	1.38E+04	3.30E+03
33	45.701	0.0127	0.40	0.0004	2.726	0.086	1.38E+04	6.60E+03

Test Point	Gas flow rate (m^3/hr)	Gas flow rate (m^3/s)	Liquid flow rate (l/s)	Liquid flow rate (m^3/s)	Superficial gas velocity (m/s)	Superficial liquid velocity (m/s)	Superficial gas Reynold's number	Superficial Liquid Reynold's number
34	45.701	0.0127	0.60	0.0006	2.726	0.129	1.38E+04	9.90E+03
35	45.701	0.0127	0.80	0.0008	2.726	0.172	1.38E+04	1.32E+04
36	45.701	0.0127	1.00	0.0010	2.726	0.215	1.38E+04	1.65E+04
37	45.701	0.0127	2.00	0.0020	2.726	0.429	1.38E+04	3.30E+04
38	22.851	0.0063	0.20	0.0002	1.363	0.043	6.92E+03	3.30E+03
39	22.851	0.0063	0.40	0.0004	1.363	0.086	6.92E+03	6.60E+03
40	22.851	0.0063	0.60	0.0006	1.363	0.129	6.92E+03	9.90E+03
41	22.851	0.0063	0.80	0.0008	1.363	0.172	6.92E+03	1.32E+04
42	22.851	0.0063	1.00	0.0010	1.363	0.215	6.92E+03	1.65E+04
43	22.851	0.0063	2.00	0.0020	1.363	0.429	6.92E+03	3.30E+04
44	22.851	0.0063	4.00	0.0040	1.363	0.859	6.92E+03	6.60E+04
45	22.851	0.0063	6.00	0.0060	1.363	1.288	6.92E+03	9.90E+04
46	15.995	0.0044	0.20	0.0002	0.954	0.043	4.85E+03	3.30E+03
47	15.995	0.0044	0.40	0.0004	0.954	0.086	4.85E+03	6.60E+03
48	15.995	0.0044	2.00	0.0020	0.954	0.429	4.85E+03	3.30E+04
49	15.995	0.0044	4.00	0.0040	0.954	0.859	4.85E+03	6.60E+04
50	15.995	0.0044	6.00	0.0060	0.954	1.288	4.85E+03	9.90E+04
51	9.140	0.0025	0.20	0.0002	0.545	0.043	2.77E+03	3.30E+03
52	9.140	0.0025	0.40	0.0004	0.545	0.086	2.77E+03	6.60E+03

Test Point	Gas flow rate (m^3/hr)	Gas flow rate (m^3/s)	Liquid flow rate (l/s)	Liquid flow rate (m^3/s)	Superficial gas velocity (m/s)	Superficial liquid velocity (m/s)	Superficial gas Reynold's number	Superficial Liquid Reynold's number
53	9.140	0.0025	2.00	0.0020	0.545	0.429	2.77E+03	3.30E+04
54	9.140	0.0025	4.00	0.0040	0.545	0.859	2.77E+03	6.60E+04
55	9.140	0.0025	6.00	0.0060	0.545	1.288	2.77E+03	9.90E+04
56	2.285	0.0006	0.20	0.0002	0.136	0.043	6.92E+02	3.30E+03
57	2.285	0.0006	0.40	0.0004	0.136	0.086	6.92E+02	6.60E+03
58	2.285	0.0006	1.00	0.0010	0.136	0.215	6.92E+02	1.65E+04
59	2.285	0.0006	2.00	0.0020	0.136	0.429	6.92E+02	3.30E+04
60	2.285	0.0006	4.00	0.0040	0.136	0.859	6.92E+02	6.60E+04
61	2.285	0.0006	6.00	0.0060	0.136	1.288	6.92E+02	9.90E+04
62	53.699	0.0149	3.71	0.0037	3.203	0.797	1.63E+04	6.12E+04
63	5.621	0.0016	9.27	0.0093	0.335	1.991	1.70E+03	1.53E+05
64	7.769	0.0022	5.56	0.0056	0.463	1.194	2.35E+03	9.18E+04
65	19.560	0.0054	5.56	0.0056	1.167	1.194	5.93E+03	9.18E+04
66	24.400	0.0068	3.71	0.0037	1.456	0.797	7.39E+03	6.12E+04
67	2.692	0.0007	9.27	0.0093	0.161	1.991	8.16E+02	1.53E+05
68	3.921	0.0011	5.56	0.0056	0.234	1.194	1.19E+03	9.18E+04
69	9.149	0.0025	5.56	0.0056	0.546	1.194	2.77E+03	9.18E+04
70	17.760	0.0049	0.24	0.0002	1.059	0.050	5.38E+03	3.88E+03
71	35.519	0.0099	4.69	0.0047	2.119	1.007	1.08E+04	7.74E+04

Test Point	Gas flow rate (m^3/hr)	Gas flow rate (m^3/s)	Liquid flow rate (l/s)	Liquid flow rate (m^3/s)	Superficial gas velocity (m/s)	Superficial liquid velocity (m/s)	Superficial gas Reynold's number	Superficial Liquid Reynold's number
72	177.586	0.0493	1.41	0.0014	10.593	0.303	5.38E+04	2.33E+04
73	45.701	0.0127	0.50	0.0005	2.726	0.107	1.38E+04	8.25E+03
74	45.701	0.0127	1.00	0.0010	2.726	0.215	1.38E+04	1.65E+04
75	45.701	0.0127	3.71	0.0037	2.726	0.797	1.38E+04	6.12E+04
76	24.400	0.0068	5.56	0.0056	1.456	1.194	7.39E+03	9.18E+04
77	45.701	0.0127	5.56	0.0056	2.726	1.194	1.38E+04	9.18E+04
78	68.552	0.0190	5.56	0.0056	4.089	1.194	2.08E+04	9.18E+04

Appendix C Time series plots of pressure measurements for different blind tee lengths in the flow loop

C.1 Time series of pressures in blind tee of different lengths (0D, 1D and 2D)

C.1.1 Time series of pressures in blind tee of different lengths for intermittent flows

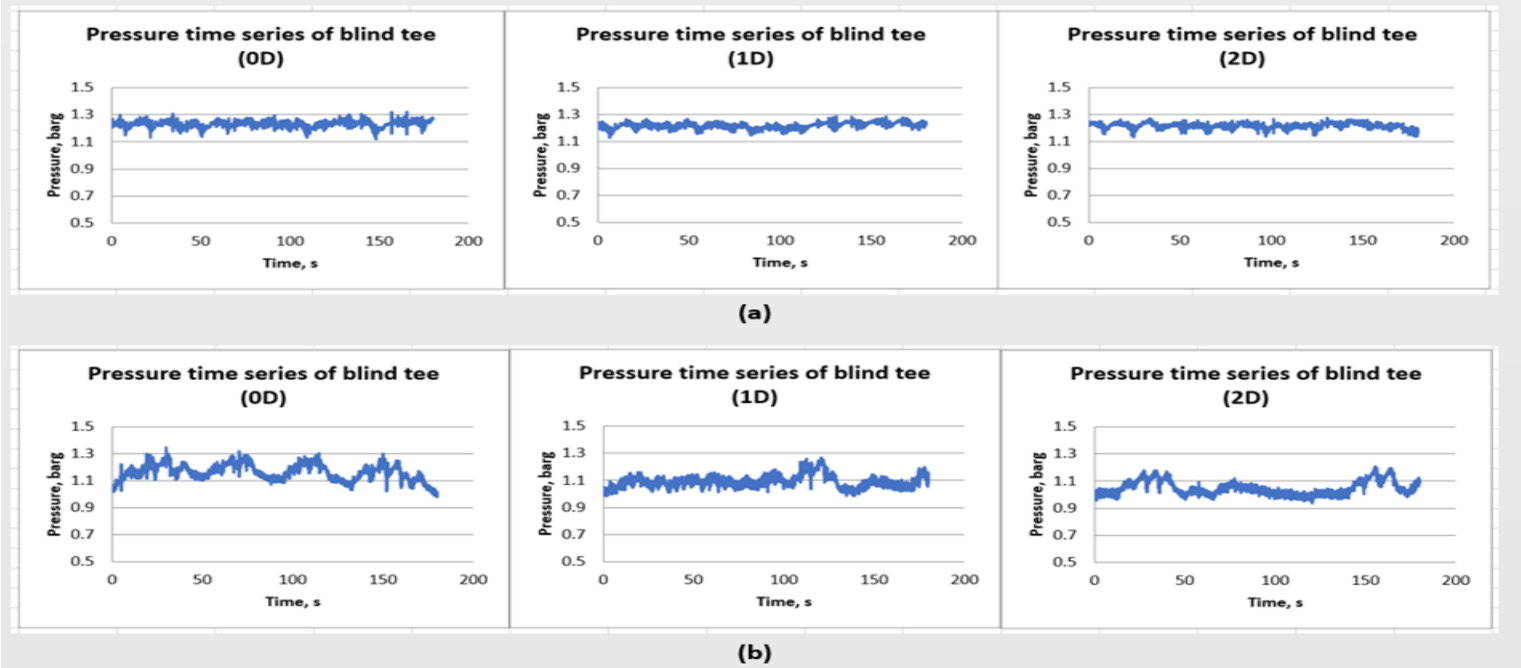

Figure C-1 Time series of pressures in blind tee of different lengths (0D, 1D and 2D) for flows with superficial liquid velocity of 0.086 m/s and superficial gas velocities of (a) 0.14 m/s and (b) 0.55 m/s.

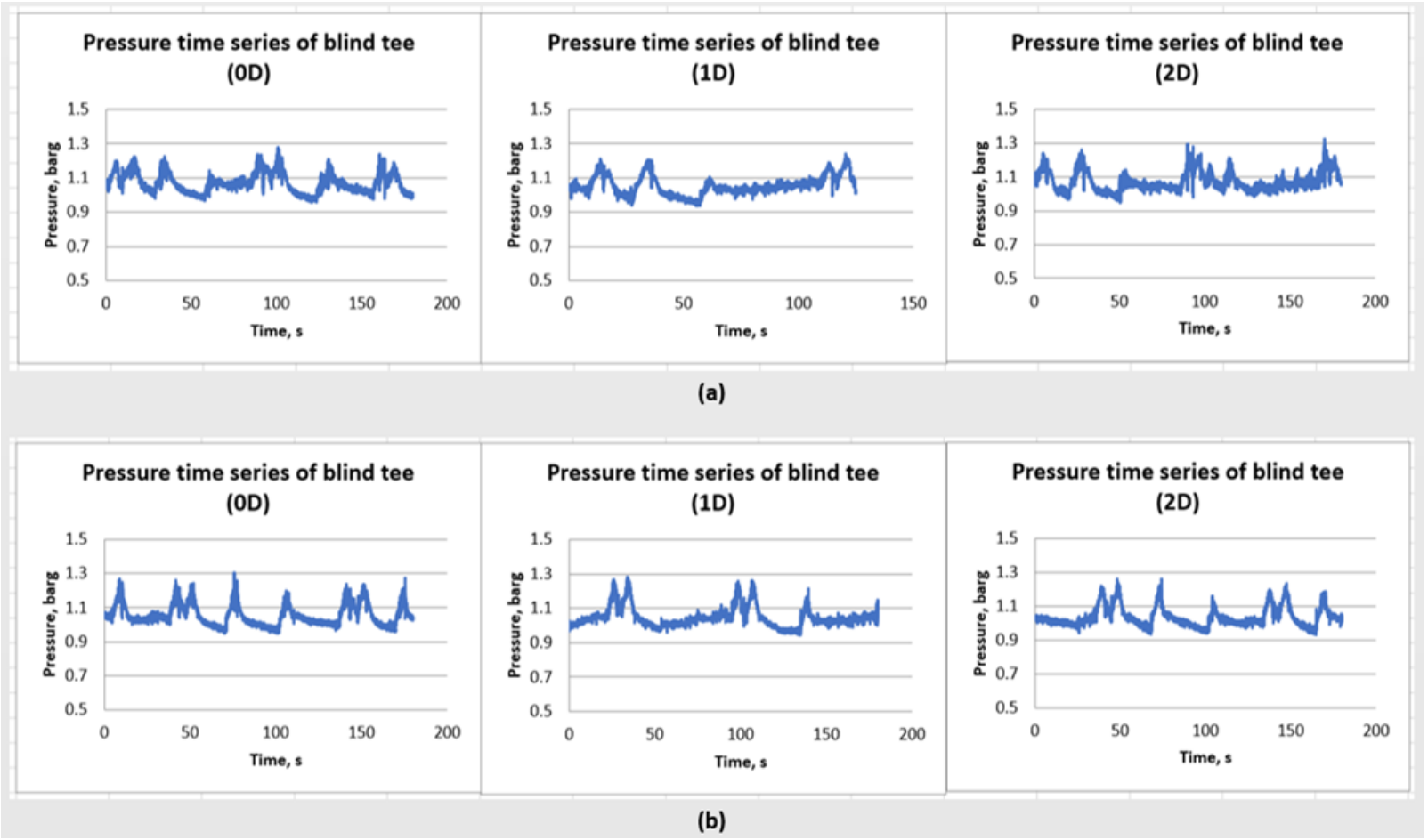

Figure C-2 Time series of pressures in blind tee of different lengths (0D, 1D and 2D) for flows with superficial liquid velocity of 0.086 m/s and superficial gas velocities of (a) 0.95 m/s and (b) 1.36 m/s.

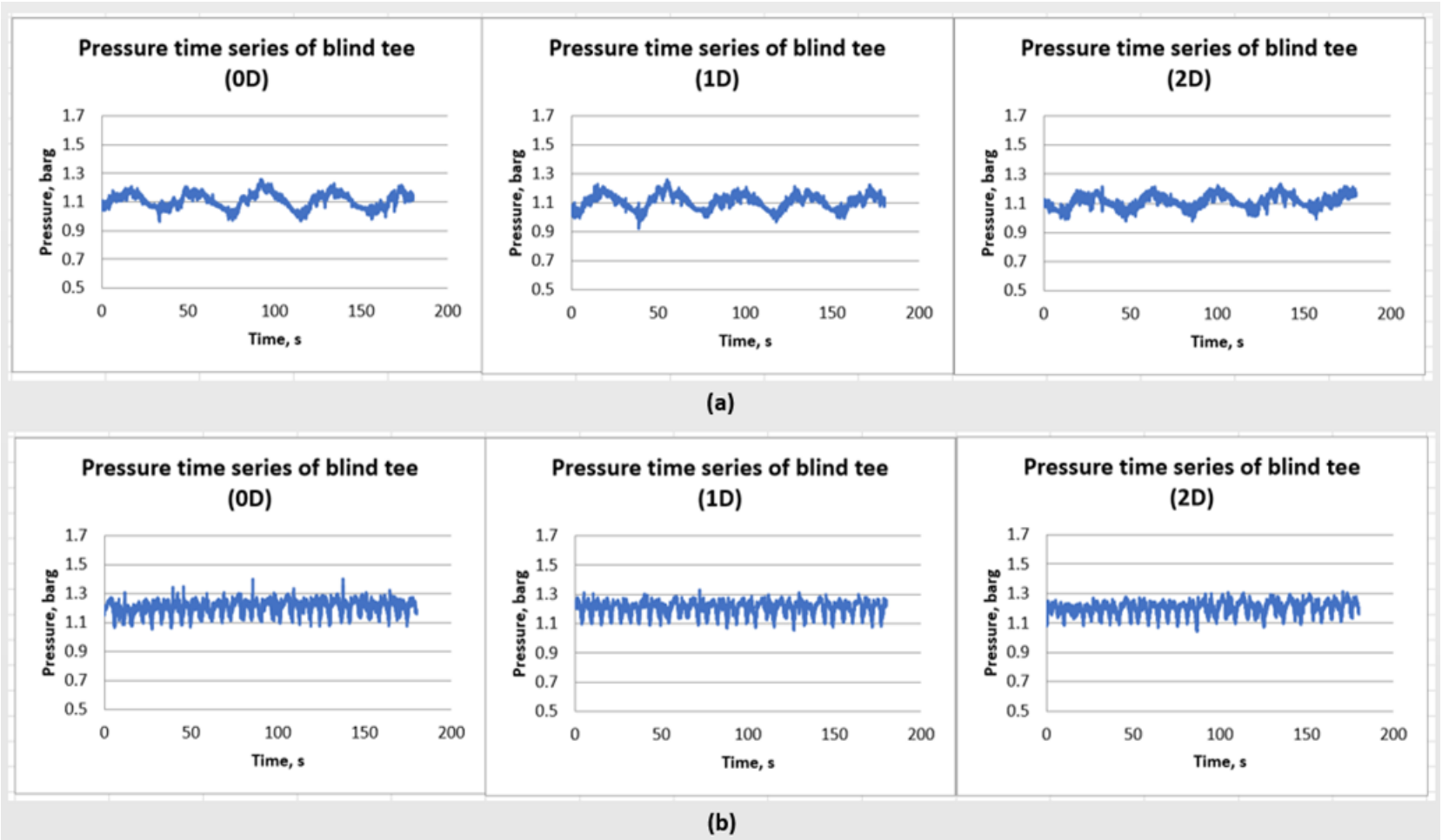

Figure C-3 Time series of pressures in blind tee of different lengths (0D, 1D and 2D) for flows with superficial liquid velocity of 0.86 m/s and superficial gas velocities of (a) 0.14 m/s and (b) 0.55 m/s.

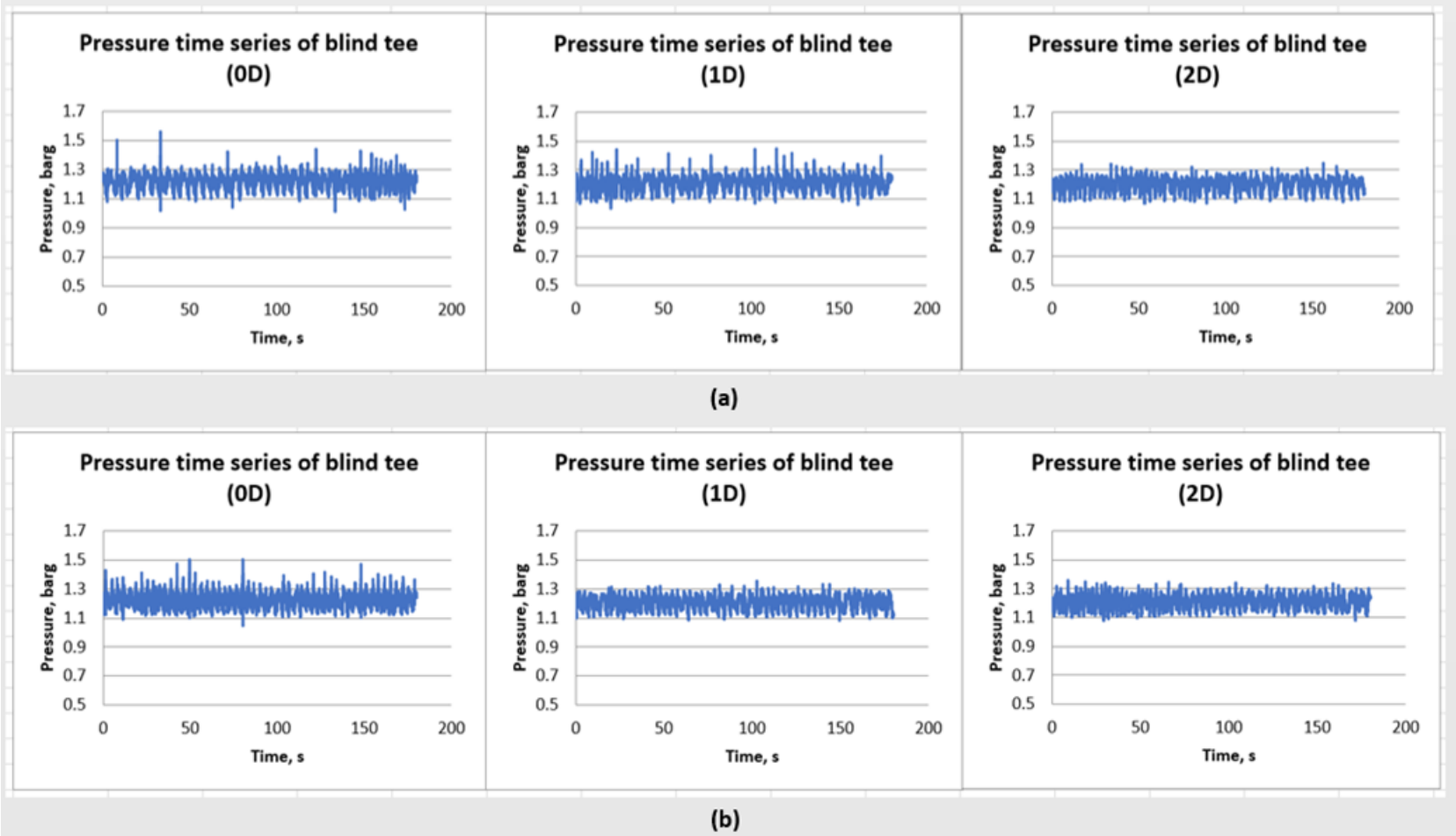

Figure C-4 Time series of pressures in blind tee of different lengths (0D, 1D and 2D) for flows with superficial liquid velocity of 0.86 m/s and superficial gas velocities of (a) 0.95 m/s and (b) 1.36 m/s.

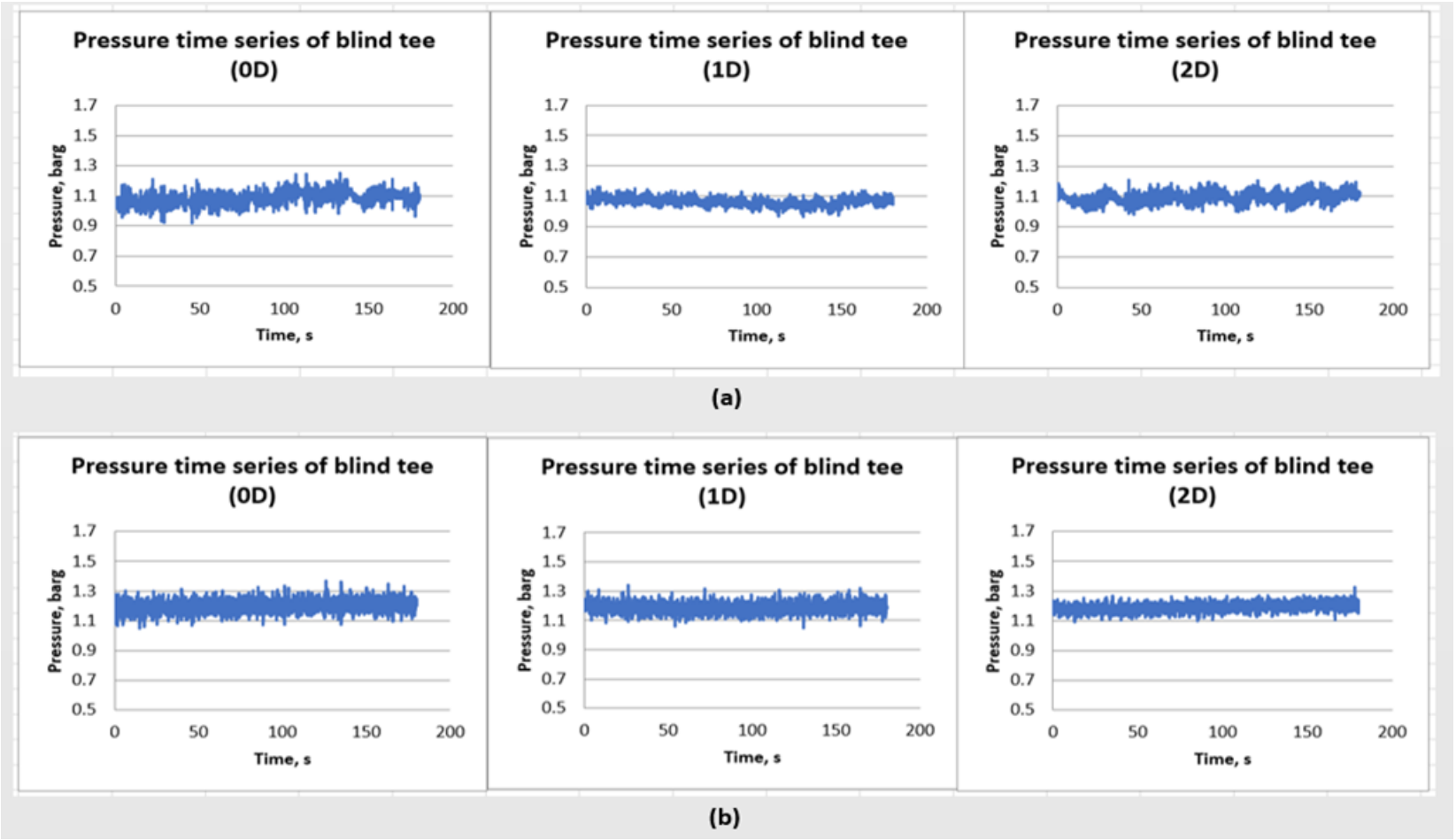

Figure C-5 Time series of pressures in blind tee of different lengths (0D, 1D and 2D) for flows with superficial liquid velocity of 1.3 m/s and superficial gas velocities of (a) 0.14 m/s and (b) 0.55 m/s.

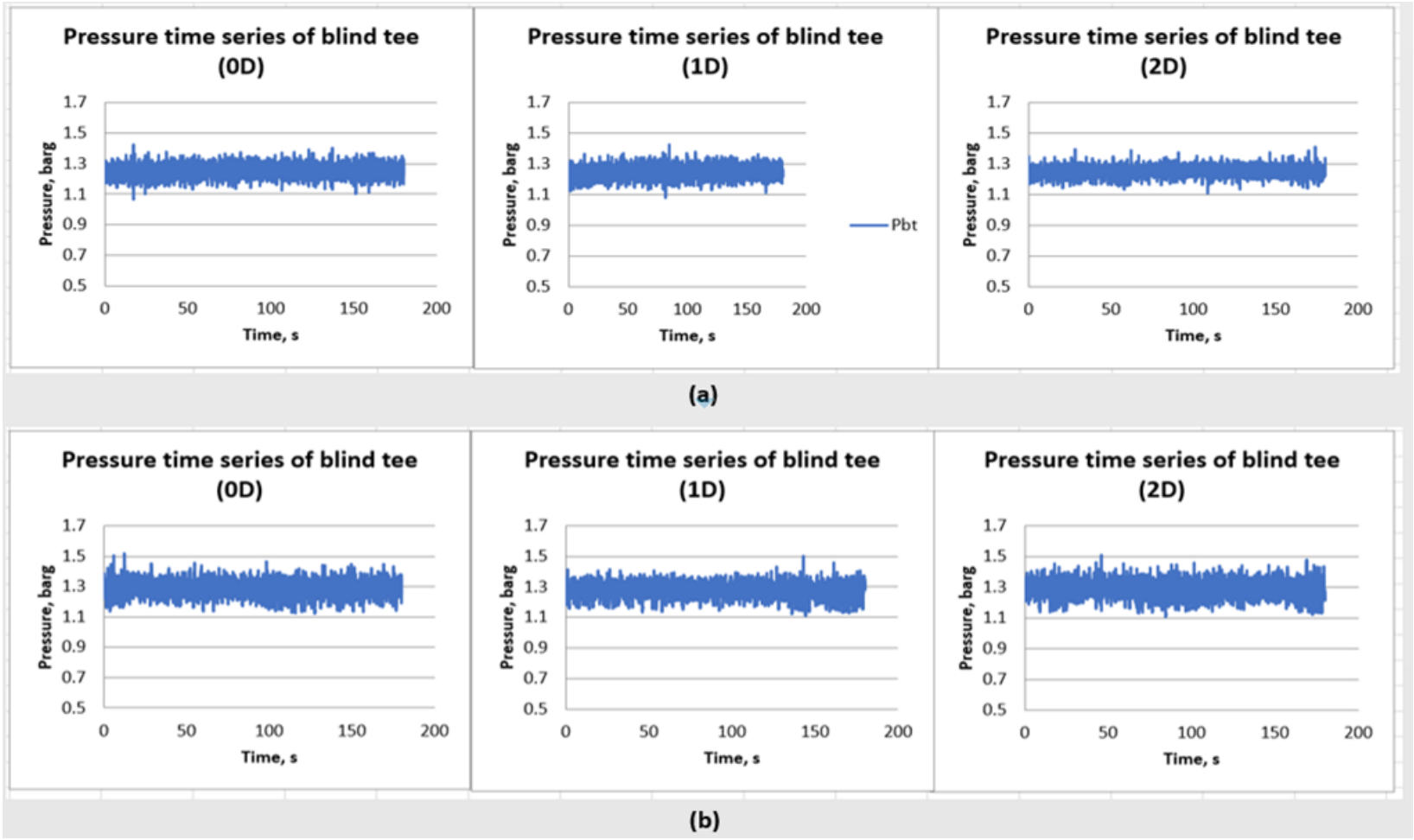

Figure C-6 Time series of pressures in blind tee of different lengths (0D, 1D and 2D) for flows with superficial liquid velocity of 1.3 m/s and superficial gas velocities of (a) 0.95 m/s and (b) 1.36 m/s.

C.1.2 Time series of pressures in blind tee of different lengths for separated flows

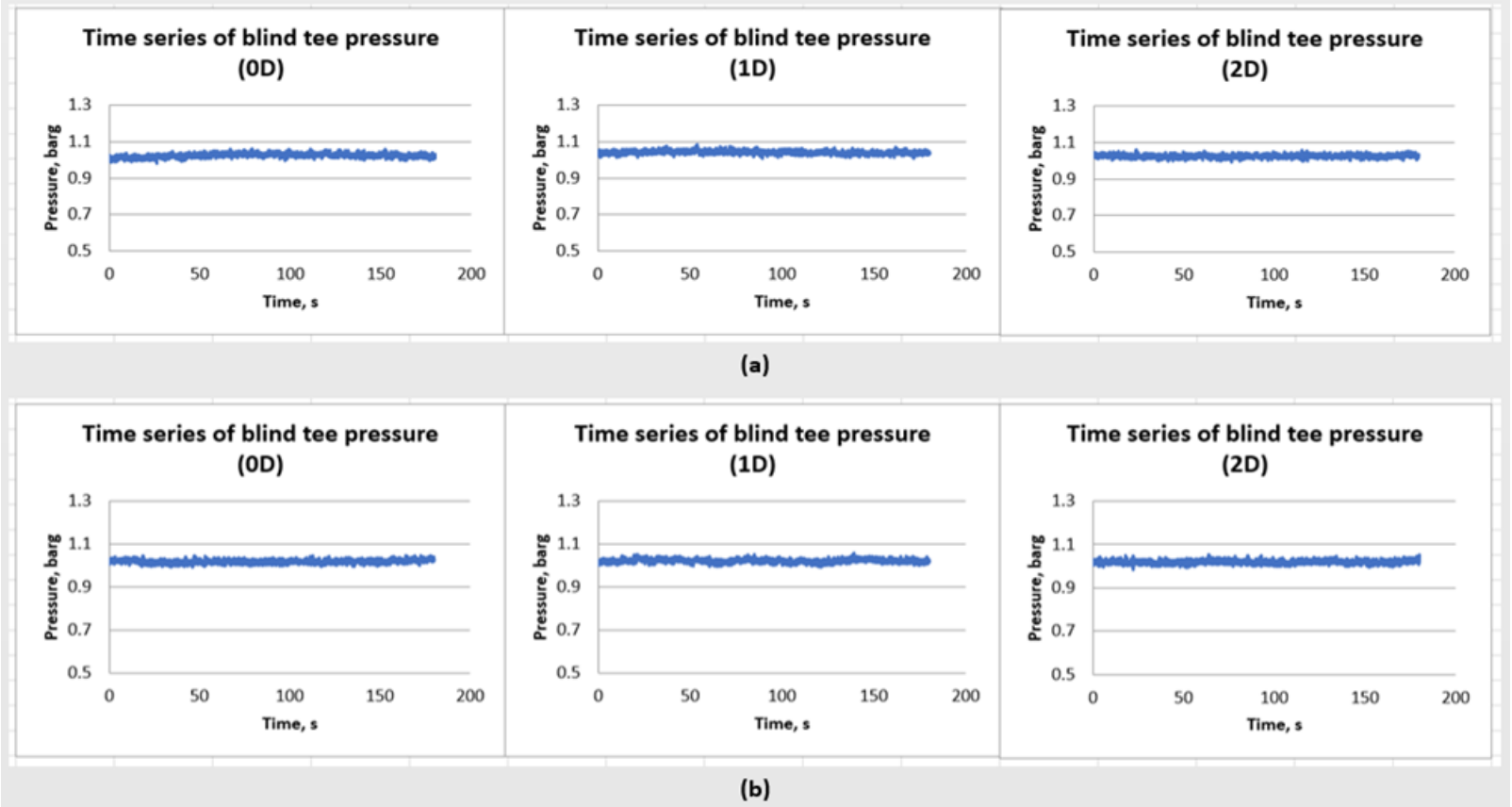

Figure C-7 Time series of pressures in blind tee of different lengths (0D, 1D and 2D) for flows with superficial liquid velocity of 0.043 m/s and superficial gas velocities of (a) 2.73 m/s and (b) 5.45 m/s.

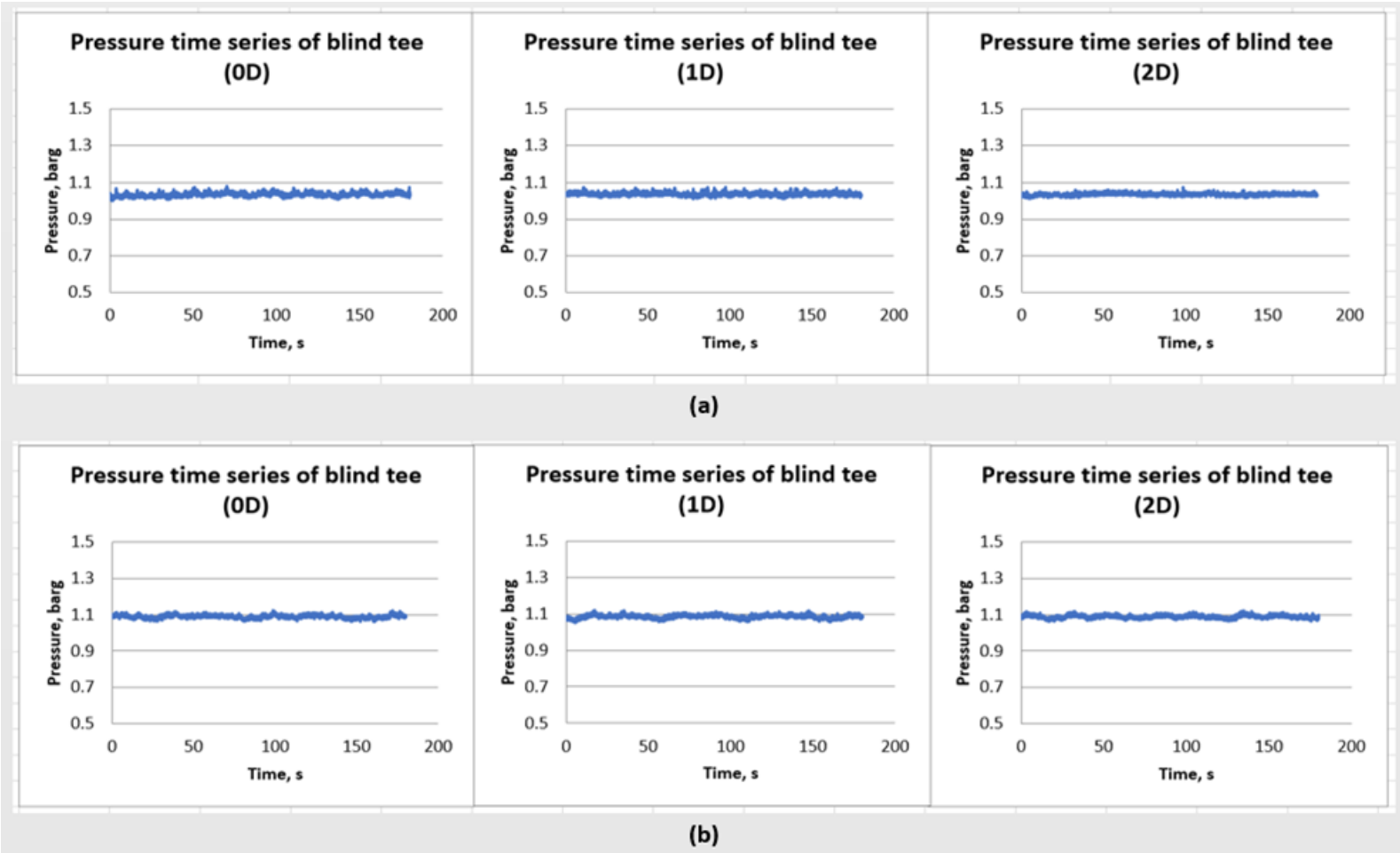

Figure C-8 Time series of pressures in blind tee of different lengths (0D, 1D and 2D) for flows with superficial liquid velocity of 0.043 m/s and superficial gas velocities of (a) 10.91 m/s and (b) 16.36 m/s.

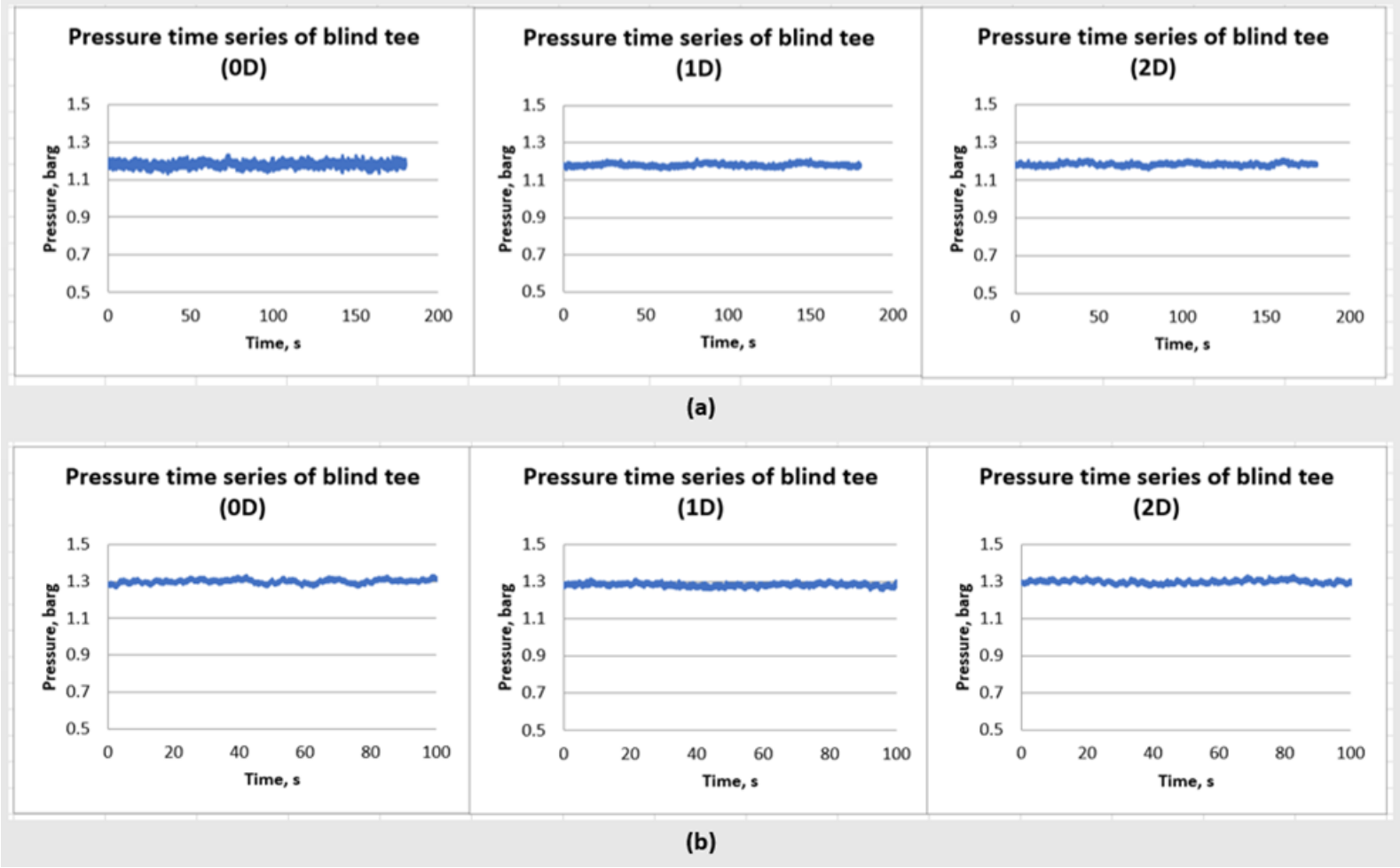

Figure C-9 Time series of pressures in blind tee of different lengths (0D, 1D and 2D) for flows with superficial liquid velocity of 0.043 m/s and superficial gas velocities of (a) 21.81 m/s and (b) 27.26 m/s.

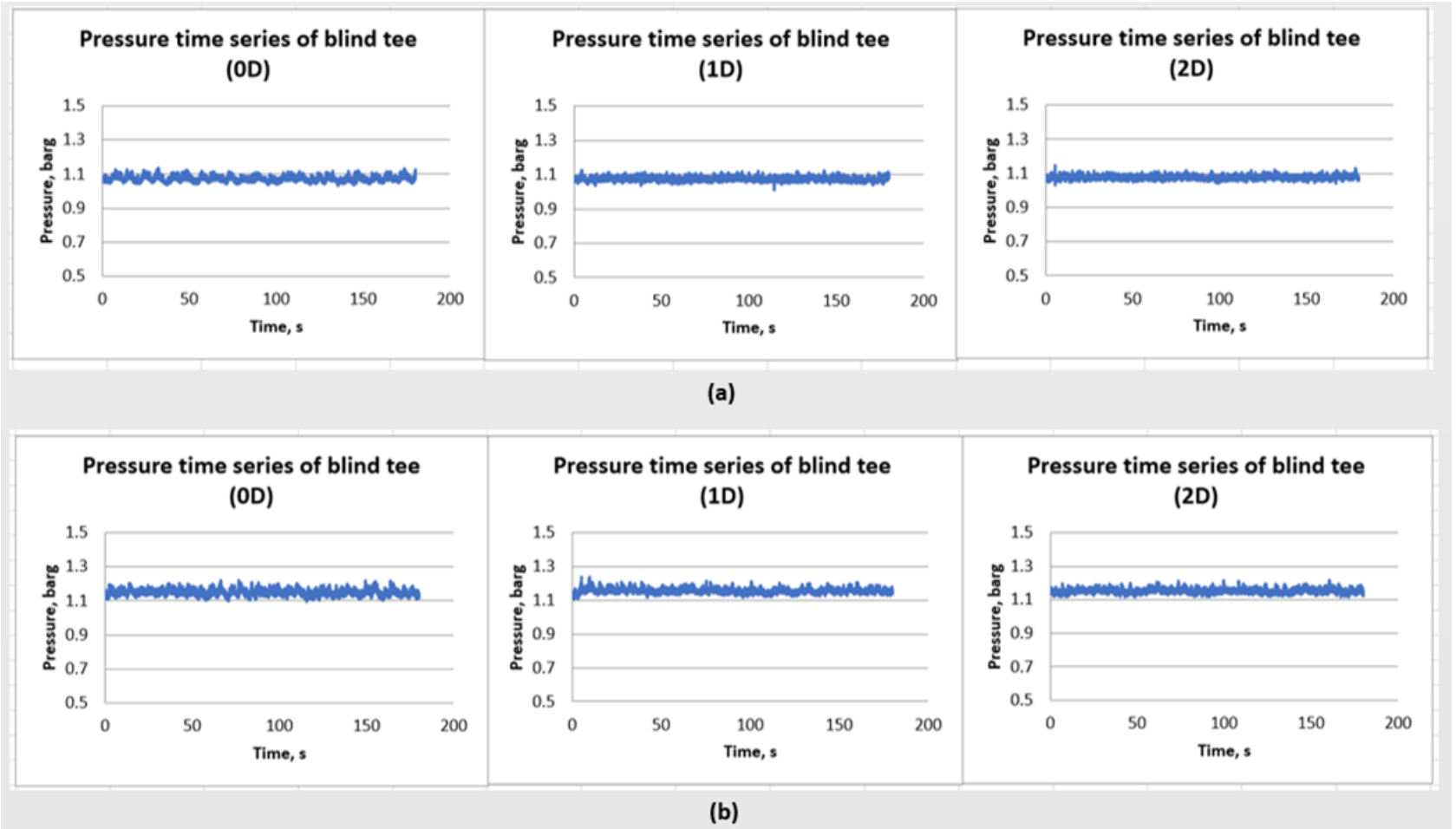

Figure C-10 Time series of pressures in blind tee of different lengths (0D, 1D and 2D) for flows with superficial liquid velocity of 0.086 m/s and superficial gas velocities of (a) 10.91 m/s and (b) 16.36 m/s.

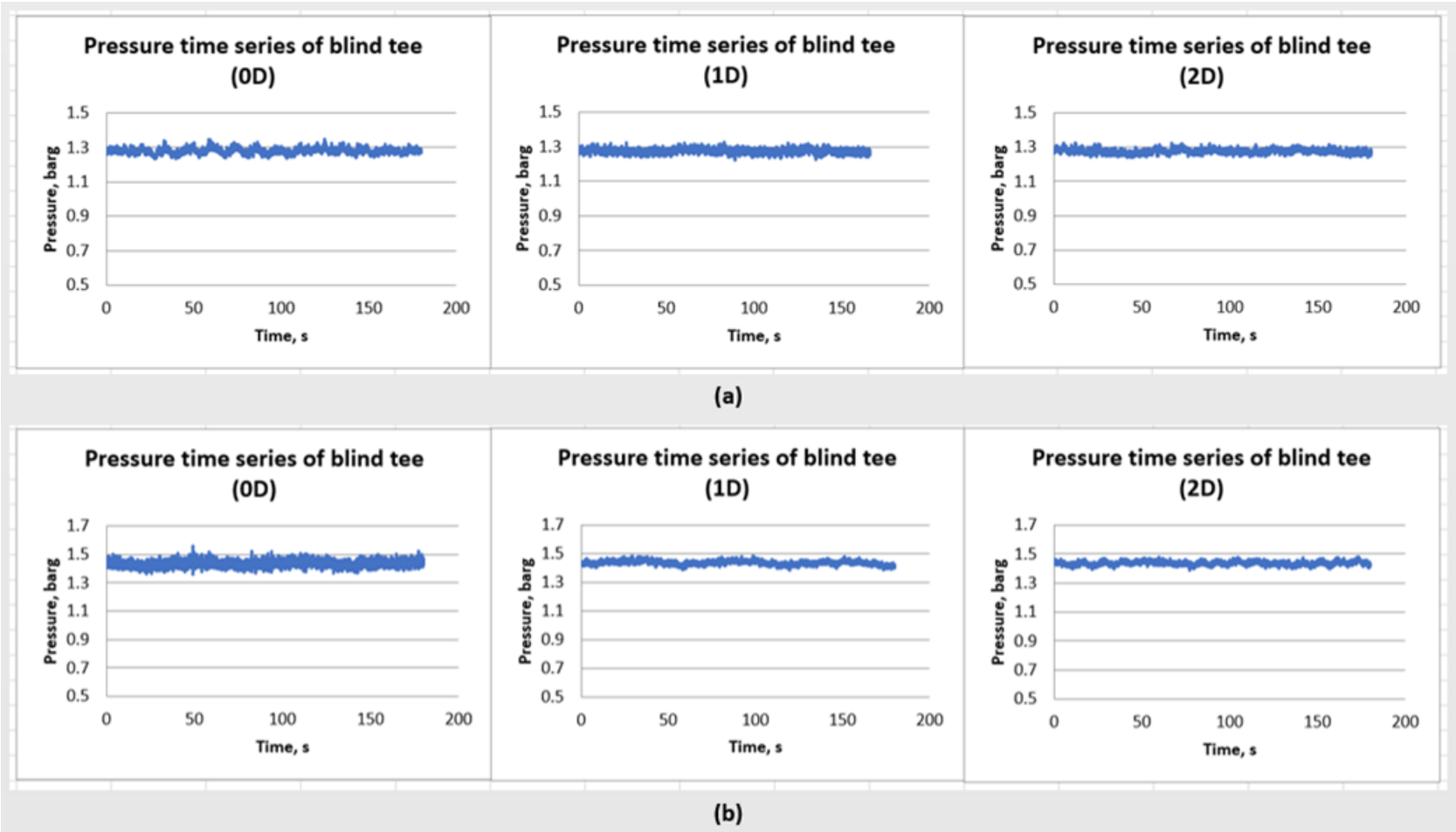

Figure C-11 Time series of pressures in blind tee of different lengths (0D, 1D and 2D) for flows with superficial liquid velocity of 0.086 m/s and superficial gas velocities of (a) 21.81 m/s and (b) 27.26 m/s.

C.2 Time series of pressures upstream of blind tee of different lengths

C.2.1 Time series of pressures upstream of blind tee for intermittent flows

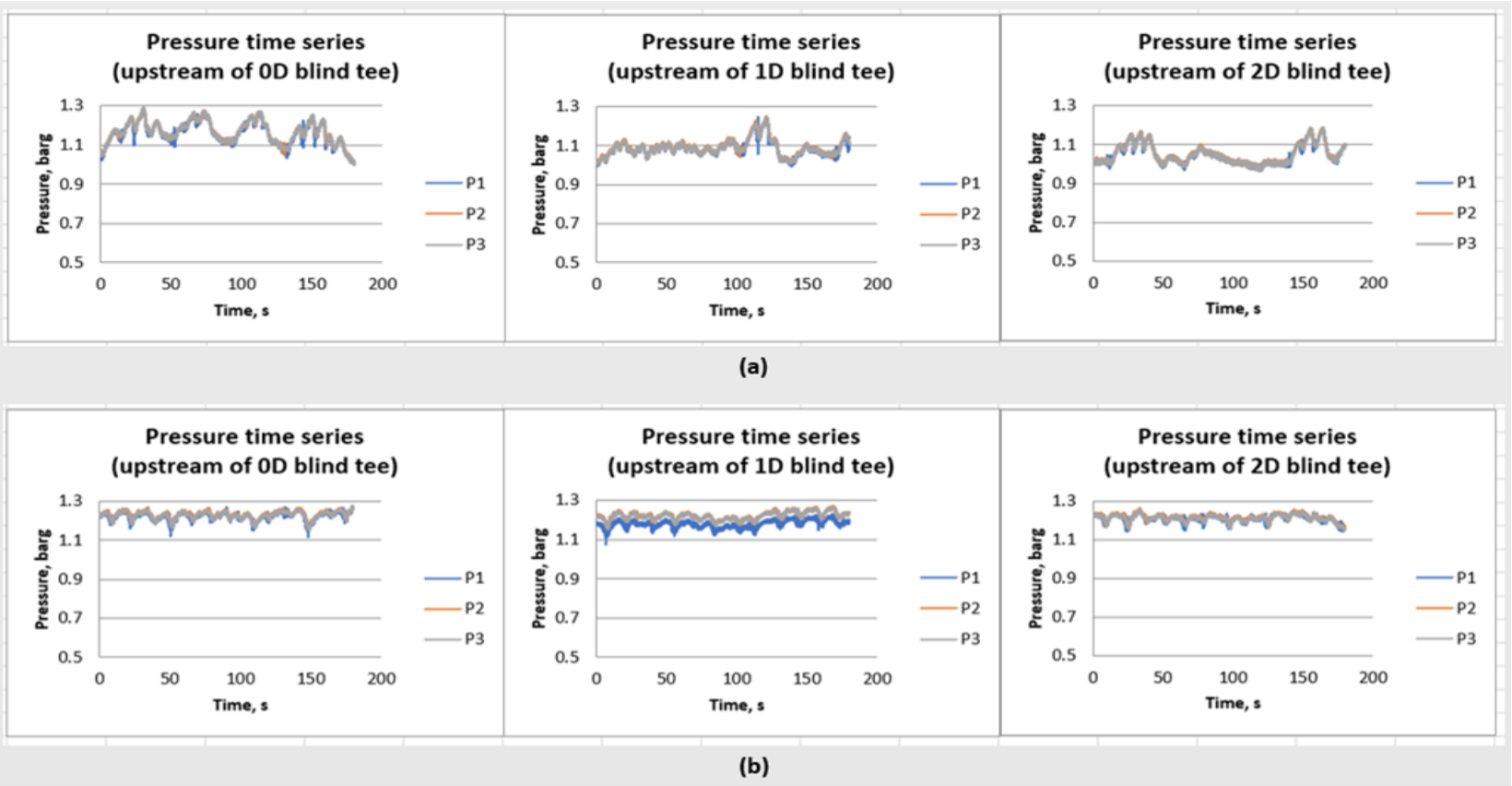

Figure C-12 Time series of pressures upstream of blind tee of different lengths (0D, 1D, and 2D) for flows with superficial liquid velocity of 0.086 m/s and superficial gas velocities of (a) 0.14 m/s and (b) 0.55 m/s.

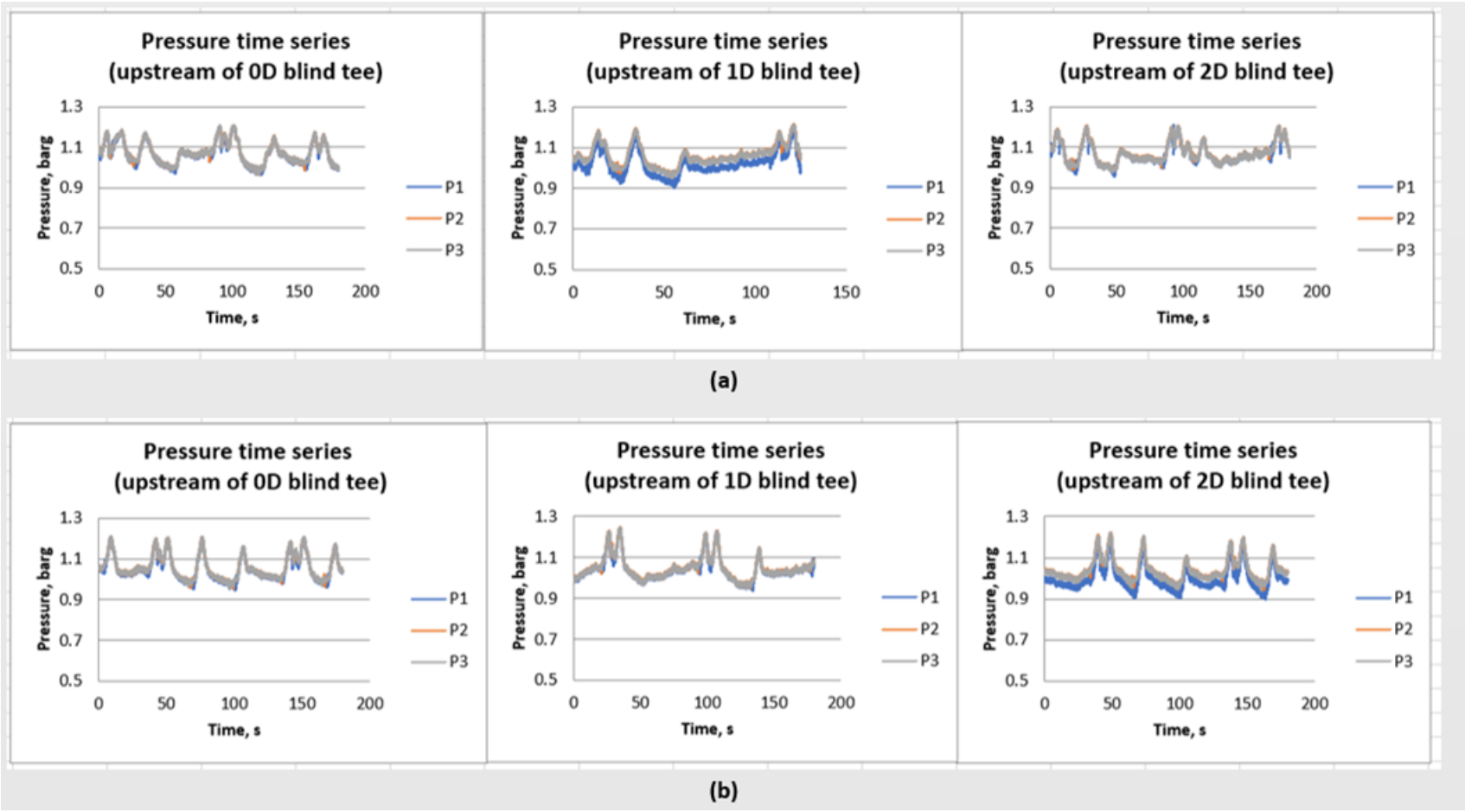

Figure C-13 Time series of pressures upstream of blind tee of different lengths (0D, 1D, and 2D) for flows with superficial liquid velocity of 0.086 m/s and superficial gas velocities of (a) 0.95 m/s and (b) 1.36 m/s.

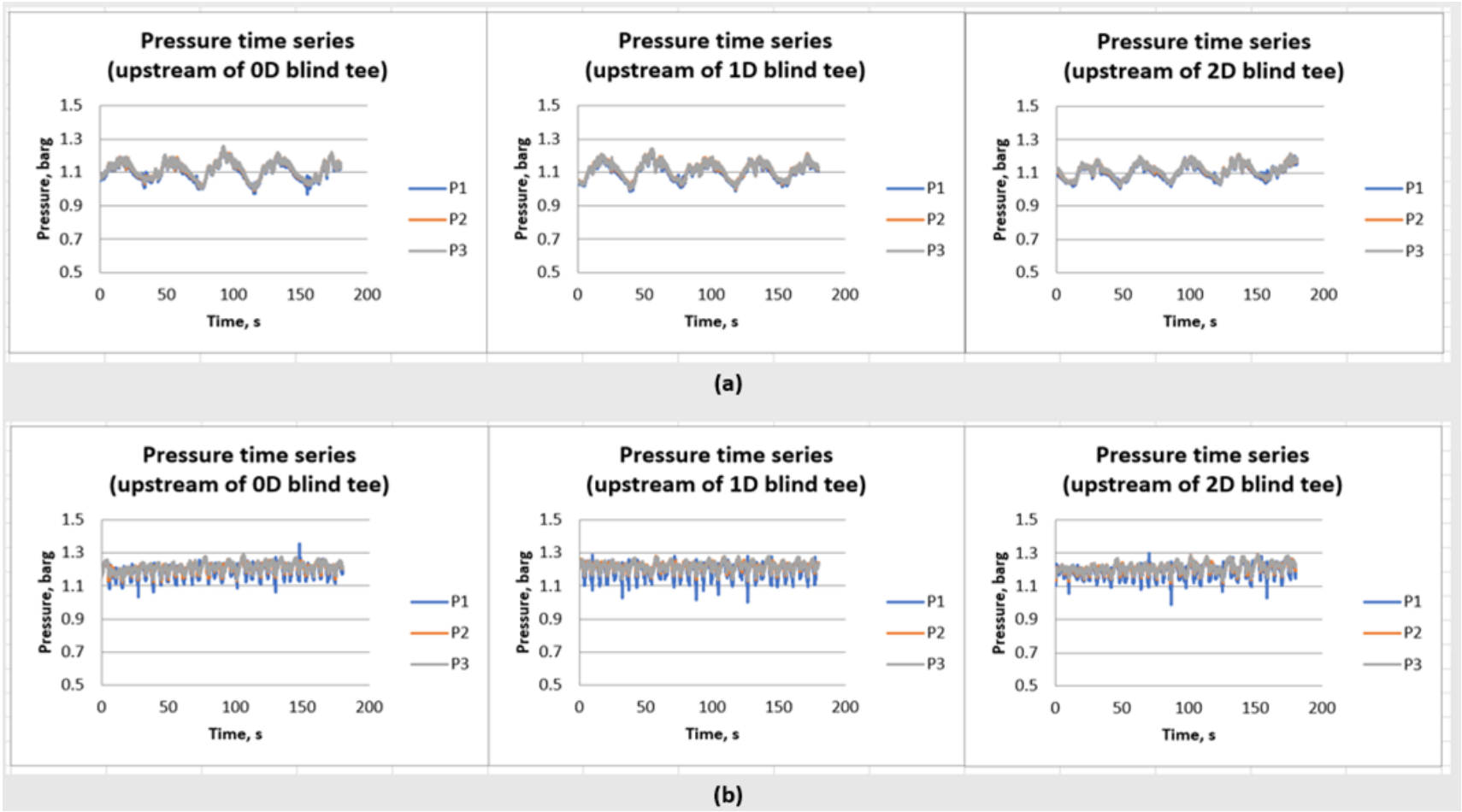

Figure C-14 Time series of pressures upstream of blind tee of different lengths (0D, 1D, and 2D) for flows with superficial liquid velocity of 0.86 m/s and superficial gas velocities of (a) 0.14 m/s and (b) 0.55 m/s.

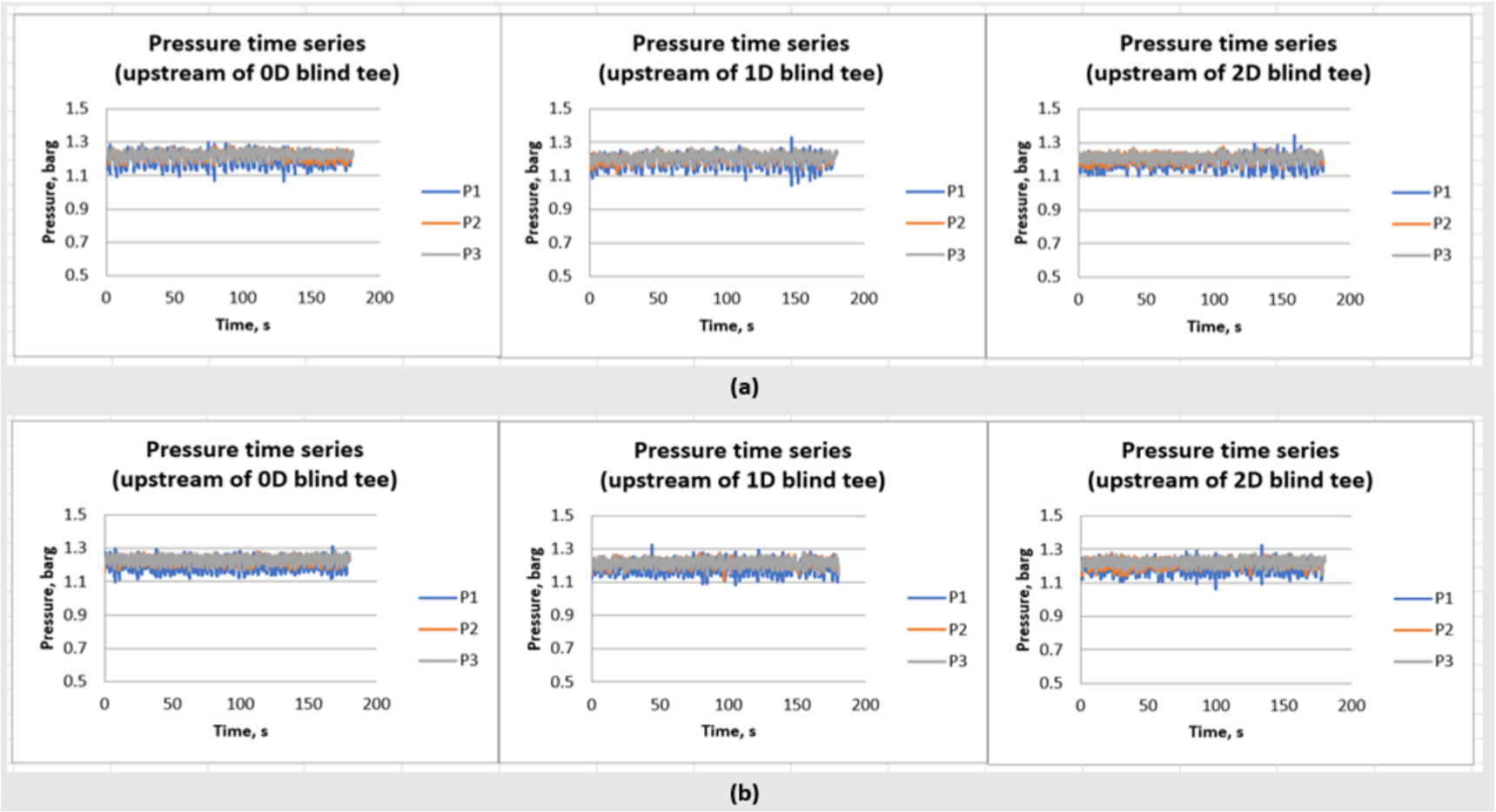

Figure C-15 Time series of pressures upstream of blind tee of different lengths (0D, 1D, and 2D) for flows with superficial liquid velocity of 0.86 m/s and superficial gas velocities of (a) 0.95 m/s and (b) 1.36 m/s.

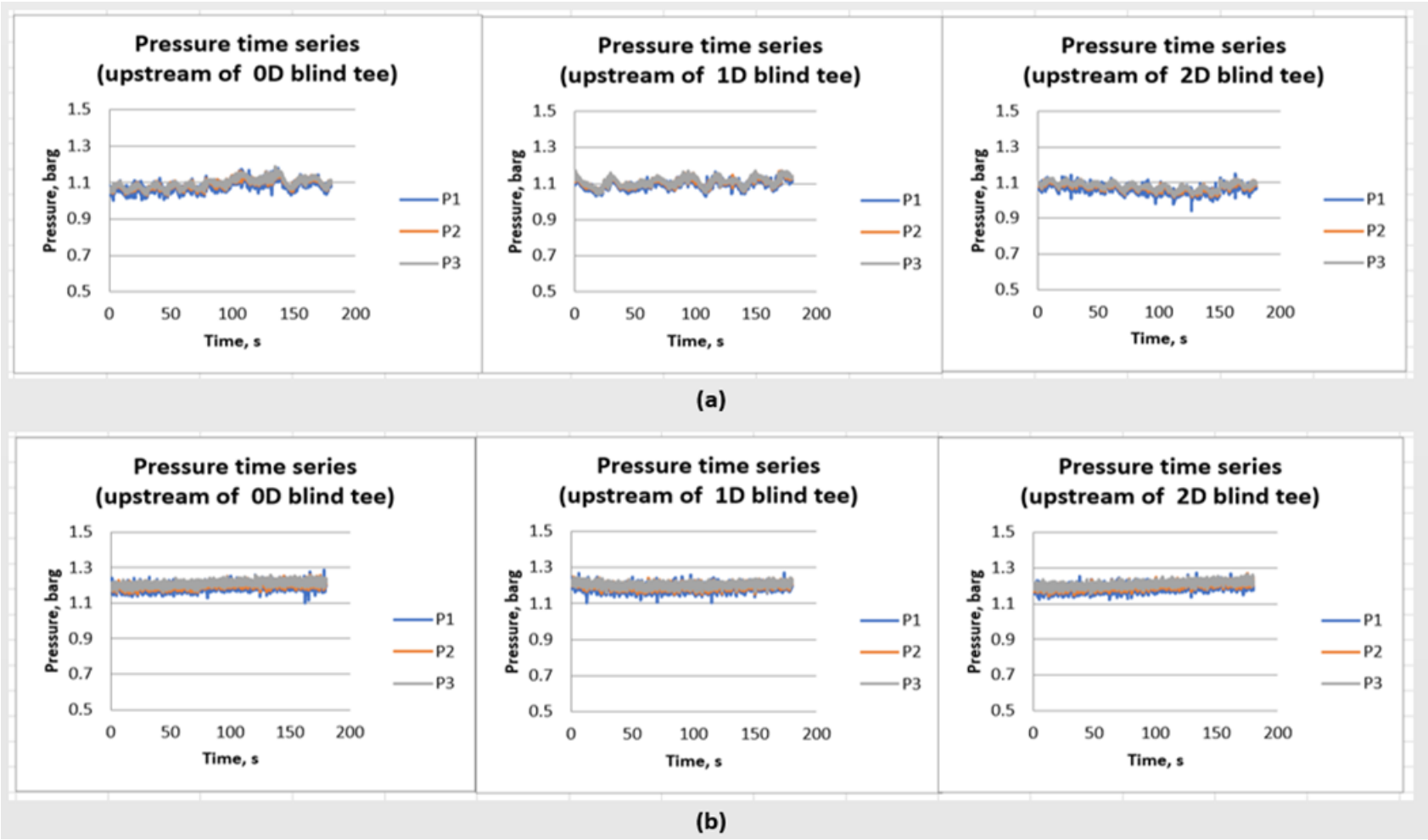

Figure C-16 Time series of pressures upstream of blind tee of different lengths (0D, 1D, and 2D) for flows with superficial liquid velocity of 1.3 m/s and superficial gas velocities of (a) 0.14 m/s and (b) 0.55 m/s.

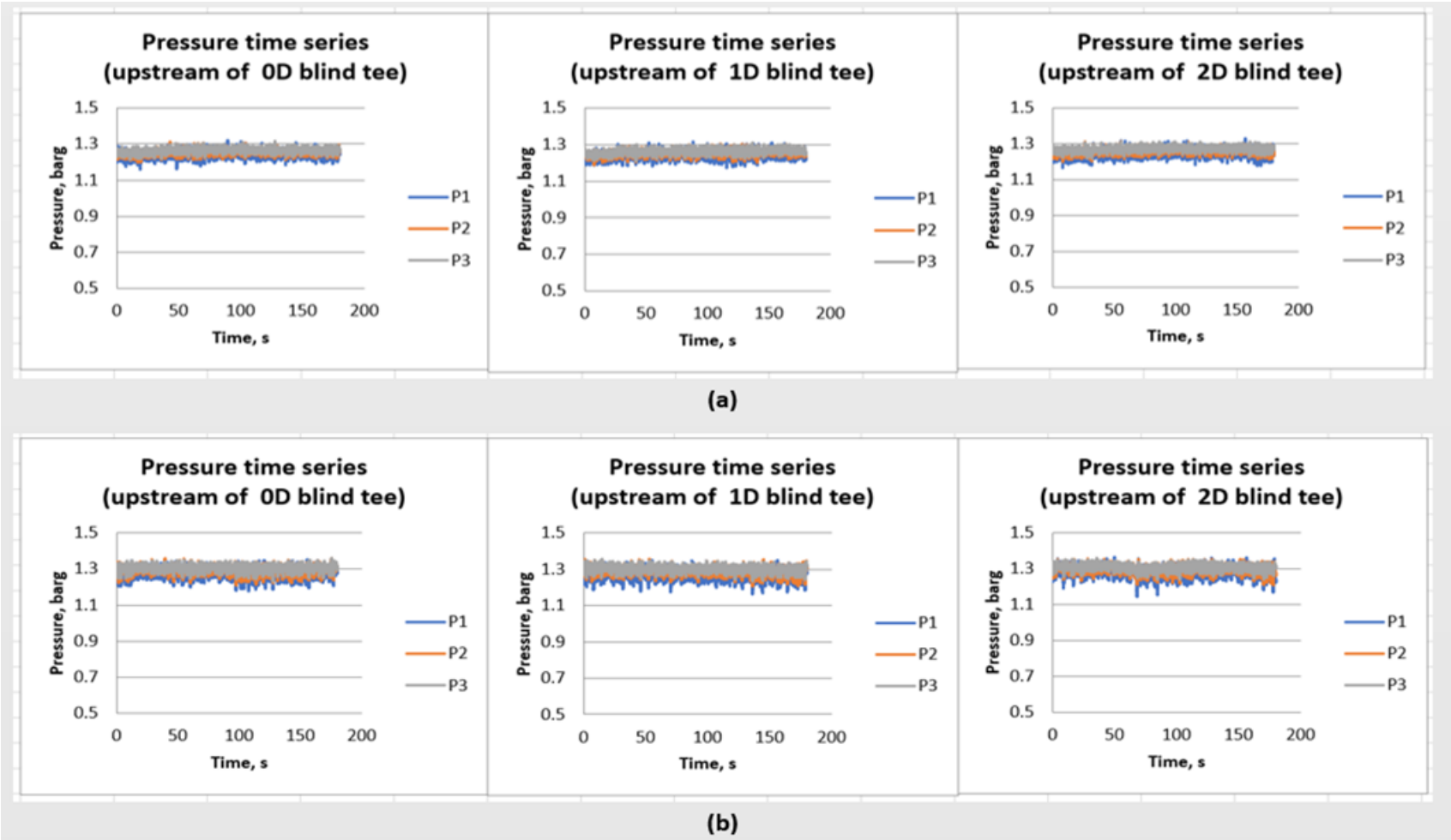

Figure C-17 Time series of pressures upstream of blind tee of different lengths (0D, 1D, and 2D) for flows with superficial liquid velocity of 1.3 m/s and superficial gas velocities of (a) 0.95 m/s and (b) 1.36 m/s.

C.2.2 Time series of pressures upstream of blind tee for separated flows

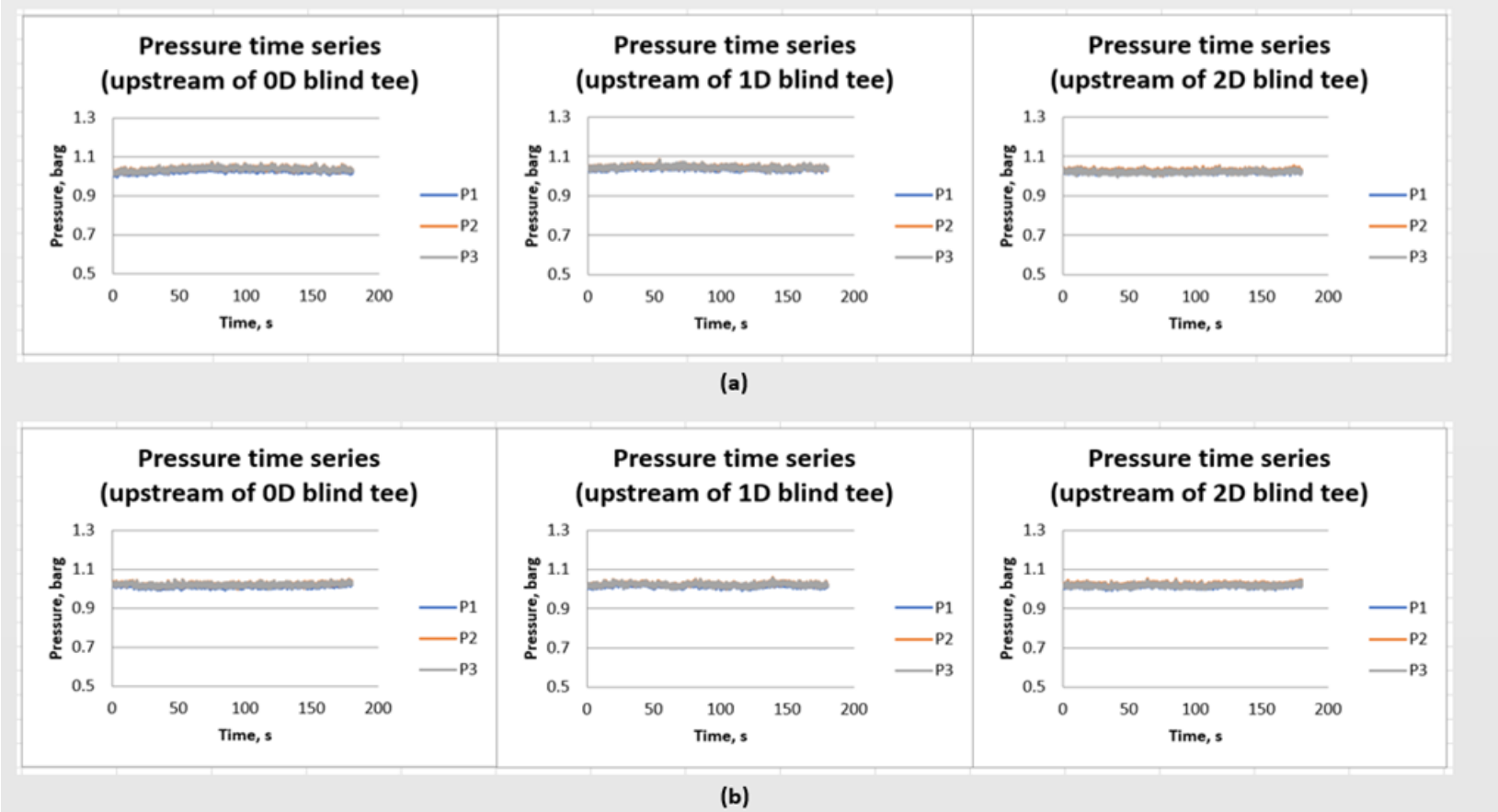

Figure C-18 Time series of pressures upstream of blind tee of different lengths (0D, 1D, and 2D) for flows with superficial liquid velocity of 0.043 m/s and superficial gas velocities of (a) 2.73 m/s and (b) 5.45 m/s.

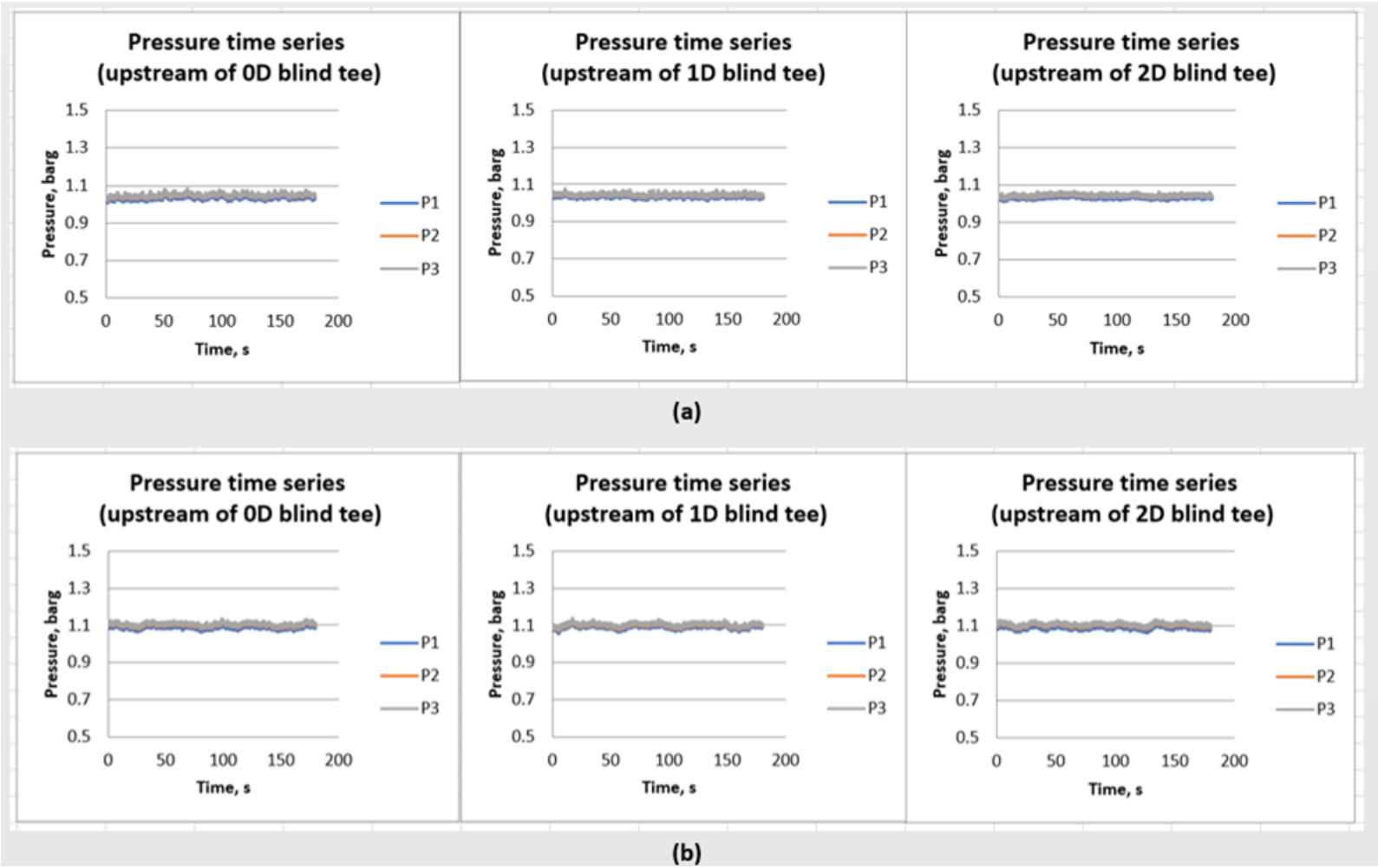

Figure C-19 Time series of pressures upstream of blind tee of different lengths (0D, 1D, and 2D) for flows with superficial liquid velocity of 0.043 m/s and superficial gas velocities of (a) 10.91 m/s and (b) 16.36 m/s.

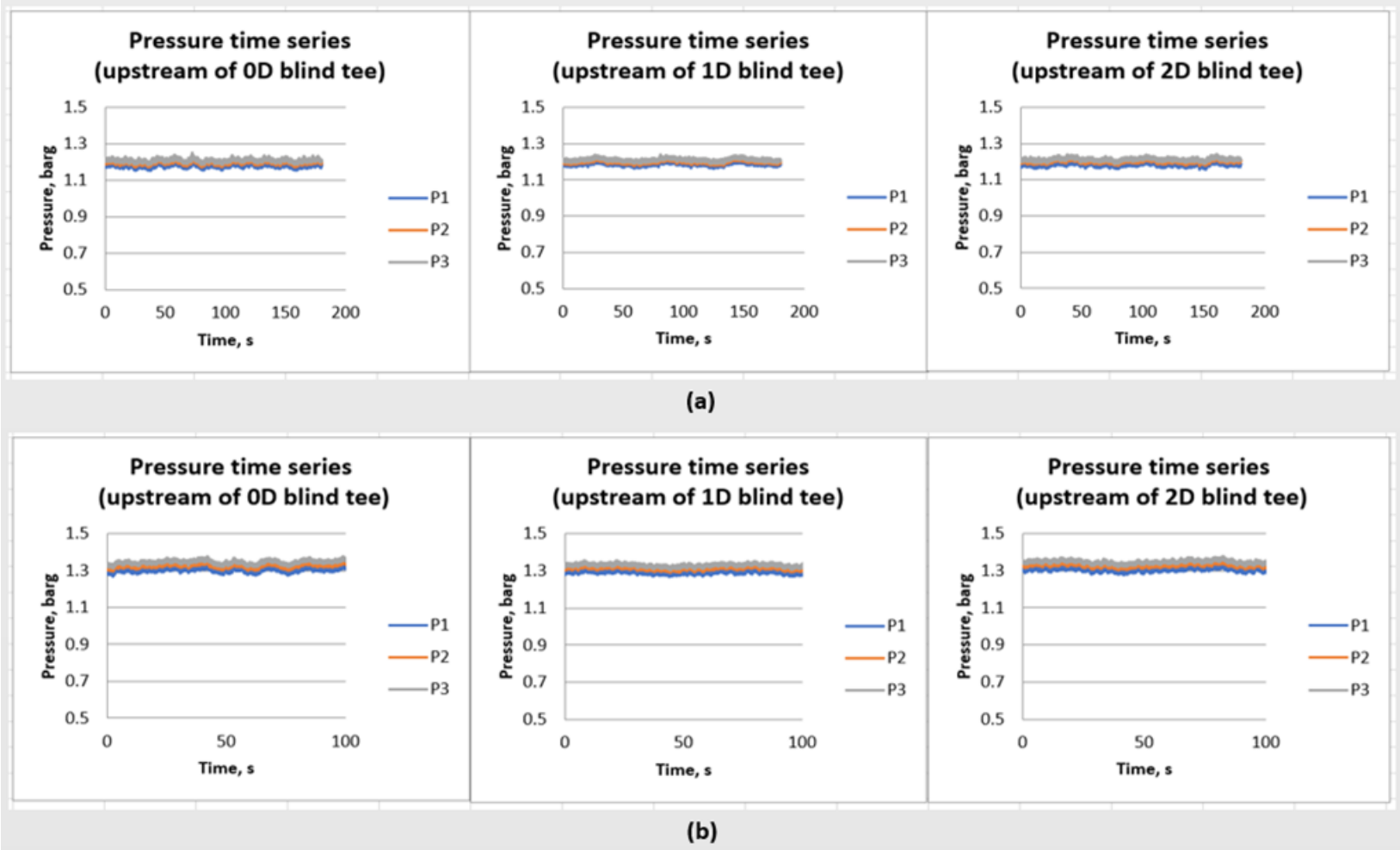

Figure C-20 Time series of pressures upstream of blind tee of different lengths (0D, 1D, and 2D) for flows with superficial liquid velocity of 0.043 m/s and superficial gas velocities of (a) 21.81 m/s and (b) 27.26 m/s.

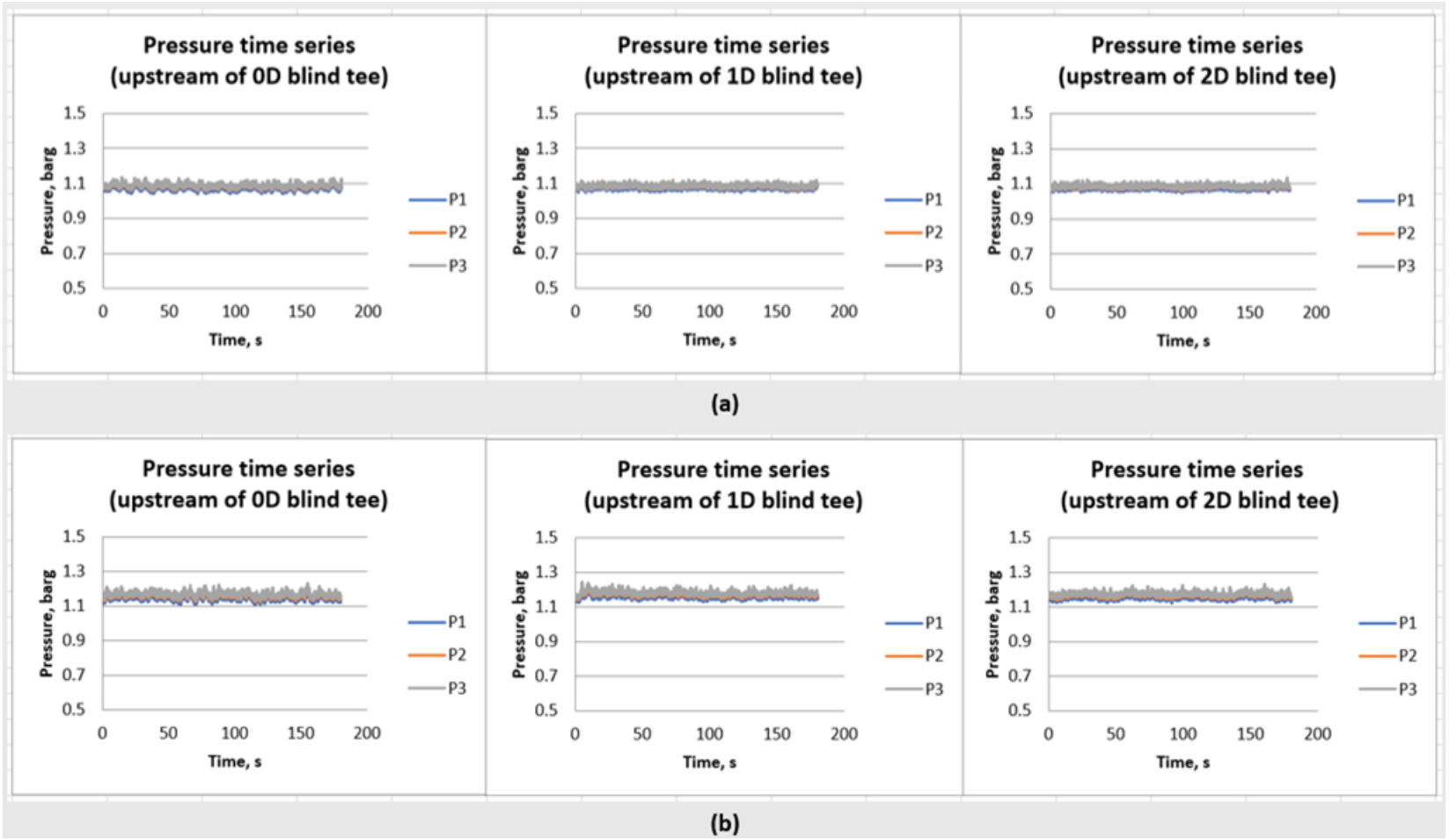

Figure C-21 Time series of pressures upstream of blind tee of different lengths (0D, 1D, and 2D) for flows with superficial liquid velocity of 0.086 m/s and superficial gas velocities of (a) 10.91 m/s and (b) 16.36 m/s.

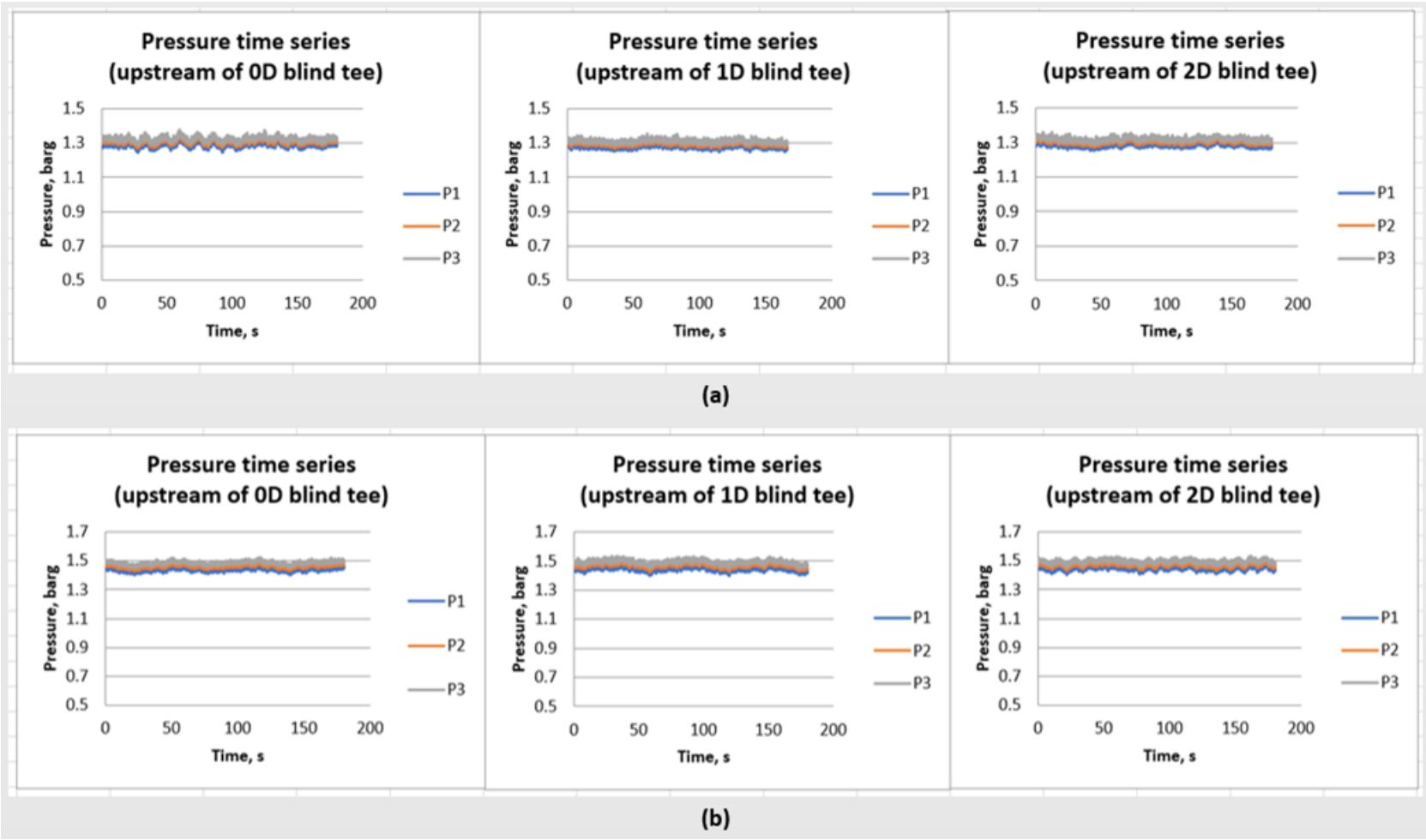

Figure C-22 Time series of pressures upstream of blind tee of different lengths (0D, 1D, and 2D) for flows with superficial liquid velocity of 0.086 m/s and superficial gas velocities of (a) 21.81 m/s and (b) 27.26 m/s.

C.3 Time series of pressures downstream of blind tee of different lengths

C.3.1 Time series of pressures downstream of blind tee for intermittent flows

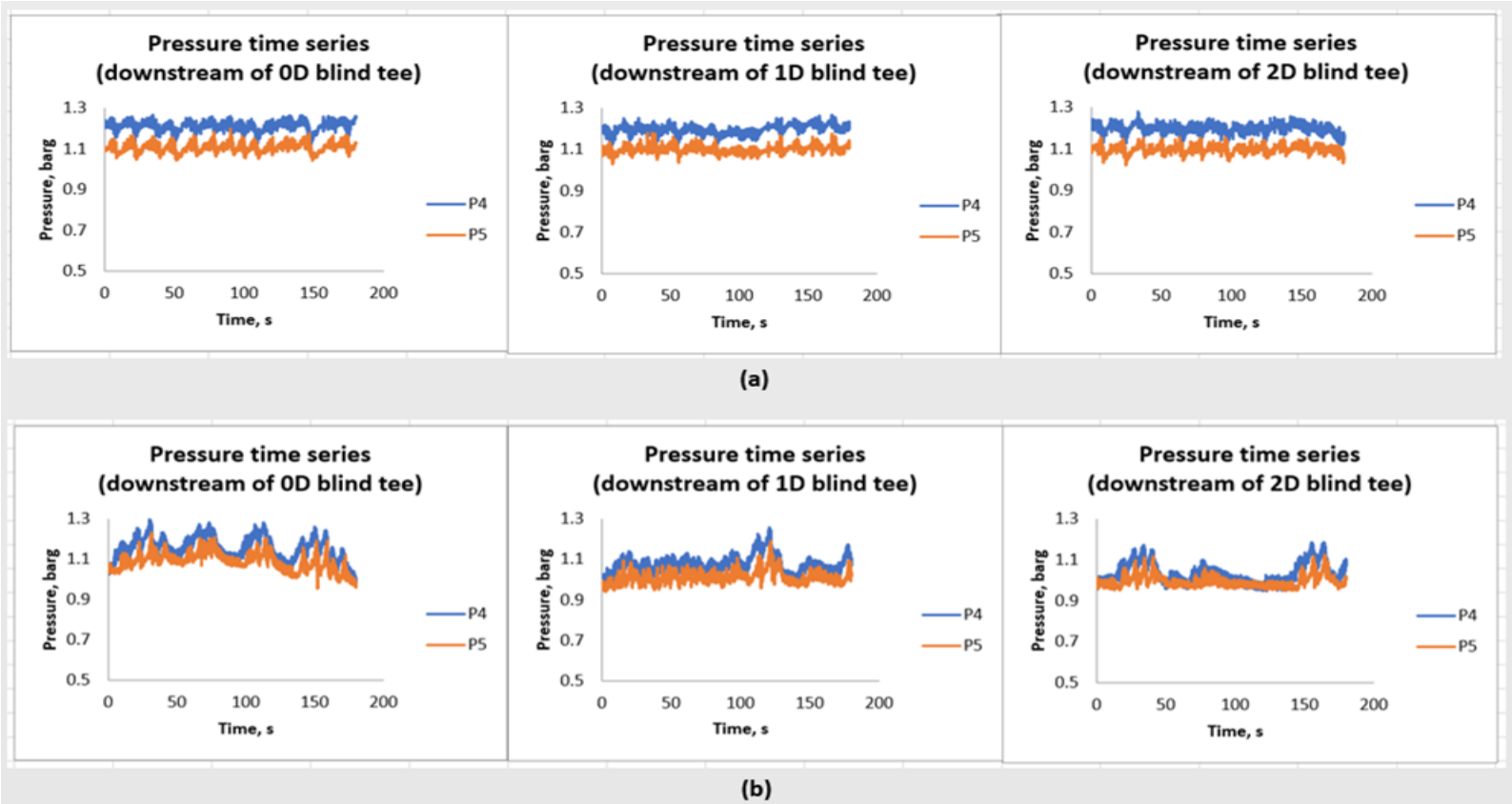

Figure C-23 Time series of pressures downstream of blind tee of different lengths (0D, 1D, and 2D) for flows with superficial liquid velocity of 0.086 m/s and superficial gas velocities of (a) 0.14 m/s and (b) 0.55 m/s.

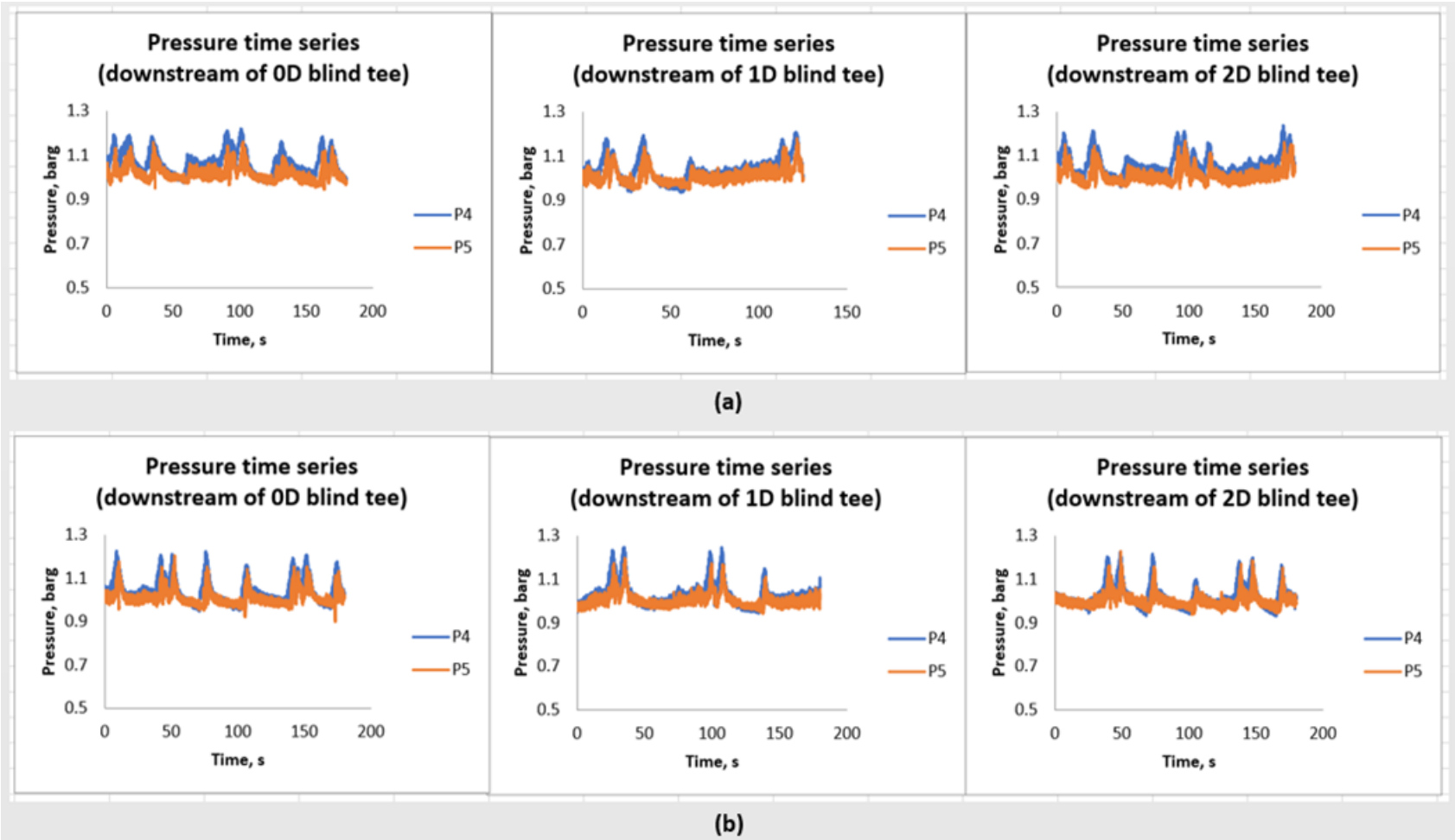

Figure C-24 Time series of pressures downstream of blind tee of different lengths (0D, 1D, and 2D) for flows with superficial liquid velocity of 0.086 m/s and superficial gas velocities of (a) 0.95 m/s and (b) 1.36 m/s.

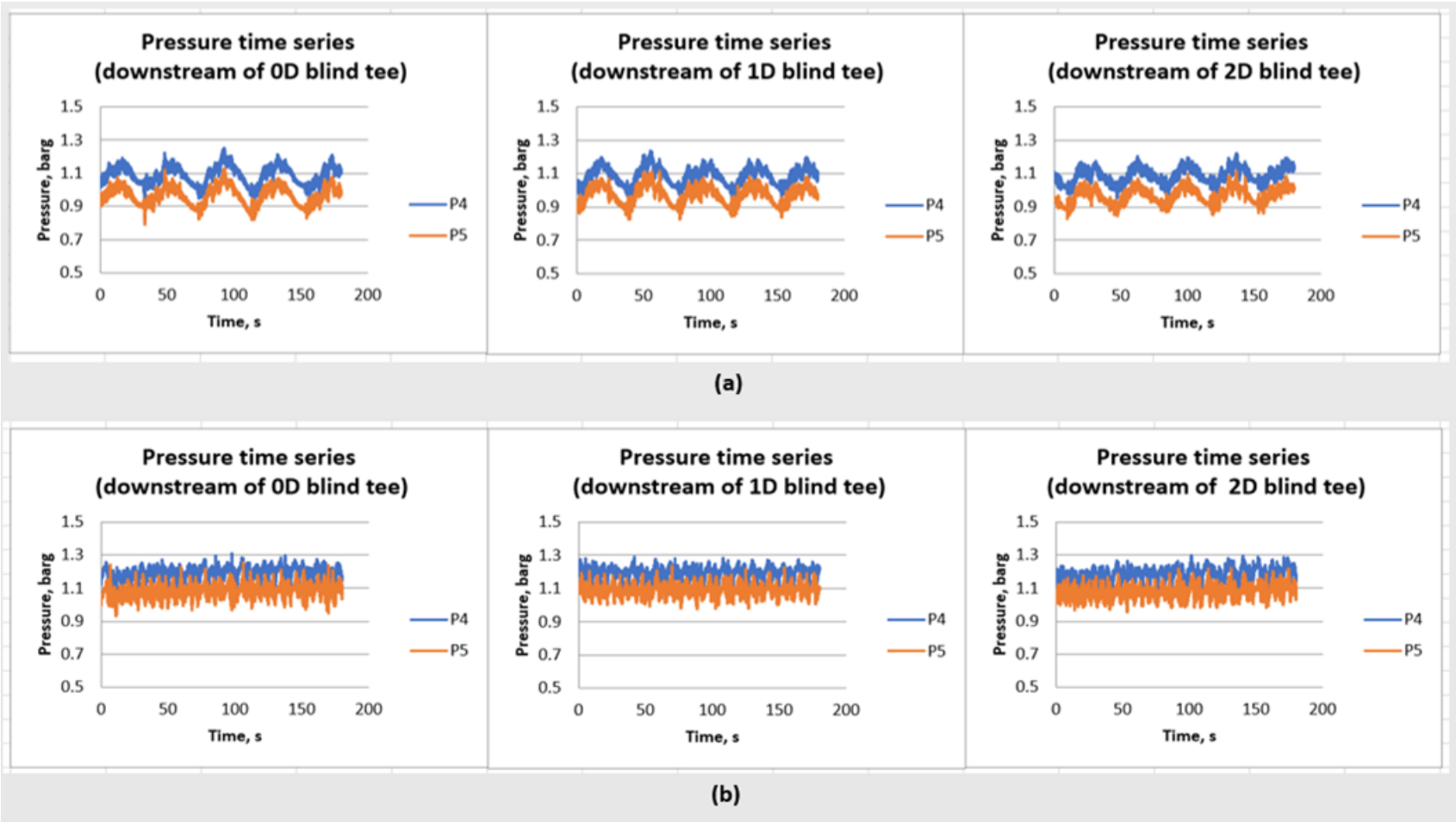

Figure C-25 Time series of pressures downstream of blind tee of different lengths (0D, 1D, and 2D) for flows with superficial liquid velocity of 0.86 m/s and superficial gas velocities of (a) 0.14 m/s and (b) 0.55 m/s.

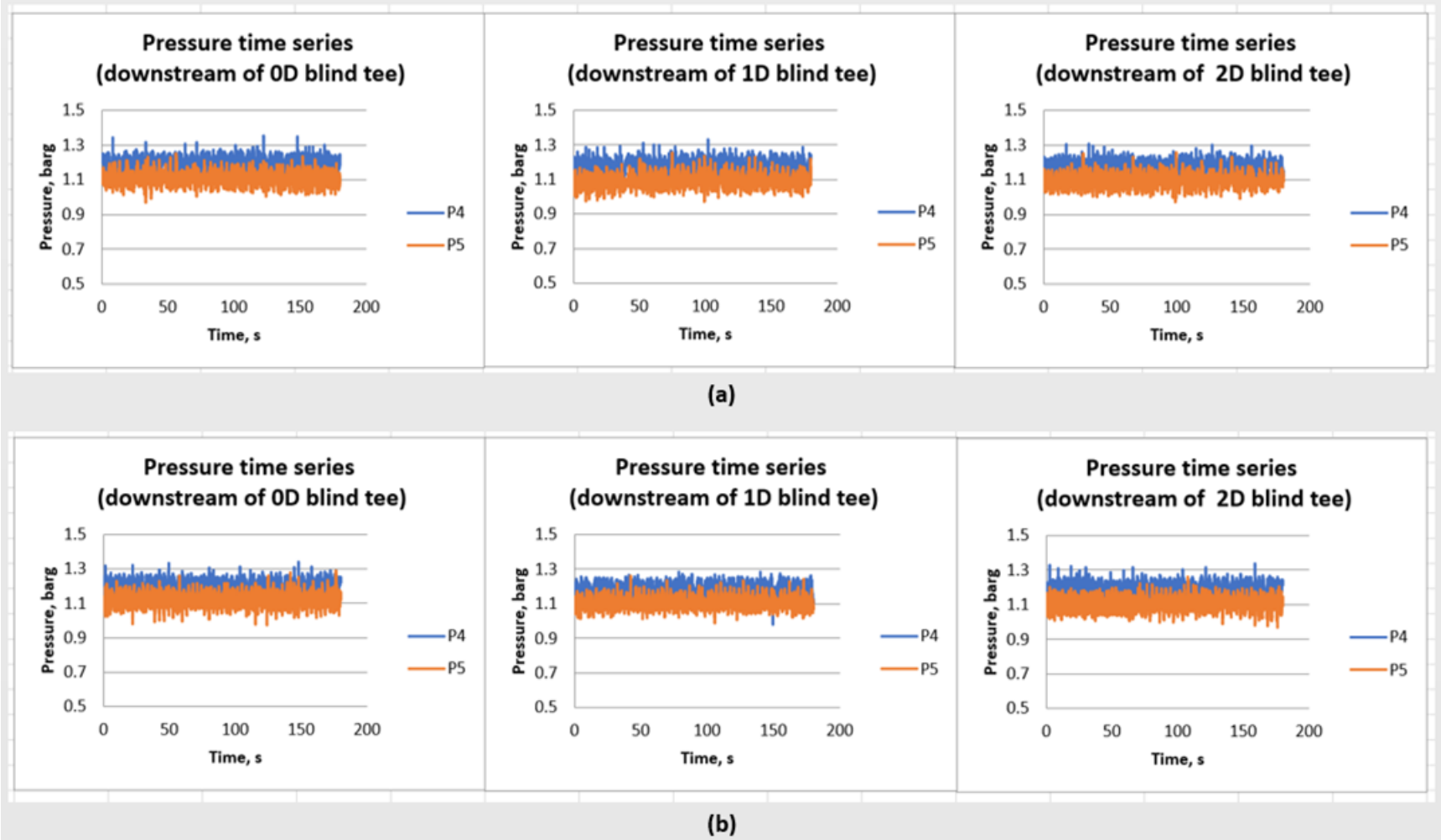

Figure C-26 Time series of pressures downstream of blind tee of different lengths (0D, 1D, and 2D) for flows with superficial liquid velocity of 0.86 m/s and superficial gas velocities of (a) 0.95 m/s and (b) 1.36 m/s.

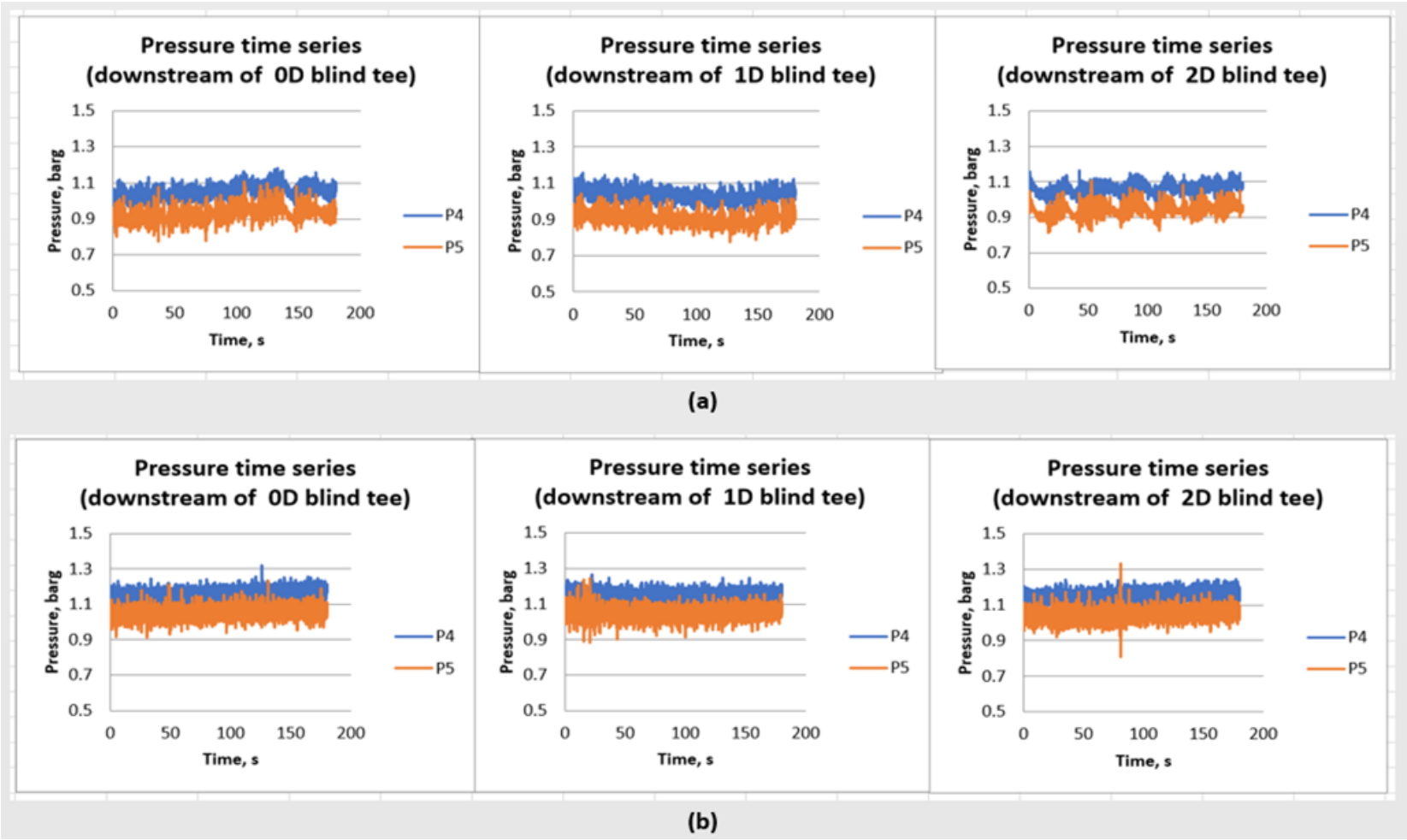

Figure C-27 Time series of pressures downstream of blind tee of different lengths (0D, 1D, and 2D) for flows with superficial liquid velocity of 1.3 m/s and superficial gas velocities of (a) 0.14 m/s and (b) 0.55 m/s.

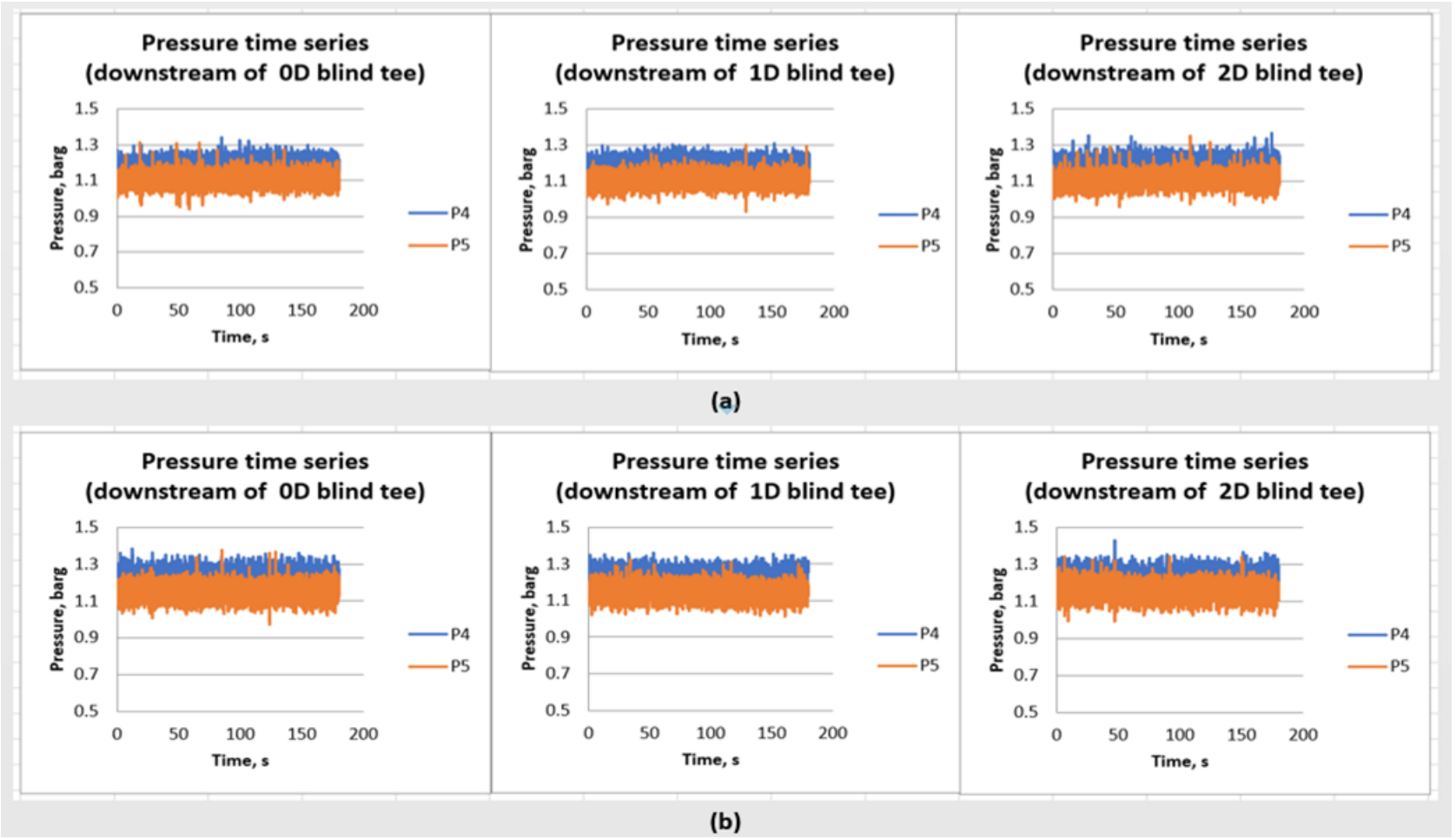

Figure C-28 Time series of pressures downstream of blind tee of different lengths (0D, 1D, and 2D) for flows with superficial liquid velocity of 1.3 m/s and superficial gas velocities of (a) 0.95 m/s and (b) 1.36 m/s.

C.3.2 Time series of pressures downstream of blind tee for separated flows

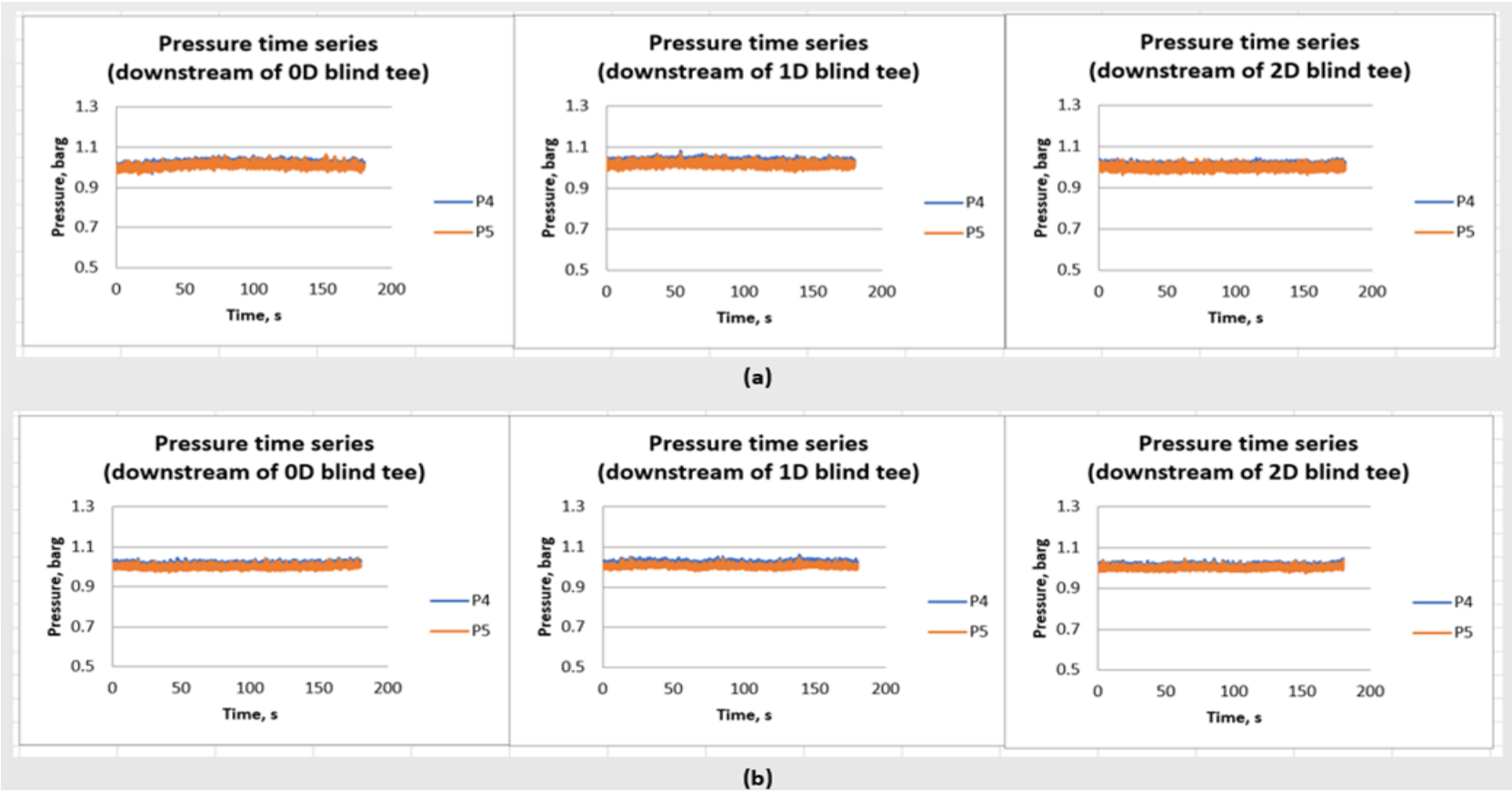

Figure C-29 Time series of pressures downstream of blind tee of different lengths (0D, 1D, and 2D) for flows with superficial liquid velocity of 0.043 m/s and superficial gas velocities of (a) 2.73 m/s and (b) 5.45 m/s.

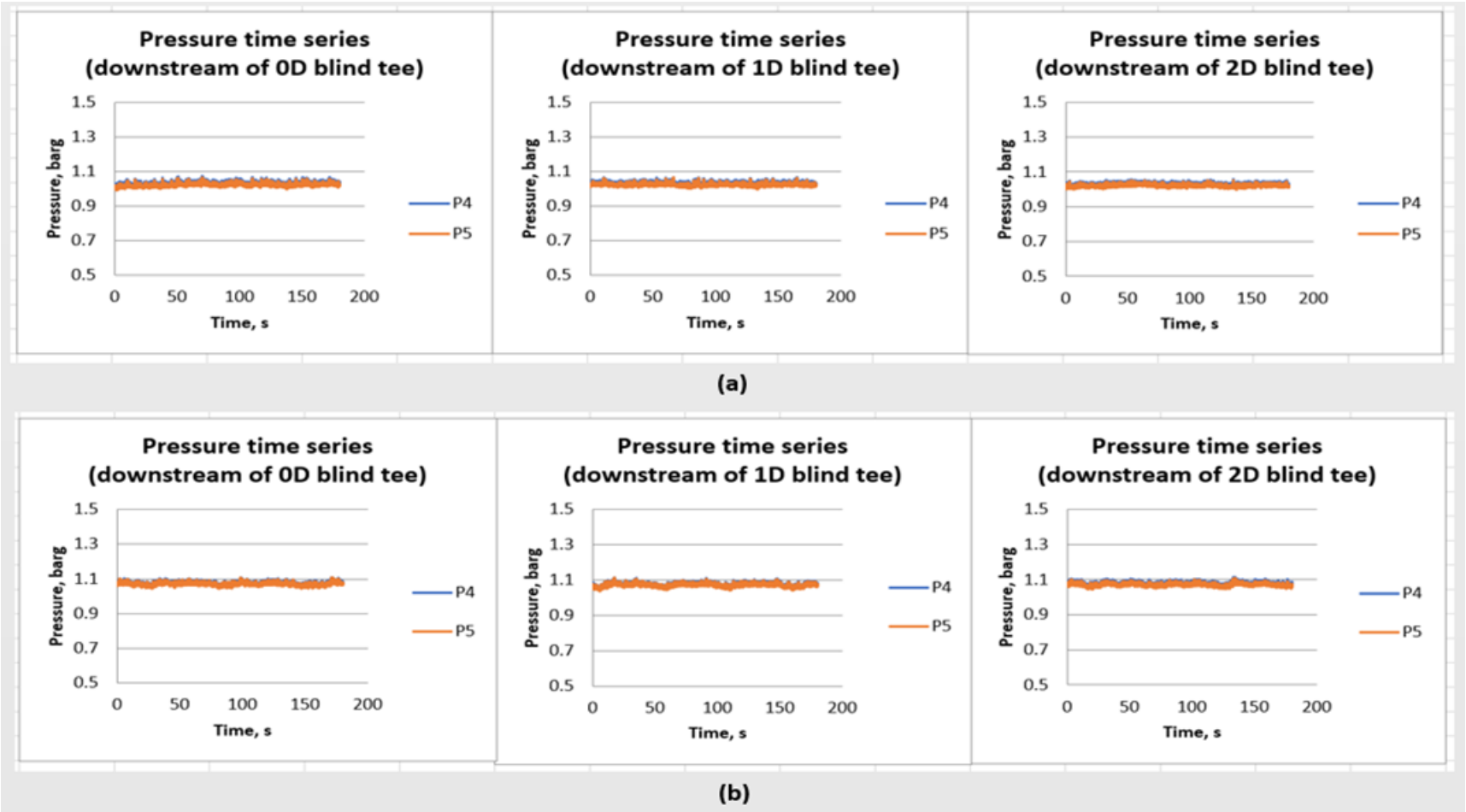

Figure C-30 Time series of pressures downstream of blind tee of different lengths (0D, 1D, and 2D) for flows with superficial liquid velocity of 0.043 m/s and superficial gas velocities of (a) 10.91 m/s and (b) 16.36 m/s.

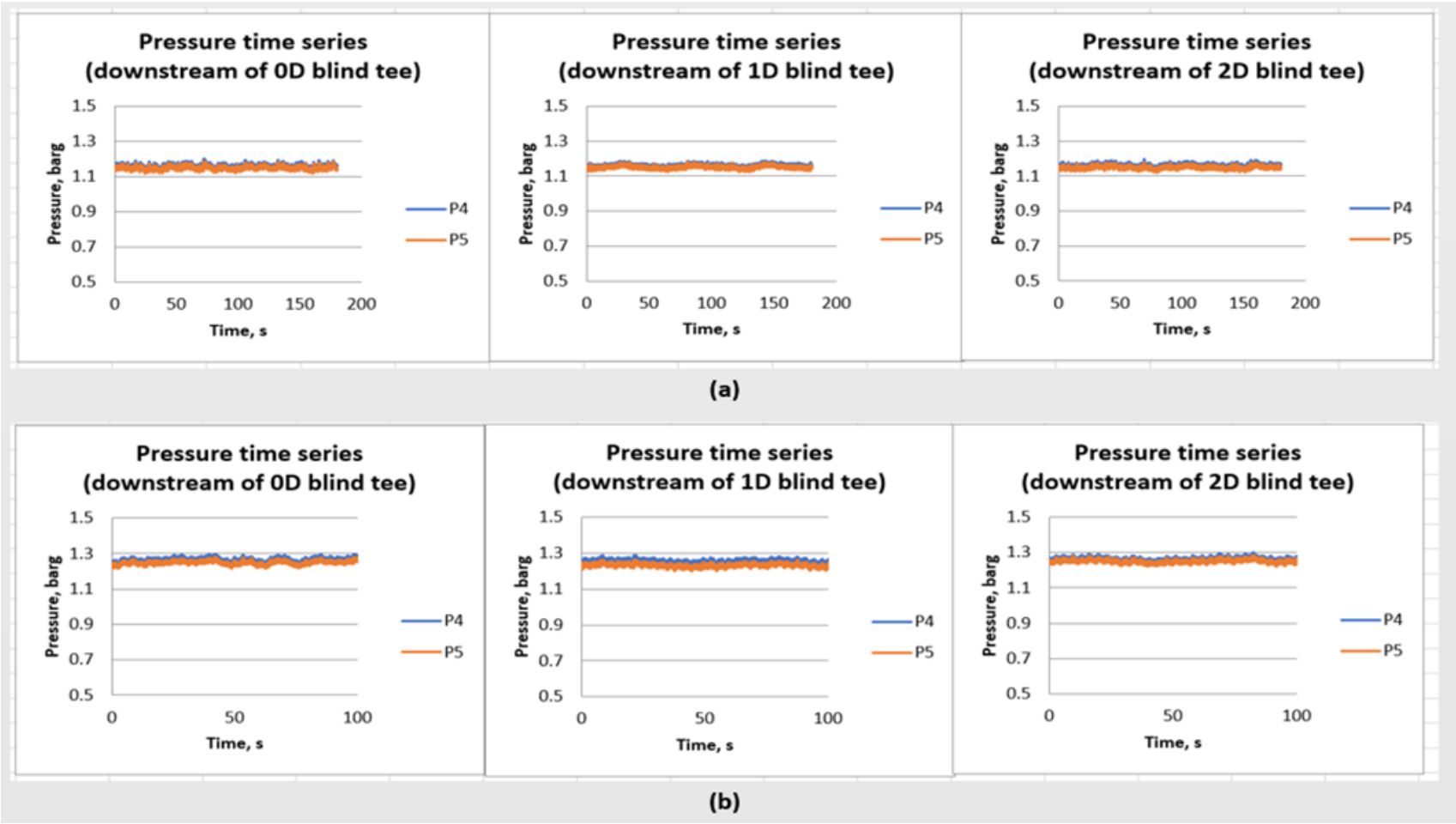

Figure C-31 Time series of pressures downstream of blind tee of different lengths (0D, 1D, and 2D) for flows with superficial liquid velocity of 0.043 m/s and superficial gas velocities of (a) 21.81 m/s and (b) 27.26 m/s.

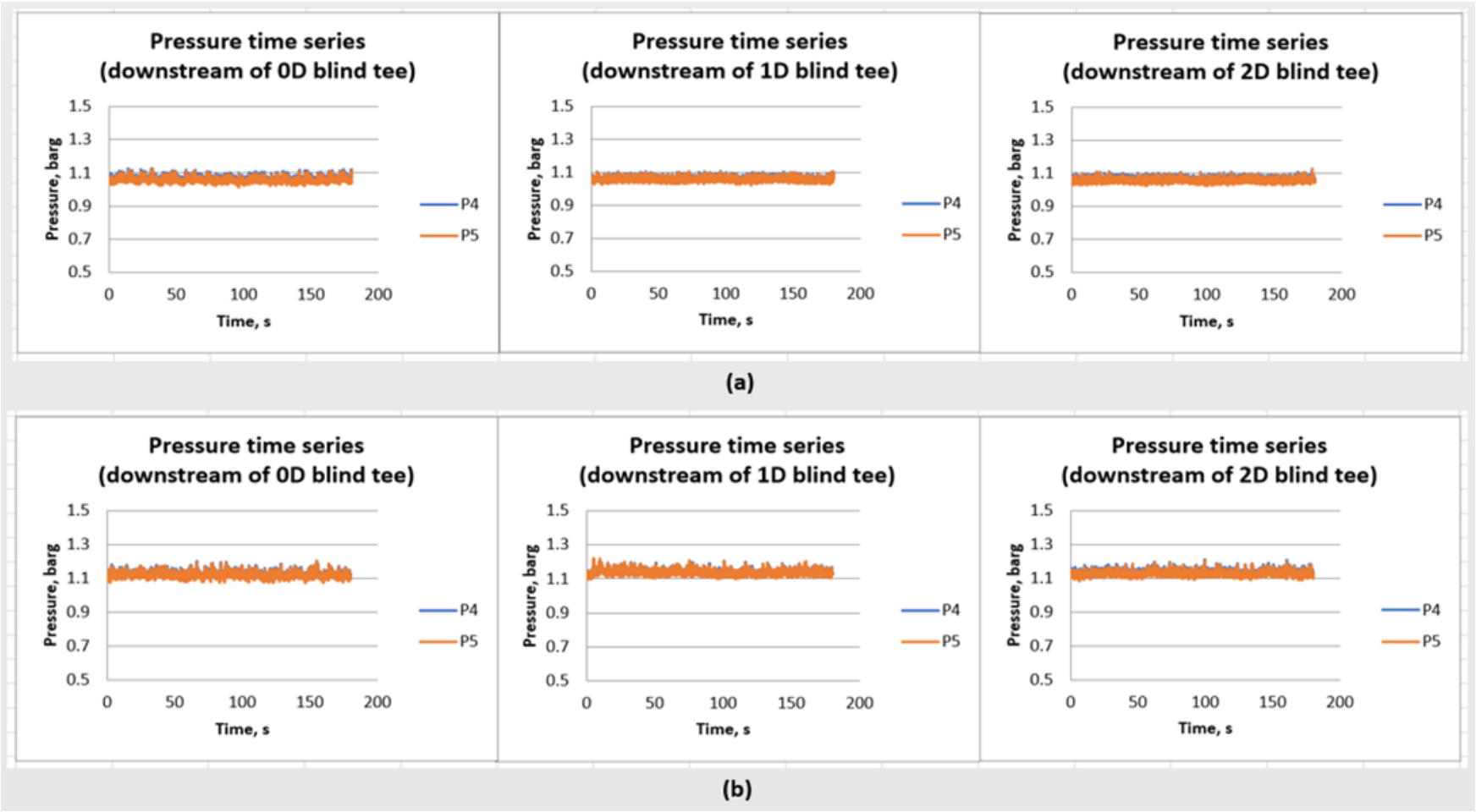

Figure C-32 Time series of pressures downstream of blind tee of different lengths (0D, 1D, and 2D) for flows with superficial liquid velocity of 0.086 m/s and superficial gas velocities of (a) 10.91 m/s and (b) 16.36 m/s.

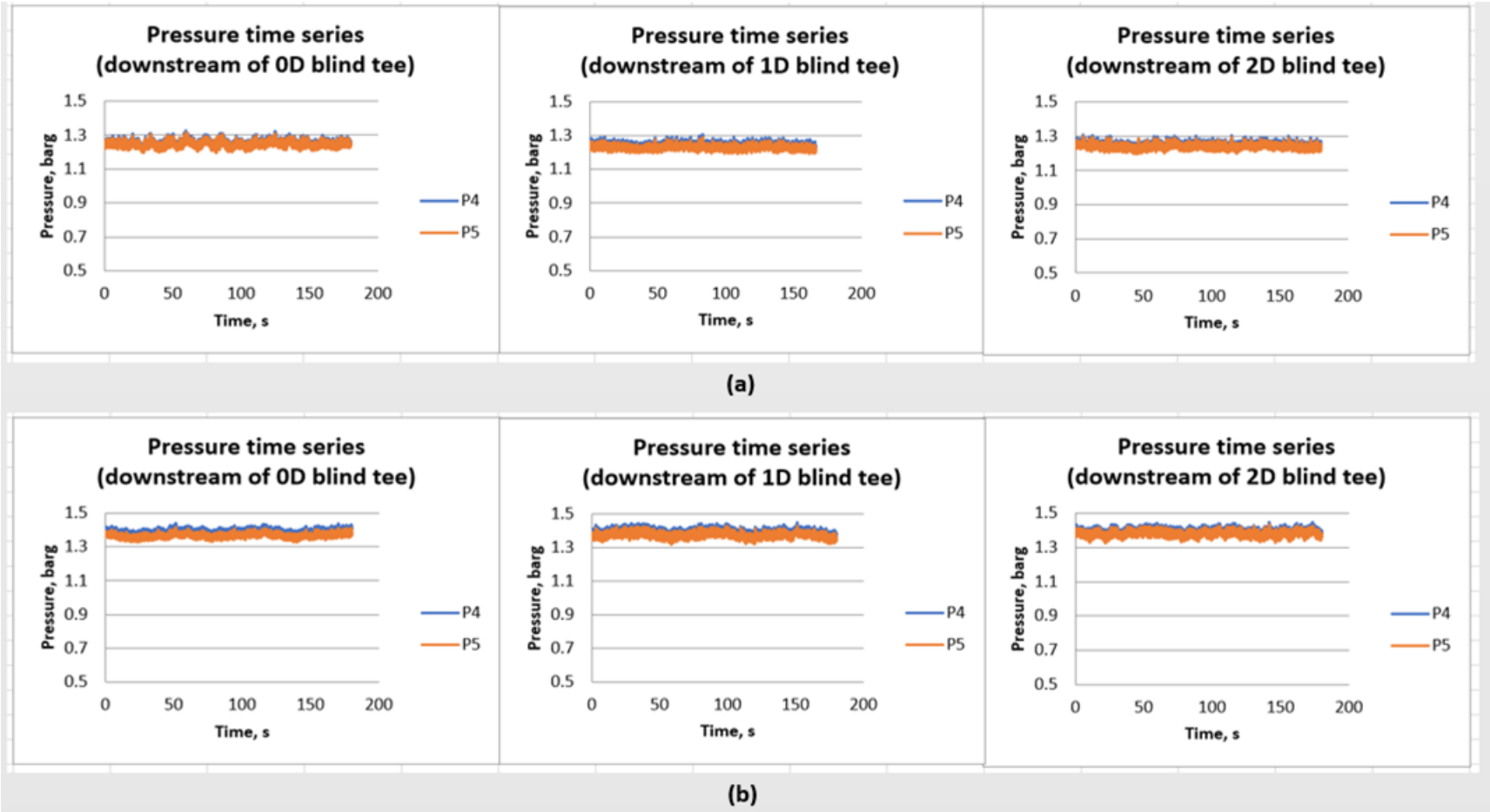

Figure C-33 Time series of pressures downstream of blind tee of different lengths (0D, 1D, and 2D) for flows with superficial liquid velocity of 0.086 m/s and superficial gas velocities of (a) 21.81 m/s and (b) 27.26 m/s.